ISSN 2686-7575 (Online)

ТОНКИЕ ХИМИЧЕСКИЕ ТЕХНОЛОГИИ

Fine Chemical Technologies

- Theoretical Basis of Chemical Technology
- Chemistry and Technology of Organic Substances
- Chemistry and Technology of Medicinal Compounds and Biologically Active Substances
- Industrial Pharmacy, Pharmaceutical Chemistry, Pharmacognosy
- Biochemistry and Biotechnology
- Synthesis and Processing of Polymers and Polymeric Composites
- Chemistry and Technology of Inorganic Materials
- Analytical Methods in Chemistry and Chemical Technology
- Mathematical Methods and Information Systems in Chemical Technology

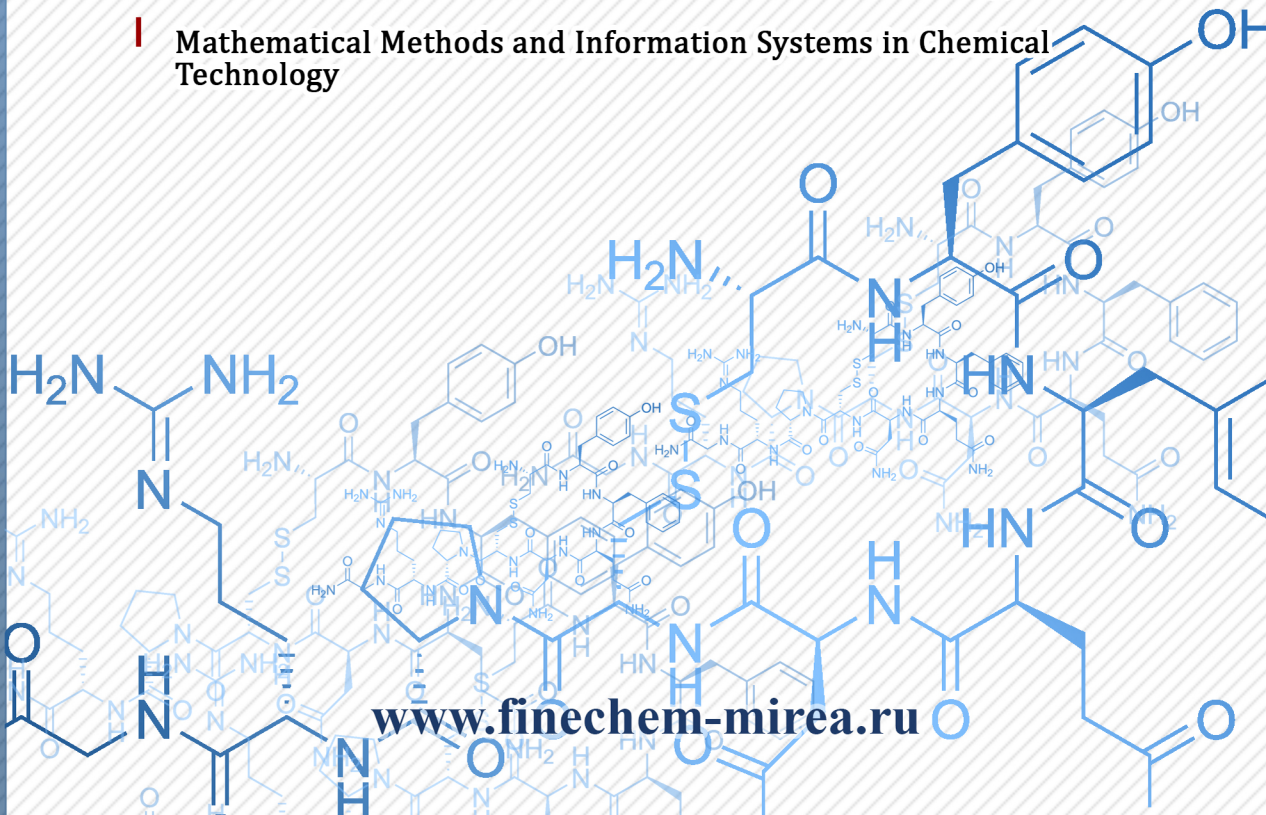

21(2)
2026

www.finechem-mirea.ru

ISSN 2686-7575 (Online)

ТОНКИЕ ХИМИЧЕСКИЕ ТЕХНОЛОГИИ

Fine Chemical Technologies

- Theoretical Basis of Chemical Technology
- Chemistry and Technology of Organic Substances
- Chemistry and Technology of Medicinal Compounds and Biologically Active Substances
- Industrial Pharmacy. Pharmaceutical Chemistry. Pharmacognosy
- Biochemistry and Biotechnology
- Synthesis and Processing of Polymers and Polymeric Composites
- Chemistry and Technology of Inorganic Materials
- Analytical Methods in Chemistry and Chemical Technology
- Mathematical Methods and Information Systems in Chemical Technology

Tonkie Khimicheskie Tekhnologii =
Fine Chemical Technologies.
Vol. 21, No. 2, 2026

Тонкие химические технологии =
Fine Chemical Technologies.
Том 21, № 2, 2026

https://doi.org/10.32362/2410-6593-2026-21-2
www.finechem-mirea.ru

https://doi.org/10.32362/2410-6593-2026-21-2
www.finechem-mirea.ru ISSN 2686-7575 (Online)

**Tonkie Khimicheskie Tekhnologii =
Fine Chemical Technologies
2026, Vol. 21, No. 2**

The peer-reviewed scientific and technical journal Fine Chemical Technologies highlights the modern achievements of fundamental and applied research in the field of fine chemical technologies, including the theoretical basis of chemical technology, chemistry and technology of medicinal compounds and biologically active substances, organic substances and inorganic materials, biochemistry and biotechnology, synthesis and processing of polymers and polymeric composites, analytical and mathematical methods and information systems in chemistry and chemical technology.

Founder and Publisher

Federal State Budget
Educational Institution of Higher Education
"MIREA – Russian Technological University"
78, Vernadskogo pr., Moscow, 119454, Russian Federation.
Publication frequency: bimonthly.
The journal was founded in 2006. The name was Vestnik MITHT until 2015 (ISSN 1819-1487).

The journal is included into the List of peer-reviewed science press of the State Commission for Academic Degrees and Titles of the Russian Federation; the Unified State List of Scientific Publications – White List (K1).

The journal is indexed: SCOPUS, DOAJ, Chemical Abstracts, Science Index, RSCI, Ulrich's International Periodicals Directory

86, Vernadskogo pr., Moscow, 119571, Russian Federation.
Phone: +7 (499) 600-80-80 (#31288)
E-mail: *seredina@mirea.ru*

The registration number ПИ № ФС 77-74580 was issued in December 14, 2018 by the Federal Service for Supervision of Communications, Information Technology, and Mass Media of Russia

The subscription index of *Pressa Rossii*: **36924**

Publication date 30.04.2026.

**Тонкие химические технологии =
Fine Chemical Technologies
2026, том 21, № 2**

Научно-технический рецензируемый журнал «Тонкие химические технологии» освещает современные достижения фундаментальных и прикладных исследований в области тонких химических технологий, включая теоретические основы химической технологии, химию и технологию лекарственных препаратов и биологически активных соединений, органических веществ и неорганических материалов, биохимию и биотехнологию, синтез и переработку полимеров и композитов на их основе, аналитические и математические методы и информационные системы в химии и химической технологии.

Учредитель и издатель

федеральное государственное бюджетное
образовательное учреждение высшего образования
«МИРЭА – Российский технологический университет»
119454, РФ, Москва, пр-т Вернадского, д. 78.
Периодичность: один раз в два месяца.
Журнал основан в 2006 году. До 2015 года издавался под названием «Вестник МИТХТ» (ISSN 1819-1487).

Журнал входит в Перечень ведущих рецензируемых научных журналов ВАК РФ, в Единый государственный перечень научных изданий – Белый список (К1).

Индексируется: SCOPUS, DOAJ, Chemical Abstracts, РИНЦ (Science Index), RSCI, Ulrich's International Periodicals Directory

РФ, 119571, Москва, пр. Вернадского, 86, оф. Р-108.
Тел.: +7 (499) 600-80-80 (#31288)
E-mail: *seredina@mirea.ru*

Регистрационный номер и дата принятия решения о регистрации СМИ: ПИ № ФС 77-74580 от 14.12.2018 г. СМИ зарегистрировано Федеральной службой по надзору в сфере связи, информационных технологий и массовых коммуникаций (Роскомнадзор)

Индекс по Объединенному каталогу «Пресса России»: **36924**

Дата опубликования 30.04.2026 г.

EDITORIAL BOARD

РЕДАКЦИОННАЯ КОЛЛЕГИЯ

Alexander N. Ozerin – Corresponding Member of the RAS, Dr. Sci. (Chem.), Professor, Enikolopov Institute of Synthetic Polymeric Materials of the RAS, Moscow, Russian Federation.
Scopus Author ID 7006188944, ResearcherID J-1866-2018, https://orcid.org/0000-0001-7505-6090, *ozerin@ispm.ru.*

Tapani A. Pakkanen – PhD, Professor, Department of Chemistry, University of Eastern Finland, Joensuu, Finland.
Scopus Author ID 7102310323, *tapani.pakkanen@uef.fi.*

Armando J.L. Pombeiro – Academician at the Academy of Sciences of Lisbon, PhD, Professor, President of the Center for Structural Chemistry of the Higher Technical Institute of the University of Lisbon, Lisbon, Portugal.
Scopus Author ID 7006067269, ResearcherID I-5945-2012, https://orcid.org/0000-0001-8323-888X, *pombeiro@ist.utl.pt.*

Dmitrii V. Pyshnyi – Corresponding Member of the RAS, Dr. Sci. (Chem.), Professor, Institute of Chemical Biology and Fundamental Medicine, Siberian Branch of the RAS, Novosibirsk, Russian Federation.
Scopus Author ID 7006677629, ResearcherID F-4729-2013, https://orcid.org/0000-0002-2587-3719, *pyshnyi@niboch.nsc.ru.*

Natalya V. Pyatigorskaya – Corresponding Member of the RAS, Dr. Sci. (Pharm.), Professor, Institute for Translational Medicine and Biotechnology, I.M. Sechenov First Moscow State Medical University (Sechenov University) of the Ministry of Health of the Russian Federation, Moscow, Russian Federation.
Scopus Author ID 55640443500, Researcher ID K-6918-2015, https://orcid.org/0000-0003-4901-4625, *pyatigorskaya_n_v@staff.sechenov.ru.*

Alexander S. Sigov – Academician at the RAS, Dr. Sci. (Phys. and Math.), Professor, President of MIREA – Russian Technological University, Moscow, Russian Federation.
Scopus Author ID 35557510600, ResearcherID L-4103-2017, *sigov@mirea.ru.*

Alexander M. Toikka – Dr. Sci. (Chem.), Professor, Institute of Chemistry, Saint Petersburg State University, St. Petersburg, Russian Federation.
Scopus Author ID 6603464176, ResearcherI D A-5698-2010, http://orcid.org/0000-0002-1863-5528, *a.toikka@spbu.ru.*

Andrzej W. Trochimczuk – Dr. Sci. (Chem.), Professor, Faculty of Chemistry, Wrocław University of Science and Technology, Wrocław, Poland.
Scopus Author ID 7003604847, *andrzej.trochimczuk@pwr.edu.pl.*

Aslan Yu. Tsivadze – Academician at the RAS, Dr. Sci. (Chem.), Professor, A.N. Frumkin Institute of Physical Chemistry and Electrochemistry of the RAS, Moscow, Russian Federation.
Scopus Author ID 7004245066, ResearcherID G-7422-2014, *tsiv@phyche.ac.ru.*

Озерин Александр Никифорович – член-корр. РАН, д.х.н., профессор, Институт синтетических полимерных материалов им. Н.С. Ениколопова РАН, Москва, Российская Федерация.
Scopus Author ID 7006188944, ResearcherID J-1866-2018, https://orcid.org/0000-0001-7505-6090, *ozerin@ispm.ru.*

Пакканен Тапани – PhD, профессор, Департамент химии, Университет Восточной Финляндии, Йоенсуу, Финляндия.
Scopus Author ID 7102310323, *tapani.pakkanen@uef.fi.*

Помбейро Армандо – академик Академии наук Лиссабона, PhD, профессор, президент Центра структурной химии Высшего технического института Университета Лиссабона, Португалия.
Scopus Author ID 7006067269, ResearcherID I-5945-2012, https://orcid.org/0000-0001-8323-888X, *pombeiro@ist.utl.pt.*

Пышный Дмитрий Владимирович – член-корр. РАН, д.х.н., профессор, Институт химической биологии и фундаментальной медицины Сибирского отделения РАН, Новосибирск, Российская Федерация.
Scopus Author ID 7006677629, ResearcherID F-4729-2013, https://orcid.org/0000-0002-2587-3719, *pyshnyi@niboch.nsc.ru.*

Пятигорская Наталья Валерьевна – член-корр. РАН, д.фарм.н., профессор, Институт трансляционной медицины и биотехнологии, Первый Московский государственный медицинский университет имени И.М. Сеченова Минздрава России (Сеченовский Университет), Москва, Российская Федерация.
Scopus Author ID 55640443500, Researcher ID K-6918-2015, https://orcid.org/0000-0003-4901-4625, *pyatigorskaya_n_v@staff.sechenov.ru.*

Сигов Александр Сергеевич – академик РАН, д.ф.-м.н., профессор, президент МИРЭА – Российского технологического университета, Москва, Российская Федерация.
Scopus Author ID 35557510600, ResearcherID L-4103-2017, *sigov@mirea.ru.*

Тойкка Александр Матвеевич – д.х.н., профессор, Институт химии, Санкт-Петербургский государственный университет, Санкт-Петербург, Российская Федерация.
Scopus Author ID 6603464176, Researcher ID A-5698-2010, http://orcid.org/0000-0002-1863-5528, *a.toikka@spbu.ru.*

Трохимчук Андржей – д.х.н., профессор, Химический факультет Вроцлавского политехнического университета, Вроцлав, Польша.
Scopus Author ID 7003604847, *andrzej.trochimczuk@pwr.edu.pl.*

Цивадзе Аслан Юсупович – академик РАН, д.х.н., профессор, Институт физической химии и электрохимии им. А.Н. Фрумкина РАН, Москва, Российская Федерация.
Scopus Author ID 7004245066, ResearcherID G-7422-2014, *tsiv@phyche.ac.ru.*

21(2) 2026 | Tonkie Khimicheskie Tekhnologii
Fine Chemical Technologies

CONTENTS

СОДЕРЖАНИЕ

SYNTHESIS AND PROCESSING OF POLYMERS AND POLYMERIC COMPOSITES

СИНТЕЗ И ПЕРЕРАБОТКА ПОЛИМЕРОВ И КОМПОЗИТОВ НА ИХ ОСНОВЕ

Tonkie Khimicheskie Tekhnologii = Fine Chemical Technologies.
2026;21(2):143–156 ISSN 2686-7575 (Online)

Theoretical basis of chemical technology

Теоретические основы химической технологии

UDC 66.011
https://doi.org/10.32362/2410-6593-2026-21-2-143-156
EDN VSRQYI

RESEARCH ARTICLE

Steady state analysis of the flow continuous stirred tank reactor on instance exothermic dimerization reaction

Natalia A. Korol'kova, Sergei L. Nazanskii✉, Michael A. Solokhin

MIREA – Russian Technological University, Moscow, 119454 Russia

✉ *Corresponding author, e-mail: nazanski@yandex.ru*

Abstract

Objectives. Due to the complexity of their behavior, chemical process flowsheets are characterized by steady state multiplicity, in other words, the presence of multiple steady state operating modes having the same set of parameters. The steady states differ from each other in terms of their reagent conversion, selectivity, product flow composition, and stability. Therefore, in order to be able to identify the steady state having optimal technological indicators, the objective of searching all steady states of a chemical process flowsheet is relevant. The aim of the study is to research all possible steady states for a continuous stirred tank reactor (CTSR) according to the exothermic dimerization reaction and investigate the influence of different operation parameters on the technological indicators of found states.

Methods. Mathematical simulations of material and energy balance equations for reactor were used. The quantity of steady states was estimated by the number of energy balance discrepancy function intersection with the O*x* axis. The Newton method in Microsoft Excel was used to solve nonlinear material balance equations of the reactor. The initial value of productivity was in range from zero to feed rate value of reagent of 100 kmol/h.

Results. It is shown that up to three steady states may exist for the reactor in dependence on the reaction volume, composition, and temperature feed flow, as well as the heat carrier flow rate. The results of this study correspond with earlier obtained results, which were obtained for irreversible reactions in adiabatic conditions. These states differ in productivity, internal reactor temperature, and stability. Steady state stability analysis of small parameter deviations was carried out. The analysis demonstrated that real characteristic values are in all found steady states of the reactor. Therefore, no oscillations in stable steady states of reactor and asymptotical operating time dependencies are implemented.

Conclusions. The technique of steady state analysis of a continuous stirred tank reactor developed over the course of this study, which reveals all steady states of the reactor with heat exchange, can be used to perform steady state analysis of recycled chemical process flowsheets, including continuous stirred tank reactors and separation blocks.

Keywords

reactors, exothermic reactions, steady states, steady state stability, mathematical simulation

Submitted: 27.07.2025
Revised: 09.09.2025
Accepted: 17.02.2026

For citation

Korol'kova N.A., Nazanskii S.L., Solokhin M.A. Steady state analysis of the flow continuous stirred tank reactor on instance exothermic dimerization reaction. *Tonk. Khim. Tekhnol. = Fine Chem. Technol.* 2026;21(2):143–156. https://doi.org/10.32362/2410-6593-2026-21-2-143-156

НАУЧНАЯ СТАТЬЯ

Анализ стационарных состояний проточного реактора идеального смешения на примере экзотермической реакции димеризации

Н.А. Королькова, С.Л. Назанский✉, М.А. Солохин

МИРЭА – Российский технологический университет, Москва, 119454 Россия

✉ *Автор для переписки, e-mail: nazanski@yandex.ru*

Аннотация

Цели. Химико-технологические системы в силу сложности своего поведения во многих случаях характеризуются полистационарностью, то есть наличием множественных стационарных режимов работы при одном и том же наборе рабочих параметров. Данные стационарные состояния отличаются конверсией, селективностью, составами продуктовых потоков и устойчивостью. В связи с этим, актуальной задачей является выявление всех возможных стационарных состояний химико-технологических систем для того, чтобы в дальнейшем была возможность выбора состояния с наилучшими технологическими показателями. Цель работы — поиск всех возможных стационарных состояний проточного реактора идеального смешения на примере реакции димеризации и анализ влияния различных параметров на технологические показатели реактора для найденных состояний.

Методы. Работа выполнялась методом математического моделирования с использованием материальных балансов по веществам и энергетического баланса реактора. Количество стационарных состояний оценивалось по числу точек пересечения функции невязки энергетического баланса с осью O*x*. Нелинейные алгебраические уравнения материального баланса реактора решались методом Ньютона в среде Microsoft Excel. Начальное приближение по производительности выбиралось в диапазоне от нуля до количества реагента 100 кмоль/ч в питании реактора.

Результаты. В ходе работы установлено, что в зависимости от объема реактора, температуры и состава входящего потока и расхода теплоносителя в проточном реакторе идеального смешения может реализовываться до трех стационарных состояний, которые отличаются производительностью реактора и температурой в нем. Результаты настоящей работы согласуются с литературными данными, полученными ранее для случаев необратимых реакций, протекающих в адиабатическом режиме. Кроме этого, проведен анализ устойчивости стационарных состояний при малых изменениях параметров, который показал, что характеристические корни в стационарных состояниях действительны, следовательно, колебания при работе реактора не реализуются, и в окрестности устойчивого состояния характер изменения параметров асимптотический.

Выводы. Разработана методика, которая позволяет выявить все возможные стационарные состояния проточного реактора идеального смешения с внешним теплообменом. Методику, примененную в данной работе, можно использовать для анализа стационарных состояний рециркуляционных химико-технологических систем, включающих реактор идеального смешения и блок разделения.

Ключевые слова

реакторы, экзотермические реакции, стационарные состояния,
устойчивость стационарных состояний, математическое моделирование

Поступила: 27.07.2025
Доработана: 09.09.2025
Принята в печать: 17.02.2026

Для цитирования

Королькова Н.А., Назанский С.Л., Солохин М.А. Анализ стационарных состояний проточного реактора идеального смешения на примере экзотермической реакции димеризации. *Тонкие химические технологии*. 2026;21(2):143–156. https://doi.org/10.32362/2410-6593-2026-21-2-143-156

INTRODUCTION

Any chemicotechnological system, regardless of its scale and product range, consists of a sequence of technological processes linked by direct and reverse connections. These processes include receipt and preparation of raw materials, chemical conversions, separation of the reaction mixture to obtain the target product, and formation of recirculation flows for unreacted raw materials. Experience in operating chemical plants shows that the main contribution to the economic efficiency criterion is made by the costs of chemical conversion processes (reactor subsystem) and reaction mass separation (separation subsystem) [1]. In addition to general economic indicators, an assessment of the efficiency of individual stages of the process also includes efficiency criteria that more fully reflect the chemical and physicochemical phenomena occurring in individual units of the technological system. One of the most important quantitative criteria reflecting the efficiency of a chemical reactor is the specific productivity and selectivity of the process.

In the case of kinetically reversible reactions, the overall reaction rate decreases as the chemical transformation proceeds due to an increase in the rate of reverse processes; as a result, a state of equilibrium is eventually achieved. Such a chemical equilibrium state comprises the main thermodynamic limitation that prevents the complete conversion of reactants into products in a single pass through a chemical reactor [2, 3]. In practice, many reactions require a long contact time and large reactor volume to achieve chemical equilibrium due to kinetic difficulties (low reaction rate). Under industrial conditions, the process should be carried out in such a way as to prevent the achievement of an equilibrium state of the chemical reaction, which would result in a lower yield of products. These kinetic difficulties and thermodynamic limitations of the process necessitate the use of chemicotechnological methods to overcome these difficulties. One such chemicotechnological method involves the organization of a recirculation flow of unreacted raw materials into the reactor. This reduces the residence time of the reagents in the reaction zone and consequent conversion in the reactor, which leads to an increase in the concentration of the reagents and corresponding chemical reaction rate, resulting in improved productivity [4]. However, in order to organize the recirculation flow, the chemical reactor must be supplemented with another separation unit, in which unreacted raw materials and reaction products will be separated. Using such an independent recirculation system, which is inherently more complex than a basic chemical reactor, it is possible to achieve a conversion higher than chemical equilibrium due to the absence of thermodynamic limitations on the maximum conversion value. In the case of reversible chemical reactions, recirculation can be used to achieve a degree of raw material conversion that exceeds the maximum permissible value for any type of reactor up to a theoretical maximum of 100% conversion. Thus, despite a low degree of reagent conversion in a single pass, the use of recirculation significantly increases a reactor's productivity. Similarly, with the proper organization of recirculation flows, it is possible to reduce the rate of side reactions to increase the overall selectivity of the process [5].

The presence of recirculating flows in the system causes feedback, which can lead to the emergence of multiple steady states under the same operating parameters of the system[1] [6]. In certain cases, steady state continua can be realized in recirculating reaction-rectification processes, which however disappear when transitioning from infinite separation capacity to a finite number of plates [7, 8]. In this regard, it is relevant to study the evolution of steady states of a given chemicotechnological scheme subject to changing design and operating parameters. Furthermore, in the presence of multiple steady states, the task of analyzing the stability of these states arises. The solution of this task in turn determines the strategy for starting the chemicotechnological process and the ability to maintain the operating parameters set for the desired steady state.

In view of the above, the present study set out to analyze the steady states of the reactor, taking into account heat exchange and changes in design and operating parameters, as well as the composition of the feed stream.

MATHEMATICAL MODEL OF THE REACTOR

In the first stage of the computational part of the study, research was conducted of the steady states of a continuous stirred tank reactor (CSTR) in which a liquid-phase reversible exothermic dimerization reaction $2A \leftrightarrow B$ takes place. The reaction was considered hypothetical, with the thermophysical properties of the components (heat capacity, density) used for the reaction under study corresponding to acetone (A) and diacetone alcohol (B).

[1] Blagov S.A. *Razrabotka metoda analiza statsionarnykh sostoyanii retsirkulyatsionnykh reaktsionno-rektifikatsionnykh processov* (*Development of a method for analyzing stationary states of recirculation reaction-distillation processes*). Cand. Sci. Thesis. (Eng.). Moscow: MITHT; 1999, 195 p.

Figure 1 shows a flow diagram of the CSTR for this process.

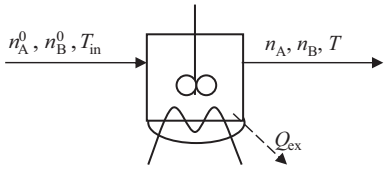

Fig. 1. Flow diagram of CSTR (all designations are given at the end of the article)

The physicochemical properties of the reaction mixture components, such as heat capacity, were taken from reference literature [9]. The thermal effect of the reaction under consideration was calculated taking into account the change in the heat capacity of the reaction mixture [10]:

$$\Delta H_T = \Delta H^0_{298.15} + \Delta C_p (T - 298.15), \quad (1)$$

where ΔH_T is the heat effect of the reaction, kJ/kmol; $\Delta H^0_{298.15}$ is the standard heat effect of the reaction at T = 298.15 K, kJ/kmol; ΔC_p is the change in the heat capacity of the reaction during the conversion of acetone to diacetone alcohol, kJ/kmol·K; T is the absolute temperature, K.

The standard heat effect of the reaction at T = 298.15 K was calculated based on the values of standard heat effects of substance formation available in the NIST TDE[2] Aspen Plus database and is equal to −95000 kJ/kmol.

The change in heat capacity during a chemical reaction is calculated using the formula:

$$\Delta C_p = C_{P_B} - C_{P_A}, \quad (2)$$

where C_{P_A} and C_{P_B} are heat capacities of components A and B, respectively, in the liquid state, kJ/(kmol·K).

The dependence of heat capacity on temperature is expressed by a power series:

$$C_p = a + bT + cT^2 + dT^3, \quad (3)$$

The coefficients *a, b, c, d* of Eq. (3) are presented in Table 1.

Table 1. Coefficients of the temperature dependence (3) of heat capacity for components A and B

Component	*a*	*b*	*c*	*d*
A	135.6	−0.177	$2.837 \cdot 10^{-4}$	$6.890 \cdot 10^{-7}$
B	59.7	0.542	0.00	0.00

For the dimerization process, it was assumed that the chemical reaction rate obeys the law of active masses and, thus, the reaction rate W has the form [12]:

$$W = k^+ \cdot C_A^2 - k^- \cdot C_B, \quad (4)$$

where k^+ (m^3/(kmol·h)) and k^- (h^{-1}) are rate constants for the forward and reverse reactions, respectively; C_A and C_B (kmol/m^3) are concentrations of components A and B, respectively.

The dependence of reaction rate on temperature obeys the Arrhenius law, according to which the following expression is valid for the reaction rate constant [11]:

$$k = Ae^{-\frac{E_a}{RT}}, \quad (5)$$

where A is the pre-exponential factor; E_a is activation energy, J/mol; R is the universal gas constant, J/(mol·K); T is absolute temperature, K.

At the preliminary calculation stage, velocity constant values were selected to ensure a sufficiently high velocity in the range of 300–400 K. The parameters of the temperature dependence of the constants (pre-exponential factors A and activation energies E) are given in Table 2.

Table 2. Arrhenius law parameters

A^+	E^+	A^-	E^-
$5.00 \cdot 10^9$	60000	$2.67 \cdot 10^{10}$	63200

The mathematical model of the CSTR shown in Fig. 1 consists of material balance equations:

$$n_A^0 - n_A - 2P = 0, \quad (6)$$

$$n_B^0 - n_B + P = 0, \quad (7)$$

where are feed rates of raw material into the reactor, kmol/h; n_A and n_B are product flow rates, kmol/h; P is reactor performance, kmol/h.

Reactor productivity depends on the volume V of the CSTR and the chemical reaction rate W. Thus, using formula (4) for W, we obtain the kinetic equation for productivity [12]:

$$P = W \cdot V = \left(k^+ \cdot C_A^2 - k^- \cdot C_B\right) \cdot V, \quad (8)$$

where V is a reactor volume, m^3; k^+ and k^- are constants of the forward and reverse reaction rates, respectively.

In order to reduce the problem to a single unknown parameter, we will relate the molar concentrations in the reactor to the molar fractions and molar flows using the molar volume of the mixture.

[2] NIST Standard Reference Data (SRD); © 2022 by the U.S. Secretary of Commerce on behalf of the United States of America.

Let us assume that the molar volume of the mixture obeys Amaga's law [9]:

$$\nu = \nu_A x_A + \nu_B x_B, \quad (9)$$

where ν_A and ν_B are the molar volumes of components A and B, respectively, in the mixture, m^3/kmol; x_A and x_B are mole fractions of components A and B, respectively.

The molar volume of a component depends on temperature and is calculated using the formula:

$$\nu_i = \frac{1}{a} \cdot b^{\left[1+\left(1-\frac{T}{c}\right)^d\right]}, \; i = \text{A, B}. \quad (10)$$

The coefficients *a, b, c, d* in Eq. (10) are given in Table 3.

Table 3. Coefficients for the mole volume calculation by (10)

Component	*a*	*b*	*c*	*d*
A	1.2298	0.2576	508.2	0.29903
B	0.6727	0.2603	606	0.2511

Molar concentrations in the reactor are related to molar fractions by the ratio:

$$C_A = \frac{x_A}{\nu}, \quad (11)$$

$$C_B = \frac{x_B}{\nu}. \quad (12)$$

Molar fractions are related to molar flows in the reactor by the following ratios:

$$x_A = \frac{n_A}{N}, \quad (13)$$

$$x_B = \frac{n_B}{N}, \quad (14)$$

$$N = n_A + n_B. \quad (15)$$

From Eqs. (6) and (7) of the component material balance of the reactor, we express the product molar flows through the known input flows and the unknown reactor productivity *P*:

$$n_A = n_A^0 - 2P, \quad (16)$$

$$n_B = n_B^0 + P. \quad (17)$$

Thus, using (9), (11)–(17), we obtain relations reflecting the connection between molar concentrations and molar fractions and molar flows in the reactor through one unknown quantity *P*:

$$C_A = \frac{x_A}{\nu_A x_A + \nu_B x_B} = \frac{\frac{n_A}{N}}{\nu_A \cdot \frac{n_A}{N} + \nu_B \cdot \frac{n_B}{N}} = \frac{n_A}{\nu_A n_A + \nu_B n_B} = \frac{n_A^0 - 2P}{\nu_A\left(n_A^0 - 2P\right) + \nu_B\left(n_B^0 + P\right)}, \quad (18)$$

$$C_B = \frac{x_B}{\nu_A x_A + \nu_B x_B} = \frac{\frac{n_B}{N}}{\nu_A \cdot \frac{n_A}{N} + \nu_B \cdot \frac{n_B}{N}} = \frac{n_B}{\nu_A n_A + \nu_B n_B} = \frac{n_B^0 + P}{\nu_A\left(n_A^0 - 2P\right) + \nu_B\left(n_B^0 + P\right)}. \quad (19)$$

To find the reactor performance, we will transform Eq. (8) using the obtained expressions for the chemical reaction rate (4) and molar concentrations (18) and (19).

As a result of the transformations, we will obtain a nonlinear equation expressing the material balance of the CSTR through one unknown quantity *P*:

$$P - V\left[\frac{k^+ \cdot \left(n_A^0 - 2P\right)^2}{\left(\nu_A\left(n_A^0 - 2P\right) + \nu_B\left(n_B^0 + P\right)\right)^2} - \frac{k^- \cdot \left(n_B^0 + P\right)}{\nu_A\left(n_A^0 - 2P\right) + \nu_B\left(n_B^0 + P\right)}\right] = 0. \quad (20)$$

The mathematical model of CSTR also includes the reactor heat balance equation (ΔQ is the heat balance discrepancy, kJ/h):

$$\Delta Q = \left(n_A^0 \cdot C_{P_A}^{\text{in}} + n_B^0 \cdot C_{P_B}^{\text{in}}\right) T_{\text{in}} - \left(n_A \cdot C_{P_A} + n_B \cdot C_{P_B}\right) T - \Delta H_T \cdot P + Q_{\text{ex}} = 0 \quad (21)$$

where are heat capacity of components A and B at inlet temperature, kJ/(kmol·K); T_{in} is the temperature at the reactor inlet, K; Q_{ex} is the amount of heat supplied by external heat exchange, kJ/h.

To simplify the study, let us assume that the CSTR has a cylindrical shape with a flat bottom enclosed in a jacket. The flow structure in the reactor jacket is assumed to correspond to ideal mixing. The amount of heat supplied by external heat exchange is calculated based on the temperature difference between the reactor and the jacket [13].

The equation for calculating the amount of heat supplied by external heat exchange is as follows:

$$Q_{\text{ex}} = K_t \cdot F(T - T''), \quad (22)$$

where K_t is the heat transfer coefficient, kJ/(h·m^2·K); *F* is the heat exchange surface area, m^2; *T* is the reactor

temperature, K; T'' is the refrigerant temperature in the jacket, K.

To solve the problem of analyzing steady states under conditions of external heat exchange, it is necessary to specify the design characteristics, comprising the diameter and height of the reactor, the heat exchange surface, as well as the amount of refrigerant supplied to the jacket, its inlet temperature, and its thermophysical properties.

The heat balance equation for the refrigerant is expressed as follows:

$$G_{\text{ref}} \cdot C_{P_{\text{ref}}} \cdot T' - G_{\text{ref}} \cdot C_{P_{\text{ref}}} \cdot T'' + K_{\text{t}} \cdot F\left(T - T''\right) = 0, \quad (23)$$

where G_{ref} is the refrigerant consumption, kmol/h; $C_{P_{\text{ref}}}$ is the heat capacity of refrigerant, kJ/(kmol·K); T' is the refrigerant inlet temperature, K.

When calculating the material balance of the reactor and the thermal balance mismatch, the input parameters were the feed flow rate, its composition and temperature, as well as the refrigerant flow rate and its inlet temperature. The influence of the feed flow input parameters on the steady-state conditions when varying the temperature and composition of the feedstock, as well as the influence of heat exchange, were studied. The following parameters were set: reactor volume, refrigerant quantity, and refrigerant temperature.

Thus, we obtained a problem in which the known parameters are: reactor volume V; feed rate of the raw material n_{A}^0 and n_{B}^0; inlet flow temperature T_{in}; standard heat effect of reaction $\Delta H_{298.15}^0$; refrigerant consumption G_{ref}; refrigerant inlet temperature T'. The unknown parameters are: the temperature in the reactor and the composition of the product stream.

To solve this problem, the current temperature value in the CSTR was set and Eq. (20) was solved to find the reactor performance value. Then, using Eqs. (16) and (17), the material balance of the reactor was calculated at a given temperature. To solve Eq. (20), the Newton method was used, which is implemented in Microsoft Excel in the Solver module. Next, based on the information obtained, the reactor heat balance discrepancy (21) was calculated. By graphically plotting the dependence $\Delta Q = f(T)$ according to the number of points of intersection of this dependence with the Ox axis, the number of steady states of the reactor was determined. For this purpose, the thermal balance discrepancy was calculated in the temperature range of 200–500 K. When selecting the temperature range, the possibility of lowering the temperature in the reactor by removing heat with an external heat carrier, as well as heating the reaction mass due to the thermal effect, was taken into account.

Analysis of steady states of a flow adiabatic CSTR at different inlet temperatures of reagents

Let us consider the influence of the inlet flow temperature on the steady-state parameters. To do this, we will specify the design parameters of the reactor and the composition of the reagent flow, and its temperature will act as a variable.

Initial data for the calculation were as follows: reactor volume V = 1.4 m^3; feed rate of raw material $n_{\text{A}}^0 = 100$ kmol/h; $n_{\text{B}}^0 = 0$; no external heat exchange, $Q_{\text{ex}} = 0$.

Next, we obtain the dependencies of the thermal balance discrepancies of the adiabatic reactor on temperature at various values of the inlet flow temperature. The calculation results are shown in Fig. 2.

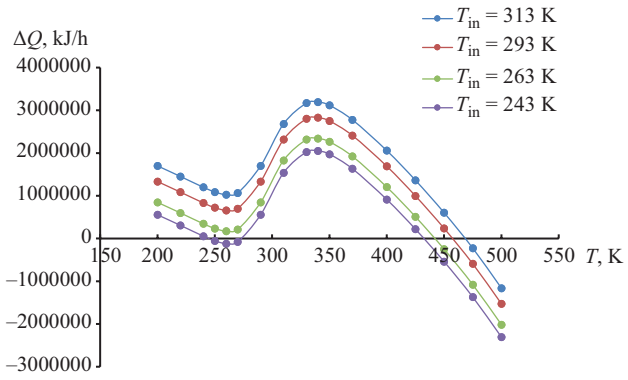

Fig. 2. Reactor temperature dependencies of the energetic balance discrepancy for adiabatic reactor with different feed temperature

Based on the data obtained from the thermal balance discrepancies from the temperature, the parameters of the reactor's steady states were determined, the results of which are shown in Fig. 3.

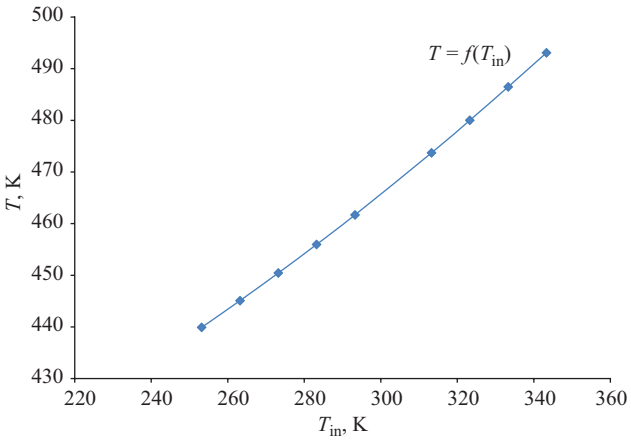

Fig. 3. Feed flow temperature dependence of the internal reactor temperature

The results shown in Fig. 2 indicate that when the inlet flow temperature decreases below a certain value (below 248 K), three steady states become possible, differing in reactor temperature and productivity. For example, at $T_{in} = 243$ K, three steady states are realized: $T_1 = 244.70$ K, $P_1 = 0.229$ kmol/h; $T_2 = 274.79$ K, $P_2 = 4.545$ kmol/h, and $T_3 = 432.46$ K, $P_3 = 37.263$ kmol/h. The calculations showed that the temperature in the reactor increases with an increase in the inlet flow temperature, while the productivity decreases. The decrease in productivity is due to the fact that as the temperature in the reactor increases, the reverse reaction rate constant begins to prevail, which leads to a significant increase in its rate.

Analysis of steady states of a flow adiabatic CSTR at different values of its volume

Let us consider the effect of the CSTR volume on the steady-state parameters. This can be achieved by setting the input values for the reagent flow (its composition and temperature), while the reactor volume will vary.

Initial data for the calculation were as follows: inlet flow temperature $T_{in} = 263.15$ K, feed rate of raw material $n_A^0 = 100$ kmol/h; $n_B^0 = 0$; $Q_{ex} = 0$.

Next, we will obtain the dependencies of the thermal balance discrepancies of an adiabatic reactor on temperature at different values of its volume, m^3. The calculation results are shown in Fig. 4.

From Fig. 4, it can be concluded that, with a decrease in the reactor volume, three steady states can be achieved. At high volume values, one steady state is achieved with a high temperature in the reactor (approximately 450 K). At low volume values, two more steady states appear with lower temperatures and, accordingly, lower reactor productivity.

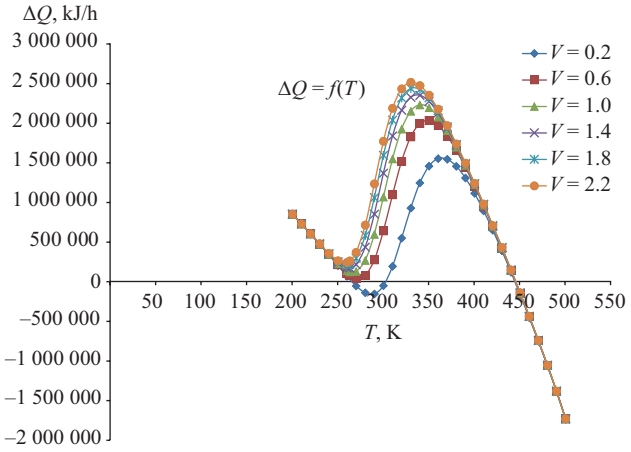

Fig. 4. Reactor temperature dependencies of the energetic balance discrepancy for adiabatic reactor with different reaction volumes

Analysis of steady states in a flow adiabatic CSTR at various inlet flow compositions

Let us consider the influence of the inlet stream composition on the steady-state parameters. This can be achieved by setting the design parameters of the reactor and the inlet stream temperature, while its composition will vary.

Initial data for calculation: reactor volume $V = 1.4$ m^3; inlet flow temperature $T_{in} = 263.15$ K; $Q_{ex} = 0$. The calculation results are shown in Fig. 5.

The data obtained (Fig. 5) show that, as the content of component A in the input stream decreases, the heat balance discrepancy curve decreases relative to the Oy axis and straightens. The temperature and productivity of the reactor decrease as the molar fraction of component A in the initial mixture decreases. Furthermore, when the

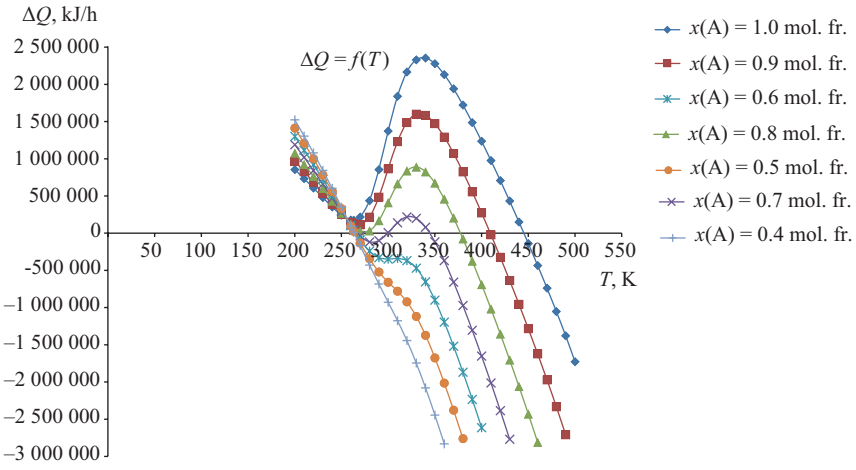

Fig. 5. Reactor temperature dependencies of the energetic balance discrepancy for adiabatic reactor with different composition of feed flow. x(A) is the mole fraction A in the feed flow

ratio of reagents changes, there is a range of values (0.65–0.80 molar fractions of component A) in which three steady states are realized.

Analysis of steady states in a flow isothermal CSTR at different amounts of heat removal

The results of the analysis of the steady states of the adiabatic reactor demonstrate the possibility of three points of intersection of the $\Delta Q(T)$ curve with the Ox axis and consequent likelihood of three steady states of the reactor. The achievement of multiple steady states in the presence of heat removal Q_{ex} can be assumed, since the presence of an additional negative term in (21) will lead to the appearance of new points of intersection of the mismatch curve with the Ox axis. In this regard, calculations of a mathematical model of a reactor with heat removal were performed.

Let us consider the effect of the amount of heat supplied to the refrigerant jacket on the steady-state parameters. This can be achieved by setting the design parameters of the reactor, the temperature and composition of the inlet flow, while the refrigerant supply rate will vary.

Initial data for solving the problem were as follows: inlet temperature of the reactants T_{in} = 263.15 K; reactor volume V = 1.4 m^3; reactor diameter d = 1.2 m; reactor height h = 1.24 m; feed rate of the raw material $n_A^0 = 100$ kmol/h; $n_B^0 = 0$.

The heat transfer coefficient K_t generally depends on the hydrodynamic conditions in the reactor and jacket and the composition of the reaction mass. To simplify calculations, we will assume K_t to be constant in accordance with the recommended parameters [13]: K_t = 5400 kJ/(h·m^2·K); heat capacity of the refrigerant $C_{P_{ref}}$ = 83.4 kJ/(kmol·K). Refrigerant inlet temperature T' = 250.15 K.

We can calculate the heat exchange surface area F knowing the diameter d and height h of the reactor:

$$F = \pi dh + \frac{\pi d^2}{4} = 3.14 \cdot 1.2 \cdot 1.24 + \frac{3.14 \cdot 1.2}{4} = 5.80 \text{ m}^2.$$

To calculate the outlet temperature of the refrigerant and the amount of heat removed, we will use Eqs. (22) and (23). Using the reactor model, we will obtain the dependencies of the heat balance discrepancies of the isothermal reactor on the temperature at different refrigerant flow rates. The calculation results are shown in Fig. 6.

Based on the obtained dependencies of heat balance discrepancies on temperature, the parameters of steady states of an isothermal reactor were determined as given in Table 4.

Table 4. Steady states of the isothermal reactor with different flow rates of heat carrier

G_{ref}, kmol/h	T, K	P, kmol/h	Q_{ex}, kJ/h	T'', K
0	445.07	37.06	0.00	–
200	267.60	2.48	$1.90 \cdot 10^5$	261.53
	271.22	3.40	$2.29 \cdot 10^5$	263.90
	388.78	38.01	$1.51 \cdot 10^6$	340.59
400	260.75	1.30	$1.71 \cdot 10^5$	255.28
	282.60	7.98	$5.24 \cdot 10^5$	265.86
	369.94	37.95	$1.93 \cdot 10^5$	308.14

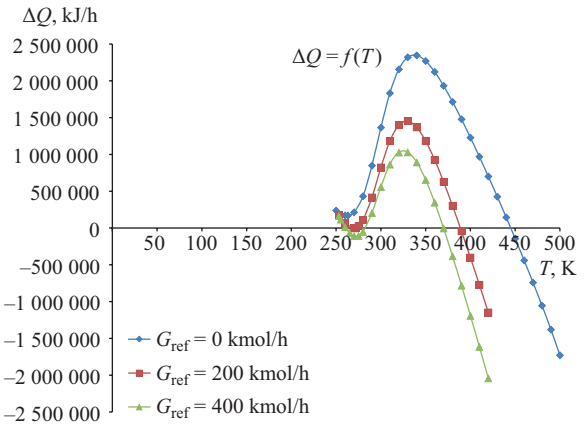

Fig. 6. Reactor temperature dependencies of the energetic balance discrepancy for isothermal reactor with different flow rates of heat carrier

The results show that, in the case of heat exchange with an increased quantity of refrigerant, three steady states of the reactor occur, differing in temperature and performance. The presence of several steady states is realized at refrigerant flow rates above 200 kmol/h.

Thus, numerical modeling of the reactor made it possible to identify its possible steady states. If we assume that the reactor under consideration is an element of a recirculation system, then the reactor feed flow is formed by mixing some external flow with the recirculation flow. Thus, it can be assumed that the recirculation system, including the reactor and the separation unit, can also implement several steady states with different reactor capacities and, consequently, conversion throughout the system.

Stability of steady states in a dimerization reactor under small parameter changes

For a CSTR, whose mathematical model is a system of ordinary differential equations, the concentrations of reactants and the temperature in the reactor play the role of variables. The behavior of the object is described by a system of first-order differential equations [14]:

$$\begin{cases} \dfrac{dC_A}{dt} = \dfrac{n_A^0 - qC_A}{V} - 2k^+C_A^2 + 2k^-C_B \equiv f_1, \\ \dfrac{dC_B}{dt} = \dfrac{n_B^0 - qC_B}{V} + k^+C_A^2 - k^-C_B \equiv f_2, \\ \dfrac{dT}{dt} = \dfrac{\left(n_A^0 C_{P_A} + n_B^0 C_{P_B}\right)T_{in}}{V\left(C_A C_{P_A} + C_B C_{P_B}\right)} - \dfrac{qT}{V} - \dfrac{\Delta H_T\left(k^+C_A^2 - k^-C_B\right)}{C_A C_{P_A} + C_B C_{P_B}} \equiv f_3, \end{cases} \quad (24)$$

where q is the volume flow rate of the mixture, m^3/h, which is calculated using the expression:

$$q = (\nu_A x_A + \nu_B x_B)L, \quad (25)$$

where L is the flow rate at the reactor outlet, kmol/h.

The coefficients of system (24) are the values of partial derivatives from the right-hand sides of the equations corresponding to the equilibrium position coordinates, namely matrix **B**:

$$\mathbf{B} = \begin{pmatrix} \dfrac{\partial f_1}{\partial C_A} & \dfrac{\partial f_1}{\partial C_B} & \dfrac{\partial f_1}{\partial T} \\ \dfrac{\partial f_2}{\partial C_A} & \dfrac{\partial f_2}{\partial C_B} & \dfrac{\partial f_2}{\partial T} \\ \dfrac{\partial f_3}{\partial C_A} & \dfrac{\partial f_3}{\partial C_B} & \dfrac{\partial f_3}{\partial T} \end{pmatrix} \quad (26)$$

The equation of system (24) with respect to characteristic roots λ has the form of a third-degree polynomial [15]:

$$\lambda^3 + \sigma\lambda^2 + \Delta\lambda + \theta = 0, \quad (27),$$

whose coefficients are calculated in accordance with the following expressions:

$$\sigma = -\left(\frac{\partial f_1}{\partial C_A} + \frac{\partial f_2}{\partial C_B} + \frac{\partial f_3}{\partial T}\right), \quad (28)$$

$$\Delta = \begin{vmatrix} \dfrac{\partial f_1}{\partial C_A} & \dfrac{\partial f_2}{\partial C_A} \\ \dfrac{\partial f_1}{\partial C_B} & \dfrac{\partial f_2}{\partial C_B} \end{vmatrix} + \begin{vmatrix} \dfrac{\partial f_1}{\partial C_A} & \dfrac{\partial f_3}{\partial C_A} \\ \dfrac{\partial f_1}{\partial T} & \dfrac{\partial f_3}{\partial T} \end{vmatrix} + \begin{vmatrix} \dfrac{\partial f_2}{\partial C_B} & \dfrac{\partial f_3}{\partial C_B} \\ \dfrac{\partial f_2}{\partial T} & \dfrac{\partial f_3}{\partial T} \end{vmatrix} \quad (29)$$

$$\theta = -\begin{vmatrix} \dfrac{\partial f_1}{\partial C_A} & \dfrac{\partial f_1}{\partial C_B} & \dfrac{\partial f_1}{\partial T} \\ \dfrac{\partial f_2}{\partial C_A} & \dfrac{\partial f_2}{\partial C_B} & \dfrac{\partial f_2}{\partial T} \\ \dfrac{\partial f_3}{\partial C_A} & \dfrac{\partial f_3}{\partial C_B} & \dfrac{\partial f_3}{\partial T} \end{vmatrix} \quad (30)$$

$$\Omega = -\sigma^2\Delta^2 + 4\sigma^3\theta + 4\Delta^3 - 18\sigma\Delta\theta + 27\theta^2. \quad (31)$$

To solve system (24), we express the partial derivatives of matrix **B** in analytical form:

$$\frac{\partial f_1}{\partial C_A} = -\frac{q}{V} - 4k^+C_A, \quad (32)$$

$$\frac{\partial f_1}{\partial C_B} = 2k^-, \quad (33)$$

$$\frac{\partial f_1}{\partial T} = -2C_A^2\frac{\partial k^+}{\partial T} + 2C_B\frac{\partial k^-}{\partial T}, \quad (34)$$

$$\frac{\partial f_2}{\partial C_A} = 2k^+C_A, \quad (35)$$

$$\frac{\partial f_2}{\partial C_B} = -\frac{q}{V} - k^-, \quad (36)$$

$$\frac{\partial f_2}{\partial T} = C_A^2\frac{\partial k^+}{\partial T} - C_B\frac{\partial k^-}{\partial T}, \quad (37)$$

$$\frac{\partial k}{\partial T} = \frac{\partial\left[A\cdot e^{\frac{-E_a}{RT}}\right]}{\partial T} = A\cdot e^{\frac{-E_a}{RT}}\frac{E_a}{RT^2}. \quad (38)$$

We express the derivative functions f_3 as:

$$\frac{\partial f_3}{\partial C_A} \approx \frac{\Delta f_3}{\Delta C_A} = \frac{f_3\left(C_{A_S} + 0.001; C_{B_S}; T_S\right) - f_3\left(C_{A_S}; C_{B_S}; T_S\right)}{0.001}, \quad (39)$$

$$\frac{\partial f_3}{\partial C_B} \approx \frac{\Delta f_3}{\Delta C_B} = \\ = \frac{f_3\left(C_{A_S}; C_{B_S} + 0.001; T_S\right) - f_3\left(C_{A_S}; C_{B_S}; T_S\right)}{0.001}, \quad (40)$$

$$\frac{\partial f_3}{\partial T} \approx \frac{\Delta f_3}{\Delta T} = \\ = \frac{f_3\left(C_{A_S}; C_{B_S}; T_S + 0.001\right) - f_3\left(C_{A_S}; C_{B_S}; T_S\right)}{0.001}. \quad (41)$$

Here, C_{A_S} and C_{B_S} are concentrations of components A and B at steady states, respectively, kmol/m^3; T_S is the reactor temperature at steady states, K.

We will analyze the obtained steady states of the adiabatic reactor for stability; the parameters of the steady states are given in Table 5.

For these values, we will analyze the stability of steady states in the small. We will calculate the values of the derivatives using formulas (32)–(41) and find the values of the coefficients of the characteristic Eq. (27) using formulas (28)–(31). The results are presented in Table 6.

From the Routh–Hurwitz conditions, it follows that the equilibrium position under investigation is stable if the following inequalities are satisfied [15]:

$$\sigma > 0;\ \Delta > 0;\ \theta > 0;\ \sigma\Delta - \theta > 0. \quad (42)$$

From this, it can be concluded that systems characterized by a single steady state are stable. For example, steady states 1, 2 and 3, which when occurring in isolation (as shown by qualitative analysis), are characterized by stable reactor operation. However, when several steady states are realized, not all of them correspond to a stable reactor state. In a reactor with a volume of 0.2 m^3, three steady states are realized, two

Table 5. Steady states of the reactor

No.	V, m^3	T_{in}, K	x_A, mol. fr.	T, K	P, kmol/h
1	1.4	253.15	1.0	439.89	37.18
2	1.4	263.15	1.0	445.07	37.06
3	1.4	273.15	1.0	492.98	35.72
4	0.2	263.15	1.0	265.22	0.30
5				302.73	6.31
6				444.22	36.88
7	1.4	263.15	0.7	266.85	0.75
8				299.77	7.90
9				344.27	18.99

Table 6. Coefficients of the characteristic Eq. (27)

No.	σ	Δ	θ	σΔ − θ	Ω
1	6020	$2.11 \cdot 10^6$	$1.19 \cdot 10^7$	$1.27 \cdot 10^{10}$	$-1.16 \cdot 10^{20}$
2	7270	$3.07 \cdot 10^6$	$1.75 \cdot 10^7$	$2.23 \cdot 10^{10}$	$-3.64 \cdot 10^{20}$
3	8800	$4.47 \cdot 10^6$	$2.58 \cdot 10^7$	$3.93 \cdot 10^{10}$	$-1.14 \cdot 10^{21}$
4	119	4670	59900	498000	−224000
5	15.3	−4510	−136000	67300	$-4.13 \cdot 10^{10}$
6	6990	$1.76 \cdot 10^6$	$5.99 \cdot 10^7$	$1.23 \cdot 10^{10}$	$-6.14 \cdot 10^{19}$
7	20.3	135	293	2440	−22.9
8	4.78	−157	−925	172	$-5.98 \cdot 10^6$
9	52.8	−1340	−10400	−60300	$-3.11 \cdot 10^{10}$

of which (Nos. 4 and 6) are stable, and one (No. 5) is a saddle [15]. When a mixture of components A and B in a ratio of 0.7/0.3 is fed into the reactor, it is also possible to implement three steady states, where one state is a stable node (No. 7) and the other two are saddles (Nos. 8 and 9).

DISCUSSION OF RESULTS AND CONCLUSIONS

By calculating the thermal balance discrepancies, possible steady states of a CSTR were identified. The influence of the inlet temperature and composition of the reagent flow, reactor volume, heat exchange, and inlet flow composition on the parameters of steady states was considered along with a determination of their type.

As the inlet flow temperature increases, the steady-state temperature also increases along with a decrease in their productivity. This is due to the fact that, as the temperature in the reactor increases, the reverse reaction rate begins to increase.

A decrease in the reactor volume leads to the realization of three steady states (when the reactor volume is less than 0.6 m^3), which can lead to unstable operation or low productivity values.

As the product content in the feed stream increases due to the composition approaching chemical equilibrium, the reactor productivity decreases, and two more steady states appear in the range of 0.65–0.8 molar fractions of component A.

The analysis of the steady states demonstrates that the realized steady states are stable nodes and saddles. It follows that oscillatory modes for the reaction under consideration are not realized in a CSTR.

Symbols

A, B — reaction mixture components;
C_A, C_B — concentrations of components A and B, respectively, kmol/m^3;
C_{A_S}, C_{B_S} — concentrations of components A and B at steady states, respectively, kmol/m^3;
C_{P_A}, C_{P_B} — heat capacity of components A and B, respectively, kJ/(kmol·K);
$C_{P_{ref}}$ — heat capacity of refrigerant, kJ/(kmol·K);
E_a — activation energy, J/mol;
F — surface area of heat exchange, m^2;
G_{ref} — refrigerant consumption, kmol/h;
ΔH_T — change in enthalpy during the reaction, kJ/kmol;
k — speed constant;
K_t — heat transfer coefficient, kJ/(h·m^2·K);
L — reactor outlet flow, kmol/h;
n_A^0 and n_B^0 — feed rate of raw material into the reactor, kmol/h;
n_A and n_B — product flow rates, kmol/h;
P — reactor performance, kmol/h;
q — volume flow rate of the mixture, m^3/h;
Q_{ex} — heat removal from the reactor, kJ/h;
ΔQ — energy imbalance, kJ/h;
R — universal gas constant, 8.314 J/(mol·K);
T_{in} — inlet flow temperature to the reactor, K;
T' — refrigerant inlet temperature, K;
T'' — refrigerant outlet temperature, K;
T — reactor temperature, K;
T_S — reactor temperature at steady states, K;
V — reactor volume, m^3;
ν — molar volume of mixture, m^3/kmol;
ν_A and ν_B — molar volumes of components A and B, respectively, in the mixture, m^3/kmol;
x_A and x_B — molar fractions of components A and B in the mixture, respectively;
W — chemical reaction rate.

Authors' contributions

N.A. Korol'kova—search for data for reaction mixture physical and chemical properties, development of the reactor mathematical model, development of the steady state analysis for the reactor.

S.L. Nazanskii—statement the problem, development of the reactor mathematical model, development of the steady state stability analysis of reactor, conclusions.

M.A. Solokhin—search for data for reaction mixture physical and chemical properties, thermodynamical consistency of the reaction rate model, development of the steady state stability analysis of the reactor.

The authors declare no conflicts of interest.

REFERENCES

1. Timofeev B.C., Serafimov L.A. *Printsipy tekhnologii osnovnogo organicheskogo i neftekhimicheskogo sinteza* (*Principles of Basic Organic and Petrochemical Synthesis Technology*): A Textbook for Universities. Moscow: Vysshaya shkola; 1992, 536 p. (In Russ.).
2. Nagiev M.F. *Teoriya retsirkulyatsii i povyshenie optimal'nosti khimiko-tekhnologicheskikh protsessov* (*Theory of Recirculation and Improving the Optimality of Chemicotechnological Processes*). Moscow: Nauka; 1970, 390 p. (In Russ.).
3. Aliev A.M., Safarov A.R., Osmanova I.I., Guseinova A.M., Mamedov Z.A., Ismailov O.A. Intensification of gasoline pyrolysis process taking into account recirculation. *Azerbaidzhanskii khimicheskii zhurnal = Azerbaijan Chemical Journal*. 2017;1:20–27 (in Russ.). https://elibrary.ru/vpecho
4. Solokhin A.V., Blagov S.A., Timofeev V.S. Effect of recycling on reactor productivity. *Teoreticheskie osnovy khimicheskoi tekhnologii = Theor. Found. Chem. Eng.* 1995;29(5):528–534 (in Russ.). https://www.elibrary.ru/ktdvsn
5. Solokhin A.V., Nazanskii S.L., Miliaeva T.V. Recycling techniques for enhancing the selectivity of complex chemical reactions. *Theor. Found. Chem. Eng*. 2011;45(3):267–271. https://doi.org/10.1134/S0040579511030122
[Original Russian Text: Solokhin A.V., Nazanskii S.L., Miliaeva T.V. Recycling techniques for enhancing the selectivity of complex chemical reactions. *Teoreticheskie osnovy khimicheskoi tekhnologii.* 2011;45(3):284–288 (in Russ.). https://www.elibrary.ru/ntvznn]
6. Ponomarev V.N., Saksonova O.I., Timofeev B.C. Polystationarity in continuous distillation processes. *Teoreticheskie osnovy khimicheskoi tekhnologii.* 1996;30(4): 383–389 (in Russ.).
7. Duev S.I., Borianov A.I. Conditions for the existence of families of stationary states in a recirculation system: a perfectly mixed reactor – a separation unit. *Teoreticheskie osnovy khimicheskoi tekhnologii.* 2000;34(1):50–56 (in Russ.).
8. Solokhin A.V., Nazanskii S.L., Timofeev V.S. Prediction of steady-state operating modes in recycle reactive-distillation systems using the mode of infinite separation efficiency. *Theor. Found. Chem. Eng*. 2009;43(2):151–159. https://doi.org/10.1134/S0040579509020043
[Original Russian Text: Solokhin A.V., Nazanskii S.L., Timofeev V.S. Prediction of steady-state operating modes in recycle reactive-distillation systems using the mode of infinite separation efficiency. *Teoreticheskie osnovy khimicheskoi tekhnologii.* 2009;43(2):163–172 (in Russ.). https://www.elibrary.ru/jxouyj]
9. Reid R.C., Prausnitz G.M., Sherwood T.K. *Svoistva gazov i zhidkostei* (*The Properties of Gases and Liquids*): transl. from Engl. Leningrad: Khimiya; 1982, 592 p. (In Russ.).
[Reid R.C., Prausnitz G.M., Sherwood T.K. *The Properties of Gases and Liquids.* New York: MCGraw-Hill; 1977, 710 p.]
10. Zobnina A.N., Morozova T.A. *Raschet khimischeskogo ravnovesia* (*Calculation of Chemical Equilibrium*): Guidelines. Moscow: MITHT Publ.; 2003, 25 p. (In Russ.).
11. Levanda O.G., Evstigneeva E.M., Flid V.R. *Khimicheskaya kinetika* (*Chemical Kinetics*): Textbook. Moscow: MITHT Publ.; 2009, 52 p. (In Russ.).
12. Zakgeim A.Yu. *Obshchaya khimicheskaya tekhnologiya. Vvedenie v modelirovanie khimiko-tekhnologicheski protsessov* (*General Chemical Technology. Introduction to Modeling of Chemical-Engineering Processes*): Tutorial. Moscow: Logos; 2009, 304 p. (In Russ.).

СПИСОК ЛИТЕРАТУРЫ

1. Тимофеев В.С., Серафимов Л.А. *Принципы технологии основного органического и нефтехимического синтеза:* учебное пособие для вузов. М.: Высшая школа; 1992, 536 с.
2. Нагиев М.Ф. *Теория рециркуляции и повышение оптимальности химико-технологических процессов.* М.: Наука; 1970, 390 с.
3. Алиев А.М., Сафаров А.Р., Османова И.И., Гусейнова А.М., Мамедов З.А., Исмайлов О.А. Интенсификация процесса пиролиза бензина с учетом рециркуляции. *Азербайджанский химический журнал.* 2017;1:20–27. https://elibrary.ru/vpecho
4. Солохин А.В., Благов С.А., Тимофеев В.С. Влияние рецикла на производительность реактора. *Теор. основы хим. технологии.* 1995;29(5):528–534. https://www.elibrary.ru/ktdvsn
5. Солохин А.В., Назанский С.Л., Миляева Т.В. Использование рециркуляции для увеличения селективности сложных химических реакций. *Теор. основы хим. технологии.* 2011;45(3):284–288. https://www.elibrary.ru/ntvznn
6. Пономарев В.Н., Саксонова О.И., Тимофеев В.С. Полистационарность в процессах непрерывной ректификации. *Теор. основы хим. технологии*. 1996;30(4):383–389.
7. Дуев С.И., Бояринов А.И. Условия существования семейств стационарных состояний в рециркуляционной системе: реактор идеального смешения – блок разделения. *Теор. сновы хим. технологии.* 2000;34(1):50–56.
8. Солохин А.В., Назанский С.Л., Тимофеев В.С. Возможность использования режима бесконечной эффективности по разделению для анализа стационарных состояний рециркуляционных реакционно-ректификационных систем. *Теор. основы хим. технологии*. 2009;43(2): 163–172. https://www.elibrary.ru/jxouyj
9. Рид Р., Праусниц Дж., Шервуд Т. *Свойства газов и жидкостей:* пер. с англ. Химия; 1982, 592 с.
10. Зобнина А.Н., Морозова Т.А. *Расчет химического равновесия:* методические указания. М.: ИПЦ МИТХТ; 2003, 25 с.
11. Леванда О.Г., Евстигнеева Е.М., Флид В.Р. *Химическая кинетика:* учебно-методическое пособие. М.: МИТХТ; 2009, 52 с.
12. Закгейм А.Ю. *Общая химическая технология. Введение в моделирование химико-технологически процессов:* учебное пособие. М.: Логос; 2009, 304 с.
13. Павлов К.Ф., Романков П.Г., Носков А.А. *Примеры и задачи по курсу процессов и аппаратов химической технологии*. Л.: Химия; 1981, 560 с.
14. Арис Р. *Анализ процессов в химических реакторах:* пер. с англ. Л.: Химия; 1967, 328 с.
15. Вольтер Б.В., Сальников И.Е. *Устойчивость режимов работы химических реакторов.* М.: Химия; 1981, 198 с.

13. Pavlov K.F., Romankov P.G., Noskov A.A. *Primery i zadachi po kursu protsessov i apparatov khimicheskoi tekhnologii* (*Examples and Tasks for the Course on Processes and Apparatus of Chemical Technology*). Leningrad: Khimiya; 1981, 560 p. (In Russ.).
14. Aris R. *Analiz protsessov v khimicheskikh reaktorakh* (*Analysis of Processes in Chemical Reactors*): transl. from Engl. Leningrad: Khimiya; 1967, 328 p. (In Russ.).
[Aris R. *Introduction to the Analysis of Chemical Reactors.* Prentice-Hall; 1965, 337 p.]
15. Vol'ter B.V., Sal'nikov I.E. *Ustoichivost' rezhimov raboty khimicheskikh reaktorov* (*Stability of Operating Modes of Chemical Reactors*). Moscow: Khimiya; 1981, 198 p. (In Russ.).

About the Authors

Natalia A. Korol'kova, Postgraduate Student, Department of Chemistry and Technology of Basic Organic Synthesis, M.V. Lomonosov Institute of Fine Chemical Technologies, MIREA – Russian Technological University (78, Vernadskogo pr., Moscow, 119454, Russia). E-mail: korolkova@mirea.ru

Sergei L. Nazanskii, Dr. Sci. (Eng.), Professor, Department of Chemistry and Technology of Basic Organic Synthesis, M.V. Lomonosov Institute of Fine Chemical Technologies, MIREA – Russian Technological University (78, Vernadskogo pr., Moscow, 119454, Russia). E-mail: nazanski@yandex.ru. Scopus Author ID 6506699314, https://orcid.org/0000-0002-6612-4343

Michael A. Solokhin, Cand. Sci. (Eng.), Associate Professor, Department of Chemistry and Technology of Basic Organic Synthesis, M.V. Lomonosov Institute of Fine Chemical Technologies, MIREA – Russian Technological University (78, Vernadskogo pr., Moscow, 119454, Russia). E-mail: i@solohin.ru.

Об авторах

Королькова Наталья Анатольевна, аспирант, кафедра химии и технологии основного органического синтеза, Институт тонких химических технологий им. М.В. Ломоносова, ФГБОУ ВО «МИРЭА – Российский технологический университет» (119454, Россия, Москва, пр-т Вернадского, д. 78). E-mail: korolkova@mirea.ru.

Назанский Сергей Леонидович, д.т.н., профессор, кафедра химии и технологии основного органического синтеза, Институт тонких химических технологий им. М.В. Ломоносова, ФГБОУ ВО «МИРЭА – Российский технологический университет» (119454, Россия, Москва, пр-т Вернадского, д. 78). E-mail: nazanski@yandex.ru. Scopus Author ID 6506699314, https://orcid.org/0000-0002-6612-4343

Солохин Михаил Аркадьевич, к.т.н., доцент, кафедра информационных систем в химической технологии, Институт тонких химических технологий им. М.В. Ломоносова, ФГБОУ ВО «МИРЭА – Российский технологический университет» (119454, Россия, Москва, пр-т Вернадского, д. 78). E-mail: i@solohin.ru.

Translated from Russian into English by H. Moshkov
Edited for English language and spelling by Thomas A. Beavitt

Tonkie Khimicheskie Tekhnologii = Fine Chemical Technologies.
2026;21(2):157–164 ISSN 2686-7575 (Online)

UDC 665.6
https://doi.org/10.32362/2410-6593-2026-21-2-157-164
EDN ZMHSIV

RESEARCH ARTICLE

Changes in the hydrocarbon composition of petroleum products under the influence of cavitation

Alexandr I. Nikolaev, Boris V. Peshnev, Alexandr N. Korolev✉, Denis V. Nikishin

MIREA – Russian Technological University (M.V. Lomonosov Institute of Fine Chemical Technologies), Moscow, 119454 Russia

✉ *Corresponding author, e-mail: waterpolist2000@yandex.ru*

Abstract

Objectives. While the phenomenon of cavitation is of interest for treatment of hydrocarbon mixtures, in particular crude oil and petroleum products, the literature lacks a systematic approach to conducting such research. This gap stimulates the need for a more in-depth study of the influence of this physical effect on the characteristics and detailed hydrocarbon composition of petroleum feedstock. Thus, the present work set out to explore the influence of the conditions leading to cavitation on the physicochemical properties and hydrocarbon composition of crude oil and petroleum products.

Methods. The objects of the study were two crude oil samples and four straight-run fractions—gasoline, kerosene, diesel, and fuel oil—having different characteristics and hydrocarbon compositions. Cavitation treatment was carried out in a hydrodynamic mode using a Donor-2 apparatus within a range of pressure changes from 20 to 50 MPa. The number of treatment cycles was from 1 to 20. The density was determined by pycnometry using the refractive index, an Abbe refractometer, and the fractional composition or fraction yield, as well as by distillation at atmospheric or reduced pressure for light or dark petroleum products, respectively. The hydrocarbon composition of the gasoline fraction was determined by chromatography and mass spectrometry.

Results. Changes in the densities and fractional compositions of the objects of study following their treatment under various conditions were recorded. Particular attention was paid to the hydrocarbon composition of the gasoline fraction: an increase in the content of normal alkanes was shown to be due to an increase in the number of structures with shorter carbon chains in comparison with the components of raw materials not subjected to cavitation.

Conclusions. The results of the study of the effect of cavitation treatment of crude oil and its individual fractions on their physicochemical characteristics showed that the nature of the changes depends on the treatment conditions and the initial characteristics of the sample. It is suggested that cavitation treatment causes cracking and compaction processes. The possibility of cracking reactions was confirmed by chromatographic determination of the group hydrocarbon composition of the samples.

Keywords

crude oil, petroleum products, cavitation, hydrocarbon composition, classes of hydrocarbons

Submitted: 16.12.2024
Revised: 11.07.2025
Accepted: 13.02.2026

For citation

Nikolaev A.I., Peshnev B.V., Korolev A.N., Nikishin D.V. Changes in the hydrocarbon composition of petroleum products under the influence of cavitation. *Tonk. Khim. Tekhnol. = Fine Chem. Technol.* 2026;21(2):157–164. https://doi.org/10.32362/2410-6593-2026-21-2-157-164

НАУЧНАЯ СТАТЬЯ

Изменение углеводородного состава нефтепродуктов под воздействием кавитации

А.И. Николаев, Б.В. Пешнев, А.Н. Королев✉, Д.В. Никишин

МИРЭА – Российский технологический университет (Институт тонких химических технологий им. М.В. Ломоносова), Москва, 119454 Россия

✉ *Автор для переписки, e-mail: waterpolist2000@yandex.ru*

Аннотация

Цели. Интерес к применению явления кавитации для обработки углеводородных смесей, в частности нефти и нефтепродуктов, и отсутствие в литературе системного подхода к проведению подобных исследований открывает необходимость более глубокого изучения влияния этого физического воздействия на характеристики и детальный углеводородный состав нефтяного сырья. В связи с этим, цель данной работы заключается в изучении влияния условий, при которых возникает кавитация, на изменение физико-химических свойств и углеводородного состава нефти и нефтепродуктов.

Методы. В качестве объектов исследования были взяты два образца нефти и четыре прямогонные фракции — бензиновая, керосиновая, дизельная и мазут, обладающие различными характеристиками и углеводородным составом. Кавитационную обработку проводили в гидродинамическом режиме на аппарате Донор-2 в диапазоне перепадов давления от 20 до 50 МПа. Количество циклов обработки составляло от 1 до 20. Плотность определяли пикнометрическим методом, показатель преломления — на рефрактометре типа Аббе, а фракционный состав или выход фракций — перегонкой при атмосферном или пониженном давлении соответственно для светлых или темных нефтепродуктов. Углеводородный состав бензиновой фракции определяли хромато-масс-спектрометрическим методом.

Результаты. В работе показано изменение плотности и фракционного состава объектов исследования после их обработки при различных условиях. Уделено особое внимание углеводородному составу бензиновой фракции: показано увеличение содержания в ней нормальных алканов за счет увеличения количества структур, обладающих меньшей длиной углеродной цепи, по сравнению с компонентами сырья, не подвергнутого кавитационному воздействию.

Выводы. Представлены результаты исследования влияния кавитационной обработки нефти и ее отдельных фракций на изменение физико-химических характеристик объектов исследования. Установлено, что характер изменений зависит от условий обработки и исходных характеристик образца. Высказано предположение о том, что в результате кавитационного воздействия могут протекать процессы крекинга и уплотнения. Возможность протекания реакций крекинга подтверждена результатами хроматографии и определения группового углеводородного состава образцов.

Ключевые слова

нефть, нефтепродукты, кавитация, углеводородный состав, классы углеводородов

Поступила: 16.12.2024
Доработана: 11.07.2025
Принята в печать: 13.02.2026

Для цитирования

Николаев А.И., Пешнев Б.В., Королев А.Н., Никишин Д.В. Изменение углеводородного состава нефтепродуктов под воздействием кавитации. *Тонкие химические технологии*. 2026;21(2):157–164. https://doi.org/10.32362/2410-6593-2026-21-2-157-164

INTRODUCTION

The alternation of high- and low-pressure regions in a liquid medium leads to cavitation involving the formation and collapse of gas bubbles [1, 2]. The study of this phenomenon confirms its role not only as a destructive factor for ship propellers and hydroelectric turbine blades, but also as an efficient agent in processes taking place agriculture [3], medicine [4], the food industry [5], construction [6], and the oil industry [7–9].

In the oil production and refining industries, cavitation is used as a means of modifying the rheological properties of crude oil and its fractions to reduce the viscosity of petroleum disperse systems and consequent cost of transportation [10], as well as increasing the yield of light fractions [11] and improving the quality of hydrocarbon fuels [12]. The potential for using cavitation to intensify chemical engineering processes has also been noted [13]. However, despite the wide variety of publications on the use of cavitation in oil refining processes, they lack a systematic approach for relating the conditions leading to cavitation phenomena with the observed changes in feedstock characteristics, particularly in terms of their hydrocarbon composition.

The present study set out to explore the influence of the conditions for the occurrence of cavitation on

the characteristics and hydrocarbon compositions of petroleum and petroleum products.

EXPERIMENTAL

The objects of study were samples of heavy (O1) and light (O2) crude oils obtained from the Ilskoe field (Krasnodar krai, Russia); straight-run fractions of crude oil: gasoline (G), kerosene (K), and diesel (D); and fuel oil (F) (all of *Gazpromneft-MNPZ*, Russia). Table 1 presents some of their characteristics.

Cavitation treatment was performed in a Donor-2 apparatus (Russia) [14, 15]. In this apparatus, cavitation occurs in the hydrodynamic flow of a petroleum product through a diffuser under elevated pressure. The pressure in the discharge cylinder was varied from 20 to 50 MPa; the number of treatment cycles, from 1 to 20. The treatment temperature was determined by the viscosity of the samples. Samples G, K, and D were treated at 20°C; Samples O1 and O2, at 50°C; Sample F, at 70°C.

The density of the samples was measured pycnometrically in accordance with GOST R 50.2.075-2010[1].

The fractional composition of light petroleum products was characterized using an ARNP-1 apparatus (*NPP SKIF-PRIBOR*, Ukraine) in accordance with GOST 2177-99[2]. The yields of dark fractions of crude oil and fuel oil were determined by vacuum distillation at a residual pressure of ~2 mm Hg [16].

The hydrocarbon composition of the gasoline fraction was determined using an Agilent GC 7890 chromatograph (*Agilent Technologies*, USA) on an HP-5MS quartz capillary column (30 m × 0.25 mm × 0.25 μm) with a modified methyl silicone (5% phenylmethyl silicone) liquid stationary phase. The chromatograph was equipped with an MSD 5975C mass-selective detector (*Agilent Technologies*, USA) having a quadrupole mass analyzer. Mass spectra were obtained by electron impact ionization with an ionization energy of 70 eV and recorded in the mass range of 29–550 amu at an evaporator temperature of 320°C and a carrier gas (helium) flow rate of 1 mL/min.

RESULTS AND DISCUSSION

The most obvious changes in the characteristics of petroleum products under the influence of cavitation involve variations in the sample density (Fig. 1) and its fractional composition. For example, the initial boiling points of Samples O1, F, and G following five treatment cycles at a pressure of 50 MPa decreased by 30, 25, and 8°C, respectively. It was observed that,

Table 1. Characteristics of objects of study

Property	Object of study					
	O1*	O2	G	K	D	F
Density, g/cm^3	0.9693	0.8810	0.7112	0.7880	0.8333	0.9684
Refractive index	–	–	1.4345	1.4501	1.4709	–
Initial boiling point, °C	160	56	40	144	175	290
Distillation point, °C 10 vol % 50 vol % 90 vol %	–	–	 71 116 186	 162 192 218	 213 280 335	–
Yield of fractions, wt % Up to 160°C 160–230°C 230–350°C 350–400°C 400–480°C Above 480°C	 – 0.5 5.2 93.4 93.4 93.4	 11.9 19.2 19.5 49.4 49.4 49.4	–	–	–	 – – 4.9 9.3 27.9 57.9

* O1, heavy crude oil; O2, light crude oil; G, gasoline; K, kerosene; D, diesel; and F, fuel oil.

[1] GOST R 50.2.075-2010. State system for ensuring the uniformity of measurements. Crude petroleum and petroleum products. Laboratory methods for determination of density, relative density and API gravity. Moscow: Standartinform; 2011.

[2] GOST 2177-99. Interstate Standard. Petroleum products. Methods for determination of distillation characteristics. Moscow: Standartinform; 2006.

the higher the initial density of the petroleum product, the more noticeable were the changes occurring in its physicochemical characteristics (density, fractional composition, etc.).

The changes occurring in the parameters of a sample with changing treatment conditions were noted to be significantly affected by the nature of the sample. Increasing the pressure and the number of treatment cycles (up to 10) for Sample F led to a decrease in the initial boiling point and density and an increase in the yields of fractions whose initial boiling points were up to 400°C. Conversely, the yields of fractions boiling above 400°C decreased. For example, after one treatment cycle at a pressure of 20 MPa, the initial boiling point of Sample F decreased from 290 to 287°C, while the yield of fractions boiling up to 400°C increased from 14.4 to 14.8 wt %. Following 10 processing cycles, these parameters amounted to 273°C and 23.4 wt %, respectively. If the treatment was carried out at 50 MPa, then after 10 cycles, the initial boiling point decreased to 257°C, and the yield of fractions boiling up at 400°C increased to 29.2 wt %. No significant changes were observed with a further increase in the number of treatment cycles.

When treating light fractions (G, K, D), their initial boiling points also decreased with increasing pressure and number of treatment cycles. The dependence of the density of these samples on treatment pressure was similar to that for Sample F: increasing pressure led to a greater decrease in density. However, the dependence of the density of the light products on the number of treatment cycles differed significantly. Unlike Sample F, the density of the light petroleum products began to increase with repeated treatments (Fig. 2).

The number of treatment cycles after which an increase in density was detected depended on the nature of the sample (its initial density) and the treatment pressure. For example, at a treatment pressure of 30 MPa, the density of Samples G and K increased after 10 cycles. For Sample D, no significant change in density occurred following 10 treatment cycles at this pressure. After 10 treatment cycles, its density was 0.8293 g/cm^3, while after 20 cycles, the density was 0.8295 g/cm^3. However, when the treatment pressure for Sample D was increased to 40 MPa, an increase in its density was detected already after 10 treatment cycles (after 5 cycles, the density was 0.8298 g/cm^3; after 10 cycles, 0.8294 g/cm^3; and

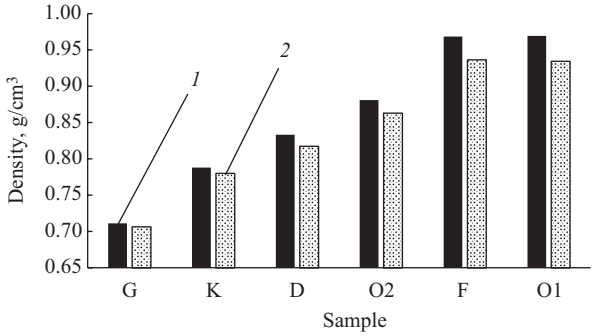

Fig. 1. Influence of cavitation treatment on the density of samples in five treatment cycles at 50 MPa: sample density (*1*) before and (*2*) after treatment

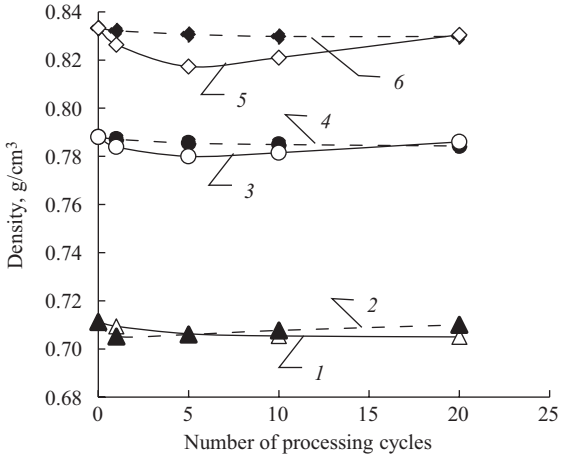

Fig. 2. Influence of conditions of cavitation treatment of light petroleum products on their density: Samples G (*1*, *2*), K (*3*, *4*), and D (*5*, *6*) at treatment pressures of 20 (*1*, *3*, *5*) and 50 MPa (*2*, *4*, *6*)

after 20 cycles, 0.8301 g/cm^3). At a treatment pressure of 50 MPa, an increase in the density of Sample D was noted after the fifth cycle.

Similar behavior with increasing number of treatment cycles was observed for the refractive indices of light petroleum products. For Samples G and K, increasing the number of treatment cycles to 10 (at a pressure of 30 MPa) resulted in a decrease in the refractive index to 1.4185 and 1.4408, respectively. After 20 treatment cycles, the refractive indices were 1.4205 and 1.4422, respectively. At a pressure of 50 MPa, the refractive index of Sample G after 5 processing cycles was 1.4205, and after 10 cycles, it increased to 1.4225.

Noteworthy is the effect of the number of treatment cycles on the fractional composition of light petroleum products and their distillation points. The initial boiling points of Samples G, K, and D decreased with both increasing pressure and increasing number of treatment cycles. When treating these samples at a pressure of 20 MPa, the 10, 20, …, and 95% distillation points of the samples also decreased with increasing number of cycles. If the treatment was carried out at higher pressures, then, after an initial decrease (after 1–5 cycles), subsequent treatment led to an increase in the 40%+ distillation point of the sample (Fig. 3).

For Sample D, an increase in distillation points was detected only at treatment pressures of 40 and 50 MPa; moreover, the higher the treatment pressure, the earlier this increase began. For example, if the treatment was carried out at 40 MPa, then, after 10 cycles, an increase in the distillation point was noted after distilling 60% of the sample. And if the treatment was performed at 50 MPa, then, after 10 cycles, the increase in the distillation point was observed after distilling 40% of the sample.

The effect of treatment conditions on the fractional composition of Samples G and K was similar. Moreover, an increase in the 40% distillation point was detected at a treatment pressure of 30 MPa.

The decreases in the densities, initial boiling points, and fractional compositions of the samples as a result of cavitation treatment can be explained by cracking reactions under the influence of heat released during the collapse of cavitation bubbles [17]. In the resulting lower-molecular-weight hydrocarbons, all of the above parameters are reduced. The interaction of long-lived radicals leads to the formation of products with a molecular weight higher than that of the feedstock. As manifested by an increase in the distillation points, this phenomenon is most noticeable after the treatment of light, low-boiling fractions. Although no such changes are observed following the treatment of dark petroleum products, an increase in density after cavitation treatment was noted for fractions boiling at temperatures above 480°C [14, 18].

Table 2 and Fig. 4 present data on the group hydrocarbon composition of Sample G and the number of carbon atoms in alkane molecules before and after treatment (5 cycles at a pressure of 50 MPa), confirming the occurrence of cracking reactions.

Table 2. Effect of treatment on the group hydrocarbon composition of Sample G after 5 treatment cycles at a pressure of 50 MPa

Hydrocarbons	Group hydrocarbon composition of Sample G, wt %	
	Before treatment	After treatment
Total alkanes	75.0	73.9
n-Alkanes	22.6	25.8
iso-Alkanes	20.0	18.0
Cycloalkanes	32.4	30.1
Arenes	22.5	22.6
Not identified	2.5	3.5

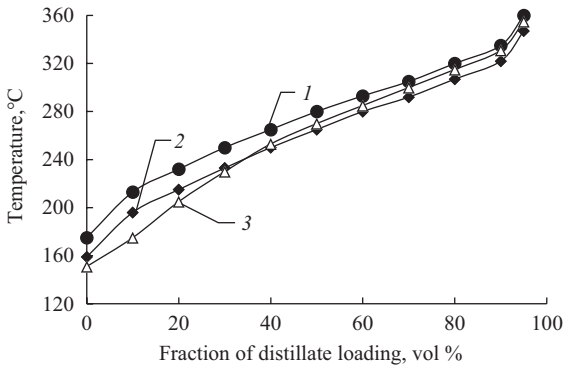

Fig. 3. Influence of the number of treatment cycles (pressure 50 MPa) on the fractional composition of Sample D: (*1*) initial sample and the sample after (*2*) 10 and (*3*) 20 treatment cycles at a pressure of 50 MPa

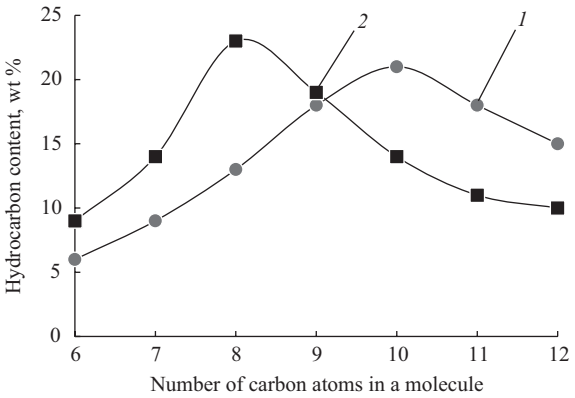

Fig. 4. Distributions of alkanes by number of carbon atoms in Sample G (*1*) before and (*2*) after treatment in 5 cycles at a pressure of 50 MPa

It is of particular significance that cavitation treatment was shown to alter the ratio of normal alkanes, isoalkanes, and naphthenes in the samples. While the fraction of *n*-alkanes increased, the contents of isoalkanes and naphthenes decreased. Following cavitation, the content of saturated hydrocarbons with 6–8 carbon atoms in a molecule increased, while the content of structures with 10–12 carbon atoms in a molecule decreased. No changes in the content of arenes were observed.

CONCLUSIONS

The results confirm the occurrence of cracking reactions during cavitation treatment of hydrocarbons. Depending on the treatment conditions and the initial characteristics of the sample, these reactions form products having lower and higher molecular weights than the feedstock. The results also suggest that arene hydrocarbons exhibit the greatest stability under cavitation conditions, while isoalkanes and naphthenes are more susceptible to degradation.

Authors' contributions

A.I. Nikolaev—development of the idea and concept of the study, formulation of the purpose and objectives of the study, identification of research objects, analysis of literary sources and obtained results, writing and editing the text of the article.

B.V. Peshnev—analysis of literary sources, writing and editing of the text of the article, development of methodology, analysis and presentation of the results obtained.

A.N. Korolev—conducting experiments, analysis and processing of the experimental data obtained, editing the text of the article.

D.V. Nikishin—consulting on methodology and research, providing equipment and consulting on the instrument base, editing the text of the article.

The authors declare no conflicts of interest.

REFERENCES

1. Birkhoff G., Zarantello E.H. *Strui, sledy i kaverny* (*Jets, Wakes and Cavities*): transl. from Engl. Moscow: Mir; 1964, 466 p. (In Russ.).
[Birkhoff G., Zarantello E.H. *Jets, Wakes and Cavities*. New York: Academic Press; 1957, 353 p.]
2. Knapp R., Daily J., Hammit F. *Kavitatsiya* (*Cavitation*): transl. from Engl. Moscow: Mir; 1974, 687 p. (In Russ.).
[Knapp R., Daily J., Hammit F. *Cavitation*. McGraw-Hill; 1970, 567 p.]
3. Shestakov S.D. *Osnovy tekhnologii kavitatsionnoi dezintegratsii. Teoriya kavitatsionnogo reaktora i ee prilozheniya v proizvodstve khleboproduktov* (*Fundamentals of Cavitation Disintegration Technology. Theory of the Cavitation Reactor and its Applications in Bakery Production*). Moscow: EVA-Press; 2011, 173 p. (In Russ.).
4. Promtov M.A. *Pul'satsionnye apparaty rotornogo tipa: teoriya i praktika* (*Pulsating rotary devices: Theory and practice*). Moscow. Mashinostroenie-1; 2001, 260 p. (In Russ.).
5. Dumitrash P.G., Bologa M.K., Kuchuk T.V. *et al.* Cavitation technologies for dispergation and homogenization. *Surf. Eng. Appl. Electrochem.* 2009;45(4):342–345. https://doi.org/10.3103/S1068375509040152
[Original Russian Text: Dumitrash P.G., Bologa M.K., Kuchuk T.V., Shemyakova T.D. Cavitation technologies for dispergation and homogenization. *Elektronnaya obrabotka materialov.* 2009;4(258):102–107 (in Russ.). https://elibrary.ru/qyxcrh]

СПИСОК ЛИТЕРАТУРЫ

1. Биркгоф Г., Сарантонелло Э. *Струи, следы и каверны:* пер. с англ. М.: Мир; 1964, 466 с.
2. Кнэпп Р., Дейли Дж., Хэммит Ф. *Кавитация:* пер. с англ. М.: Мир; 1974, 687 с.
3. Шестаков С.Д. *Основы технологии кавитационной дезинтеграции. Теория кавитационного реактора и ее приложения в производстве хлебопродуктов.* М.: ЕВА-пресс; 2001, 173 с.
4. Промтов М.А. *Пульсационные аппараты роторного типа: теория и практика*. М.: Машиностроение-1; 2001, 260 с.
5. Думитраш П.Г., Болога М.К., Кучук Т.В., Шемякова Т.Д. Кавитационные технологии при диспергировании и гомогенизации. *Электронная обработка материалов.* 2009;4(258):102–107. https://elibrary.ru/qyxcrh, https://doi.org/10.3103/S1068375509040152
6. Агранат Б.А. *Ультразвуковая технология.* М.: Металлургия; 1974, 504 с.
7. Хафизов Ф.Ш., Хафизов Н.Ф., Ванчухин Н.П. *Процессы нефтепереработки в кавитационно-вихревых аппаратах*. Уфа: Изд-во Фонда содействия развитию научных исследований; 1999, 110 с.
8. Промтов М.А. Изменение фракционного состава нефти при гидроимпульсной кавитационной обработке. *Вестник ТГТУ.* 2017;23(3):412–419. https://doi.org/10.17277/vestnik.2017.03.pp.412-419

6. Agranat B.A. *Ul'trazvukovaya tekhnologiya* (*Ultrasonic Technology*). Moscow: Metallurgiya; 1974, 504 p. (In Russ.).
7. Khafizov F.Sh., Khafizov N.F., Vanchukhin N.P. *Protsessy neftepererabotki v kavitatsionno-vikhrevykh apparatakh* (*Oil Refining Processes in Cavitation-Vortex Devices*). Ufa; 1999, 110 p. (In Russ.).
8. Promtov M.A. Change in fractional composition of oil in hydro-pulse cavitation processing. *Vestnik TGTU = Transactions TSTU.* 2017;23(3):412–419 (in Russ.). https://doi.org/10.17277/vestnik.2017.03.pp.412-419
9. Vorobyev S.I., Torhovsky V.N., Tutorskiy I.A., Kazmaly I.K. Mechaniodestruction of raw oil hydrocarbons by high-pressure disintegrator. *Vestnik MITHT.* 2008;3(3):77–84 (in Russ.).
10. Mullakaev M.S., Abramov V.O., Bayazitov V.M., Baranov D.A., Novotortsev V.M., Eremenko I.L. Studying of cavitation impact on heavy oil rheological characteristics. *Oborudovanie i tekhnologii dlya neftegazovogo kompleksa = Equipment and Technologies for Oil and Gas Complex.* 2011;5:24–27 (in Russ.). https://elibrary.ru/oimnnj
11. Galimov R.A., Mardanshin R.N., Kharlampidi Kh.E., Dakhnavi Kh.E. The influence of electromagnetic field on the selection of narrow fractions of light petroleum products. *Vestnik Kazanskogo tekhnologicheskogo universiteta = Herald of the Kazan Technological University*. 2010;5: 171–177 (in Russ.). https://elibrary.ru/motycd
12. Promtov M.A. Cavitation technology for quality improvement of hydrocarbon fuels. *Chem. Petrol. Eng*. 2008;44(1-2): 63–66. https://doi.org/10.1007/s10556-008-9014-x
[Original Russian Text: Promtov M.A. Cavitation technology for quality improvement of hydrocarbon fuels. *Khimicheskoe i neftegazovoe mashinostroenie.* 2008;2:6–8 (in Russ.). https://elibrary.ru/ilgqdp]
13. Ivanov S.V., Vorobyev S.I., Torhovsky V.N., Gerzeliev I.M. The application of hydrodynamic cavitation to increase the efficiency of the catalytic cracking of vacuum gas oil. *Vestnik MITHT.* 2013;8(3):67–69 (in Russ.). https://elibrary.ru/qgslud
14. Terenteva V.B., Peshnev B.V., Nikolaev A.I. Hydrodynamic activation of heavy oil residues. *Tonk. Khim. Tekhnol. = Fine Chem. Technol.* 2021;16(5):390–398. https://doi.org/10.32362/2410-6593-2021-16-5-390-398
15. Nikolaev A.I., Peshnev B.V., Alhamedi M.H.I. Cavitation treatment of watered oil products. *Izvestiya vysshikh uchebnykh zavedenii. Khimiya i khim. Tekhnologiya = ChemChemTech*. 2022;65(7):94–99. https://doi.org/10.6060/ivkkt.20226507.6611
16. Rybak B.M. *Analiz nefti i nefteproduktov* (*Analysis of Oil and Petroleum Products*). Moscow: Gostoptekhizdat; 1962, 888 p. (In Russ.).
17. Avvaru B., Venkateswaran N., Uppara P., Iyengar S.B., Katti S.S. Current knowledge and potential applications of cavitation technologies for the petroleum industry. *Ultrason. Sonochem*. 2018;42:493–507. https://doi.org/10.1016/j.ultsonch.2017.12.010
18. Peshnev B.V., Nikolaev A.I., Nikishin D.V., Alhamedi M.Kh.I. Prospects of using the cavitation phenomenon in oil refining. *Izvestiya vysshikh uchebnykh zavedenii. Khimiya i khim. Tekhnologiya = ChemChemTech*. 2023;66(4):110–116. https://doi.org/10.6060/ivkkt.20236604.6760
9. Воробьев С.И., Торховский В.Н., Туторский И.А., Казмалы И.К. Механодеструкция углеводородов нефти с помощью дезинтегратора высокого давления. *Вестник МИТХТ.* 2008;3(3):77–84.
10. Муллакаев М.С., Абрамов В.О., Баязитов В.М., Баранов Д.А., Новоторцев В.М., Еременко И.Л. Изучение воздействия кавитации на реологические свойства тяжелой нефти. *Оборудование и технологии для нефтегазового комплекса.* 2011;5:24–27. https://elibrary.ru/oimnnj
11. Галимов Р.А., Мардиншин Р.Н., Харлампиди Х.Э., Дахнави Х.Э. Влияние электромагнитного поля на отбор узких фракций светлых нефтепродуктов. *Вестник Казанского технологического университета.* 2010;5: 171–177. https://elibrary.ru/motycd
12. Промтов М.А. Кавитационная технология улучшения качества углеводородных топлив. *Химическое и нефтегазовое машиностроение*. 2008;2:6–8. https://elibrary.ru/ilgqdp
13. Иванов С.В., Воробьев С.И., Торховский В.Н., Герзелиев И.М. Применение гидродинамической кавитации для повышения эффективности каталитического крекинга вакуумного газойля. *Вестник МИТХТ.* 2013;8(3): 67–69. https://elibrary.ru/qgslud
14. Терентьева В.Б., Пешнев Б.В., Николаев А.И. Гидродинамическая активация тяжелых нефтяных остатков. *Тонкие химические технологии.* 2021;16(5):390–398. https://doi.org/10.32362/2410-6593-2021-16-5-390-398
15. Николаев А.И., Пешнев Б.В., Алхамеди М.Х.И. Кавитационная обработка обводненных нефтепродуктов. *Известия высших учебных заведений. Химия и хим. технология.* 2022;65(7): 94–99. https://doi.org/10.6060/ivkkt.20226507.6611
16. Рыбак Б.М. *Анализ нефти и нефтепродуктов*. М.: Гостоптехиздат; 1962, 888 с.
17. Avvaru B., Venkateswaran N., Uppara P., Iyengar S.B., Katti S.S. Current knowledge and potential applications of cavitation technologies for the petroleum industry. *Ultrason. Sonochem*. 2018;42:493–507. https://doi.org/10.1016/j.ultsonch.2017.12.010
18. Пешнев Б.В., Николаев А.И., Никишин Д.В., Алхамеди М.Х.И. Перспективы использования явления кавитации при переработке нефти. *Известия высших учебных заведений. Химия и хим. технология*. 2023;66(4): 110–116. https://doi.org/10.6060/ivkkt.20236604.6760

About the Authors

Alexander I. Nikolaev, Dr. Sci. (Eng.), Professor, Department of Chemistry and Technology of Basic Organic Synthesis, M.V. Lomonosov Institute of Fine Chemical Technologies, MIREA – Russian Technological University (78, Vernadskogo pr., Moscow, 119454, Russia). E-mail: nikolaev_a@mirea.ru. Scopus Author ID 57197582338, https://orcid.org/0000-0001-8594-2985

Boris V. Peshnev, Dr. Sci. (Eng.), Professor, Department of Chemistry and Technology of Basic Organic Synthesis, M.V. Lomonosov Institute of Fine Chemical Technologies, MIREA – Russian Technological University (78, Vernadskogo pr., Moscow, 119454, Russia). E-mail: peshnev@mirea.ru. Scopus Author ID 6507362823, https://orcid.org/0000-0002-0507-2754

Alexandr N. Korolev, Postgraduate Student, Department of Chemistry and Technology of Basic Organic Synthesis, M.V. Lomonosov Institute of Fine Chemical Technologies, MIREA – Russian Technological University (78, Vernadskogo pr., Moscow, 119454, Russia). E-mail: waterpolist2000@yandex.ru. https://orcid.org/0000-0003-2709-3342

Denis V. Nikishin, Assistant, Department of Chemistry and Technology of Basic Organic Synthesis, M.V. Lomonosov Institute of Fine Chemical Technologies, MIREA – Russian Technological University (78, Vernadskogo pr., Moscow, 119454, Russia). E-mail: nikishin@mirea.ru. RSCI SPIN-code 4089-6391, https://orcid.org/0000-0002-4466-4402

Об авторах

Николаев Александр Игоревич, д.т.н., профессор, кафедра химии и технологии основного органического синтеза, Институт тонких химических технологий им. М.В. Ломоносова, ФГБОУ ВО «МИРЭА – Российский технологический университет» (119454, Россия, Москва, пр-т Вернадского, д. 78). E-mail: nikolaev_a@mirea.ru. Scopus Author ID 57197582338, https://orcid.org/0000-0001-8594-2985

Пешнев Борис Владимирович, д.т.н., профессор, кафедра химии и технологии основного органического синтеза, Институт тонких химических технологий им. М.В. Ломоносова, ФГБОУ ВО «МИРЭА – Российский технологический университет» (119454, Россия, Москва, пр-т Вернадского, д. 78). E-mail: peshnev@mirea.ru. Scopus Author ID 6507362823, https://orcid.org/0000-0002-0507-2754

Королев Александр Николаевич, аспирант, кафедра химии и технологии основного органического синтеза, Институт тонких химических технологий им. М.В. Ломоносова, ФГБОУ ВО «МИРЭА – Российский технологический университет» (119454, Россия, Москва, пр-т Вернадского, д. 78). E-mail: waterpolist2000@yandex.ru. https://orcid.org/0000-0003-2709-3342

Никишин Денис Васильевич, ассистент, кафедра химии и технологии основного органического синтеза, Институт тонких химических технологий им. М.В. Ломоносова, ФГБОУ ВО «МИРЭА – Российский технологический университет» (119454, Россия, Москва, пр-т Вернадского, д. 78). E-mail: nikishin@mirea.ru. SPIN-код РИНЦ 4089-6391, https://orcid.org/0000-0002-4466-4402

Translated from Russian into English by V. Glyanchenko
Edited for English language and spelling by Thomas A. Beavitt

Tonkie Khimicheskie Tekhnologii = Fine Chemical Technologies.
2026;21(2):165–178
ISSN 2686-7575 (Online)

Chemistry and technology of medicinal compounds
and biologically active substances

Химия и технология лекарственных препаратов
и биологически активных соединений

UDC 577.1
https://doi.org/10.32362/2410-6593-2026-21-2-165-178
EDN SNRUWU

RESEARCH ARTICLE

Development, characterization, and stability assessment of a lyophilized Eculizumab formulation for use as a reference material

Dmitry I. Zybin[1,✉], Anatoly A. Klishin[1], Natalia V. Orlova[1], Tatiana S. Sorokina[1], Dmitry V. Kapustin[2]

[1] *PHARMAPARK, Moscow, 117246 Russia*

[2] *M.M. Shemyakin and Yu.A. Ovchinnikov Institute of Bioorganic Chemistry, Russian Academy of Sciences, Moscow, 117997 Russia*

✉ *Corresponding author, e-mail: mithtchem@gmail.com*

Abstract

Objectives. The study set out to develop a stable lyophilized formulation of the monoclonal antibody Eculizumab, comprehensively characterize the resulting material, and assess its stability for qualifying it as a reference material. This involved developing a matching placebo formulation, determining the optimal lyophilization conditions, and conducting a rigorous stability study.

Methods. In the development of the formulation and lyophilization conditions for Eculizumab, we tested various buffer systems and cryoprotectants. The residual moisture content in the resulting lyophilized samples was determined by Karl Fischer titration. Peptide mapping was performed using reversed-phase high-performance liquid chromatography (RP-HPLC) following enzymatic hydrolysis with trypsin. The structural, physicochemical, and biological properties were analyzed using various analytical methods, including RP-HPLC, high-performance liquid chromatography mass spectrometry, capillary sodium dodecyl sulfate electrophoresis, size-exclusion high-performance liquid chromatography, and enzyme-linked immunosorbent assay.

Results. A placebo solution for lyophilization of Eculizumab was selected with the following composition: 20 mM sodium phosphate, 4% trehalose, 0.2% polysorbate 80, pH 7.0. The results demonstrated a high degree of similarity between the candidate reference material and Eculizumab EU. Stability studies under storage conditions at 2–8°C demonstrated the material's stability for one year, with control points at 3, 6, 9, and 12 months.

Conclusions. The absence of any effect of the drying process on the primary and spatial structure, post-translational modifications, content of related impurities, composition of isoforms, and specific activity was confirmed. Furthermore, stability studies demonstrated no significant changes in protein quality during storage at 2–8°C for at least 12 months, which represents the entire available data period at the time of manuscript preparation. The results indicate that the developed lyophilized material is a viable candidate for an international reference material, although its official qualification would require additional collaborative trials and long-term stability data.

Keywords

reference material, lyophilization, monoclonal antibody, Eculizumab

Submitted: 02.09.2025
Revised: 18.11.2025
Accepted: 17.02.2026

For citation

Zybin D.I., Klishin A.A., Orlova N.V., Sorokina T.S., Kapustin D.V. Development, characterization, and stability assessment of a lyophilized Eculizumab formulation for use as a reference material. *Tonk. Khim. Tekhnol. = Fine Chem. Technol.* 2026;21(2):165–178. https://doi.org/10.32362/2410-6593-2026-21-2-165-178

НАУЧНАЯ СТАТЬЯ

Разработка, характеризация и оценка стабильности лиофилизированной формы экулизумаба для использования в качестве стандартного образца

Д.И. Зыбин[1],✉, А.А. Клишин[1], Н.В. Орлова[1], Т.С. Сорокина[1], Д.В. Капустин[2]

[1] *ООО ФАРМАПАРК, Москва, 117246 Россия*

[2] *Институт биоорганической химии им. академиков М.М. Шемякина и Ю.А. Овчинникова Российской академии наук, Москва, 117997 Россия*

✉ *Автор для переписки, e-mail: mithtchem@gmail.com*

Аннотация

Цели. Целью данного исследования была разработка стабильной лиофилизированной формы моноклонального антитела экулизумаб, характеризация полученного материала и оценка его стабильности для аттестации в качестве стандартного образца. Для достижения поставленных целей требовались разработка соответствующего состава плацебо, определение оптимальных условий лиофилизации и проведение исследования стабильности.

Методы. В ходе разработки состава плацебо и условий лиофилизации экулизумаба были протестированы различные буферные системы и криопротекторы. Содержание остаточной воды в лиофилизированных образцах определяли методом титрования по Карлу Фишеру. Пептидное картирование проводили методом обращенно-фазовой высокоэффективной жидкостной хроматографии (ВЭЖХ) после ферментативного гидролиза трипсином. Структурные, физико-химические и биологические свойства анализировали с использованием широкого ряда аналитических методов, включая обращенно-фазовую ВЭЖХ, жидкостную хромато-масс-спектрометрию, капиллярный гель-электрофорез, эксклюзионную ВЭЖХ и иммуноферментный анализ.

Результаты. Для лиофилизации экулизумаба был выбран буферный раствор следующего состава: 20 мМ фосфат натрия, 4% трегалозы, 0.2% полисорбата 80, pH 7.0. Полученные результаты продемонстрировали высокую степень сходства между кандидатом на стандартный образец и референсным образцом экулизумаба. Исследования стабильности при хранении при 2–8°C показали стабильность материала в течение одного года с контрольными точками через 3, 6, 9 и 12 месяцев.

Выводы. Подтверждено отсутствие влияния процесса лиофилизации на первичную и пространственную структуру, посттрансляционные модификации, содержание родственных примесей, состав изоформ и специфическую активность. Кроме того, исследования стабильности показали отсутствие значимых изменений качества белка при хранении при 2–8°C в течение по меньшей мере 12 месяцев, что соответствует всему доступному объему данных на момент подготовки рукописи. Полученные результаты свидетельствуют о том, что разработанный лиофилизированный материал является перспективным кандидатом на роль международного стандартного образца, однако его официальная аттестация потребует проведения дополнительных межлабораторных исследований и получения данных по долгосрочной стабильности.

Ключевые слова

стандартный образец, лиофилизация, моноклональное антитело, экулизумаб

Поступила: 02.09.2025
Доработана: 18.11.2025
Принята в печать: 17.02.2026

Для цитирования

Зыбин Д.И., Клишин А.А., Орлова Н.В., Сорокина Т.С., Капустин Д.В. Разработка, характеризация и оценка стабильности лиофилизированной формы экулизумаба для использования в качестве стандартного образца. *Тонкие химические технологии.* 2026;21(2):165–178. https://doi.org/10.32362/2410-6593-2026-21-2-165-178

1. INTRODUCTION

A biosimilar medicinal product is defined as a biological product that has no clinically significant differences in purity, safety or efficacy as compared to the reference medicinal product [1]. The scale of application of biosimilars is increasing every year. The increasing number of biosimilar monoclonal antibodies (mAbs)—both registered and mAbs—currently under development dictates the necessity for primary reference materials. The National Institute for Biological Standards and Control (NIBSC) is the official laboratory in the United Kingdom approved by the World Health Organization (WHO) for performing the control of biological medicines. This institute is the world's largest manufacturer and distributor of international reference materials (supplying more than 95% of WHO standards worldwide). However, due to the current lack

of an international reference material of Eculizumab, we publish for the first time in this paper the conditions of lyophilization technology, the results of the stability study, as well as the methods for validation of the authenticity of the reference material of the Eculizumab monoclonal antibody. Both the aim and the number of the studies involving the use of reference samples (RSs) depend on the type of the sample and the purposes of its use. RSs can be categorized as primary or secondary depending on the certification procedure. In addition, there are RSs of the following categories: international, interstate (regional), state, pharmacopeial, industry RSs, as well as enterprise RSs[1]. Each RS is limited to a specific area of application and cannot be used for other purposes.

Eculizumab is a recombinant humanized IgG2/4k monoclonal antibody in which the CH1 and hinge regions are related to IgG2, while the CH2 and CH3 regions are related to IgG4, and the complementarity determining regions (CDRs) are murine [2]. Having an approximate mass (including glycosylation) of about 148 kDa, Eculizumab contains two light chains of 214 amino acid residues and two heavy chains of 448 amino acid residues with a conservative *N*-glycosylation site at the Asn297 position in both heavy chains. Eculizumab, which inhibits the terminal lytic pathway of complement by blocking of the enzymatic cleavage of complement factor 5 [3–5], is used to treat patients with paroxysmal nocturnal hemoglobinuria (PNH) [6–8], atypical hemolytic uremic syndrome (aHUS) [9–14], refractory generalized myasthenia gravis (gMG) in patients aged 6 years and above [15–17], and neuromyelitis optical spectrum disorder (NMOSD) [18–21]. The wide range of biosimilar drugs of Eculizumab approved for the use in Europe and Russia includes: EPYSQLI™ (*Samsung Bioepis*, South Korea) and Bekemv® (*Amgen*, USA), which was approved in Europe by the European Commission in 2023; Elizaria® (licensed by *GENERIUM* in the Russian Federation in 2019 and in Turkey in 2022); Eculizumab (licensed by *PHARMAPARK* in the Russian Federation in 2024).

Both the Soliris® (the original product developed by *Alexion Pharmaceuticals*, USA) and the various biosimilar products are supplied as the concentrates for solution for infusion. Although liquid forms of Eculizumab demonstrate high stability during the storage at 2–8°C for at least 2.5 years, they have a number of limitations that make them less suitable for the use as international reference materials. The use of liquid forms in international practice is significantly limited by their sensitivity to temperature fluctuations and the requirement of strict cold chain conditions at all stages of transportation and storage. Here, it can be noted that the instructions for medical use of all Eculizumab preparations explicitly prohibit state freezing, which may indicate potential instability of the molecule as a result of freezing and thawing (e.g., aggregation or denaturation). This is a particular problem in the course of developing reference materials due to the requirement of optimal resilience to external influences and consequent suitability for long-term storage. Typically, WHO international standards produced by NIBSC are supplied as lyophilized material in hermetically sealed glass ampoules under nitrogen. The absence of a lyophilized form of the Eculizumab protein to date is likely due to the sensitivity of the molecule to freezing and drying stress. However, our data demonstrate that optimal formulation and correct selection of the process parameters provide effective lyophilization of Eculizumab without loss of structural integrity and biological activity. Thus, the present study describes for the first time the production of a lyophilized form of the Eculizumab monoclonal antibody. In addition, an assessment of the stability of the obtained material for 12 months at a temperature of 2–8°C and 2 months at 25°C was carried out along with a study of its structural, physicochemical, and biological properties.

2. METHODS

2.1. Preparation of the formulation

Two of the most widely used buffer solutions [22] were tested, namely 20 mM phosphate buffer solution, pH 6.0 and 30 mM histidine buffer solution, pH 7.0 in combination with different cryoprotectants, such as sucrose, trehalose, and mannose. After concentrating the samples of Eculizumab (*PHARMAPARK,* Russia) (to a concentration of 12 mg/mL) using the concentrator Vivaspin 20 with polyethersulfone membrane (MWCO[2] 30000 Da; *Sartorius*, Germany), the buffer solution was exchanged using Slider-A-Lyzer dialysis cassettes (MWCO 10000 Da; *Thermo Scientific*, USA) for 24 h. The concentration after the dialysis was measured using UV5 Nano ultraviolet (UV) spectrophotometer (*Mettler Toledo*, Switzerland) at 280 nm. The content of Eculizumab in the samples was normalized to 10 mg/mL and 1 mL of the solution was transferred into 2R vials (*SCHOTT Pharma AG & Co. KGaA*, Germany) for lyophilization.

[1] World Health Organization. WHO good practices for pharmaceutical reference standards. Annex 3, WHO Technical Report Series, No. 943. Geneva: World Health Organization. 2007.

[2] Molecular weight cut-off.

2.2. Freeze-drying process

The samples were placed into a metal rack and pre-frozen for 4 h at the temperature of −30°C. Then they were transferred to a shelf of a laboratory-scale freeze-dryer Christ Beta 1-8K (*Martin Christ*, Germany) at a pre-equilibrated shelf temperature of −30°C. Primary drying was performed at the pressure of 0.10 mbar and a shelf temperature of −30°C for 20 h. Secondary drying was carried out at the pressure of 0.05 mbar with a gradual increase of the shelf temperature from −30 to 0°C for 3 h and from 0 to 25°C for 3 h. Desorption was carried out at the temperature of 25°C at the pressure of 0.05 mbar for 4 h.

2.3. Estimation of residual moisture content

The residual water content was estimated using V20 volumetric titrator (*Mettler Toledo*, Switzerland) using the Karl Fischer method according to the manufacturer's recommendations. The results were calculated as relative water content (w/w).

2.4. Peptide mapping by reversed-phase high-performance liquid chromatography (RP-HPLC)

The test samples were denatured with 6 M guanidine hydrochloride and reduced with dithiothreitol followed by alkylation with iodoacetic acid. Excesses of reagents were removed and samples were re-buffered into ammonium bicarbonate using Vivaspin 500 microcentrifuge concentrators retaining the particles with a MWCO 10000 Da (*Sartorius*, Germany). Trypsin proteolysis was carried out at 37°C for 16 h. Analysis of the hydrolysates was performed using Aeris WIDEPORE XB-C18 chromatography column (250 × 4.6 mm, 3.6 μm, purchased from *Phenomenex*, USA) with Vanquish Flex system (*Thermo Fisher Scientific*, USA). The flow rate was 0.5 mL/min, mobile phase A: HPLC-grade water containing 0.1% formic acid, mobile phase B: acetonitrile containing 0.1% formic acid. Separation was performed in a gradient mode (*t*, min / content of mobile phase A, %): 0/100, 4/100, 60/64, 62/50, 65/0, 66/100. Detection was performed at wavelength of 214 nm.

2.5. Mass spectrometric studies

A Bruker Q-TOF Maxis Impact mass spectrometric detector (*Bruker Corporation*, USA) with electrospray ionization and qTOF Control data management and processing software was used to study the protein structure. To remove *N*-linked glycans, 1 μL of PNGase F solution (*NEB*, USA) was added to 100 μL of 0.5 mg/mL sample and incubated at 37°C for 4 h. The end groups of cysteine were protected by addition of 4 μL of 500 mM iodoacetamide solution to 100 μL of 0.5 mg/mL sample followed by incubation in the dark for 30 min at 25°C. For heavy and light chain analysis, disulfide bonds were reduced by addition of 5 μL of 100 mM dithiothreitol to 100 μL of 0.5 mg/mL sample, followed by incubation for 30 min at 56°C. In order to analyze the full-length protein and the protein following removal of *N*-linked glycans, heavy and light chains, the samples were diluted with 0.1% formic acid to a concentration of 0.1 mg/mL. High-performance liquid chromatography mass spectrometry (HPLC-MS) was performed using an Elute liquid chromatograph (*Bruker Corporation*, USA) on a BIOshell 400A Protein C4 UHPLC[3] chromatographic column (100 × 2.1 mm) at a column temperature of 80°C. The following parameters were applied: mobile phase A: 0.1% formic acid in water, mobile phase B: acetonitrile, mobile phase flow rate: 0.3 mL/mL. Separation was performed in a gradient mode (*t*, min / content of mobile phase A, %): 0/80, 1/80, 2/50, 3/10, 4/80, 7/80. Mass spectrometric detector settings for full-length protein analysis were: desiccant gas flow rate, 8 L/min; gas pressure in the nebulizer, 26.1 psi; conductive capillary temperature, 220°C; capillary voltage, 4500 V. Detection in full ion current scanning mode with ion registration was carried out in the *m*/*z* range from 400 to 5000 21amu with positive ionization.

In order to determine the position of disulfide bonds, enzymatic hydrolysis in the presence of trypsin was performed using the SMART Digest Trypsin Kit (*Thermo Scientific*, USA). Separation of peptide fragments was performed on a Chromolith® Performance RP-18 end-capped chromatographic column (100 × 2.0 mm). The column temperature was 40°C. Mobile phase A: 0.1% formic acid in water, mobile phase B: acetonitrile, mobile phase flow rate 0.3 mL/mL. Separation was performed in a gradient mode (*t*, min / content of mobile phase A, %): 0/95, 1/95, 24/30, 25/10, 27/10, 28/95. Settings for peptide analysis were as follows: desiccant gas flow, 6 L/min; gas pressure in the nebulizer, 29.0 psi; temperature of the conducting capillary, 220°C; voltage on the capillary, 4500 V. Detection in AutoMS mode with registration of precursor ions and fragment ions was carried out in the *m*/*z* range from 150 to 2200 amu with positive ionization.

[3] Ultra-high-performance liquid chromatography.

2.6. Size-exclusion high-performance liquid chromatography (SEC-HPLC)

The analysis was performed using TSKgel G3000SWxl at 300 × 7.8 mm with a 5 µm chromatography column (*Tosoh*, Japan) with the Vanquish Flex system (*Thermo Fisher Scientific*, USA) in isocratic mode. The flow rate was 0.5 mL/min, mobile phase: 20 mM solution of sodium hydrogen phosphate, 150 mM solution of sodium chloride, pH 7.0. Elution time was 35 min. Detection was performed at wavelength of 214 nm.

2.7. Capillary electrophoresis sodium dodecyl sulfate (CE-SDS) in non-reduced form

CE-SDS in non-reduced form was performed using PA 800 Plus Pharmaceutical Analysis System (*SCIEX*, USA). Bare-fused silica capillaries, SDS-MW gel buffer, acidic and basic wash solutions, Tris/SDS sample buffer (pH 9.0) were purchased from *SCIEX* (USA). Separation was performed using a capillary with a total length of 30 cm (effective length 10 cm). Samples were injected from the short end of the capillary for 20 s at 5 kV (normal polarity). Separation was performed at 15 kV (normal polarity) for 25 min. Detection was performed using a UV detector at 214 nm. The capillary temperature was 25°C.

2.8. Capillary isoelectric focusing (cIEF)

cIEF was performed using PA 800 Plus Pharmaceutical Analysis System (*SCIEX*, USA). Pharmalyte 5–8 carrier ampholytes were purchased from *Cytiva* (USA); neutral capillary, pI marker set and ready-made gel for cIEF were obtained from *SCIEX* (USA). Phosphoric acid, sodium hydroxide, iminodiacetic acid, acetic acid, L-arginine, and urea for electrophoresis were purchased from *Sigma-Aldrich* (USA). Separation was performed using the capillary with a total length of 30 cm (effective length 20 cm). 200 mM phosphoric acid solution was used as anolyte, 300 mM sodium hydroxide solution was used as catholyte, 350 mM acetic acid solution was used as chemical mobilizer. The sample focusing stage was carried out at 25 kV for 13 min, while chemical mobilization was carried out at 30 kV for 25 min. Detection was performed using UV detector at 280 nm. The capillary temperature was 20°C.

2.9. Cation-exchange high-performance liquid chromatography (CEX-HPLC)

Analysis of Eculizumab charged forms distribution was performed using a YMC BioPro SP-F chromatography column (100 × 4.6 mm, 5 µm, purchased from *YMC*, Japan) with the Vanquish Flex system (*Thermo Fisher Scientific*, USA). At a flow rate of 0.5 mL/min, the following parameters were applied; mobile phase A: 20 mM MES, 0.02% isopropanol, pH 5.7; mobile phase B: 20 mM solution of sodium hydrogen phosphate, 100 mM solution of sodium tetraborate decahydrate, 0.05% isopropanol, pH 9.0. Separation was performed in a gradient mode (*t*, min / content of mobile phase A, %): 0/100, 5/85, 35/50, 40/50, 41/0, 43/0, 50/100. Detection was performed at wavelength of 280 nm.

2.10. C5-binding specific activity by ELISA (C5-ELISA)

In order to analyze the specific activity of Eculizumab, an enzyme-linked immunosorbent assay (ELISA) was used. Eculizumab specifically forms a complex of C5-Eculizumab, for the detection of which secondary antibodies to the Fc fragment of human IgG4 are subsequently introduced. Detection of the formed complex C5-Eculizumab–IgG4 HRP was performed by introducing a ready-made solution of 3,3',5,5'-tetramethylbenzidine containing hydrogen peroxide (*Sigma-Aldrich*, USA). The reaction was stopped with 0.5 M sulfuric acid. Data were read using an Infiniti M200 Pro plate spectrophotometer (*Tecan Austria GmbH*, Austria) at a main wavelength of 450 nm and a reference wavelength of 650 nm. The dependence of Eculizumab concentration on the obtained optical density was approximated using a 4-parameter logistic curve in GraphPad Prism 6.0 software (*GraphPad Software*, *Inc*., San Diego, CA, USA). A detailed description of the method was previously published along with the validation results in [23].

3. RESULTS AND DISCUSSION

Lyophilization is widely used to increase the stability and shelf life of biopharmaceutical products. In the freeze-drying process, a protein solution is successively subjected to freezing, primary drying (mainly to remove ice by sublimation) and secondary drying (to remove the retained water) [24, 25]. It is evident that protein molecules undergo significant environmental effects during both the freezing and the drying processes. Typically, even minor changes in the compositional characteristics of a drug solution, such as pH, buffer capacity, and drug or excipient concentration, lead to striking differences in the behavior of molecules during the freezing and freeze-drying.

The main object of the study was Eculizumab, a recombinant humanized monoclonal antibody of IgG2/4k subclass that specifically binds the

Table 1. Characteristics of the studied formulations

Abbreviations	PhT	PhS	HisT	HisS	PhSN	PhSM
Buffer solution	20 mM NaPh	20 mM NaPh	30 mM His	30 mM His	20 mM NaPh	20 mM NaPh
Trehalose	+	–	+	–	–	–
Sucrose	–	+	–	+	+	+
Mannose	–	–	–	–	–	+
NaCl, 0.9% w/v	–	–	–	–	+	–
Polysorbate 80, % w/v	0.2					
pH	7.0					
Eculizumab, mg	10.0					

Note: PhT—phosphate buffer with trehalose; PhS—phosphate buffer with sucrose; HisT—histidine buffer with trehalose; HisS—histidine buffer with sucrose; PhSN—phosphate buffer with sucrose and NaCl; NaPh—phosphate buffer; PhSM—phosphate buffer with a mixture of sucrose and mannose; His—histidine.

protein C5 of the complement to inhibit its cleavage. The initial preparation of Eculizumab produced by *PHARMAPARK* (Russia) as part of the development of a biosimilar drug (hereinafter referred to as Eculizumab Lyo) was subsequently lyophilized. The stock solution (bulk drug substance) at a concentration of 12 mg/mL and pH 7.0 contained 20 mM sodium phosphate and 0.2% (w/v) polysorbate 80. Prior to lyophilization, the sample was dialyzed to change the buffer solution and brought to a concentration of 10 mg/mL. The resulting solution was poured into 2R vials and lyophilized. All physicochemical and biological studies within the framework of the work were carried out using the samples obtained from the same batch. This sample is not certified as an RS, but is considered in this study as a preparation potentially suitable for the use as a national or international RS after passing of the appropriate qualification procedures.

The preparation was supplied as a concentrate for obtaining an infusion solution (300 mg/30 mL) and stored according to the manufacturer's instructions. It is should be noted that, unlike classical studies on the biosimilarity of drugs, for example [26], the main emphasis was placed in this study on the development of a lyophilized form of Eculizumab for possible use as a national or international standard sample.

To assess the structural and physicochemical comparability, the original drug Soliris® (Eculizumab, *Alexion Pharmaceuticals*, approved for use in the European Union (EU), hereinafter referred to as Eculizumab EU) was used. The substance was supplied as a concentrate for the preparation of an infusion solution (300 mg/30 mL) and stored in accordance with the manufacturer's instructions.

3.1. Determination of the optimal composition of the formulation buffer solution

In order to select the composition of the formulation buffer solution for lyophilization, we applied two widely used buffer systems based on phosphate and histidine. Selection of the appropriate composition was carried out at pH value of 7.0. This value was chosen taking into account our previous study of the stability of Eculizumab protein under various stress conditions [26], as well as the results of a study of the long-term stability of the protein in solution carried out as part of the development of the drug Eculizumab (licensed by *PHARMAPARK* in the Russian Federation in 2024). Trehalose and sucrose or mixture of sucrose and mannose were used as cryoprotectants. Mannose was included in one of the formulations during the screening phase due to its use for stabilizing of glycoproteins as it was described earlier [27–29]. Furthermore, an effect of sodium chloride adding to the formulation buffer solution was studied. As reported in [27], the addition of sodium chloride ensured a decrease in the residual water content and the formation of an optimal cake shape. The formulations shown in Table 1 were considered in the primary screening stage, whose purpose was to quickly identify the acceptable options in terms of moisture content and physical characteristics.

In the first experiment, combinations of phosphate (Ph) and histidine (His) buffer solutions with trehalose (T), sucrose (S), and a mixture of sucrose and mannose (SM) without the addition of sodium chloride were compared. Cryoprotectant/protein ratio was 5 : 1 in all cases. With the exception of the formulation with the addition of sucrose

Table 2. Compositions of the studied variants of the formulation buffer solution in the experiment with variation of the cryoprotectant content

Abbreviations	T2	T3	T4	S2	S3	S4	T4N	S4N
Buffer solution	20 mM NaPh							
Trehalose, % w/v	2	3	4	–	–	–	4	–
Sucrose, % w/v	–	–	–	2	3	4	–	4
NaCl, 0.9% w/v	–	–	–	–	–	–	+	+
Polysorbate 80, % w/v	0.2							
pH	7.0							
Eculizumab, mg	10.0							

Note: T2—phosphate buffer with 2% trehalose; T3—phosphate buffer with 3% trehalose; T4—phosphate buffer with 4% trehalose; S2—phosphate buffer with 2% sucrose; S3—phosphate buffer with 3% sucrose; S4—phosphate buffer with 4% sucrose; T4N—phosphate buffer with 4% trehalose and NaCl; S4N—phosphate buffer with 4% sucrose and NaCl.

and mannose (PhSM), where the value was 3.7%, the residual water content in the samples after freeze-drying varied from 1 to 3%. Due to the high residual water content, this formulation was excluded from the further studies. Changes in the protein activity and increase in the number of aggregates were not detected in all of the studied formulations. According to WHO recommendations[4], satisfactory long-term stability is demonstrated by the preparations with a residual water content of less than 1% w/v, although higher values are acceptable in some cases. In a number of studies, the authors predictably pointed out the detrimental influence of low moisture content (less than 1% residual water) on the protein stability [28].

The next experiment was carried out to optimize the cryoprotectant/protein ratio and to evaluate the effect of addition of sodium chloride to the formulation. The content of cryoprotectant was varied only in the phosphate buffer solution. The use of this buffer solution was determined by the absence of significant differences between the used buffer systems in the first experiment, the relatively low cost, as well as the obtained data relating to the stability of Eculizumab during the development of the Eculizumab drug (licensed by *PHARMAPARK* in the Russian Federation in 2024). The compositions of the studied variants of the formulation buffer solution in the experiment with variation of the cryoprotectant content are given in Table 2.

The obtained (with varying cryoprotectant content) lyophilizates were evaluated for cake appearance, residual water content, pH shift, and changes in the protein purity and activity (using SEC-HPLC and C5-ELISA).

The samples containing sucrose demonstrated higher levels of residual water (2.0–2.7%) in comparison with the trehalose-containing formulation (1.0–1.5%). The addition of 0.9% w/v sodium chloride resulted in a number of cake defects as compared to other formulations. No pH shift or changes in the protein purity or activity were detected.

A scaled-up series of the samples of Eculizumab Lyo was prepared using the formulation buffer containing 20 mM sodium phosphate, 4% trehalose, 0.2% polysorbate 80, pH 7.0 (Fig. 1).

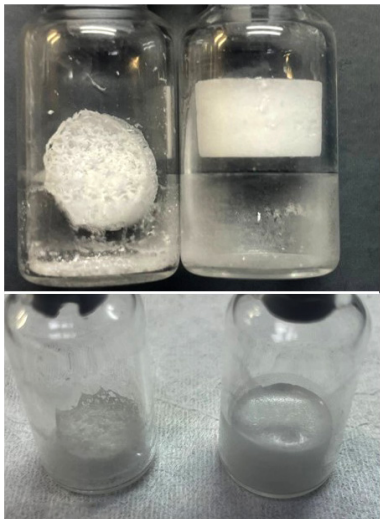

(a) (b)

Fig. 1. An appearance of the cakes after drying of the samples. (a) 4% trehalose with NaCl; (b) 4% trehalose without NaCl

[4] World Health Organization, Recommendations for the preparation, characterization and establishment of international and other biological reference standards (Revised 2004), WHO Tech. Rep. Ser., no. 932, Geneva: WHO, 2006.

The scaling up process presupposed use of the maximal number of available vials in the laboratory's equipment. Thus, to evaluate the stability and impact of the lyophilization process on the physicochemical and biological properties of Eculizumab, more than 400 vials filled with the same bulk solution were prepared. Analysis of the resulting samples confirmed the absence of pH shift, as well as the retention of the protein purity and activity. To analyze the residual water content, the samples were taken into vials from both the central part and the edges of the lyophilizer shelf. This approach ensured the data representativeness insofar as the distribution of temperature and heat transfer might differ between the center and the periphery of the shelf. The residual water content in the selected samples did not exceed 1.1 ± 0.2% (± standard deviation (SD), n = 5). Although the scalability of the process was limited in our case by the capabilities of the laboratory freeze drying plant, the used process can be directly transferred to a pilot plant providing the required drying parameters.

3.2. Study of physicochemical and biological properties

The study of the effect of lyophilization on the physicochemical and biological properties of Eculizumab Lyo was performed using various complementary analytical methods. The corresponding methods and the results of analysis of the structural, physicochemical, and biological properties are as presented in Table 3.

The intact protein mass before and after *N*-glycan removal, as well as the mass of the light and heavy chains of the antibody after disulfide bond reduction, were estimated using reversed-phase liquid chromatography with mass spectrometric detection. The average isotopic molecular mass of the main glycoform (G0F) of the studied protein was shown to be 147875 Da. The intact and subunit molecular mass, amino acid sequence, disulfide bonds positions, and glycosylation site corresponded to theoretical expectations.

Table 3. Methods used to assess the structure, physicochemical and biological properties of Eculizumab Lyo

Characteristic	Parameter and research method	Results
Primary structure	Intact molecular weight (HPLC-MS)*	G0F/G0F: 147875 ± 1 Da G0F/G1F: 148037 ± 1 Da G1F/G1F: 148199 ± 1 Da
	Intact molecular weight of deglycosylated molecule (HPLC-MS)*	144987 ± 1 Da
	Molecular weight of the heavy chain (HPLC-MS)*	G0F: 50817 ± 1 Da G1F: 50979 ± 1 Da
	Molecular weight of the light chain (HPLC-MS)*	23130 ± 1 Da
	Free thiols content (HPLC-MS)	0.2%
	Glycosylation site (HPLC-MS/MS)	Asn298
	Isoelectric point (cIEF)	Main form: 6.1
Product-related substances and impurities	Size variants (SEC-HPLC)	HMW: 0.3% Monomer: 99.6% LMW: 0.1%
	Non-reduced CE-SDS	Monomer: 98.5%
	Charge variants (CEX-HPLC)	Acidic form: 12.2% Main form: 82.7% Basic form: 5.1%
Biological activities	C5-component binding by ELISA	1053321 U/mg

*Data were expressed as mean ± SD, n = 3. HMW—high molecular weight, LMW—low molecular weight.

Peptide mapping of the protein after deglycosylation was performed by RP-HPLC with UV detection (Fig. 2). The query cover of amino acid sequence (obtained using mass spectrometric identification of peptides) was 100%. The chromatographic profile of the studied sample completely coincided with the RSs. The content of oxidized forms in Eculizumab Lyo, which was comparable to that of the reference product (Eculizumab EU), did not exceed 2% in either sample. Oxidation is presented as the most illustrative and representative post-translational modification (PTM), while the full range of PTMs was assessed during the studies.

The monomer of Eculizumab (recombinant IgG2/4k antibody) consists of two heavy and two light chains linked by disulfide bonds. As such, protein fragmentation and aggregation may occur during the production and storage. CE-SDS is typically used to assess the protein fragmentation, while size exclusion chromatography is used to determine the relative content of various aggregated forms. The profiles of high- and low-molecular impurities were obtained as a result of analysis of the sample after freeze-drying using such methods as SEC-HPLC and CE-SDS in non-reduced form in comparison with the RSs (these are shown in Figs. 3 and 4). The results demonstrated a high degree of similarity between the Eculizumab Lyo and Eculizumab EU, not only in the chromatographic profiles of the peptide map, but also in the relative content of aggregates and fragments. No statistically significant differences were observed between the two materials, thus confirming the compossibility of the candidate material with the reference product.

Charge heterogeneity is a consequence of post-translational modifications of a protein. As a rule, monoclonal antibodies have three groups of isoforms: the main isoform, as well as acidic and alkaline forms. Acidic isoforms have a different nature; the most common mechanism of their formation is deamidation of asparagine or glutamine residues, oxidation, and sialylation. Alkaline forms are mainly formed due to incomplete hydrolysis of *C*-terminal lysine residues by the action of carboxypeptidases. During the biosynthesis of heavy chains of antibodies, each chain has one lysine residue at the end, some of which are subsequently removed by the action of carboxypeptidases during the secretion and incubation in culture fluid. As a result, the purified antibody contains three forms having 0, 1, and 2 lysine residues [29]. In our studies, we used a cation exchange chromatography (CEX-HPLC) method to assess the charge heterogeneity in the sample. The obtained data confirmed the comparability of the profile of charged forms between Eculizumab Lyo and Eculizumab EU.

A comprehensive study of Eculizumab Lyo was carried out using complementary analytical methods (HPLC-MS, cIEF, SEC-HPLC, CE-SDS, CEX-HPLC, C5-ELISA, and RP-HPLC with UV detection). Figures 3 and 4 represent the quality attributes that are most relevant for assessing the lyophilization process and formulation, while the results from additional complementary methods are summarized in Table 3. The study demonstrated a high degree of comparability between Eculizumab Lyo and the reference product (Eculizumab EU). No statistically significant differences were observed in high molecular weight impurities, fragments, charge variant profiles, or specific activity. These results confirm that the lyophilization process does not affect the physicochemical or functional properties of Eculizumab Lyo.

3.3. Study of stability

The stability of medicinal products depends on many factors, such as storage temperature, illumination, composition of the surrounding atmosphere, technology of manufacturing of the dosage form, presence of

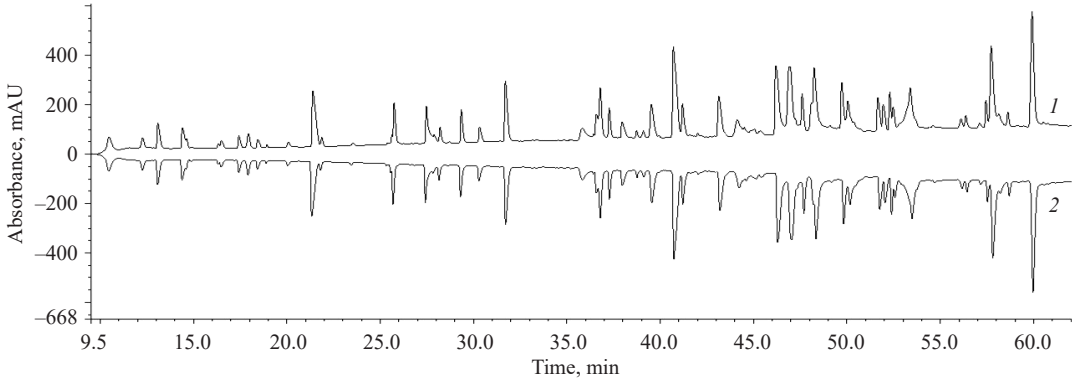

Fig. 2. Peptide mapping of Eculizumab samples. (*1*) Scaled up series of Eculizumab Lyo, (*2*) Eculizumab EU

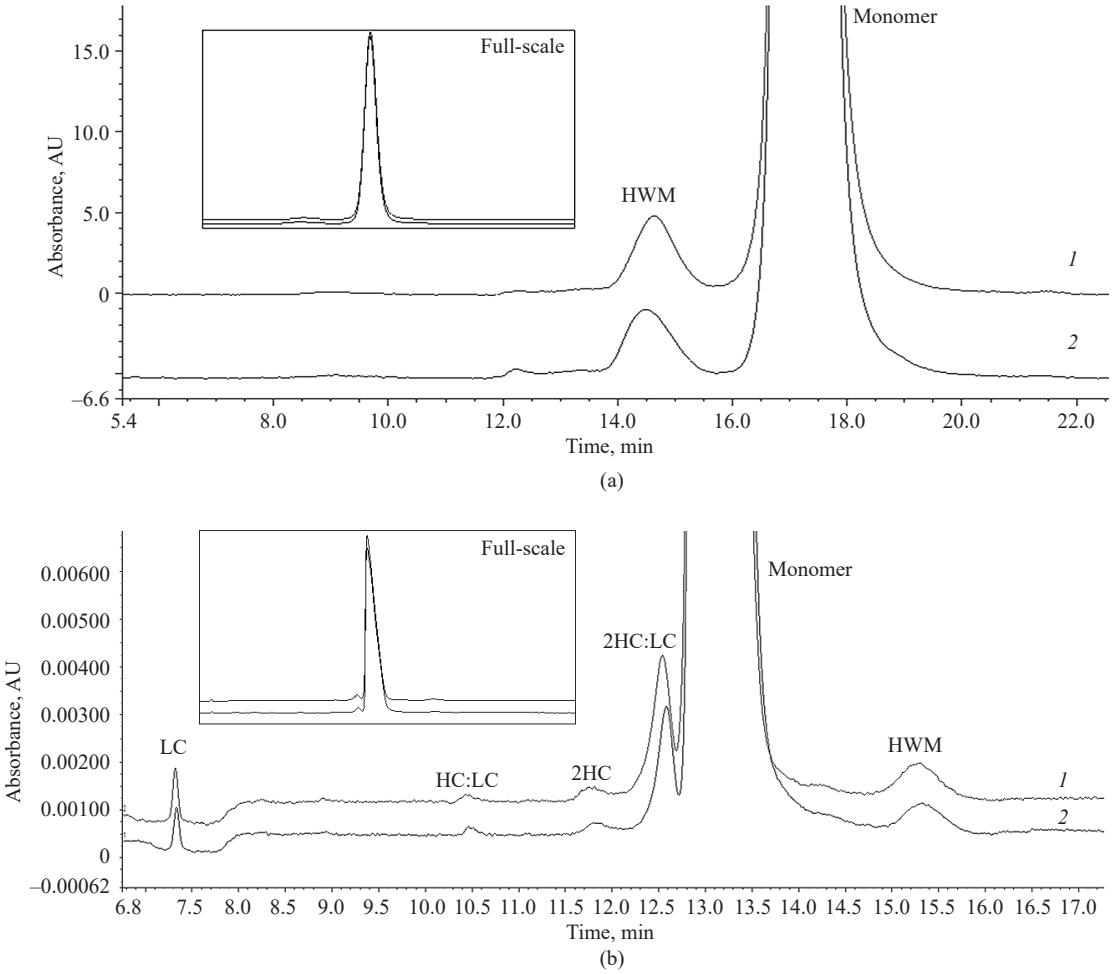

Fig. 3. Results of the study of Eculizumab using SEC-HPLC (a) and CE-SDS (b) in non-reduced form methods. (*1*) Scaled up series of Eculizumab Lyo, (*2*) Eculizumab EU. HC—heavy chain, LC—light chain, HMW—high molecular weight

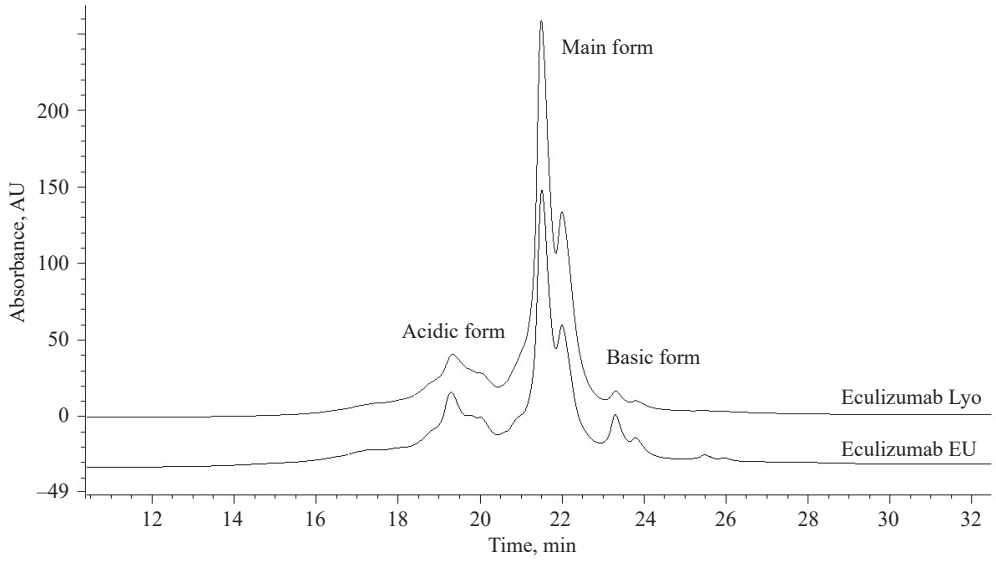

Fig. 4. Chromatograms of Eculizumab Lyo and Eculizumab EU (the last one is given for comparison) obtained by the CEX-HPLC method

excipients, type of dosage form, and especially their aggregate state, nature of material and method of packaging, etc. Classical programs for studying of the stability of biological medicinal products envisage long-term-, accelerated-, and stress tests, including assessment of photostability. Thus, the stability of a drug is a characteristic of a biologically active substance, which describes the degree of preserving of physicochemical properties and pharmacological activity during the established shelf life.

When determining the storage temperature, we wanted to avoid the necessity of the use of low and ultra-low temperatures (from −18 to −30 or −80°C), as this significantly complicates the transportation of the RS. Both the original Soliris® preparation and biosimilar drugs are supplied as a concentrate for solution for infusion at a storage temperature of 2–8°C. Based on the instructions for Eculizumab preparations, which were approved for the use in Europe and Russia, the storage temperature of 5 ± 3°C was identical for all manufacturers. The data regarding obtained by us regarding the stability of Eculizumab during the development of the Eculizumab drug (licensed by *PHARMAPARK* in the Russian Federation in 2024) confirm the absence of significant changes in protein quality over 3 years of storage. In view of this, additional stability studies at low and ultra-low temperatures were not performed.

Long-term stability of the scaled-up series was studied at the temperature of 2–8°C, protected from light, with checkpoints every 3 months during the first year and every 6 months thereafter. At the time of submission of the publication, the study had been carried out at four checkpoints: 3, 6, 9, and 12 months. Accelerated stability was studied at a temperature of 25 ± 2°C and humidity of 65 ± 5%, quality control of parameters was performed at checkpoints of 3 and 6 months. Stress stability tests were not performed due to the well-described degradation profile of Eculizumab in the scientific literature [26]. The results of stability assessment are presented in Table 4.

The data on stability at 25°C confirm that the sample retains its physicochemical properties and activity for at least 6 months. It suggests that short-term transportation and storage outside the cold chain is acceptable, for example, when moving between laboratories or under conditions of temporary lack of temperature control. The observed slight increase in the proportion of acidic isoforms (about 1%) is consistent with the expected degradation processes [26, 30] and is not accompanied by a decrease in biological activity. At the same time, when the preparations are stored at 2–8°C, all the monitored parameters remained stable for 12 months, confirming the suitability of this form for long-term storage under standard refrigeration conditions. Despite the advantages of lyophilization for long-term storage, the process carries inherent risks, such as protein denaturation during freezing and the potential possibility of oxidation or aggregation upon removal of the hydration shell. Although our data (e.g., SEC-HPLC, ELISA) confirm the structural and functional integrity of the protein after lyophilization and throughout the studied period, continuous monitoring of these quality attributes is essential to mitigate potential long-term risks associated with the mentioned degradation pathways.

CONCLUSIONS

The development of biosimilar medical preparations based on monoclonal antibodies represents a complex multi-stage process. The critical parameters of quality, such as primary and spatial structure, post-translational

Table 4. Results of the stability study

Quality parameter		Zero point	Long-term stability, months				Accelerated stability, months	
			3	6	9	12	3	6
Residual moisture, %		1.1	1.2	1.2	1.2	1.2	1.2	1.2
SEC-HPLC (Eculizumab monomer), %		99.5	99.5	99.5	99.5	99.5	99.2	98.9
Non-reduced CE-SDS (Eculizumab monomer), %		98.5	98.5	98.4	98.4	98.4	98.1	97.8
CEX-HPLC	Acidic form, %	12.3	12.3	12.4	12.5	12.5	12.6	13.5
	Main form, %	82.6	82.6	82.5	82.4	82.4	82.4	81.5
	Basic form, %	5.1	5.1	5.1	5.1	5.1	5.1	5.0
C5-ELISA, U/mg		1 052 213	1 046 524	1 053 314	1 052 781	1 053 256	1 042 249	1 041 994

modifications, product isoforms, and biological activity, must be studied in detail at each step of this process. When considering several products supplied by different manufacturers, there is always a risk of discrepancies in the results of determination of quality indicators between the biosimilar drugs and following their comparison with the reference preparation. The availability of an international reference material permits independent assessments of the quality of biosimilar preparations worldwide. The use of certified international reference materials thus facilitates the introduction of uniform quality standards for the production and registration of biosimilar preparations.

Currently, although a wide range of biosimilar Eculizumab drugs are approved for use worldwide, no international standard sample of Eculizumab has yet been released. In our study we obtained a lyophilized form of the monoclonal antibody Eculizumab, which was characterized by the following formulation buffer solution composition: 20 mM sodium phosphate, 4% trehalose, 0.2% polysorbate 80, pH 7.0. The absence of any effect of the drying process on the primary and spatial structure, post-translational modifications, content of related impurities, product isoforms and biological activity was rigorously demonstrated. Furthermore, stability studies demonstrated no significant changes in the critical quality attributes of the protein during storage at 2–8°C for the entire available data period of 12 months at the time of manuscript preparation. The confirmed stability provides a strong foundation for near-term application of the material. To substantiate the shelf-life required for an international reference material, continuous monitoring of long-term stability (up to 36 months) is currently in progress. Collectively, these results indicate that the developed lyophilized material is a viable candidate for an international reference material; however, its official qualification depends on the outcomes of the ongoing stability program and future collaborative trials.

Authors' contributions

D.I. Zybin—writing: original draft.

A.A. Klishin—visualization.

N.V. Orlova—conceptualization.

T.S. Sorokina—writing: review and editing.

D.V. Kapustin—writing: review and editing.

Conflict of interest

The authors work for *PHARMAPARK*. However, when writing this paper, the authors were guided by considerations of the scientific value of the material obtained; the authors declare their impartiality in its assessment.

REFERENCES

1. Sheridan M., Massich M., Ashourian N. Biosimilars: From production to patient. *J. Infus. Nurs*. 2024;47(1):19–29. https://doi.org/10.1097/NAN.0000000000000528
2. An Z., Forrest G., Moore R., Cukan M., Haytko P., Huang L., Strohl W. IgG2m4, an engineered antibody isotype with reduced Fc function. *mAbs*. 2009;1(6):572–579. https://doi.org/10.4161/mabs.1.6.10185
3. Thomas T.C., Rollins S.A., Rother R.P., Giannoni M.A., Hartman S.L., Elliott E.A., Nye S.H., Matis L.A., Squinto S.P., Evans M.J. Inhibition of complement activity by humanized anti-C5 antibody and single-chain Fv. *Mol. Immunol*. 1996;33(17–18):1389–1401. https://doi.org/10.1016/S0161-5890(96)00078-8
4. Rother R.P., Rollins S.A., Mojcik C.F., Brodsky R.A., Bell L. Discovery and development of the complement inhibitor eculizumab for the treatment of paroxysmal nocturnal hemoglobinuria. *Nat. Biotechnol*. 2007;25:(11):1256–1264. https://doi.org/10.1038/nbt1344
5. Wijnsma K.L., ter Heine R., Moes D.J.A.R., Langemeijer S., Schols S.E.M., Volokhina E.B., van den Heuvel L.P., Wetzels F.M., van de Kar N.C.A.J., Brüggemann R.J. Pharmacology, pharmacokinetics and pharmacodynamics of eculizumab, and possibilities for an individualized approach to eculizumab. *Clin. Pharmacokinet*. 2019;58(7):859–874. https://doi.org/10.1007/s40262-019-00742-8
6. Hillmen P., Hall C., Marsh J.C., Elebute M., Bombara M.P., Petro B.E., *et al*. Effect of eculizumab on hemolysis and transfusion requirements in patients with paroxysmal nocturnal hemoglobinuria. *N. Engl. J. Med*. 2004;350(6): 552–559. https://doi.org/10.1056/NEJMoa031688
7. Brodsky R.A., Young N.S., Antonioli E., Risitano A.M., Schrezenmeier H., Schubert J., *et al*. Multicenter phase 3 study of the complement inhibitor eculizumab for the treatment of patients with paroxysmal nocturnal hemoglobinuria. *Blood*. 2008;111(4): 1840–1847. https://doi.org/10.1182/blood-2007-06-094136
8. Luzzatto L., Risitano A.M., Notaro R. Paroxysmal nocturnal hemoglobinuria and eculizumab. *Haematologica*. 2010;95(4): 523–526. https://doi.org/10.3324/haematol.2009.017848
9. Rondeau E., Cataland S.R. Al-Dakkak I., Miller B., Webb N.J.A., Landau D. Eculizumab safety: Five-year experience from the global atypical hemolytic uremic syndrome registry. *Kidney Int. Rep*. 2019;4(11): 1568–1576. https://doi.org/10.1016/j.ekir.2019.07.016
10. Cordero L., Cavero T., Gutiérrez E., Trujillo H., Sandino J., Auñón P., Rivero M., Morales E. Rational use of eculizumab in secondary atypical hemolytic uremic syndrome. *Front. Immunol*. 2023;14:1310469. https://doi.org/10.3389/fimmu.2023.1310469
11. Zuber J., Fakhouri F., Roumenina L.T., Loirat C., Frémeaux-Bacchi V. Use of eculizumab for atypical haemolytic uraemic syndrome and C3 glomerulopathies. *Nat. Rev. Nephrol.* 2012;8(11):643–657. https://doi.org/10.1038/nrneph.2012.214
12. Wijnsma K.L., Duineveld C., Wetzels J.F.M., van de Kar N.C.A.J. Eculizumab in atypical hemolytic uremic syndrome: Strategies toward restrictive use. *Pediatr. Nephrol.* 2019;34(12): 2261–2277. https://doi.org/10.1007/s00467-018-4091-3
13. Thomas K., Ananthula A., Lopez-Flores R., del Toro A., Chapple A.G., Loch M. The use of eculizumab for the treatment of atypical hemolytic uremic syndrome in an academic hematology center. *Permanente J.* 2023;27(2):22.073. https://doi.org/10.7812/TPP/22.073

14. Levy A.R., Chen P., Johnston K., Wang Y., Popoff E., Tomazos I. Quantifying the economic effects of ravulizumab versus eculizumab treatment in patients with atypical hemolytic uremic syndrome. *J. Med. Econ.* 2022;25(1): 249–259. https://doi.org/10.1080/13696998.2022.2027706
15. Howard J.F.Jr., Karam C., Yountz M., O'Brien F.L., Mozaffar T. Long-term efficacy of eculizumab in refractory generalized myasthenia gravis: Responder analyses. *Ann. Clin. Transl. Neurol.* 2021;8(7):1398–1407. https://doi.org/10.1002/acn3.51376
16. Patel A.D., Shah A., Avila J.D. A new era in the treatment of myasthenia gravis: Six new medications in the last 6 years. *Curr. Treat. Options Neurol.* 2024;26(2):79–96. https://doi.org/10.1007/s11940-024-00783-w
17. Brandsema J.F., Ginsberg M., Hoshino H., Mimaki M., Nagata S., Rao V., Ruzhansky K., Suresh N., Tiongson E., Yamanouchi H., Frick G., Hicks E., Liao S., Howard J. A phase 3, open-label, multicenter study to evaluate eculizumab in adolescents with refractory generalized myasthenia gravis. *Neurology.* 2023;100(17_supplement_2):1926. https://doi.org/10.1212/WNL.0000000000202200
18. Nabizadeh F., Moghadasi A.N. Eculizumab in the treatment of neuromyelitis optica spectrum disorder. *Curr. J. Neurol.* 2023;22(2):140–143. https://doi.org/10.18502/cjn.v22i2.13342
19. Enriquez M., Rosenthal S., Kammeyer R., Piquet A., Bennett J., McLedon L.A. Efficacy of eculizumab in acute refractory pediatric neuromyelitis optica: A case report. *Neurology.* 2024;102(7_supplement_1):4052. https://doi.org/10.1212/WNL.0000000000205538
20. Pittock S.J., Lennon V.A., McKeon A., Mandrekar J., Weinshenker B.G., Lucchinetti C.F., *et al*. Eculizumab in AQP4-IgG-positive relapsing neuromyelitis optica spectrum disorders: An open-label pilot study. *Lancet Neurol.* 2013;12(6): 554–562. https://doi.org/10.1016/S1474-4422(13)70076-0
21. Digala L., Katyal N., Narula N., Govindarajan R. Eculizumab in the treatment of aquaporin-4 seronegative neuromyelitis optica spectrum disorder: A case report. *Front. Neurol.* 2021;12:660741. https://doi.org/10.3389/fneur.2021.660741
22. Gervasi V., Dall Agnol R., Cullen S., McCoy T., Vucen S., Crean A. Parenteral protein formulations: An overview of approved products within the European Union. *Eur. J. Pharm. Biopharm.* 2018;131:8–24. https://doi.org/10.1016/j.ejpb.2018.07.011
23. Zybin D.I., Seregin A.S., Askretkov A.D., Orlova N.V., Seregin Y.A., Prostyakova A.I., Kapustin D.V. Development and validation of a method for the determination of the specific activity of recombinant monoclonal antibody eculizumab. *Tonk. Khim. Tekhnol. = Fine Chem. Technol.* 2020:15(2): 77–85. https://doi.org/10.32362/2410-6593-2020-15-2-77-85
24. Thakral S., Sonje J., Munjal B., Suryanarayanan R. Stabilizers and their interaction with formulation components in frozen and freeze-dried protein formulations. *Adv. Drug Deliv. Rev.* 2021;173:1–19. https://doi.org/10.1016/j.addr.2021.03.003
25. Carpenter J.F., Chang B.S., Garzon-Rodriguez W., Randolph T.W. Rational design of stable lyophilized protein formulations: Theory and practice. In: *Rational Design of Stable Protein Formulations*. Springer. 2002;109–133. https://doi.org/10.1007/978-1-4615-0557-0_5
26. Zybin D.I., Zhuchenko M.A., Rassulin Y.Y., *et al*. Comparative study of the stability of eculizumab biosimilar and the original drug under extreme pH, oxidative stress, and UV irradiation conditions. *Pharm. Chem. J.* 2021:55(7);732–739. https://doi.org/10.1007/s11094-021-02485-y
27. Matejtschuk P., Bird C., Ezeajughi E., MacLellan-Gibson K., Wadhwa M. Impact of formulation choices on the freeze-drying of an interleukin-6 reference material. *Front. Mol. Biosci.* 2022;9:868460. https://doi.org/10.3389/fmolb.2022.868460
28. Bjelošević M., Pobirk A.Z., Planinšek O., Grabnar P.A. Excipients in freeze-dried biopharmaceuticals: Contributions toward formulation stability and lyophilisation cycle optimisation, *Int. J. Pharm.* 2020;583:119029. https://doi.org/10.1016/j.ijpharm.2020.119029
29. Khawli L.A., Goswami S., Hutchinson R., Kwong Z.W. Charge variants in IgG1: Isolation, characterization, *in vitro* binding properties and pharmacokinetics in rats. *mAbs.* 2010;2(6):613–624. https://doi.org/10.4161/mabs.2.6.13333
30. Tak M., Jeong H., Yun J., Kim J., Kim S., Lee Y., Park S.J. In-use stability of SB12 (eculizumab, Soliris biosimilar) diluted in saline and dextrose infusion solution after an extended storage period. *Drugs R&D.* 2023:23(4):363–375. https://doi.org/10.1007/s40268-023-00433-7

About the Authors

Dmitry I. Zybin, Cand. Sci. (Chem.), Head of the Research Laboratory, PHARMAPARK (8, b. 1, Nauchnyi proezd, Moscow, 117246, Russia). E-mail: mithtchem@gmail.com. Scopus Author ID 57189868539, Researcher ID P-8049-2016, RSCI SPIN-code 5156-8210, https://orcid.org/0000-0002-5542-982X

Anatoly A. Klishin, Head of the Research Laboratory, PHARMAPARK (8, b. 1, Nauchnyi proezd, Moscow, 117246, Russia). E-mail: klishin@pharmapark.ru. RSCI SPIN-code 5919-8724.

Natalya V. Orlova, Cand. Sci. (Biol.), Deputy Director for Science, PHARMAPARK (8, b. 1, Nauchnyi proezd, Moscow, 117246, Russia). E-mail: orlova.chemist@gmail.com. https://orcid.org/0000-0003-4161-5880

Tatiana S. Sorokina, Director of Science, PHARMAPARK (8, b. 1, Nauchnyi proezd, Moscow, 117246, Russia). E-mail: sorokina@pharmapark.ru.

Dmitry V. Kapustin, Dr. Sci. (Chem.), Senior Researcher, Laboratory of Polymers for Biology, M.M. Shemyakin and Yu.A. Ovchinnikov Institute of Bioorganic Chemistry, Russian Academy of Sciences (16/10, Miklukho-Maklaya ul., Moscow, 117997, Russia). E-mail: kapustin@ibch.ru. Scopus Author ID 6602903079, Researcher ID B-5773-2014, RSCI SPIN-code 5156-8210, https://orcid.org/0000-0002-5485-9297

Об авторах

Зыбин Дмитрий Игоревич, к.х.н., начальник лаборатории по разработке аналитических методик, ООО «ФАРМАПАРК» (117246, Россия, Москва, Научный пр-д, д. 8, корп. 1). E-mail: mithtchem@gmail.com. Scopus Author ID 57189868539, Researcher ID P-8049-2016, SPIN-код РИНЦ 5156-8210, https://orcid.org/0000-0002-5542-982X

Клишин Анатолий Анатольевич, начальник сектора контроля качества, ООО «ФАРМАПАРК» (117246, Россия, Москва, Научный пр-д, д. 8, корп. 1). E-mail: klishin@pharmapark.ru. SPIN-код РИНЦ 5919-8724

Орлова Наталья Владимировна, к.б.н., заместитель директора по науке, ООО «ФАРМАПАРК» (117246, Россия, Москва, Научный пр-д, д. 8, корп. 1). E-mail: orlova.chemist@gmail.com. https://orcid.org/0000-0003-4161-5880

Сорокина Татьяна Сергеевна, директор по науке, ООО «ФАРМАПАРК» (117246, Россия, Москва, Научный пр-д, д. 8, корп. 1). E-mail: sorokina@pharmapark.ru.

Капустин Дмитрий Валерьевич, д.х.н., старший научный сотрудник, Лаборатория полимеров для биологии, ФГБУН ГНЦ РФ Института биоорганической химии им. академиков М.М. Шемякина и Ю.А. Овчинникова Российской академии наук (117997, Россия, Москва, ул. Миклухо-Маклая, д. 16/10). E-mail: kapustin@ibch.ru. Scopus Author ID 6602903079, Researcher ID B-5773-2014, SPIN-код РИНЦ 3460-0425, https://orcid.org/0000-0002-5485-9297

The text was submitted by the Authors in English
and edited for English language and spelling by Thomas A. Beavitt

Tonkie Khimicheskie Tekhnologii = Fine Chemical Technologies.
2026;21(2):179–187 ISSN 2686-7575 (Online)

UDC 664.641.2:577.152.3
https://doi.org/10.32362/2410-6593-2026-21-2-179-187
EDN NEFNGT

RESEARCH ARTICLE

Enzymatic deglycosylation of soy proteins as a method to increase the efficiency of their hydrolysis

Viktor N. Leontiev✉, **Olesya I. Lazovskaya**

Belarusian State Technological University, Minsk, 220006 Republic of Belarus

✉ *Corresponding author, e-mail: leontiev@belstu.by*

Abstract

Objectives. Soy protein hydrolysates are now widely used in the food industry, fish farming, poultry farming, livestock farming, as well as in medical preparations. The most effective method for their production is enzymatic hydrolysis. However, even with optimal proteolysis parameters, it is not always possible to achieve the required degree of hydrolysis. For this reason, various technological approaches are used to more intensively break down soy proteins, including the addition of enzyme preparations and pretreatment of the protein substrate. β-Conglycinin, one of the main soy proteins, is a glycoprotein whose carbohydrate portion consists primarily of mannose residues. We hypothesize that deglycosylation of β-conglycinin by an enzyme preparation with mannanase activity as a pretreatment of the soy substrate will lead to change in the structure of its protein portion due to the destruction of the carbohydrate component to increase the accessibility of peptide bonds to proteolytic enzymes. Thus, the work sets out to study the effect of enzymatic deglycosylation on the efficiency of soy protein hydrolysis.

Methods. Deglycosylation of β-conglycinin, hydrolysis of polysaccharides and lipids were performed by the Complex-concentrate enzyme preparation (*Ferment*, Republic of Belarus). Protein hydrolysis was carried out by the Protozyme C330 enzyme preparation (*Ferment*, Republic of Belarus). The formation of reducing sugars was confirmed by the Miller method. The degree of protein hydrolysis was determined by the pH-stat method. The molecular weight distribution of peptide fractions was analyzed by low-pressure liquid gel chromatography on a column with Sephadex® G-50 Medium. Computer processing of the elution profile of peptide fractions was performed in the OriginPro 8.5.1 program using the Gauss function.

Results. It is established that the treatment of soy flour by the Complex-concentrate enzyme preparation (enzyme-substrate ratio 1 : 40, hydromodule 1 : 10) promotes the breakdown of both free oligo- and polysaccharides, as well as the carbohydrate component β-conglycinin. Proteolysis by the Protozyme C330 enzyme preparation (enzyme-substrate ratio 1 : 20, pH 7.5, 50°C, 3.5 h) carried out following 20 h of deglycosylation results in a product with a degree of hydrolysis of 56.3%. The content of low-molecular-weight peptides in soy hydrolysate is 83.9%. Proteolysis without enzymatic destruction of the carbohydrate part of β-conglycinin is shown to be characterized by a degree of hydrolysis of 9.2%.

Conclusions. A pretreatment approach involving deglycosylation of enzymatic β-conglycinin can be used to significantly increase the degree of hydrolysis of soy proteins.

Keywords

soy flour, enzyme preparation with mannanase activity, deglycosylation of β-conglycinin, proteolysis, degree of hydrolysis, low-molecular-weight peptides, gel chromatography

Submitted: 22.05.2025
Revised: 03.12.2025
Accepted: 13.02.2026

For citation

Leontiev V.N., Lazovskaya O.I. Enzymatic deglycosylation of soy proteins as a method to increase the efficiency of their hydrolysis. *Tonk. Khim. Tekhnol. = Fine Chem. Technol*. 2026;21(2):179–187. https://doi.org/10.32362/2410-6593-2026-21-2-179-187

НАУЧНАЯ СТАТЬЯ

Ферментативное дегликозилирование соевых белков как способ повышения эффективности их гидролиза

В.Н. Леонтьев✉, **О.И. Лазовская**

Белорусский государственный технологический университет, Минск, 220006 Республика Беларусь

✉ *Автор для переписки, e-mail: leontiev@belstu.by*

Аннотация

Цели. В настоящее время гидролизаты соевых белков находят широкое применение в пищевой промышленности, медицине, рыбоводстве, птицеводстве и животноводстве. Наиболее эффективным способом их получения является ферментативный гидролиз. Однако даже при оптимальных параметрах протеолиза не всегда возможно достичь требуемой степени гидролиза, поэтому для более интенсивного расщепления соевых белков используют различные технологические подходы: внесение нескольких ферментных препаратов и предварительную обработку белкового субстрата. β-Конглицинин — один из основных белков сои — представляет собой гликопротеин, углеводная часть которого состоит преимущественно из маннозных остатков. Предполагаем, что дегликозилирование β-конглицинина ферментным препаратом с маннаназной активностью в качестве предварительной обработки соевого субстрата приведет к изменению структуры его белковой части за счет разрушения углеводного компонента и позволит повысить доступность пептидных связей к действию протеолитических ферментов. Таким образом, целью работы является изучение влияния ферментативного дегликозилирования на эффективность гидролиза соевых белков.

Методы. Дегликозилирование β-конглицинина, гидролиз полисахаридов и липидов проводили ферментным препаратом «Комплекс-концентрат» (*ООО* «*Фермент*», Республика Беларусь). Гидролиз белков осуществляли ферментным препаратом «Протозим С330» (*ООО* «*Фермент*», Республика Беларусь). Образование редуцирующих сахаров подтверждали методом Миллера. Степень гидролиза белков определяли pH-статическим методом. Молекулярно-массовое распределение пептидных фракций анализировали методом жидкостной гель-хроматографии низкого давления на колонке с гелем Sephadex® G-50 Medium. Компьютерную обработку профиля элюирования пептидных фракций выполняли в программе OriginPro 8.5.1 с помощью функции Гаусса.

Результаты. Установлено, что обработка соевой муки ферментным препаратом «Комплекс-концентрат» (фермент-субстратное соотношение 1 : 40, гидромодуль 1 : 10) способствует расщеплению как свободных олиго- и полисахаридов, так и углеводного компонента β-конглицинина. Протеолиз ферментным препаратом «Протозим С330» (фермент-субстратное соотношение 1 : 20, pH 7.5, 50°C, 3.5 ч) после 20-часового дегликозилирования приводит к получению продукта со степенью гидролиза 56.3%. При этом содержание низкомолекулярных пептидов в соевом гидролизате составляет 83.9%. Показано, что протеолиз без ферментативного разрушения углеводной части β-конглицинина характеризуется степенью гидролиза 9.2%.

Выводы. Применение ферментативного дегликозилирования β-конглицинина в качестве предварительной обработки позволяет существенно повысить степень гидролиза соевых белков.

Ключевые слова

соевая мука, ферментный препарат с маннаназной активностью, дегликозилирование β-конглицинина, протеолиз, степень гидролиза, низкомолекулярные пептиды, гель-хроматография

Поступила: 22.05.2025
Доработана: 03.12.2025
Принята в печать: 13.02.2026

Для цитирования

Леонтьев В.Н., Лазовская О.И. Ферментативное дегликозилирование соевых белков как способ повышения эффективности их гидролиза. *Тонкие химические технологии*. 2026;21(2):179–187. https://doi.org/10.32362/2410-6593-2026-21-2-179-187

INTRODUCTION

At present, soy protein hydrolysates possessing antioxidant, hypotensive, immunomodulatory, antimicrobial, anti-inflammatory, and other properties are widely used in the food industry [1], medicine [2], fish farming [3], poultry farming [4], and livestock farming [5]. Soy proteins, which are comparable in biological value to meat and milk proteins, are rich in essential amino acids, especially lysine, which is often limited in other plant proteins. About 70% of soy proteins are represented by the storage proteins glycinin and β-conglycinin. Glycinin consists of a basic polypeptide B having a molecular mass of about 20 kDa along with an acidic polypeptide A whose molecular mass is about 38 kDa, which are linked by a disulfide bond to form an individual AB subunit. The quaternary structure of glycinin depends on pH and ionic strength of the solutions. At moderate temperatures and neutral pH values, glycinin forms hexameric complexes having a molecular mass ranging from 320 to 375 kDa, composed of heterogeneous subunits. Each hexamer contains about 2 free SH groups and 18–20 disulfide bonds. β-Conglycinin, having a molecular mass of 150–180 kDa, is a trimeric glycoprotein consisting of 3 subunits: α (72–76 kDa), α′ (68–72 kDa), and β (52–53 kDa), which form seven isomers. The subunits, which are linked mainly by hydrophobic interactions or hydrogen bonds, contain no free SH groups [6]. The carbohydrate moiety of one β-conglycinin molecule consists of 38 mannose and 12 glucosamine residues [7].

The most effective method for obtaining protein hydrolysates is enzymatic hydrolysis, which allows for selective cleavage of peptide bonds due to the specificity of proteolytic enzymes. Table 1 presents the parameters of soy protein hydrolysis using some enzyme preparations [8–13]. To achieve more intensive protein breakdown, a two-stage hydrolysis process is employed. For instance, the study [9] demonstrated that sequential application of alcalase and flavourzyme to effect a twofold increase in the degree of hydrolysis of soy protein isolate as compared to a single-stage proteolysis process using alcalase alone. Furthermore, preliminary treatment of the protein substrate significantly enhances the efficiency of enzymatic hydrolysis [14–16] (Table 2).

The authors of the study [17] demonstrated that the carbohydrate component of β-conglycinin, which exhibits pronounced IgE reactivity, is responsible for the allergenic properties of soy proteins. At the same time, it has been established [18] that deglycosylation of β-conglycinin by peptide-*N*-glycosidase F not only reduces its antigenicity compared to the native glycoprotein but also leads to significant changes in the secondary and tertiary structure of the protein moiety. Based on this, we hypothesize that the use of enzymatic deglycosylation as a pretreatment of the soy substrate will destroy the carbohydrate part of β-conglycinin to increase the susceptibility of peptide bonds to the action of proteolytic enzymes. It should be noted that the proposed approach of preliminary deglycosylation of soy proteins to increase the yield of low-molecular-weight peptides has not been described in the literature.

Thus, the aim of the present work is to investigate the influence of enzymatic deglycosylation on the efficiency of soy protein hydrolysis.

Table 1. Parameters of enzymatic hydrolysis of soy proteins

Substrate	Enzyme preparation	Hydrolysis conditions				Degree of hydrolysis		Reference
		E : S ratio**	pH	*t*, °C	τ, h	%	Method for determining	
One-step process								
Soy protein isolate*	Pepsin	1 : 20	1.6	39	5	60.5	Formol titration method	[8]
	Trypsin	1 : 30	7.8	39	5	55.7		
Soy protein concentrate*	Alcalase	4%	8.0	55	3	14.5	pH-stat method and 2,4,6-trinitrobenzenesulfonic acid method	[9]
	Papain	4%	8.0	50	1.5	14.5		
	Neutrase	4%	7.0	45	1.25	7.2		

Table 1. Continued

Substrate	Enzyme preparation	Hydrolysis conditions				Degree of hydrolysis		Reference
		E : S ratio**	pH	*t*, °C	τ, h	%	Method for determining	
Soy protein isolate	Alcalase	1%	8.0	50	3	8.0	*o*-Phthalaldehyde method	[10]
	Flavourzyme	1%	7.0	50	3	10.0		
Soy protein isolate	Flavourzyme	8%	7.0	55	4	57.0	Biuret method	[11]
Soy flour*	Alcalase	–	8.0	40	8	35.1	Ninhydrin method	[12]
	Flavourzyme	–	8.0	40	8	39.5		
	Novozym	–	8.0	40	8	33.3		
Two-step process								
Soy protein isolate	Pepsin	1 : 20	1.6	39	8	88.2	Formol titration method	[8]
	Trypsin	1 : 20	7.8					
Soy protein concentrate	Alcalase	4%	7.0	50	2.5	30.0	pH-stat method and 2,4,6-trinitrobenzenesulfonic acid method	[9]
	Flavourzyme	4%						
	Neutrase	4%	7.0	50	2.75	14.0		
	Flavourzyme	4%						

* Soy flour contains 50% protein on a dry matter basis, soy protein concentrate contains more than 65% protein, soy protein isolate contains more than 90% protein [13].

** E : S ratio is the enzyme-to-substrate ratio.

Table 2. Effect of pretreatment of soy protein isolate on the degree of hydrolysis

Pretreatment	Enzyme preparation	Hydrolysis conditions				Degree of hydrolysis		Reference
		E : S ratio	pH	*t*, °C	τ, h	%	Method for determining	
–	Papain	0.5%	7.0	55	3	0.9	pH-stat method	[14]
Ultrasound pretreatment 600 W						1.86		
–	Pancreatin	2%	7.0	55	3	9.6	pH-stat method	[15]
Extrusion pretreatment						16.4		
–	Bromelain	1 : 20	7.0	55	3	13.7	Formol titration method	[16]
Thermal pretreatment 90°C, 10 min						16.9		
High-pressure homogenization 30 MPa						23.5		

MATERIALS AND METHODS

The following materials were used in this work: defatted soy flour (protein content, 48%; fat, 1%; carbohydrates, 35%; *Irkutsk Maslozhirkombinat*, Russia); the Protozyme C330 enzyme preparation based on a neutral protease (≥250 units/g, 30–50°C, pH 6.0–7.5; *Ferment*, Republic of Belarus); an enzyme preparation based on an alkaline protease (204324 units/g, 40–50°C, pH 9.0–11.0; *Beijing Donghua Qiangsheng Biotechnology Co*., China); the Complex-concentrate enzyme preparation, possessing cellulase (1452 units/g), xylanase (21256 units/g), β-glucanase (16415 units/g), pectinase (2152 units/g), phytase (1550 units/g), mannanase (10586 units/g), and lipase (1080 units/g) activity (*Ferment*, Republic of Belarus).

Deglycosylation of β-conglycinin, hydrolysis of polysaccharides and lipids were carried out using the Complex-concentrate enzyme preparation at an enzyme-to-substrate (E : S) ratio of 1 : 40 and a hydromodule of soy flour : purified water (1 : 10) for 20 h. Protein hydrolysis was performed using a proteolytic enzyme preparation at an E : S of 1 : 20 and pH 7.5. Upon completion of proteolysis, the enzyme was inactivated at a temperature of 100°C for 10 min.

The degree of protein hydrolysis was determined by the pH-stat method [19]. The pH value of the reaction medium was controlled using an HI 83141 pH meter (*Hanna*, Germany). The constancy of pH was maintained by adding a 1 M sodium hydroxide solution.

The degree of hydrolysis (*DH*, %) of proteins was calculated using the formula:

$$DH = V \cdot N \cdot \frac{1}{\alpha} \cdot \frac{1}{m} \cdot \frac{1}{h} \cdot 100, \quad (1)$$

where V is the volume of sodium hydroxide solution added during hydrolysis, mL; N is the molar concentration of sodium hydroxide, mol/L; m is the mass of protein, g; h is the number of peptide bonds in 1 g of soy proteins, h = 7.8 mmol/g; α is the degree of dissociation of α-amino groups at the hydrolysis pH:

$$\alpha = \frac{10^{(\mathrm{pH}-\mathrm{pK})}}{1+10^{(\mathrm{pH}-\mathrm{pK})}}. \quad (2)$$

Here, the pK of the formed α-amino groups depends on the hydrolysis temperature T, in Kelvin, as follows:

$$\mathrm{pK} = 7.8 + \frac{(298 - T)}{(298 \cdot T)} \cdot 2400. \quad (3)$$

Reducing sugars were determined according to the Miller method [20] with some modifications. The essence of the method is that upon interaction of reducing sugars with 3,5-dinitrosalicylic acid, the latter is reduced to 3-amino-5-nitrosalicylic acid, which has a yellow-orange color.

To 0.5 mL of the carbohydrate hydrolysate in a test tube, 1.5 mL of dinitrosalicylic acid reagent and 1.0 mL of distilled water were added. After closing the test tube with a cotton plug and placing it in a boiling water bath for 15 min, the tube was cooled to 20°C and 0.5 mL of a 40% solution of potassium sodium tartrate (Rochelle salt) was added to stabilize the color. The optical density of the solution was measured at 582 nm using a Specord 200 Plus spectrophotometer (*Analytik Jena*, Germany) against a control sample. According to the Beer–Lambert–Bouguer law, the optical density is proportional to the concentration of reducing sugars. To prepare the dinitrosalicylic reagent, 1 g of 3,5-dinitrosalicylic acid, 1 g of sodium hydroxide, 0.05 g of sodium sulfate, and 0.2 g of phenol were weighed and dissolved in distilled water with continuous stirring, bringing the solution volume to 100 mL.

The molecular weight distribution of peptide fractions was analyzed by low-pressure liquid gel chromatography in a 1.8 × 35 cm glass column packed with Sephadex® G-50 Medium gel (separation range 1.5–30 kDa; *Pharmacia Fine Chemicals*, Sweden) and pre-calibrated using standard substances (Fig. 1): trypsin (24 kDa; *Sigma-Aldrich*, USA), cytochrome C (12.3 kDa; *Serva Fein Biochemica*, Germany), vitamin B_{12} (1.36 kDa; *Sigma-Aldrich*, USA). The void volume of the column was determined at 32.5 ± 0.1 mL by the elution volume of blue dextran 2000 (2000 kDa; *Sigma-Aldrich*, USA). Prior to loading onto the column, the hydrolysate solution was filtered through a membrane filter (pore size 0.2 μm; *Agilent Technologies*, USA). A 0.025 M Tris-HCl buffer solution (pH 8.0) was used as the eluent. Detection was performed at 280 nm.

Graphs were plotted using Microsoft Office Excel 2010 software. Computer processing of the elution profile of peptide fractions was performed in OriginPro 8.5.1 software using the Gaussian function.

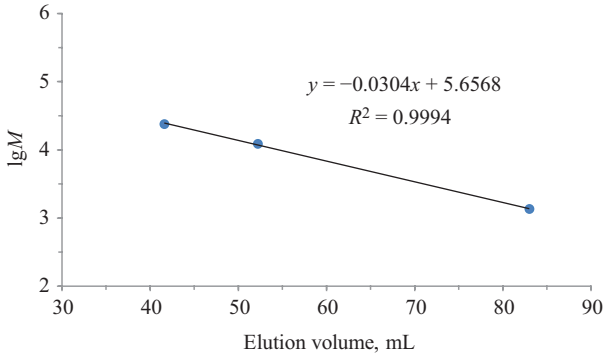

Fig. 1. Calibration curve for a column with Sephadex® G-50 Medium. *M* is molecular weight

RESULTS AND DISCUSSION

Selection of a proteolytic enzyme preparation. Protein hydrolysis was carried out with a proteolytic enzyme preparation at 40°C following preliminary deglycosylation of β-conglycinin at the same temperature. As seen from Fig. 2, when using the Protozyme C330 enzyme preparation, significant formation of proteolysis products (*DH* = 55.5%) occurs within 5.5 h, while the maximum degree of hydrolysis (*DH* = 43.3%) is achieved in 5 h with the addition of the alkaline protease-based enzyme preparation. For further research, the Protozyme C330 enzyme preparation was selected.

Influence of temperature. Protein hydrolysis was carried out using the Protozyme C330 enzyme preparation at temperatures of 40 and 50°C (the temperature range of highest catalytic activity for the neutral protease) following preliminary cleavage of the carbohydrate component of the glycoprotein at the same temperatures. As can be seen from Fig. 3, proteolysis at 40°C yields a product having a degree of hydrolysis of 55.5% over 5.5 h, while proteolysis at 50°C yields a product with the same degree of hydrolysis (*DH* = 56.3%) in 3.5 h. The results obtained indicate that the preferred temperature for protein hydrolysis is 50°C.

Influence of preliminary cleavage of the carbohydrate component of the glycoprotein. Enzymatic deglycosylation of β-conglycinin and hydrolysis of polysaccharides were carried out at 50°C. The kinetic curve of reducing sugar formation is presented in Fig. 4. Since soy flour initially contains reducing sugars (glucose, fructose) [21], their concentration on the kinetic curve is non-zero at the initial time point. The 2.5-fold increase in the concentration of reducing sugars observed 15 min after the addition of the Complex-concentrate enzyme preparation to the soy flour suspension is due to the hydrolysis of free oligo- and polysaccharides. The subsequent increase in the concentration of reducing sugars can be attributed to the slow cleavage of the carbohydrate part of the glycoprotein.

Protein hydrolysis was carried out using the Protozyme C330 enzyme preparation at 50°C both with and without preliminary deglycosylation of β-conglycinin at the same temperature. The destruction of the carbohydrate component of the glycoprotein was found to contribute to a 6-fold increase in the degree of protein hydrolysis (*DH* = 56.3% in 3.5 h) as compared to proteolysis without pretreatment (*DH* = 9.2% in 3.5 h) (Fig. 5).

Analysis of the molecular weight distribution of peptide fractions after proteolysis with preliminary deglycosylation of β-conglycinin. Analysis of the elution profile of peptide fractions (Fig. 6) showed that the soy hydrolysate contains 83.9% of peptides with a molecular weight ≤6 kDa, which potentially possess biological activity [22, 23]. Furthermore, the

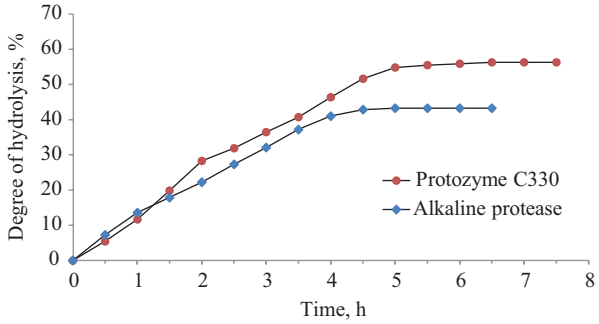

Fig. 2. Effect of proteolytic enzymes on the degree of protein hydrolysis

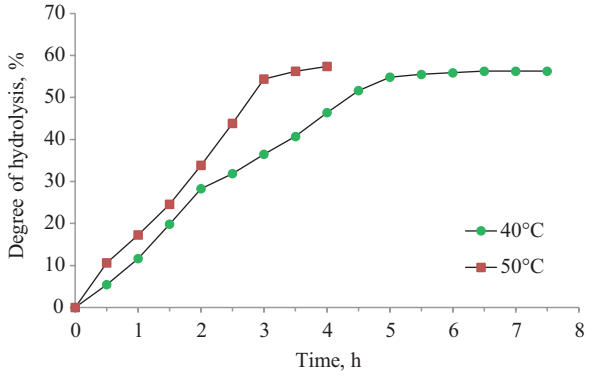

Fig. 3. Effect of temperature on the degree of protein hydrolysis by the Protozyme C330 enzyme preparation

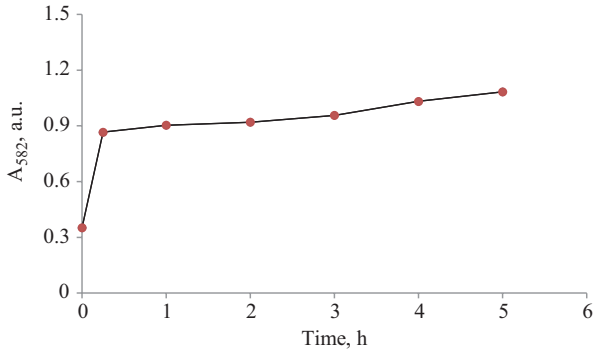

Fig. 4. Kinetic curve of reducing sugars formation

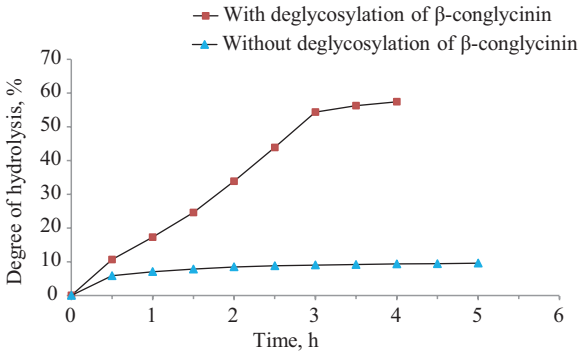

Fig. 5. Effect of preliminary cleavage of the carbohydrate part of β-conglycinin on the degree of protein hydrolysis by the Protozyme C330 enzyme preparation

peptide fraction with a molecular weight ≤1.0 kDa is predominant (58.6%), which is consistent with the degree of hydrolysis (*DH* = 56.3%). Polypeptides with a molecular weight >32 kDa and unhydrolyzed proteins elute in the void volume of the column (Table 3).

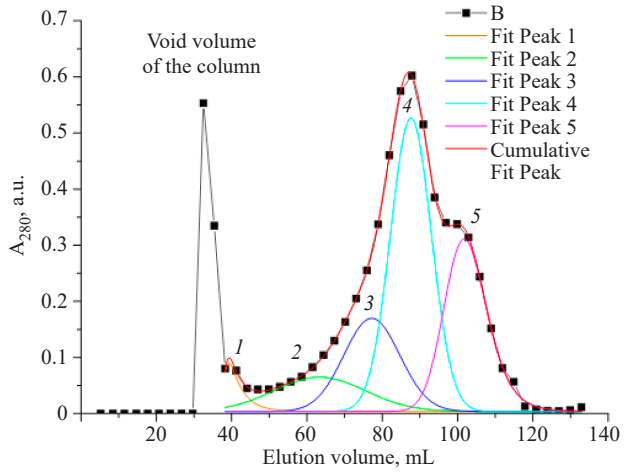

Fig. 6. Decomposition of peaks by Gaussian curves in the elution profile of peptide fractions

Table 3. Characterization of fractions in soy hydrolysate

Name of peak	Peak area	Elution volume, mL	Molecular weight of fraction, kDa	Fraction content, %
Void volume of the column	2.7	32.5	>32.0	13.6
1	0.5	38.0	31.7	2.5
2	1.9	61.5	6.1	9.6
3	3.1	75.6	2.3	15.7
4	7.1	87.5	1.0	35.9
5	4.5	98.8	0.5	22.7

CONCLUSIONS

The conducted research established that the application of enzymatic deglycosylation as a pretreatment of soy flour can be used to significantly increase the degree of protein hydrolysis. It is likely that the cleavage of the

carbohydrate moiety of β-conglycinin leads to a loss of conformational stability in the protein molecule to increase the accessibility of peptide bonds to the action of the proteolytic enzyme. Optimal conditions for the hydrolysis of soy proteins using a neutral protease-based enzyme preparation were determined. The developed approach of preliminary deglycosylation of β-conglycinin can be used to increase the yield of low-molecular-weight peptides in the production of soy hydrolysates.

Acknowledgments

The research was financially supported by the *BelAseptika CJSC* (Republic of Belarus).

Authors' contributions

V.N. Leontiev — planning experiments, discussing results, writing the text of the manuscript.

O.I. Lazovskaya — carrying out experiments, processing and discussing results, writing the text of the manuscript.

The authors declare no conflicts of interest.

REFERENCES

1. Brumă M., Banu I., Vasilean I., Grigore-Gurgu L., Dumitrașcu L., Aprodu I. Influence of soy protein hydrolysates on thermo-mechanical properties of gluten-free flour and muffin quality. *Appl. Sci.* 2024;14(9):3640. https://doi.org/10.3390/app14093640
2. Daliri E.B.-M., Ofosu F.K., Chelliah R., Park M.H., Kim J.-H., Oh D.-H. Development of a soy protein hydrolysate with an antihypertensive effect. *Int. J. Mol. Sci.* 2019;20(6):1496. https://doi.org/10.3390/ijms20061496
3. Muranova T.A., Zinchenko D.V., Miroshnikov A.I. Hydrolysates of soybean proteins for start feeds of aquaculture: behavior of proteins at fermentolysis, compositional analysis of hydrolysates. *Bioorganicheskaya khimiya.* 2019;45(4): 380–390. https://doi.org/10.1134/S0132342319030035 [Muranova T.A., Zinchenko D.V., Miroshnikov A.I. Hydrolysates of soybean proteins for starter feeds of aquaculture: the behavior of proteins upon fermentolysis and the compositional analysis of hydrolysates. *Russ. J. Bioorg. Chem.* 2019;45(3):195–203. https://doi.org/10.1134/S1068162019030038]
4. Peng H., Song X., Chen J., Xiong X., Yang L., Yu C., Qiu M., Zhang Z., Hu C., Zhu S., Xia B., Wang J., Xiong Z., Du L., Yang C. Soybean bioactive peptide supplementation improves gut health and metabolism in broiler chickens. *Poult. Sci.* 2025;104(2):104727. https://doi.org/10.1016/j.psj.2024.104727
5. Ruckman L.A., Petry A.L., Gould S.A., Kerr B.J., Patience J.F. The effects of enzymatically treated soybean meal on growth performance and intestinal structure, barrier integrity, inflammation, oxidative status, and volatile fatty acid production of nursery pigs. *Transl. Anim. Sci.* 2020;4(3):txaa170. https://doi.org/10.1093/tas/txaa170
6. Kostyleva E.V., Sereda A.S., Velikoretskaya I.A., Kurbatova E.I., Tsurikova N.V. Proteases for obtaining of food protein hydrolysates from proteinaceous by-products. *Voprosy pitaniia = Problems of Nutrition*. 2023;92(1):116–132 (in Russ.). https://doi.org/10.33029/0042-8833-2023-92-1-116-132
7. Barać M.B., Stanojević S.P., Jovanović S.T., Pešić M.B. Soy protein modification: a review. *Acta Period. Technol.* 2004;2004(35):3–16. https://doi.org/10.2298/APT0435003B
8. Sokolov D.V., Bolkhonov B.A., Zhamsaranova S.D., Lebedeva S.N., Bazhenova B.A. Enzymatic hydrolysis of soy protein. *Tekhnika i tekhnologiya pishchevykh proizvodstv* (*Food Processing: Techniques and Technology*). 2023;53(1):86–96 (in Russ.). https://doi.org/10.21603/2074-9414-2023-1-2418
9. Knežević-Jugović Z., Culetu A., Mijalković J., Duta D., Stefanović A., Šekuljica N., Đorđević V., Antov M. Impact of different enzymatic processes on antioxidant, nutritional and functional properties of soy protein hydrolysates incorporated into novel cookies. *Foods.* 2023;12(1):24. https://doi.org/10.3390/foods12010024
10. Dent T., Campanella O., Maleky F. Enzymatic hydrolysis of soy and chickpea protein with Alcalase and Flavourzyme and formation of hydrogen bond mediated insoluble aggregates. *Curr. Res. Food Sci.* 2023;6:100487. https://doi.org/10.1016/j.crfs.2023.100487
11. Kempka A.P., Honaiser T.C., Fagundes E., Prestes R.C. Functional properties of soy protein isolate of crude and enzymatically hydrolysed at different times. *Int. Food Res. J.* 2014;21(6):2229–2236.
12. Hrčková M., Rusňáková M., Zemanovič J. Enzymatic hydrolysis of defatted soy flour by three different proteases and their effect on the functional properties of resulting protein hydrolysates. *Czech J. Food Sci.* 2002;20(1):7–14. https://doi.org/10.17221/3503-CJFS
13. Agrawal R.M., Miller M.J., Singh V., Stein H.H., Takhar P.S. Enzymatic hydrolysis and fermentation of soy flour to produce ethanol and soy protein concentrate with increased polyphenols. *J. Am. Oil Chem. Soc.* 2022;99(5):379–391. https://doi.org/10.1002/aocs.12573
14. Chen L., Chen J., Ren J., Zhao M. Effects of ultrasound pretreatment on the enzymatic hydrolysis of soy protein isolates and on the emulsifying properties of hydrolysates. *J. Agric. Food Chem.* 2011;59(6):2600–2609. https://doi.org/10.1021/jf103771x
15. Chen L., Chen J., Ren J., Zhao M. Modifications of soy protein isolates using combined extrusion pre-treatment and controlled enzymatic hydrolysis for improved emulsifying properties. *Food Hydrocoll.* 2011;25(5):887–897. https://doi.org/10.1016/j.foodhyd.2010.08.013
16. Zhao F., Zhang D., Li X., Dong H. High-pressure homogenization pretreatment before enzymolysis of soy protein isolate: the effect of pressure level on aggregation and structural conformations of the protein. *Molecules.* 2018:23(7):1775. https://doi.org/10.3390/molecules23071775
17. Li C., Tian Y., Han J., Lu Y., Zou M., Jia Y., Wang C., Huang L., Wang Z. An innovative method used for the identification of *N*-glycans on soybean allergen β-conglycinin. *Food Sci. Hum. Wellness.* 2023;12(3):842–850. https://doi.org/10.1016/j.fshw.2022.09.025
18. Yang A., Deng H., Zu Q., Lu J., Wu Z., Li X., Tong P., Chen H. Structure characterization and IgE-binding of soybean 7S globulin after enzymatic deglycosylation. *Int. J. Food Prop.* 2018;21(1): 171–182. https://doi.org/10.1080/10942912.2018.1437628
19. Yolandani, Ma H., Li Y., Liu D., Zhou H., Liu X., Wan Y., Zhao X. Ultrasound-assisted limited enzymatic hydrolysis of high concentrated soy protein isolate: alterations on the functional properties and its relation with hydrophobicity and molecular weight. *Ultrason. Sonochem.* 2023;95:106414. https://doi.org/10.1016/j.ultsonch.2023.106414

20. Miller G.L. Use of dinitrosalicylic acid reagent for determination of reducing sugar. *Anal. Chem.* 1959;31(3): 426–428. https://doi.org/10.1021/ac60147a030
21. Hou A., Chen P., Shi A., Zhang B., Wang Y.-J. Sugar variation in soybean seed assessed with a rapid extraction and quantification method. *Int. J. Agron.* 2009;2009:484571. https://doi.org/10.1155/2009/484571
22. Yang C., Liu B., Pan L., Xia D., Sun C., Zheng X., Chen P., Hu H., Zhou Q. Impact of soybean bioactive peptides on growth, lipid metabolism, antioxidant ability, molecular responses, and gut microbiota of oriental river prawn (*Macrobrachium nipponense*) fed with a low-fishmeal diet. *Biology*. 2025;14(1):11. https://doi.org/10.3390/biology14010011
23. Liu C., Wen C., Olatunji O.J., Suttikhana I., Ashaolu T.J. Biologically active peptides from soy: updates on antihypertensive action and gut microbiota modulation. *J. Funct. Foods*. 2024;123:106592. https://doi.org/10.1016/j.jff.2024.106592

About the Authors

Viktor N. Leontiev, Cand. Sci. (Chem.), Head of the Department of Biotechnology, Belarusian State Technological University (13a, Sverdlova ul., Minsk, 220006, Republic of Belarus). E-mail: leontiev@belstu.by. Scopus Author ID 14052100400, RSCI SPIN-code 8653-8538, https://orcid.org/0000-0001-5348-4350

Olesya I. Lazovskaya, Assistant, Department of Biotechnology, Belarusian State Technological University (13a, Sverdlova ul., Minsk, 220006, Republic of Belarus). E-mail: lazovskaya@belstu.by. Scopus Author ID 57205667523, RSCI SPIN-code 9802-5904, https://orcid.org/0009-0006-0919-3736

Об авторах

Леонтьев Виктор Николаевич, к.х.н., заведующий кафедрой биотехнологии, учреждение образования «Белорусский государственный технологический университет» (220006, Республика Беларусь, Минск, ул. Свердлова, д. 13а). E-mail: leontiev@belstu.by. Scopus Author ID 14052100400, SPIN-код РИНЦ 8653-8538, https://orcid.org/0000-0001-5348-4350

Лазовская Олеся Илгамовна, ассистент, кафедра биотехнологии, учреждение образования «Белорусский государственный технологический университет» (220006, Республика Беларусь, Минск, ул. Свердлова, д. 13а). E-mail: lazovskaya@belstu.by. Scopus Author ID 57205667523, SPIN-код РИНЦ 9802-5904, https://orcid.org/0009-0006-0919-3736

Translated from Russian into English by N. Isaeva
Edited for English language and spelling by Thomas A. Beavitt

Tonkie Khimicheskie Tekhnologii = Fine Chemical Technologies.
2026;21(2):188–211
ISSN 2686-7575 (Online)

Biochemistry and biotechnology
Биохимия и биотехнология

UDC 60
https://doi.org/10.32362/2410-6593-2026-21-2-188-211
EDN LAJHYG

RESEARCH ARTICLE

Development and scaling of a chromatographic purification technology for single-domain antibodies fused to the Fc fragment of human IgG1

Dmitry S. Polyansky[1], ✉, Vladimir V. Prokofiev[2], Alexandra V. Samorukova[2], Fedor A. Shishkonakov[2], Dmitry V. Vasiliev[2], Ekaterina I. Ryabova[2], Artem A. Derkaev[2], Andrey I. Gosudarev[2], Yuliya A. Efimova[1], Dmitry V. Shcheblyakov[2], Andrey P. Karpov[2], Ilyas B. Esmagambetov[2]

[1] *MIREA — Russian Technological University (M.V. Lomonosov Institute of Fine Chemical Technologies), Moscow, 119454 Russia*

[2] *N.F. Gamaleya National Research Center for Epidemiology and Microbiology, Ministry of Health of the Russian Federation, Moscow, 123098 Russia*

✉ *Corresponding author, e-mail: polanskiydmitriy15@gmail.com*

Abstract

Objectives. The work set out to develop a chromatographic purification technology for drugs based on modified single-domain antibodies specific to the SARS-CoV-2 virus, as well as to select the optimal parameters for the purification process and scale up this technology for production.

Methods. The study was conducted on a culture of Chinese hamster ovary (CHO) cells GAMP2C5 clone 78, CHO B5 clone 4, and CHO B10 clone 4, which were used to produce modified single-domain antibodies GAMP2C5, GAMB5, and GAMB10, respectively. Chromatographic purification was performed using AKTA pure 25 and AKTA Pilot 600s chromatographs. Quality control of the obtained drugs was carried out using high-performance liquid chromatography, capillary gel electrophoresis, dynamic light scattering, enzyme-linked immunosorbent assay, and polymerase chain reaction.

Results. Multimodal chromatography using CA^{++}Pure-HA (*TOSOH*, Japan) resin based on type 1 ceramic hydroxyapatite can be effectively used for the removal of aggregated antibody forms. The drugs obtained after chromatography using CA^{++}Pure-HA resin based on type 1 ceramic hydroxyapatite have a purity of more than 97%. The developed purification technology was scaled up to purify 200 L of culture fluid after cultivation in an STR 200 bioreactor.

Conclusions. The described technology developed for purifying modified mono-domain antibodies using the CA^{++}Pure-HA multimodal resin based on type 1 ceramic hydroxyapatite allows for the effective removal of low-molecular-weight impurities and aggregated forms of the antibody. The antibodies obtained using the developed technology are characterized by a high degree of purity and the absence of various impurities (residual protein of the producer strain, residual protein A, and residual DNA of the producer strain), as well as offering a hydrodynamic molecular radius corresponding to the theoretical value of monomeric forms of antibodies.

Keywords

chromatographic purification, type 1 karmic hydroxyapatite, multimodal chromatography, purification technology development, scaling

Submitted: 15.01.2026
Revised: 11.02.2026
Accepted: 16.03.2026

For citation

Polyansky D.S., Prokofiev V.V., Samorukova A.V., Shishkonakov F.A., Vasiliev D.V., Ryabova E.I., Derkaev A.A., Gosudarev A.I., Efimova Yu.A., Shcheblyakov D.V., Karpov A.P., Esmagambetov I.B. Development and scaling of a chromatographic purification technology for single-domain antibodies fused to the Fc fragment of human IgG1. *Tonk. Khim. Tekhnol. = Fine Chem. Technol.* 2026;21(2):188–211. https://doi.org/10.32362/2410-6593-2026-21-2-188-211

НАУЧНАЯ СТАТЬЯ

Разработка и масштабирование технологии хроматографической очистки однодоменных антител, слитых с Fc-фрагментом IgG1 человека

Д.С. Полянский[1,✉], В.В. Прокофьев[2], А.В. Саморукова[2], Ф.А. Шишконаков[2], Д.В. Васильев[2], Е.И. Рябова[2], А.А. Деркаев[2], А.И. Государев[2], Ю.А. Ефимова[1], Д.В. Щебляков[2], А.П. Карпов[2], И.Б. Есмагамбетов[2]

[1] *МИРЭА — Российский технологический университет (Институт тонких химических технологий им. М.В. Ломоносова), Москва, 119454 Россия*

[2] *Национальный исследовательский центр эпидемиологии и микробиологии им. Н.Ф. Гамалеи Министерства Здравоохранения Российской Федерации, Москва, 123098 Россия*

✉ *Автор для переписки, e-mail: polanskiydmitriy15@gmail.com*

Аннотация

Цели. Разработать технологию хроматографической очистки для препаратов на основе модифицированных однодоменных антител, специфичных к вирусу SARS-CoV-2. Подобрать оптимальные параметры процесса очистки и масштабировать данную технологию на производстве.

Методы. Исследование проводилось на культуре клеток яичников китайского хомячка CHO GAMP2C5 клон 78, CHO B5 клон 4, CHO B10 клон 4, продуцирующих модифицированные однодоменные антитела GAMP2C5, GAMB5, GAMB10 соответственно. Хроматографическая очистка проводилась с применением хроматографов AKTA Pure 25 и AKTA Pilot 600s. Контроль качества полученных препаратов был осуществлен при помощи высокоэффективной жидкостной хроматографии, капиллярного гель-электрофореза, динамического рассеяния света, иммуноферментного анализа, полимеразной цепной реакции.

Результаты. Мультимодальная хроматография с применением сорбента Ca^{++}Pure-HA (*TOSOH*, Япония) на основе керамического гидроксиапатита 1 типа позволяет эффективно избавляться от агрегированных форм антитела. Препараты, полученные после хроматографии с применением сорбента Ca^{++}Pure-HA на основе керамического гидроксиапатита 1, имеют чистоту более 97%. Разработанная технология очистки была масштабирована до очистки объемом 200 л культуральной жидкости после культивирования в биореакторе STR 200.

Выводы. Разработана технология очистки модифицированных однодоменных антител с применением мультимодального сорбента Ca^{++}Pure-HA на основе керамического гидроксиапатита 1 типа, позволяющая эффективно избавляться от низкомолекулярных примесей и агрегированных форм антитела. Полученные с помощью разработанной технологии антитела характеризуются высокой степенью чистоты, отсутствием различных примесей (остаточного белка штамма продуцента, остаточного белка А и остаточного ДНК штамма продуцента), а также обладают гидродинамическим радиусом молекул, соответствующим теоретическому значению мономерной форм антител.

Ключевые слова

хроматографическая очистка, кармический гидроксиапатит 1 типа, мультимодальная хроматография, разработка технологии очистки, масштабирование

Поступила: 15.01.2026
Доработана: 11.02.2026
Принята в печать: 16.03.2026

Для цитирования

Полянский Д.С., Прокофьев В.В., Саморукова А.В., Шишконаков Ф.А., Васильев Д.В., Рябова Е.И., Деркаев А.А., Государев А.И., Ефимова Ю.А., Щебляков Д.В., Карпов А.П., Есмагамбетов И.Б. Разработка и масштабирование технологии хроматографической очистки однодоменных антител, слитых с Fc-фрагментом IgG1 человека. *Тонкие химические технологии.* 2026;21(2):188–211. https://doi.org/10.32362/2410-6593-2026-21-2-188-211

INTRODUCTION

Currently, many pharmaceutical companies have a number of monoclonal antibodies in their development portfolios, which are widely used in the treatment and prevention of various diseases. In addition to 100 registered antibody-based drugs, about 250 are in various stages of clinical trials [1–11]. Due to the current high demand for therapeutic antibodies in clinical practice and constantly expanding range of their application, it is advisable to optimize and improve the technologies used for their production. The main technology currently used for producing monoclonal antibodies includes two main stages: cell cultivation and chromatographic purification. An example of the development of cell cultivation technology was described earlier [12]. The antibody purification process begins with filtration of the culture fluid using depth and membrane filters to separate the medium containing monoclonal antibodies from the host cells [13].

The standard first stage of the classic three-stage chromatography purification technology consists in the purification of monoclonal antibodies by carrying out affinity chromatography on protein A (or, less commonly, protein G) to remove most impurities by means of the high selectivity of the resin. The principle of the method is based on the interaction of the Fc fragment of the antibody with protein A with high selectivity. Thus, monoclonal antibodies in the culture fluid bind to protein A and remain on the resin to allow unbound impurities to be washed out during column elution. One of the possible intermediate stages of antibody purification is anion exchange chromatography. This stage is necessary for highly efficient purification of the drugs from DNA, viruses, endotoxins, as well as acidic host cell proteins. The process is carried out due to the interaction of the charges of the molecules of the separated substances and the opposite charges of the active groups of the resin, which are covalently bound to the chromatographic matrix [14].

In order to carry out the final stage of polishing from closely related impurities (aggregates, proteolytic cleaved antibody fragments, charged forms of the target antibody), size exclusion or multimodal chromatography is usually used. This method, which separates antibodies according to their size, permits the isolation of a monomeric fraction separated from aggregates and cleaved antibody fragments. However, this type of chromatography (size exclusion chromatography) is difficult to scale up in production. When scaling up purification technology, multimodal resins are typically used. For example, ceramic hydroxyapatite-based Ca^{++}Pure-HA (*TOSOH*, Japan) resins can be conveniently used to separate aggregates from monomers based on their charge and van der Waals forces.

At the N.F. Gamaleya National Research Center for Epidemiology and Microbiology of the Ministry of Health of the Russian Federation (Gamaleya Institute), various single-domain antibodies fused with the Fc fragment of human immunoglobulin class G1, having a broad spectrum of virus-neutralizing activity against various viruses, were obtained [15–23]. The present article describes the development of a chromatographic purification technology for antibodies specific to the SARS-CoV-2 virus. After determining optimal conditions for separating the target antibody fraction from impurities, a system for verifying the purity of the obtained drugs was developed. The developed chromatographic purification technology can be applied to different single-domain antibodies containing variable domains with different specificities. Three different drugs against the SARS-CoV-2 virus developed thanks to the developed purification technology, which showed a purity of more than 98%, are at various stages of clinical trials.

MATERIALS AND METHODS

Cell line

The following cell lines were used in the study:

- Chinese hamster ovary (CHO) cells GAMP2C5 (clone 78) producing a single-domain antibody fused to the human IgG1 Fc fragment P2C5;
- CHO cell culture GAMB5 (clone 04), producing a single-domain antibody fused to the human IgG1 Fc fragment B5;
- CHO cell culture GAMB10 (clone 12), producing a single-domain antibody fused to the human IgG1 Fc fragment B10.

All three cell lines were obtained in the immunobiotechnology laboratory of the Gamaleya Institute based on CHO-K1 cells (Culture and Tissue Collection of the Gamaleya Institute).

Chromatography

The following substances were used for buffers: sodium chloride, calcium chloride, glycine, Tris, and Tris-HCl (*Neofroxx*, Germany); sodium monophosphate, sodium dihydrogen phosphate, polysorbate 80 (*PanReac*, Spain). Buffers for various types of chromatography are listed in Table 1.

Affinity chromatography: an AKTA Pure 25 chromatograph (*Cytiva*, Sweden) was used for chromatography in laboratory conditions. After clarifying one liter of culture fluid by centrifugation at 200g for 10 min, further centrifugation was carried out at 5000g

Table 1. Buffers for different stages of chromatographic purification

Designation	pH	Compound	Types of chromatography	Functions
Buffer A	7.2	Sodium chloride 150 mM Monosodium phosphate 15 mM Sodium dihydrogen phosphate 5 mM Polysorbate 80 0.01%	Affinity Size exclusion	Binding Elution
	5.0		Cation exchange	
	7.2	Sodium chloride 1000 mM Monosodium phosphate 15 mM Sodium dihydrogen phosphate 5 mM Polysorbate 80 0.01%	Hydrophobic interaction	Binding Elution
Buffer B	3.0	Glycine 200 mM Sodium chloride 150 mM Polysorbate 80 0.01%	Affinity	Elution
Buffer C	8.5	Tris-HCl 1 M	Affinity	Adjusting pH
Buffer D	6.8	Tris 20 mM Sodium chloride 150 mM	Anion exchange Multimodal	Equilibration Flushing
Buffer E	7.5	Monosodium phosphate 75 mM Sodium dihydrogen phosphate 25 mM Calcium chloride 4 ppm	Multimodal	Molecule charge Elution

for 20 min. The supernatant was then passed through syringe filters with a pore diameter of 0.8 μm. Prior to application, the pH of the clarified culture fluid was 7.1. The sample was applied to an XK 16/20 column (*Cytiva*, Sweden) with 20 mL of RUselect-P resin (*Greenvan*, Russia). Before applying the sample, the column was equilibrated with 5 column volumes (hereinafter referred to as CV) of buffer A. Chromatography was performed in the apply-remove mode at a rate of 2 mL/min. After applying the sample, the column was washed with 5 CV of buffer A. The sample was then eluted using buffer B with an acidic pH. Following elution, the intermediate product of affinity chromatography was inactivated by incubation for 30 min at a low pH (pH 3.0), then the pH was adjusted to 6.8–6.9 using buffer B.

When scaling up the technology, the culture fluid was pre-filtered using depth and clarification filtration. The volume of culture fluid prior to filtration was 200 L. For chromatography under production conditions, an AKTA Pilot 600s chromatograph (*Cytiva*, Sweden) using an AxiChrom 100/300 chromatography column (*Cytiva*, Sweden) was used with 1 L of RUselect-P resin (*Greenvan*, Russia). The volume of clarified culture fluid after filtration and washing of the filters with buffer solution to displace the residual volume of material was approximately 230 L. After dividing the resulting material into two equal parts, affinity chromatography was performed sequentially. Chromatography was performed as under laboratory conditions other than in terms of the volume and application rate (Table 2). The maximum permissible load on the resin as calculated based on experimental data (not presented in this article) was 30 g/L. Following affinity chromatography, viral inactivation was performed (pH 3, 30 min). Then, after combining both batches of the intermediate product, the next stage of purification was performed.

Anion exchange chromatography: the process was carried out at laboratory scale on an AKTA Pure 25 chromatograph (*Cytiva*, Sweden). Cytiva XK16/20 columns with 5 mL of Q Sepharose™ Fast Flow resin (*Cytiva*, Sweden) were used for this chromatography. The column was equilibrated with 5 CV of buffer G. Chromatography was performed in flow-through mode. The sample was applied at a rate of 0.5 mL/min. Fraction collection began at an optical absorption value of 20 mAU at 280 nm. After applying the sample, the column was rinsed again with buffer G until the optical absorption peak dropped to 20 mAU.

For chromatography under production conditions, an AKTA Pilot 600s chromatograph (*Cytiva*, Sweden) and AxiChrom 70/300 columns (*Cytiva*, Sweden) were used, with 1 L of Q Sepharose™ Fast Flow resin (*Cytiva*, Sweden). Chromatography was performed under conditions similar to laboratory with the exception of the volume and application rate (Table 2).

Table 2. Parameters for different stages of chromatographic purification (CF — culture fluid)

Type of chromatography	Volume of CF, L	Column	Speed, mL/min	Resin volume, mL	Contact time, min
Laboratory scale					
Affinity	1	XK 16/20	8	20	2.5
Anion exchange		XK 16/20	0.5	5	10
Multimodal		XK 16/20	2	5	2.5
Production scale					
Affinity	200	Axichrom 100/300	400	1	2.5
Anion exchange		Axichrom 100/300	100	1	10
Multimodal		Axichrom 100/300	400	1	2.5

Size exclusion chromatography: the process was carried out in laboratory conditions using an AKTA Pure 25 chromatograph (*Cytiva*, Sweden) with an XK26/100 column (*Cytiva*, Sweden) filled with Superdex™ 200 resin (*Cytiva*, Sweden). Chromatography was performed in flow-through mode. The sample was applied at a rate of 5 mL/min. Buffer A was used as the main buffer.

Hydrophobic interaction chromatography: the process was carried out under laboratory conditions on the AKTA Pure 25 system (*Cytiva*, Sweden) using an XK 16/20 column (*Cytiva*, Sweden) and 5 mL of Phenyl Sepharose™ resin (*Cytiva*, Sweden). Sodium chloride was added to samples of 30, 34, and 35 mL of GAMP2C5, GAMB5, and GAMB10 antibodies, respectively, which had previously undergone anion exchange chromatography, to a concentration of 1 M to ensure better binding to the resin. Chromatography was performed in apply-remove mode at a flow rate of 1 mL/min. The column was equilibrated with 5 CV of buffer A at a sodium chloride concentration of 1 M. Next, the sample was applied and the column was washed again with buffer A with a sodium chloride concentration of 1 M until the optical density dropped to 10 mAU. After that, elution was performed in a linear gradient to 100% concentration of buffer A without sodium chloride for 10 min. The target protein (monomeric form) was obtained in the first fractions, followed by oligomeric and aggregate forms of antibodies as the concentration of buffer A increased. The volumes of the target fractions were 17.0, 27.5, and 19.8 mL for GAMP2C5, GAMB5, and GAMB10 antibodies, respectively.

Cation exchange chromatography: the process was carried out on an AKTA Pure 25 chromatography system (*Cytiva*, Sweden) using an XK 16/20 column (*Cytiva*, Sweden) with 5 mL of SP Sepharose™ resin (*Cytiva*, Sweden). Chromatography was performed in flow-through mode at a rate of 1 mL/min. The column was equilibrated with 5 CV of buffer A with a reduced pH (pH 5). After that, samples of GAMP2C5, GAMB5, and GAMB10 antibodies transferred from anion exchange chromatography were applied to the column, 40 mL each; the pH of the samples was also reduced to 5. The target fraction contained monomeric forms of antibodies. Next, buffer A with a pH of 5 and a sodium chloride concentration of 1 M was used to remove aggregate forms of antibodies. The volumes of the target fractions were 18.0, 35.5, and 23.0 mL for GAMP2C5, GAMB5, and GAMB10 antibodies, respectively.

Multimodal chromatography: chromatography was performed on an AKTA Pure 25 chromatograph (*Cytiva*, Sweden) using a Cytiva XK16/20 column packed with 5 mL of Ca^{++}Pure-HA resin (*TOSOH*, Japan) on a laboratory scale. The optimal load for purification on a laboratory scale is the amount of anion exchange chromatography intermediate corresponding to 100 mL of culture fluid per 1 mL of resin. The column was equilibrated with buffer D, then washed with buffer G. Having adjusted the pH of the sample to 6.8, the sample was applied to the column in apply-remove mode at a rate of 2 mL/min. After applying the sample, the column was washed with buffer G, then buffer A was used to elute the monomeric form of antibodies.

At an industrial scale, chromatography was performed using an AKTA Pilot 600s chromatograph (*Cytiva*,

Sweden) and an AxiChrom 140/300 column (*Cytiva*, Sweden) packed with Ca^{++}Pure-HA resin (*TOSOH*, Japan). Chromatography was performed under similar conditions except for the volume and application rate. The parameters of the chromatography processes are shown in Table 2.

Scaling

Depth filtration was performed using a 3M™ Zeta Plus™ Encapsulated System EZP (*3M*, USA) depth filtration unit with 3M™ Zeta Plus™ Encapsulated System Capsule 1.6 m^2 filters (*3M*, USA).

Clarification filtration was performed using an ASF-006 steel filtration apparatus (*Vladisart*, Russia) with Sartoguard PES 0.2 μm (1.6 m^2) clarification capsule filters (Sartorius, Germany).

Concentration and diafiltration: the obtained filtrate was concentrated using tangential flow filtration. Filtration was performed on an AKTA Flux 6 (*Cytiva*, Sweden) system with a SARTOCON Slice Cassette 30 kDa ultrafiltration cartridge (*Sartorius*, Germany).

Antiviral filtration: a Virosart HF 200 cm^2 antiviral filter (*Sartorius*, Germany) was used for the process.

Analytical methods

The concentration of antibodies in the culture fluid and intermediate products was determined by biosensor interferometry as described previously [12].

High-performance liquid chromatography (HPLC): the authenticity of the test sample was determined by size exclusion HPLC. An Agilent 1260 Infinity Capillary LC System (*Agilent Technologies*, USA) was used with a Phenomenex SEC-s3000 column (particle size 5 μm, pore size 290 Å, geometry 300 × 7.8 mM) for analysis. Chromatography was performed under isocratic conditions. At a sample injection volume of 20 μL, the analysis duration was 35 min. The sample was applied at a rate of 0.5 mL/min. The UV detector was set to a wavelength of 214 nm.

Residual protein A: to determine the amount of residual protein A, the Immunoenzymetric Assay for the Measurement of Protein A F400 kit (*Cygnus Technologies*, USA) was used according to the manufacturer's protocol.

Residual DNA of the producer strain: to determine the amount of residual DNA of the producer strain, the PrepSEQ™ Residual DNA Sample Preparation Kit (*Thermo Fisher Scientific*, USA) and resDNASEQ™ Quantitative CHO DNA Kit (*Thermo Fisher Scientific*, USA) were used, as well as DNA extraction kits according to the manufacturers' protocols.

Residual protein of the producer strain: to determine the amount of residual protein of the producer strain, the Immunoenzymetric Assay for the Measurement of Chinese Hamster Ovary Host Cell Proteins F550 (*Cygnus*, USA) kits were used according to the manufacturer's protocol.

Particle size: particle size in solution was measured using dynamic light scattering with a Zetasizer Nano ZS (*Malvern*, United Kingdom) in accordance with the manufacturer's instructions [24].

Capillary gel electrophoresis: this analysis was performed using a Beckman/PA800 plus capillary electrophoresis system (*Beckman*, USA). The test and standard samples were diluted with purified water to a concentration corresponding to the antibody concentration. For this purpose, 12 μL of the sample and a volume of purified water calculated using the formula $V = 1.5 \times C - 12$ were placed in a 0.5 mL microcentrifuge tube, where C is the protein concentration in the sample (mg/mL). The capillary was cut such that the total length was 30.2 cm, with an effective length of approximately 20.2 cm. The capillary was installed in the cartridge in accordance with the device operating instructions, with an aperture of 100 × 200 μm.

RESULTS AND DISCUSSION

The Gamaleya Institute has developed GamCoVimab, a drug based on humanized monoclonal antibodies for the early etiotropic treatment of coronavirus infection caused by the SARS-CoV-2 virus. The active ingredient of the drug is the heavy-chain monoclonal antibody GAMP2C5, which is a single-domain antibody P2C5 fused with the Fc fragment of human IgG1 [20, 21]. Subsequently, due to the emergence of new variants of the SARS-CoV-2 virus, two new heavy-chain monoclonal antibodies (GAMB5 and GAMB10) were developed [12] (Fig. 1).

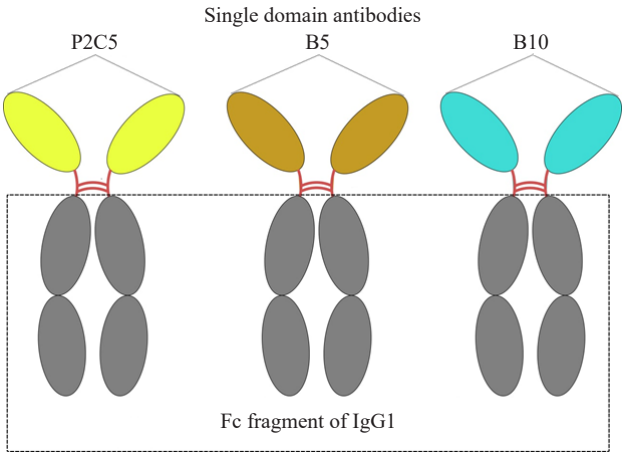

Fig. 1. Schematic representation of single-domain antibodies fused with the Fc fragment of human IgG1

In this study, a technology for purifying heavy chain antibodies using a multimodal resin based on ceramic

hydroxyapatite was developed and scaled up. The culture fluid for chromatographic purification was obtained by culturing CHO cells that stably produce GAMP2C5, GAMB5, and GAMB10 antibodies. These cell lines were cultivated using a technology developed earlier [12]. Initially, the laboratory technology for chromatographic purification consisted of three stages (Fig. 2).

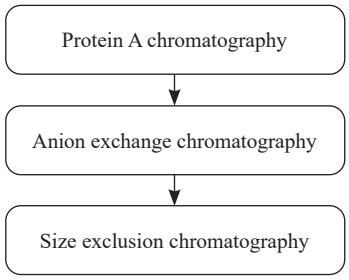

Fig. 2. Laboratory scheme for chromatographic purification of antibodies fused with the Fc fragment of human IgG1

Affinity chromatography

The classic first step in purifying monoclonal antibodies is based on affinity chromatography. Elution of the target fraction containing monoclonal antibodies is achieved by lowering the pH of the elution buffer to 3.0–4.0, which breaks the interaction between the Fc fragment and protein A. Since the antibodies under study, GAMP2C5, GAMB5, and GAMB10 contain the human IgG1 Fc fragment, affinity chromatography on protein A can also be used for their purification. Affinity chromatography allows obtaining a drug with 95–99% purity; however, residual DNA from producer cells may be present in the drug, as well as protein A, which may enter the eluate during the elution of monoclonal antibodies.

The total amounts of antibodies from intermediate products transferred from the affinity chromatography stage are shown in Table 3.

The intermediate products were then transferred to the anion exchange chromatography stage.

Anion exchange chromatography

The process was carried out in a skip mode. Due to the interaction between the charges of the separated impurities and the opposite charges of the active groups covalently linked to the resin matrix or membrane, the impurities remained bound to the active groups, while the target proteins passed through the column.

The total amounts of antibodies with intermediate products transferred from the anion exchange chromatography stage are shown in Table 4.

The intermediate products were then transferred to the size exclusion chromatography stage.

Size exclusion chromatography

As a reference stage for separating the target fraction from aggregates, as well as various non-full-size forms, the laboratory uses size exclusion chromatography based on Superdex™ 200 resin. The molecules of the chromatographic mixture are separated according to

Table 3. Total amounts of antibodies after the affinity chromatography stage

Antibody	Total amount of antibody before affinity chromatography, mg	Total amount of antibody after affinity chromatography, mg
GAMP2C5	350.0 ± 10.0	320.0 ± 10.0
GAMB5	400.0 ± 10.0	360.0 ± 10.0
GAMB10	480.0 ± 10.0	415.0 ± 10.0

Table 4. Total amounts of antibodies after the anion exchange chromatography stage

Antibody	Total amount of antibody after affinity chromatography, mg	Total amount of antibody after anion exchange chromatography, mg
GAMP2C5	320.0 ± 10.0	302.0 ± 10.0
GAMB5	360.0 ± 10.0	340.0 ± 10.0
GAMB10	415.0 ± 10.0	390.0 ± 10.0

Table 5. Total amounts of antibodies after the size exclusion chromatography stage

Antibody	Total amount of antibody after anion exchange chromatography, mg	Total amount of antibody after size exclusion chromatography, mg
GAMP2C5	302.0 ± 10.0	264.0 ± 10.0
GAMB5	340.0 ± 10.0	300.0 ± 10.0
GAMB10	390.0 ± 10.0	340.0 ± 10.0

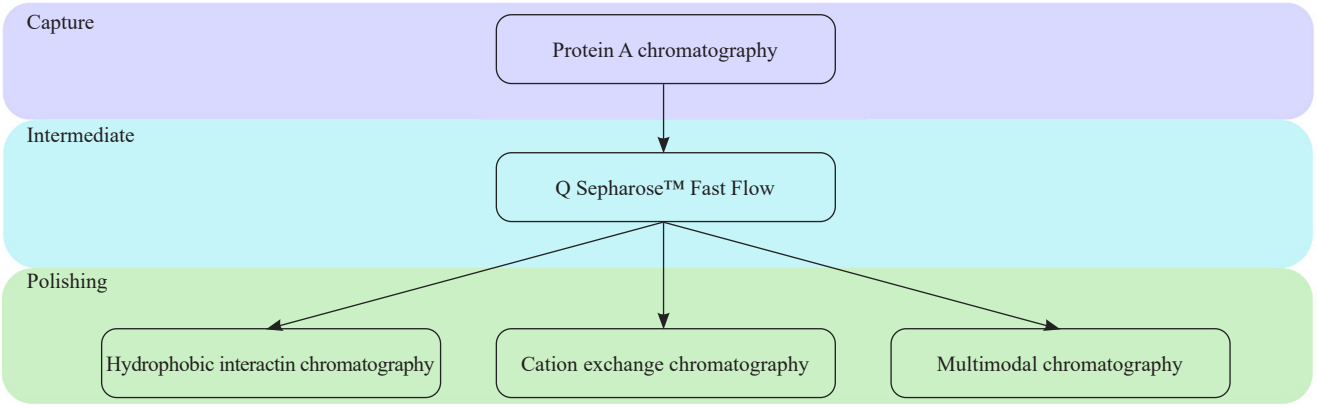

Fig. 3. Scheme for selecting a resin for the polishing final stage

their size due to differences in their ability to penetrate the pores of the resin. The aggregate forms are released in the first fractions, followed by the dimeric forms to ultimately release the target monomeric forms. To obtain sufficient resolution during size exclusion chromatography, the sample is preconcentrated on centrifugal filters with a cut-off diameter of 30 kDa prior to application to ensure an optimal sample volume of no more than 10% of the column volume.

The total amounts of antibodies with intermediate products transferred from the size exclusion chromatography stage are presented in Table 5.

Since laboratory technology using an exclusive resin is difficult to scale up for production volumes, a technology using various resins was developed. The research scheme is presented in Fig. 3.

One of the first resins studied was the hydrophobic resin Phenyl Sepharose™, whose principle of action is based on the reversible interaction of proteins with hydrophobic ligands immobilized on the resin surface. Here, target antibodies interact through hydrophobic amino acids. To increase the interaction force (hydrophobic effect), the concentration of sodium chloride in buffer A was increased to 1 M. Then the column was equilibrated with 3 CV of buffer A. In the test sample, the concentration of sodium chloride was also brought to 1 M and then applied to the column. After applying the sample, the resin was again washed with buffer A containing 1 M sodium chloride. Next, elution was performed in a linear gradient up to 100% concentration of buffer A without sodium chloride for 10 min. The target protein (monomeric form) was obtained in the first fractions, followed by the aggregate form as the salt concentration decreased.

The total amounts of antibodies from the intermediate products transferred from the hydrophobic chromatography stage using Phenyl Sepharose™ resin are presented in Table 6.

Cation exchange chromatography was also used to separate the monomer fraction from the aggregates. This type of chromatography is characterized by the interaction between the charges of the molecules of the substances being separated and the opposite charges of the active groups of the resin. In this study, we used the cation exchange resin SP Sepharose™. The active group of this resin is sulfopropyl, which is negatively charged. Since aggregates usually have a higher total positive charge, they should bind to the resin more strongly than the monomeric form. Chromatography was performed in flow-through mode. After lowering the pH of the solution to 5.0, the column was equilibrated with buffer A. Then, before applying the sample, the pH of the

Table 6. Total amounts of antibodies after the hydrophobic chromatography stage using Phenyl Sepharose™ resin

Antibody	Total amount of antibody after anion exchange chromatography, mg	Total amount of antibody after hydrophobic chromatography, mg
GAMP2C5	302.0 ± 10.0	150.0 ± 10.0
GAMB5	340.0 ± 10.0	198.0 ± 10.0
GAMB10	390.0 ± 10.0	220.0 ± 10.0

Table 7. Total amounts of antibodies after the cation exchange chromatography stage using SP Sepharose™ resin

Antibody	Total amount of antibody after anion exchange chromatography, mg	Total amount of antibody after cation exchange chromatography, mg
GAMP2C5	302.0 ± 10.0	170.0 ± 10.0
GAMB5	340.0 ± 10.0	214.0 ± 10.0
GAMB10	390.0 ± 10.0	268.0 ± 10.0

Table 8. Total amounts of antibodies after the multimodal chromatography stage using Ca^{++}Pure-HA resin

Antibody	Total amount of antibody after anion exchange chromatography, mg	Total amount of antibody after multimodal chromatography, mg
GAMP2C5	302.0 ± 10.0	260.0 ± 10.0
GAMB5	340.0 ± 10.0	301.0 ± 10.0
GAMB10	390.0 ± 10.0	344.4 ±10.0

antibody solution was lowered to 5.0. The target fraction contained monomeric forms of antibodies; the aggregate forms of antibodies were subsequently removed using a high-salt buffer (1 M NaCl). The total amounts of antibodies from the intermediate products transferred from the cation exchange chromatography stage using SP Sepharose™ resin are presented in Table 7.

Furthermore, for the final stage, we used a multimodal Ca^{++}Pure-HA resin based on type 1 ceramic hydroxyapatite.

Type 1 hydroxyapatite has three interaction groups:
1) Ca^{2+};
2) phosphate groups PO_4^{3-};
3) hydroxide groups OH^-.

The sugar phosphate backbone of nucleic acids reacts with calcium and hydroxyl groups, while antibodies interact with calcium via the carboxyl group −OOC and with phosphate groups via amino groups ^+H_3N. First, chromatography was performed on a laboratory scale using a Cytiva XK16/20 column packed with 5 mL of type 1 hydroxyapatite. Before applying the sample, the column was sequentially washed with buffer D and buffer G. After adjusting the pH to 6.8, the sample was applied to the column. Chromatography was performed in the apply-remove mode at a flow rate of 10 mL/min. Then, applying the sample, the column was washed with buffer G. Next, buffer A was used to elute the monomeric form of antibodies. The total amounts of antibodies from the intermediate products transferred from the multimodal chromatography stage using Ca^{++}Pure-HA resin are presented in Table 8.

Purity assessment

In order to select the final resin for the final purification stage, it was necessary to determine the authenticity and purity of the obtained drugs. Analytical methods were used to confirm the purity of the drugs, including analysis for residual protein of the producer strain, residual DNA of the producer strain, and residual amount of protein A.

To confirm the authenticity of the drug, the mobility of molecules was analyzed using gel filtration by HPLC and capillary gel electrophoresis of protein, while particle size was determined by dynamic light scattering (Fig. 4).

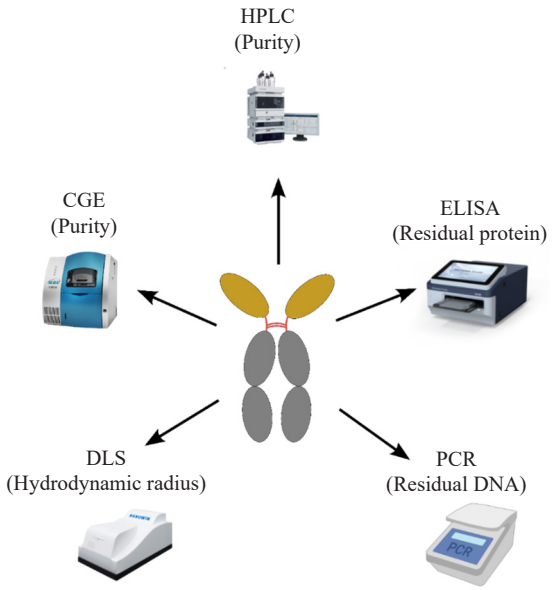

Fig. 4. Methods for assessing the purity of purified antibodies. HPLC—high-performance liquid chromatography; ELISA—enzyme-linked immunosorbent assay; PCR—polymerase chain reaction; DNA—deoxyribonucleic acid; CGE—capillary gel electrophoresis; DLS—dynamic light scattering

As a result of analyzing the presence of residual DNA from the CHO cell-producing strain using real-time polymerase chain reaction in samples of purified GAMP2C5, GAMB5, and GAMB10 antibodies on the three resins studied, it was established that the amount of residual DNA does not exceed the permissible limits at no more than 10 pg/mg of protein[1]. Immunoenzymetric analysis of purified GAMP2C5, GAMB5, and GAMB10 on three test resins showed that residual proteins from the producer strain are within acceptable concentrations, amounting to no more than 1 μg/mg of protein, while the residual protein A content is no more than 25 ng/mg of protein.

To study the authenticity of the drugs, gel filtration was performed using HPLC. The results obtained were exported to Chromeleon version 7.0 software (*Thermo Fisher Scientific*, USA) for data processing. As a result, it was found that, following chromatographic purification on Ca^{++}Pure-HA resin, the antibodies under study have a purity of 99% for all three samples. This is in contrast to the antibodies submitted for analysis after Phenyl Sepharose resins: 80% for GAMB5, 94% for GAMB10, and 60% for GAMP2C5. The purity after chromatography using SP Sepharose™ resin was 95% for GAMB5, 98% for GAMB10, and 79% for GAMP2C5. In the drug obtained after purification on Ca^{++}Pure-HA resin, there was mainly one peak and no significant impurities (Fig. 5).

[1] Note for Guidance on Production and Quality Control of Medicinal Products Derived by Recombinant DNA Technology, 3AB1A. Production and Quality Control of Medicinal Products Derived by Recombinant DNA Technology. 1995. P. 214.

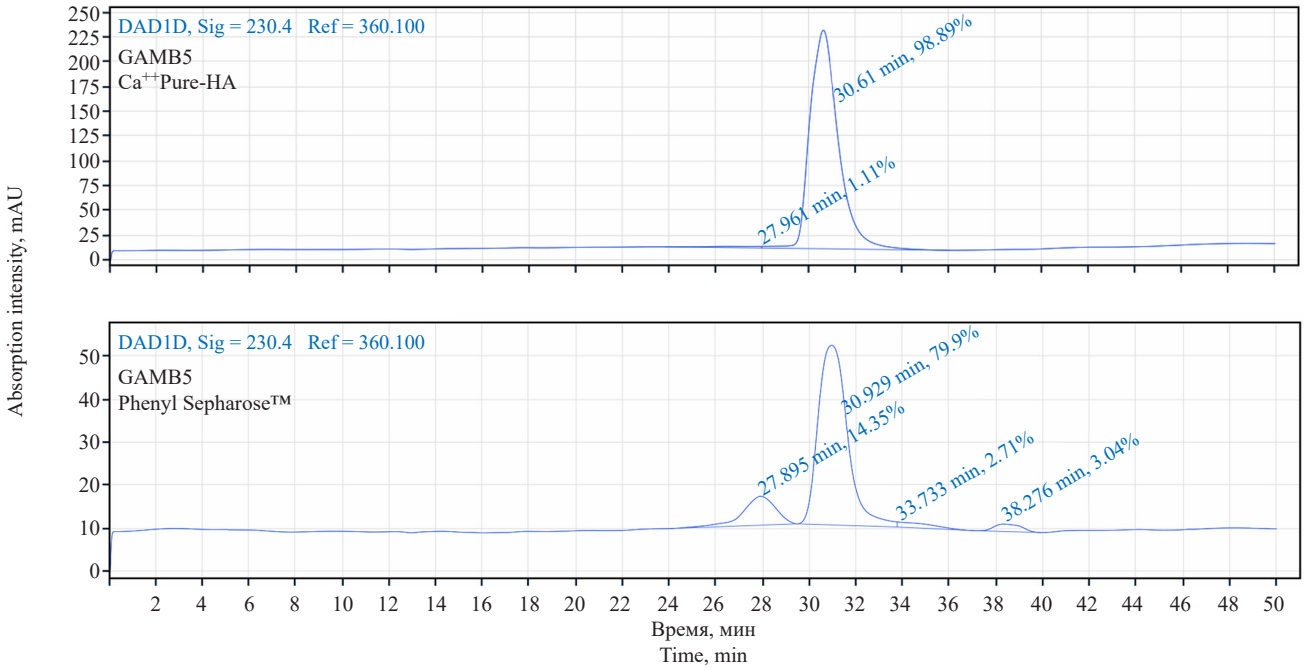

Fig. 5. Evaluation of the degree of purity by gel filtration after the final stage of purification

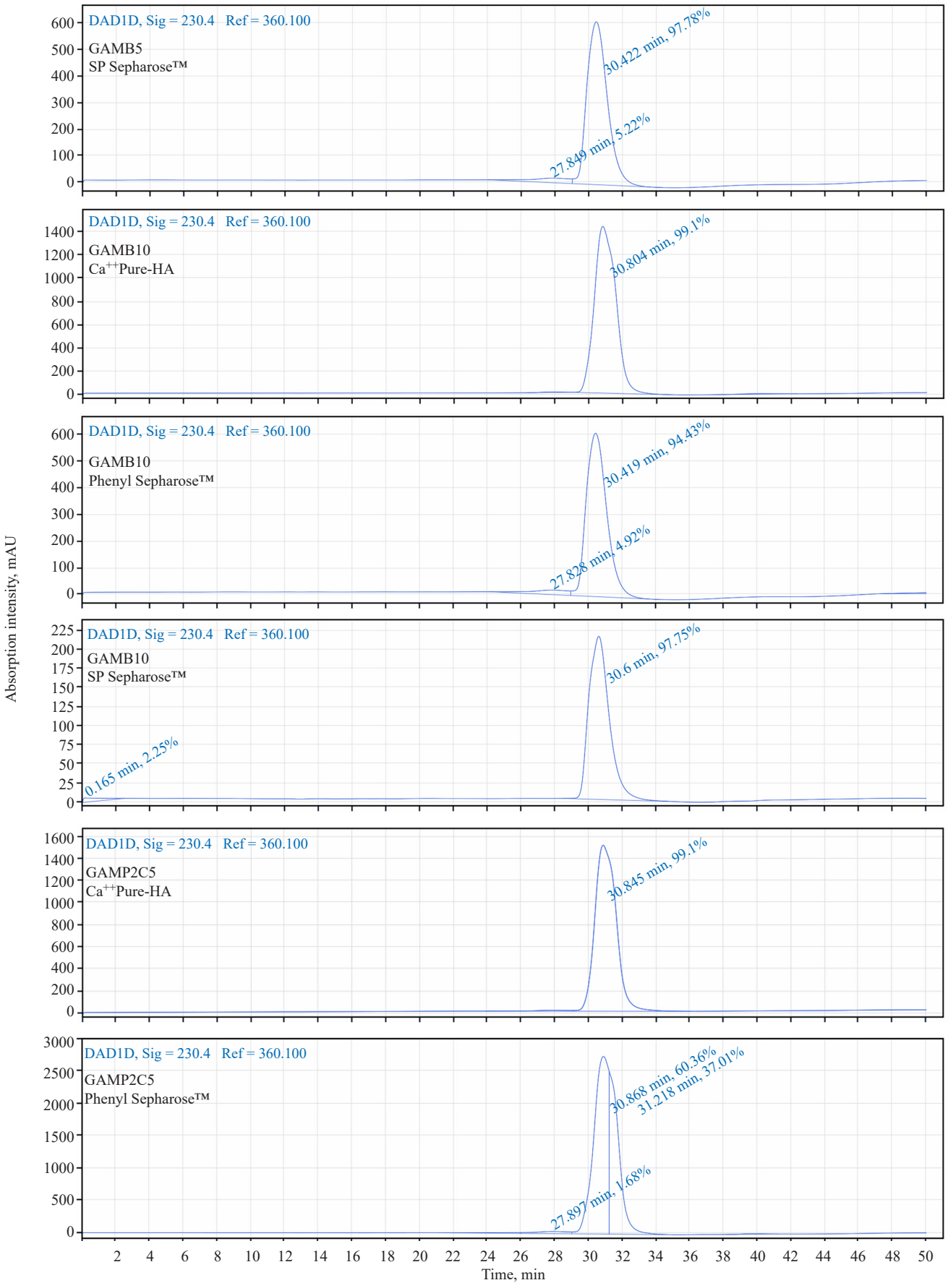

Fig. 5. Evaluation of the degree of purity by gel filtration after the final stage of purification (continued)

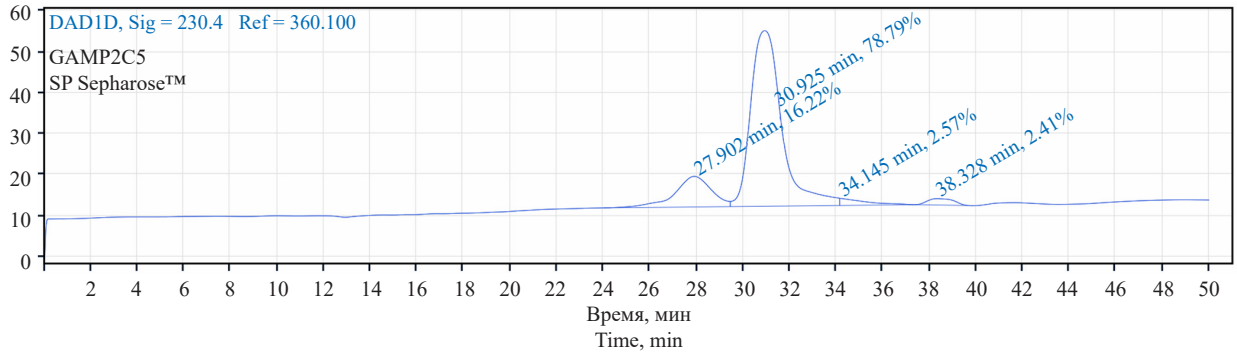

Fig. 5. Evaluation of the degree of purity by gel filtration after the final stage of purification (continued)

In addition to the gel filtration method, capillary electrophoresis was used to determine the purity of the antibodies under study. This method is based on the separation of mixture components in a quartz capillary under the influence of an electric field. The resulting electropherograms were exported to Chromeleon version 7.0 software for data processing. For the obtained antibodies, it was shown that, after using the Phenyl Sepharose™ resin, the purity of the samples was 83% for GAMB5, 83% for GAMB10, and 90% for GAMP2C5. Conversely, the purity of the samples obtained after using the SP Sepharose™ resin was 82% for GAMB5, 81% for GAMB10, and 86% for GAMP2C5. Meanwhile, the sample purity after using the Ca^{++}Pure-HA resin was 97% for GAMB5, 97% for GAMB10, and 99% for GAMP2C5 (Fig. 6).

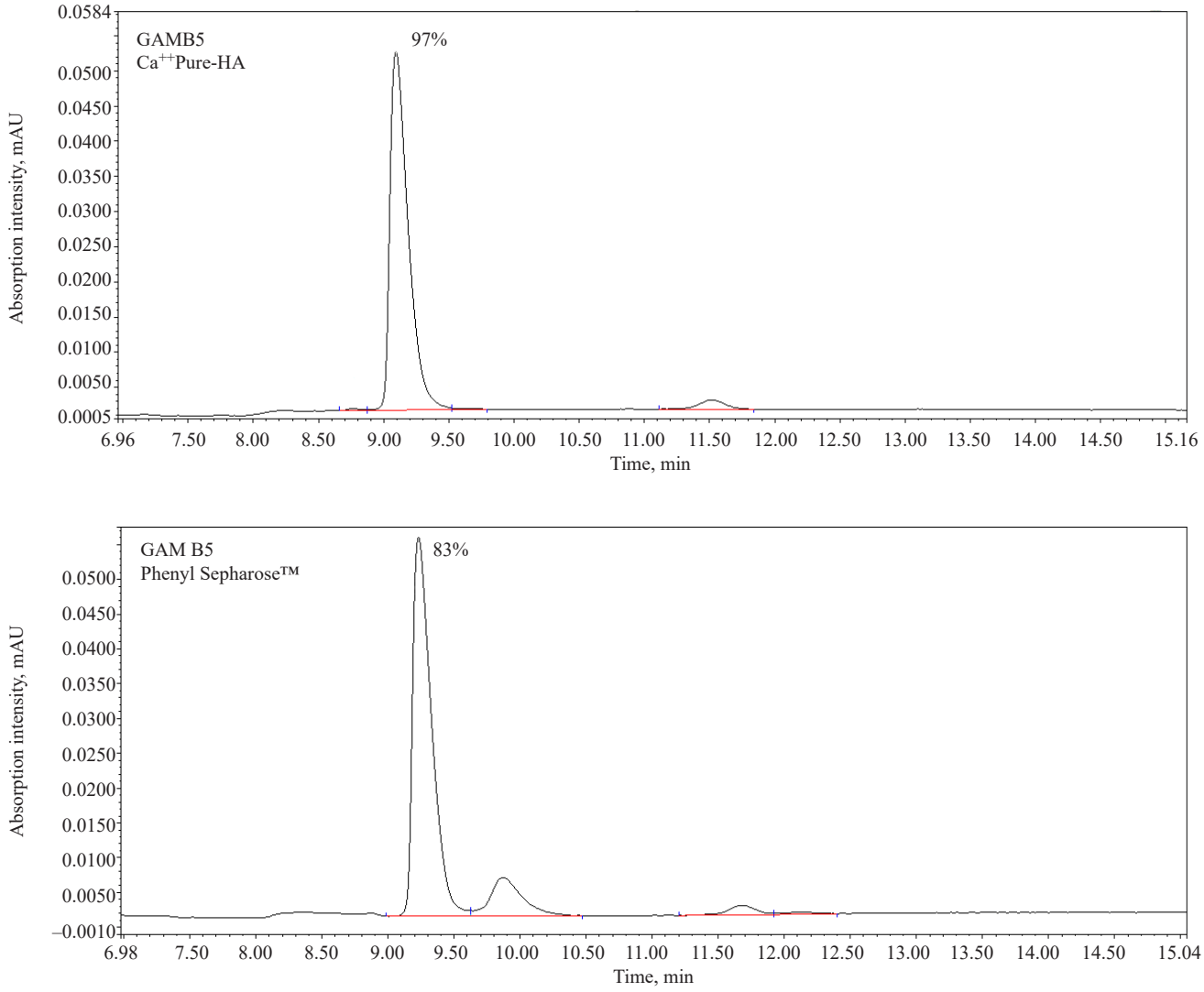

Fig. 6. Evaluation of purity by capillary gel electrophoresis after the final stage of purification

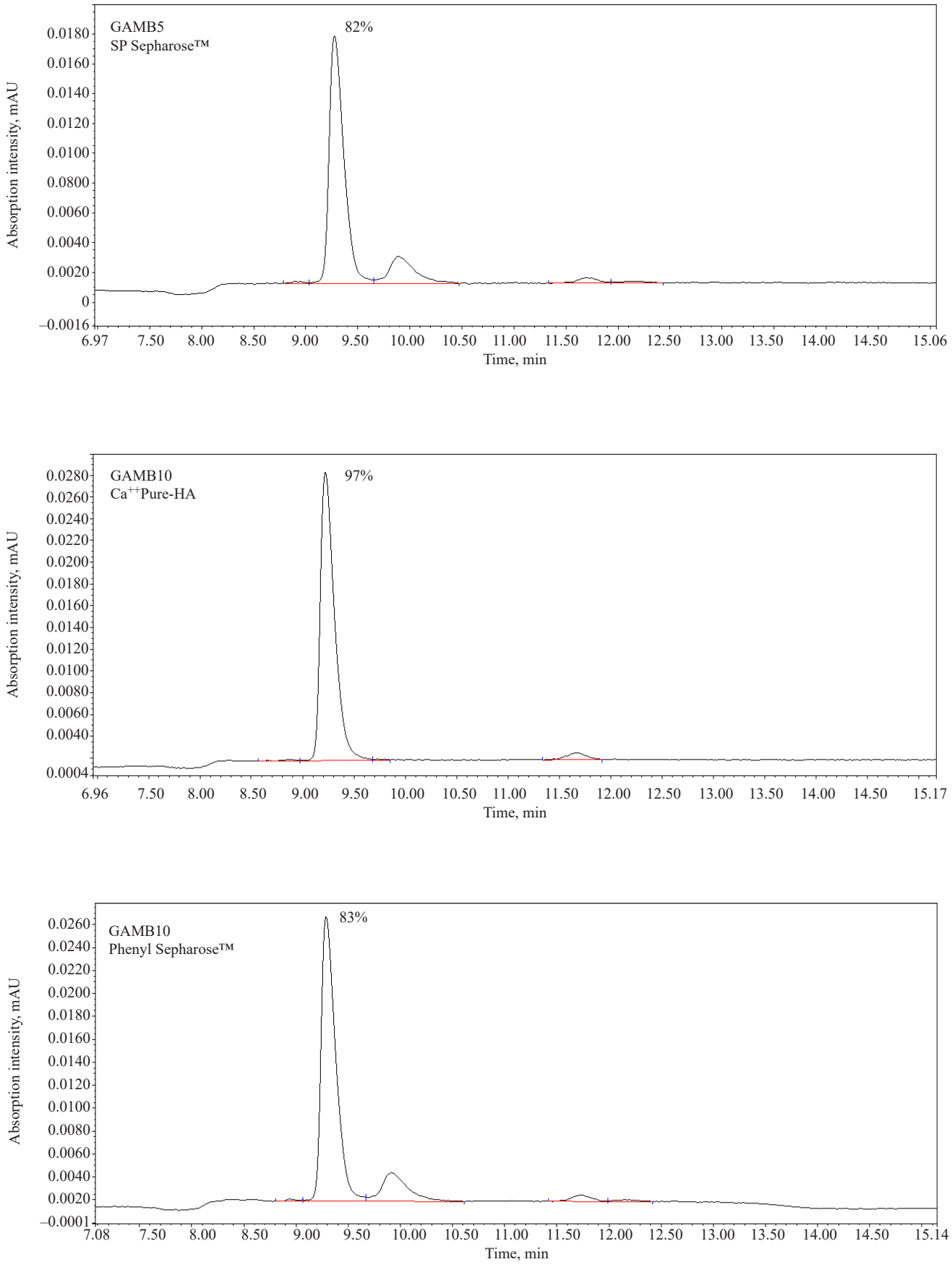

Fig. 6. Evaluation of purity by capillary gel electrophoresis after the final stage of purification (continued)

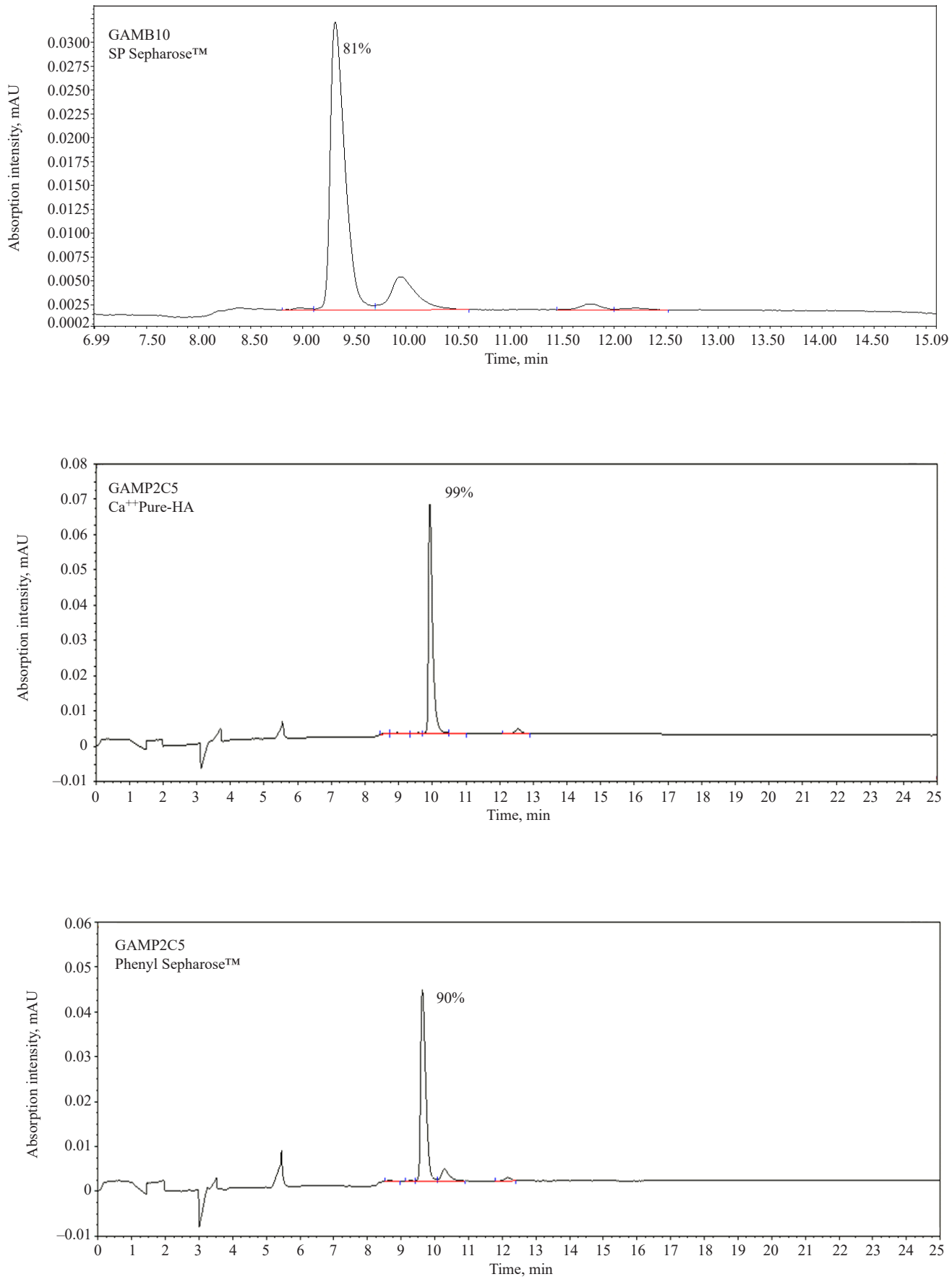

Fig. 6. Evaluation of purity by capillary gel electrophoresis after the final stage of purification (continued)

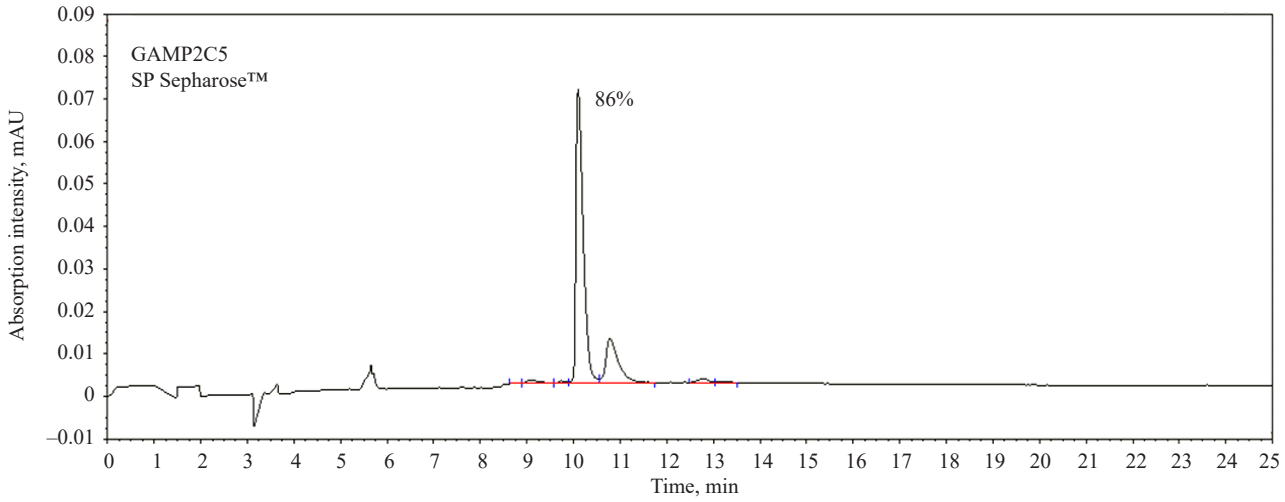

Fig. 6. Evaluation of purity by capillary gel electrophoresis after the final stage of purification (continued)

After purification using various resins, type 1 hydroxyapatite was selected as the most promising resin for the final purification stage. This decision was due to the impossibility of finding conditions for separating the target fraction from residual aggregates and non-target antibody forms using other resins.

Furthermore, to evaluate the quality of the antibodies obtained, we used the dynamic light scattering method, which allows us to determine the size of molecules and the presence of large agglomerates of particles that cannot be determined by electrophoresis and HPLC. It was shown that after purification of all three antibodies, GAMP2C5, GAMB5, and GAMB10, on the multimodal resin Ca^{++}Pure-HA, the presence of one main peak corresponding to molecules with an average diameter of 7.6–7.8 nm was detected (Fig. 7).

Scaling

After conducting laboratory-scale experiments and confirming the authenticity and purity of the drug, this technology was scaled up for production under good manufacturing practice conditions. The purification scheme for scaling up is shown in Fig. 8.

After scaling up the cultivation and purification process, the total amount of the target product remained virtually unchanged. The difference in the amount of intermediate product obtained using laboratory and scaled-up production technology was no more than 10%. The data are presented in Table 9.

During scaling, an analysis was also conducted for the content of residual proteins of the producer strain (the content was no more than 1 μg/mg of protein), residual DNA of the producer strain (no more than 10 pg/mg of protein), and residual protein A content (no more than 25 ng/mg of protein). The impurity content depending on the scale of production is shown in Table 10.

To confirm the purity of the drugs during technology scaling, gel filtration was performed using HPLC. The impurity content was no more than 5%. The degree of purity is shown in Table 11. Chromatograms for each antibody are shown in Fig. 9.

In order to study changes in the size and structure of molecules during scaling, capillary electrophoresis was also performed. The percentage of target protein content in the intermediate product is shown in Table 12. Chromatograms for each antibody are shown in Fig. 10.

To further confirm the successful scaling of the chromatographic purification technology for modified single-domain antibodies, the dynamic light scattering method was used. After purification of all three antibodies, GAMB5, GAMP2C5, and GAMB10, on the multimodal resin Ca^{++}Pure-HA at the production facility in accordance with GMP (Good Manufacturing Practice) principles, values were detected that correspond to those previously obtained during purification on a laboratory scale (Fig. 11).

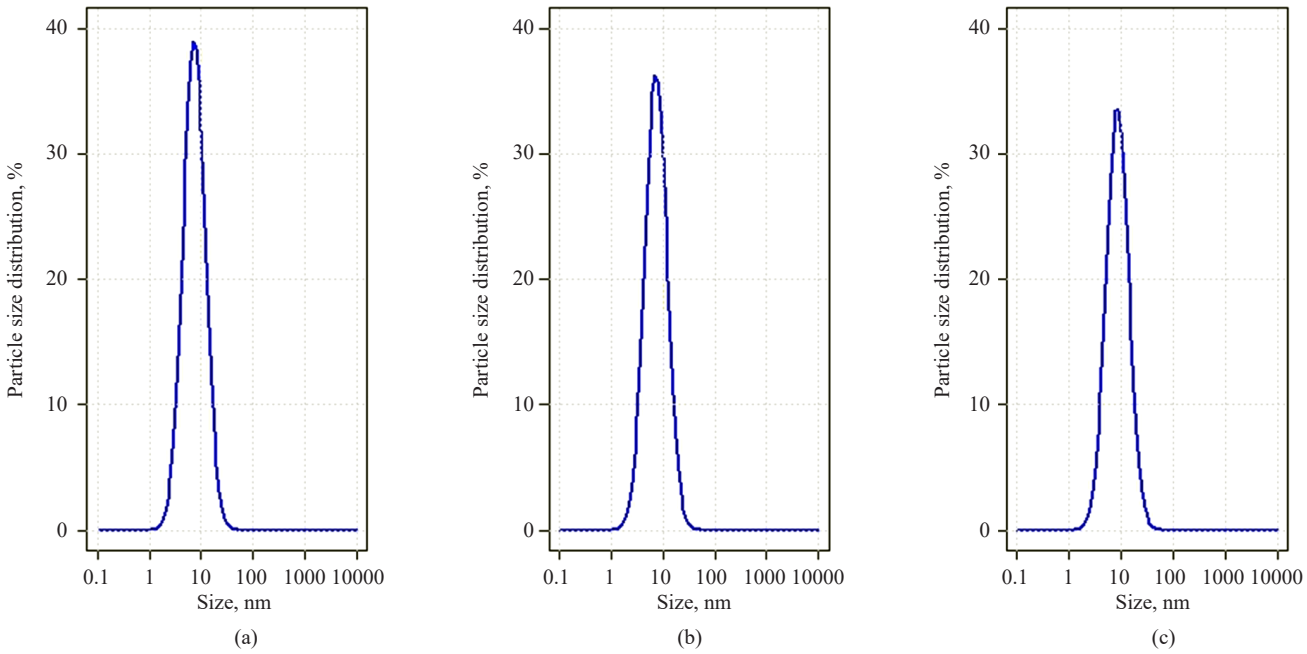

Fig. 7. Particle size evaluation after the final stage of cleaning using dynamic light scattering at the laboratory scale: (a) GAMB5, (b) GAMP2C5, and (c) GAMB10

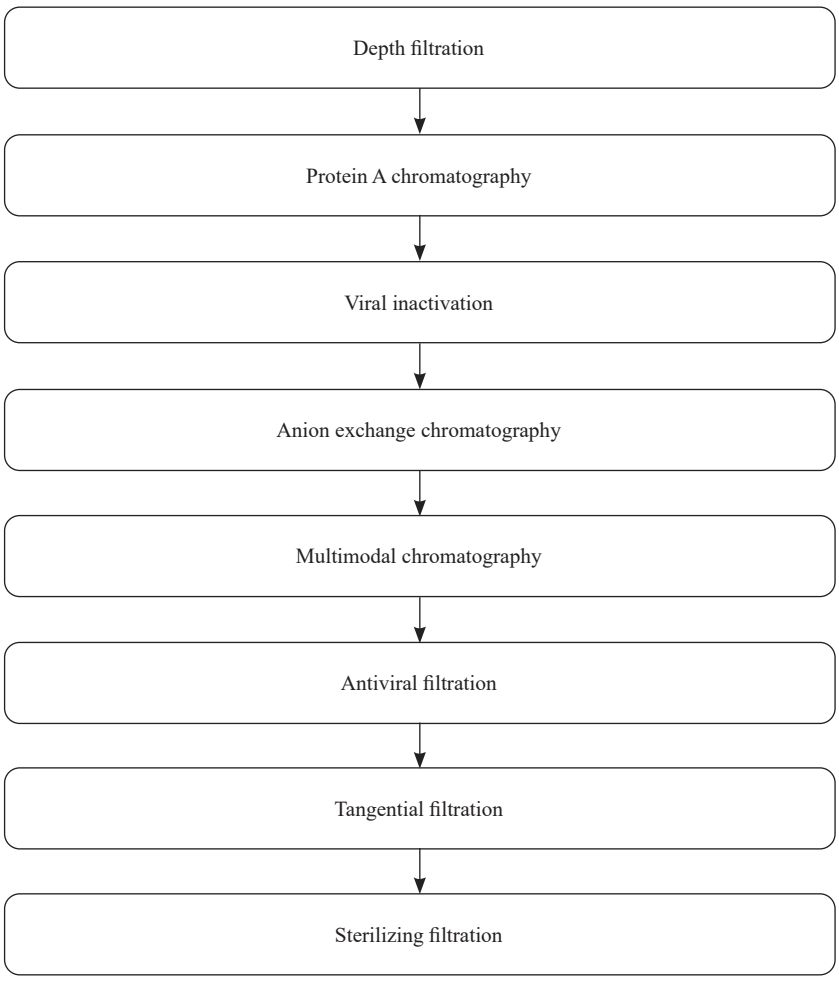

Fig. 8. Scheme of chromatographic purification technology during scaling

Table 9. Total amount of target protein after 3 stages of chromatographic purification

Antibody	Laboratory scale		Production scale	
	Volume of CF, L	Total amount of antibody after purification, mg	Volume of CF, L	Total amount of antibody after purification, g
GAMP2C5	1.0	260.0	200.0	46.0
GAMB5		301.0		58.0
GAMB10		344.0		64.0

Table 10. Impurity content at scaling

Antibody	Laboratory scale			Production scale		
	Residual protein of the producer strain, µg/mg	Residual protein A, ng/mg	Residual DNA, pg/mg	Residual protein of the producer strain, µg/mg	Residual protein A, ng/mg	Residual DNA, pg/mg
GAMP2C5	0.111	2.85	Not defined	0.241	3.29	Not defined
GAMB5	0.029	4.62	3.2	0.107	2.85	Not defined
GAMB10	0.036	Not defined	Not defined	0.022	2.0	4.0

Table 11. Target protein content in the intermediate product (HPLC)

Intermediate product	Target protein content, %
GAMP2C5	96.1
GAMB5	98.9
GAMB10	99.89

Table 12. Percentage of target protein content in the intermediate product (capillary electrophoresis)

Intermediate product	Target protein content, %
GAMP2C5	92.3
GAMB5	94.0
GAMB10	95.8

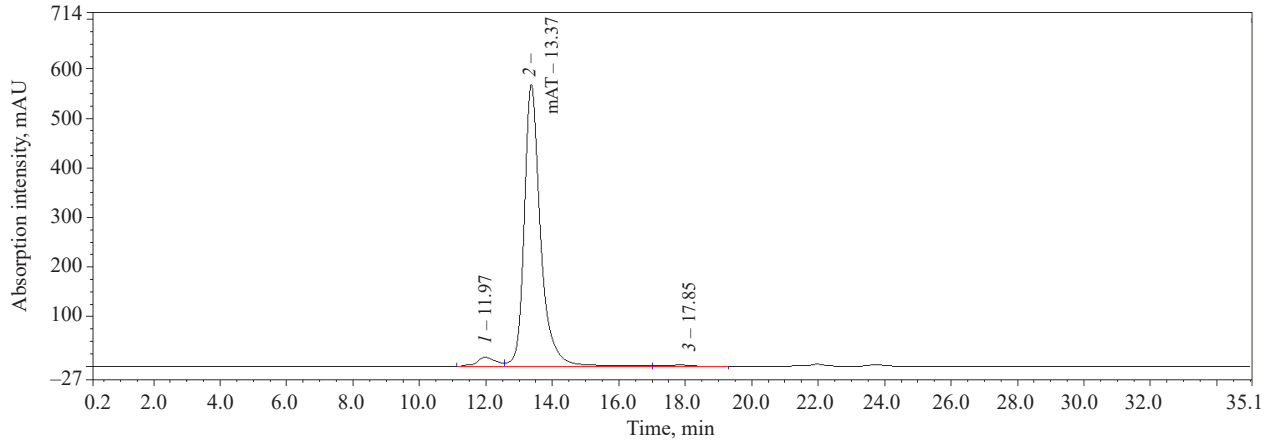

(a)

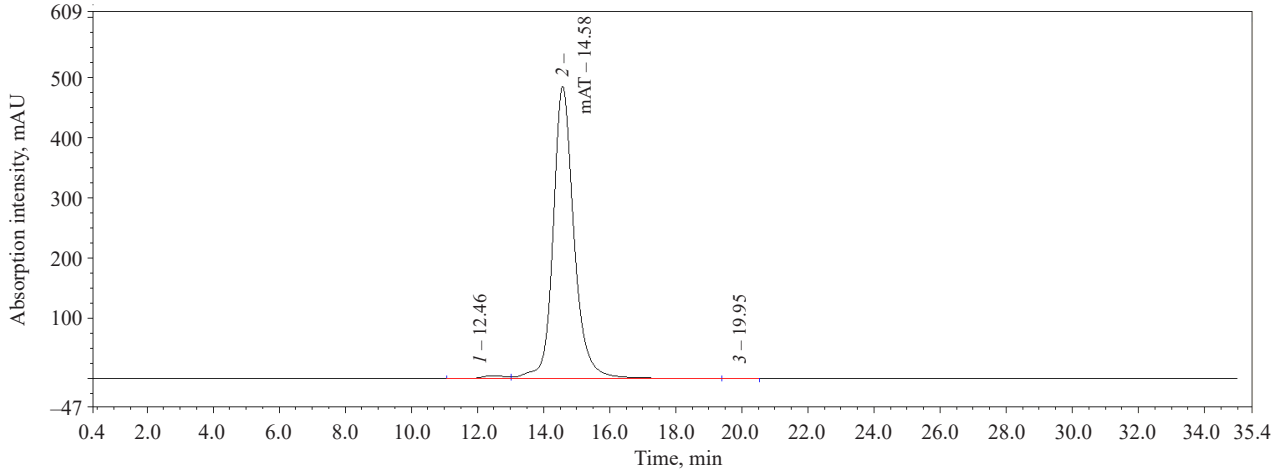

(b)

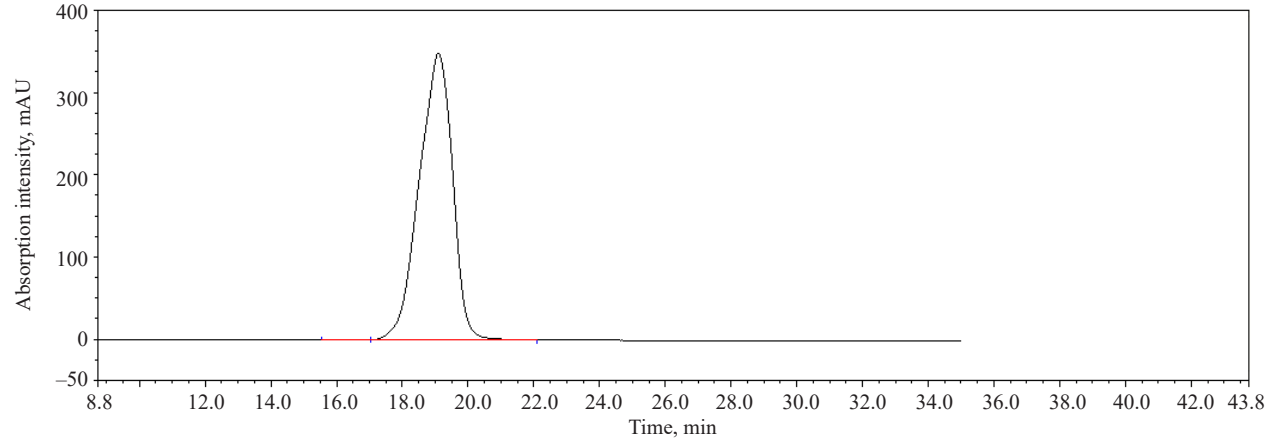

(c)

Fig. 9. Chromatograms of semifinished products obtained by gel filtration after the final stage of purification; the target protein content: (a) GAMP2C5, 96.1%; (b) GAMB5, 99.8%; (c) GAMB10, 99.89%

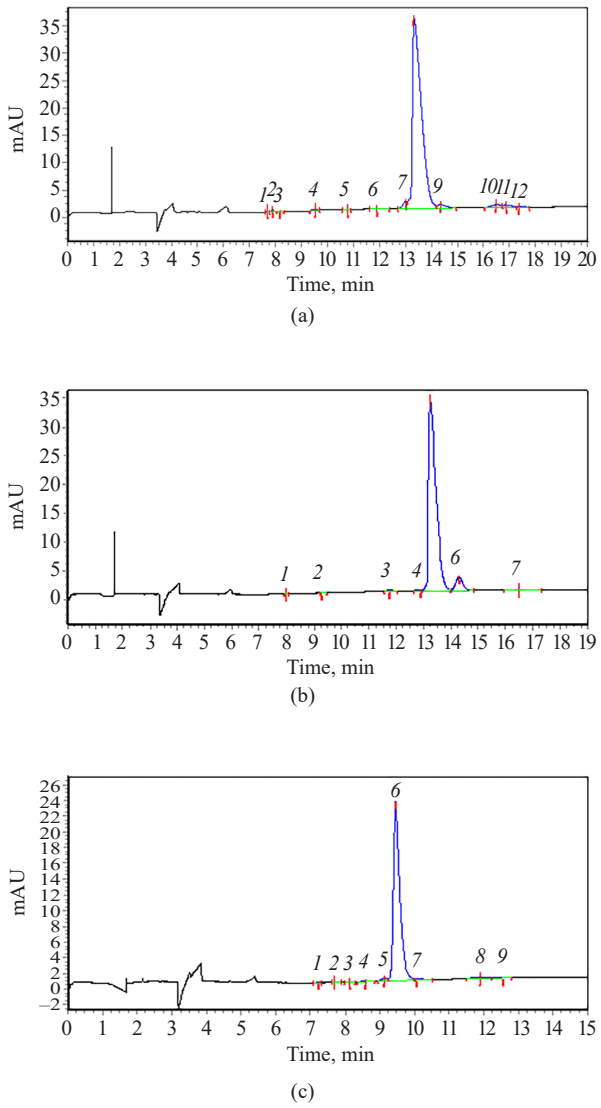

Fig. 10. Chromatograms of semifinished products obtained by capillary electrophoresis after the final stage of purification; the target protein content: (a) GAMP2C5, 92.3%; (b) GAMB5, 94.0%; (c) GAMB10, 95.8%

CONCLUSIONS

As a result of the study, a laboratory purification technology was developed for single-domain antibodies modified with the human IgG1 Fc fragment specific to the SARS-CoV-2 virus. In the first stage of chromatographic purification, a protein A-based resin was used. For the intermediate stage, a quaternary amine-based anion exchange resin was employed. Type 1 ceramic hydroxyapatite was selected as the resin for the final chromatographic purification stage. The latter is optimally suited for various single-domain antibodies modified with the human IgG1 Fc fragment since it allows the target antibody fraction to be separated from residual impurities of aggregates and non-target antibody forms. After purification of three different antibodies, it was possible to obtain a drug with a high degree of purity. Quality control of the obtained drugs by HPLC, capillary gel electrophoresis, dynamic light scattering, enzyme-linked immunosorbent assay, and polymerase chain reaction confirmed the purity of more than 95% of the obtained drug.

The developed technology for chromatographic purification of CHO-GAMP2C5, CHO-GAMB5, and CHO-GAMB10 antibodies was transferred to production. This technology can be used to obtain intermediate products from 200 L of culture fluid. Quality control was performed on the obtained intermediate products in accordance with regulatory documentation. These drugs had quality and purity characteristics comparable to those of drugs obtained in the laboratory. It is concluded

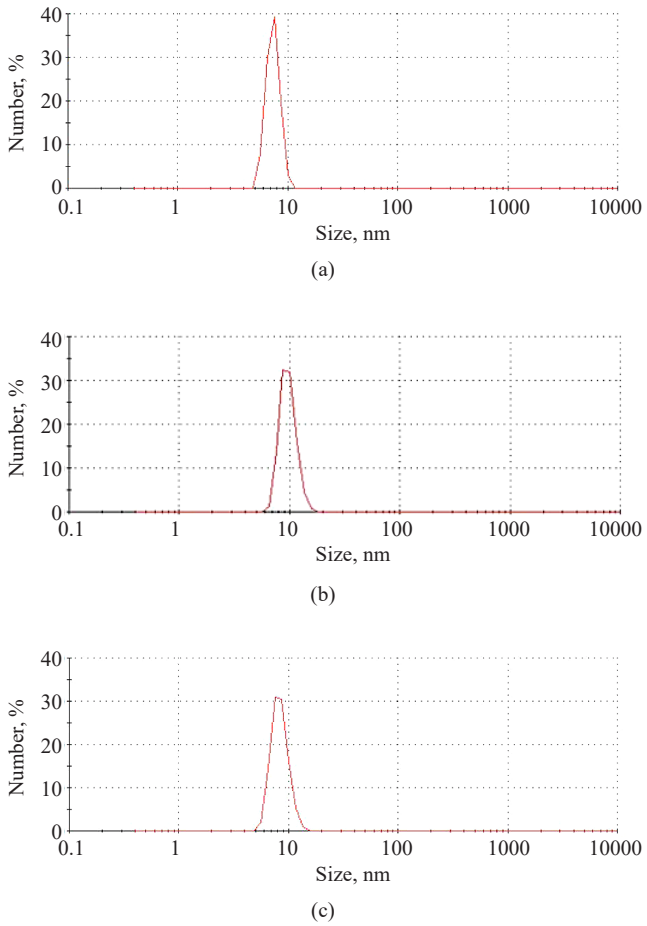

Fig. 11. Evaluation of particle size after the final stage of cleaning using dynamic light scattering at the industry scale: (a) GAMB5, (b) GAMP2C5, and (c) GAMB10

that the Ca^{++}Pure-HA resin (*TOSOH*, Japan) based on type 1 ceramic hydroxyapatite is the optimal resin for the final stage of purification of single-domain antibodies modified with the human IgG1 Fc fragment specific to the SARS-CoV-2 virus.

Authors' contributions

D.S. Polyansky—conducting experiments to develop a laboratory technology for the chromatographic purification of modified single-domain antibodies, collecting and analyzing data, writing the manuscript.

V.V. Prokofiev—conducting experiments to develop a laboratory technology for the chromatographic purification of modified single-domain antibodies.

A.V. Samorukova, F.A. Shishkonakov, D.V. Vasiliev—scaling up the technology for the chromatographic purification of modified single-domain antibodies.

E.I. Ryabova, A.A. Derkaev, A.I. Gosudarev, Yu.A. Efimova—studying the purity and authenticity of purified preparations based on modified single-domain antibodies.

D.V. Shcheblyakov—overall management of the development of drugs based on modified single-domain antibodies.

A.P. Karpov—management of the scaling-up of the chromatographic purification technology for antibodies, proofreading the manuscript, approval of the final version of the manuscript for publication.

I.B. Esmagambetov—management of the development of the laboratory technology for chromatographic purification, proofreading the manuscript, approval of the final version of the manuscript for publication.

The authors declare no conflicts of interest.

REFERENCES

1. Mekala J.R., Nalluri H.P., Reddy P.N., Sainath S.B., Sampath Kumar N.S., Sai Kiran G.V.S.D., Dhiman R., Chamarthy S., Komaragiri R.R., Manyam R.R., Dirisala V.R. Emerging trends and therapeutic applications of monoclonal antibodies. *Gene*. 2024;20(925):148607. https://doi.org/10.1016/j.gene.2024.148607
2. Esposito S., Amirthalingam G., Bassetti M., Blasi F., De Rosa F.G., Halasa N.B., Principi N. Monoclonal antibodies for prophylaxis and therapy of respiratory syncytial virus, SARS-CoV-2, human immunodeficiency virus, rabies and bacterial infections: An update from the world association of infectious diseases and immunological disorders and the Italian society of antinfective therapy. *Front. Immunol*. 2023;14:1162342. https://doi.org/10.3389/fimmu.2023.1162342
3. Wang Z., Wang G., Lu H., Li H., Tang M., Tong A. Development of therapeutic antibodies for the treatment of diseases. *Mol. Biomed*. 2022;3:35. https://doi.org/10.1186/S43556-022-00100-4
4. Paul S., Konig M.F., Pardoll D.M., Bettegowda C., Papadopoulos N., Wright K.M., Gabelli S.B., Ho M., van Elsas A., Zhou S. Cancer therapy with antibodies. *Nature Reviews Cancer*. 2024;24(6):399–426. https://doi.org/10.1038/s41568-024-00690-x
5. Kumar M., Jalota A., Sahu S.K., Haque S. Therapeutic antibodies for the prevention and treatment of cancer. *J. Biomed. Sci*. 2024;31(1):6. https://doi.org/10.1186/s12929-024-00996-w
6. Kügler M., Stein C., Schwenkert M., Saul D., Vockentanz L., Huber T., *et al*. Stabilization and humanization of a single-chain Fv antibody fragment specific for human lymphocyte antigen CD19 by designed point mutations and CDR-grafting onto a human framework. *Protein Eng. Des. Sel*. 2009;22(3): 135–147. https://doi.org/10.1093/protein/gzn079
7. Jin B.K., Odongo S., Radwanska M., Magez S. Nanobodies: A review of generation, diagnostics and therapeutics. *Int. J. Mol. Sci.* 2023;24(6):5994. https://doi.org/10.3390/IJMS24065994
8. Klein C., Brinkmann U., Reichert J.M., Kontermann R.E. The present and future of bispecific antibodies for cancer therapy. *Nat. Rev. Drug Discov.* 2024;23(4):301–319. https://doi.org/10.1038/s41573-024-00896-6
9. Wang M., Ying T., Wu Y. Single-domain antibodies as therapeutics for solid tumor treatment. *Acta Pharmaceutica Sinica B*. 2024;14(7):2854–2868. https://doi.org/10.1016/j.apsb.2024.03.016
10. Cheng L., Chen L., Shi Y., Gu W., Ding W., Zheng X., Liu Y., Jiang J., Zheng Z. Efficacy and safety of bispecific antibodies vs. immune checkpoint blockade combination therapy in cancer: A real-world comparison. *Mol. Cancer*. 2024;23(1):77. https://doi.org/10.1186/s12943-024-01956-6
11. Zacharias N., Podust V.N., Kajihara K.K., Leipold D., Del Rosario G., Thayer D., Dong E., Paluch M., Fischer D., Zheng K., Lei C. A homogeneous high-DAR antibody–drug conjugate platform combining THIOMAB antibodies and XTEN polypeptides. *Chem. Sci*. 2022;13(11):3147–3160. https://doi.org/10.1039/D1SC05243H
12. Polyansky D.S., Ryabova E.I., Derkaev A.A., Starkov N.S., Kashapova I.S., Shcheblyakov D.V., Karpov A.P., Esmagambetov I.B. Development of technology for culturing a cell line producing a single-domain antibody fused with the Fc fragment of human IgG1. *Tonk. Khim. Tekhnol. = Fine Chem. Technol.* 2024;19(3):240–257. https://doi.org/10.32362/2410-6593-2024-19-3-240-257
13. Kelley B. Industrialization of mAb production technology: The bioprocessing industry at a crossroads. *MAbs*. 2009;1(5): 443–452. https://doi.org/10.4161/mabs.1.5.9448
14. Ulmer N., Vogg S., Müller-Späth T., Morbidelli M. Purification of Human Monoclonal Antibodies and Their Fragments. In: Steinitz M. (Ed.). *Human Monoclonal Antibodies. Methods in Molecular Biology*. 2019. V. 1904. P. 163–188. https://doi.org/10.1007/978-1-4939-8958-4_7
15. Esmagambetov I.B., Shcheblyakov D.V., Egorova D.A., Voronina O.L., Derkaev A.A., Voronina D.V., Popova O., Ryabova E.I., Shcherbinin D.N., Aksenova E.I., Semenov A.N., Kunda M.S., Ryzhova N.N., Zubkova O.V., Tukhvatulin A.I., Logunov D.Y., Naroditsky B.S., Borisevich S.V., Gintsburg A.L. Nanobodies Are Potential Therapeutic Agents for the Ebola Virus Infection. *Acta Naturae*. 2021;13(4):53–63. https://doi.org/10.32607/actanaturae.11487]
16. Derkaev A.A., Ryabova E.I., Esmagambetov I.B., Shcheblyakov D.V., Godakova S.A., Vinogradova I.D., Noskov A.N., Logunov D.Y., Naroditsky B.S., Gintsburg A.L. rAAV expressing recombinant neutralizing antibody for the botulinum neurotoxin type a prophylaxis. *Front. Microbiol*. 2022;13:960937. https://doi.org/10.3389/fmicb.2022.960937
17. Voronina D.V., Shcheblyakov D.V., Favorskaya I.A., Esmagambetov I.B., Dzharullaeva A.S., Tukhvatulin A.I., Zubkova O.V., Popova O., Kan V.Y., Bandelyuk A.S., Shmarov M.M., Logunov D.Y., Naroditskiy B.S., Gintsburg A.L. Cross-Reactive Fc-Fused Single-Domain Antibodies to Hemagglutinin Stem Region Protect Mice from Group 1 Influenza a Virus Infection. *Viruses*. 2022;14(11):2485. https://doi.org/10.3390/v14112485
18. Panova E.A., Kleymenov D.A., Shcheblyakov D.V., Bykonia E.N., Mazunina E.P., Dzharullaeva A.S., Zolotar A.N., Derkaev A.A., Esmagambetov I.B., Sorokin I.I., Usachev E.V., Noskov A.N., Ivanov I.A., Zatsepin T.S., Dmitriev S.E., Gushchin V.A., Naroditsky B.S., Logunov D.Y., Gintsburg A.L. Single-domain antibody delivery using an mRNA platform protects against lethal doses of botulinum neurotoxin A. *Front. Immunol*. 2023;14:1098302. https://doi.org/10.3389/fimmu.2023.1098302
19. Godakova S.A., Noskov A.N., Vinogradova I.D., Ugriumova G.A., Solovyev A.I., Esmagambetov I.B., Tukhvatulin AI., Logunov D.Y., Naroditsky B.S., Shcheblyakov D.V., Gintsburg A.L. Camelid VHHs Fused to Human Fc Fragments Provide Long Term Protection Against Botulinum Neurotoxin A in Mice. *Toxins* (Basel). 2019;11(8):464. https://doi.org/10.3390/toxins11080464

20. Esmagambetov I.B., Ryabova E.I., Derkaev A.A., Shcheblyakov D.V., Dolzhikova I.V., Favorskaya I.A., Grousova D.M., Dovgiy M.A., Prokofiev V.V., Gosudarev A.I., Byrikhina D.V., Zorkov I.D., Iliukhina A.A., Kovyrshina A.V., Shelkov A.Y., Naroditsky B.S., Logunov D.Y., Gintsburg A.L. rAAV expressing recombinant antibody for emergency prevention and long-term prophylaxis of COVID-19. *Front. Immunol.* 2023;14:1129245. https://doi.org/10.3389/fimmu.2023.1129245
21. Favorskaya I.A., Shcheblyakov D.V., Esmagambetov I.B., Dolzhikova I.V., Alekseeva I.A., Korobkova A.I., Voronina D.V., Ryabova E.I., Derkaev A.A., Kovyrshina A.V., *et al*. Single-Domain Antibodies Efficiently Neutralize SARS-CoV-2 Variants of Concern. *Front. Immunol.* 2022;13:822159. https://doi.org/10.3389/fimmu.2022.822159
22. Shcheblyakov D.V., Favorskaya I.A., Dolzhikova I.V., Korobkova A.I., Esmagambetov I.V., Voronina O.L., Zubkova O.V., Tukhvatulin A.I., Derkaev A.A., Ryabova E.I., Iliukhina A.A., Zorkov I.D., Grousova D.M., Reshetnikov D.A., Ryzhova N.N., Ermolova E.I., Kunda M.S., Matyuta I.O., Boyko K.M., Gintsburg A.L. Ultra-potent RBM-specific single-domain antibody broadly neutralizes multiple SARS-CoV-2 variants with picomolar activity. *Int. J. Biol. Macromol.* 2025; 19(Pt 3):145386. https://doi.org/10.1016/j.ijbiomac.2025.145386
23. Sedova E.S., Shcherbinin D.N., Bandelyuk A.S., Verkhovskaya L.V., Viskova N.Yu., Avdonina E.D., Prokofiev V.V., Ryabova E.I., Esmagambetov I.B., Pervoykina K.A., Bogacheva E.A., Lysenko A.A., Shmarov M.M. Method for obtaining recombinant antibodies produced by a cell line transduced with recombinant adenoviruses. *Tonk. Khim. Tekhnol. = Fine Chem. Technol.* 2023;18(1):48–64. https://doi.org/10.32362/2410-6593-2023-18-1-48-64
24. Derkaev A.A., Ryabova E.I., Esmagambetov I.B., Shcheblyakov D.V., Noskov A.N., Vinogradova I.D., Prokofiev V.V., Polyansky D.S., Logunov D.Y., Gintsburg A.L. A modified single-domain antibody candidate for the treatment of botulism caused by botulinum toxin type A. *BIOpreparaty. Profilaktika, diagnostika, lechenie = BIOpreparations. Prevention, Diagnosis, Treatment*. 2025;25(1):58–70 (in Russ.). https://doi.org/10.30895/2221-996X-2025-591

About the Authors

Dmitry S. Polyansky, Assistant Professor, I.P. Alimarin Department of Analytical Chemistry, M.V. Lomonosov Institute of Fine Chemical Technologies, MIREA – Russian Technological University (78, Vernadskogo pr., Moscow, 119454, Russia). E-mail: polanskiydmitriy15@gmail.com. Scopus Author ID 57890564200, https://orcid.org/0000-0003-0792-7063

Vladimir V. Prokofiev, Laboratory Research Assistant, Laboratory of Immunobiotechnology, N.F. Gamaleya National Research Center for Epidemiology and Microbiology (The Gamaleya National Center), Ministry of Health of the Russian Federation (18, Gamaleya ul., Moscow, 123098, Russia). E-mail: vladimir.prokofev.96@mail.ru. Scopus Author ID 57300704700, https://orcid.org/0000-0002-4130-177X

Alexandra V. Samorukova, Leading Technologist, Medgamal branch, N.F. Gamaleya National Research Center for Epidemiology and Microbiology (The Gamaleya National Center), Ministry of Health of the Russian Federation (18, Gamaleya ul., Moscow, 123098, Russia). E-mail: av.samorukova@medgamal.ru. https://orcid.org/0000-0001-8060-4370

Fedor A. Shishkonakov, Technologist, Medgamal branch, N.F. Gamaleya National Research Center for Epidemiology and Microbiology (The Gamaleya National Center), Ministry of Health of the Russian Federation (18, Gamaleya ul., Moscow, 123098, Russia). E-mail: fa.shishkonakov@medgamal.ru. https://orcid.org/0009-0009-7886-6019

Dmitry V. Vasiliev, Technologist, Medgamal branch, N.F. Gamaleya National Research Center for Epidemiology and Microbiology (The Gamaleya National Center), Ministry of Health of the Russian Federation (18, Gamaleya ul., Moscow, 123098, Russia). E-mail: vasilyevdv@medgamal.ru. https://orcid.org/0009-0002-9296-0588

Ekaterina I. Ryabova, Junior Researcher, Laboratory of Immunobiotechnology, N.F. Gamaleya National Research Center for Epidemiology and Microbiology (The Gamaleya National Center), Ministry of Health of the Russian Federation (18, Gamaleya ul., Moscow, 123098, Russia). E-mail: ryabovaei96@gmail.com. Scopus Author ID 57301278100, ResearcherID AAE-7335-2022, RSCI SPIN-code 6963-1376, https://orcid.org/0000-0002-2687-5185

Artem A. Derkaev, Junior Researcher, Laboratory of Immunobiotechnology, N.F. Gamaleya National Research Center for Epidemiology and Microbiology (The Gamaleya National Center), Ministry of Health of the Russian Federation (18, Gamaleya ul., Moscow, 123098, Russia). E-mail: derkaev.a@yandex.ru. Scopus Author ID 57381507000, ResearcherID AFU-7075-2022, RSCI SPIN-code 9339-9440, https://orcid.org/0000-0003-3776-3856

Andrey I. Gosudarev, Head of the Department of Development and Scaling, Medgamal branch, N.F. Gamaleya National Research Center for Epidemiology and Microbiology (The Gamaleya National Center), Ministry of Health of the Russian Federation (18, Gamaleya ul., Moscow, 123098, Russia). E-mail: gosudarev@medgamal.ru. https://orcid.org/0000-0001-8594-2627

Yuliya A. Efimova, Cand. Sci. (Chem.), Assistant Professor, I.P. Alimarin Department of Analitical Chemistry, M.V. Lomonosov Institute of Fine Chemical Technologies, MIREA – Russian Technological University (78, Vernadskogo pr., Moscow, 119454, Russia). E-mail: efimova_yulia@bk.ru. Scopus Author ID 25228417800, https://orcid.org/0000-0002-3582-0012

Dmitry V. Shcheblyakov, Dr. Sci. (Biol.), Leading Researcher, Head of the Laboratory of Immunobiotechnology, N.F. Gamaleya National Research Center for Epidemiology and Microbiology (The Gamaleya National Center), Ministry of Health of the Russian Federation (18, Gamaleya ul., Moscow, 123098, Russia). E-mail: sdmitryv@yahoo.com. Scopus Author ID 35073056900, ResearcherID E-5899-2014, SPIN-код РИНЦ 6357-2725, https://orcid.org/0000-0002-1289-3411

Andrey P. Karpov, Cand. Sci. (Biol.), Chief Technologist, Medgamal branch, N.F. Gamaleya National Research Center for Epidemiology and Microbiology (The Gamaleya National Center), Ministry of Health of the Russian Federation (18, Gamaleya ul., Moscow, 123098, Russia). E-mail: ap.karpov@medgamal.ru. Scopus Author ID 22834845200.

Ilias B. Esmagambetov, Cand. Sci. (Biol.), Leading Researcher, Head of the Laboratory of Stromal Regulation of Immunity, N.F. Gamaleya National Research Center for Epidemiology and Microbiology (The Gamaleya National Center), Ministry of Health of the Russian Federation (18, Gamaleya ul., Moscow, 123098, Russia). E-mail: iesmagambetov@yandex.ru. Scopus Author ID 56120429700, ResearcherID E-3327-2014, RSCI SPIN-code 8132-2320, https://orcid.org/0000-0002-2063-2449

Об авторах

Полянский Дмитрий Сергеевич, ассистент, кафедра аналитической химии им. И.П. Алимарина, Институт тонких химических технологий им. М.В. Ломоносова, ФГБОУ ВО «МИРЭА – Российский технологический университет» (119454, Россия, Москва, пр-т Вернадского, д. 78). E-mail: polanskiydmitriy15@gmail.com. Scopus Author ID 57890564200, https://orcid.org/0000-0003-0792-7063

Прокофьев Владимир Владимирович, лаборант-исследователь, лаборатория иммунобиотехнологии, ФГБУ «Национальный исследовательский центр эпидемиологии и микробиологии имени почетного академика Н.Ф. Гамалеи» Министерства здравоохранения Российской Федерации (123098, Россия, Москва, ул. Гамалеи, д. 18). E-mail: vladimir.prokofev.96@mail.ru. Scopus Author ID 57300704700, https://orcid.org/0000-0002-4130-177X

Саморукова Александра Владимировна, ведущий технолог, филиал «Медгамал», ФГБУ «Национальный исследовательский центр эпидемиологии и микробиологии имени почетного академика Н.Ф. Гамалеи» Министерства здравоохранения Российской Федерации (123098, Россия, Москва, ул. Гамалеи, д. 18). E-mail: av.samorukova@medgamal.ru. https://orcid.org/0000-0001-8060-4370

Шишконаков Федор Алексеевич, технолог, филиал «Медгамал», ФГБУ «Национальный исследовательский центр эпидемиологии и микробиологии имени почетного академика Н.Ф. Гамалеи» Министерства здравоохранения Российской Федерации (123098, Россия, Москва, ул. Гамалеи, д. 18). E-mail: fa.shishkonakov@medgamal.ru. https://orcid.org/0009-0009-7886-6019

Васильев Дмитрий Валерьевич, технолог, филиал «Медгамал», ФГБУ «Национальный исследовательский центр эпидемиологии и микробиологии имени почетного академика Н.Ф. Гамалеи» Министерства здравоохранения Российской Федерации (123098, Россия, Москва, ул. Гамалеи, д. 18). E-mail: vasilyevdv@medgamal.ru. https://orcid.org/0009-0002-9296-0588

Рябова Екатерина Игоревна, младший научный сотрудник, лаборатория иммунобиотехнологии, ФГБУ «Национальный исследовательский центр эпидемиологии и микробиологии имени почетного академика Н.Ф. Гамалеи» Министерства здравоохранения Российской Федерации (123098, Россия, Москва, ул. Гамалеи, д. 18). E-mail: ryabovaei96@gmail.com. Scopus Author ID 57301278100, ResearcherID AAE-7335-2022, SPIN-код РИНЦ 6963-1376, https://orcid.org/0000-0002-2687-5185

Деркаев Артем Алексеевич, младший научный сотрудник, лаборатория иммунобиотехнологии, ФГБУ «Национальный исследовательский центр эпидемиологии и микробиологии имени почетного академика Н.Ф. Гамалеи» Министерства здравоохранения Российской Федерации (123098, Россия, Москва, ул. Гамалеи, д. 18). E-mail: derkaev.a@yandex.ru. Scopus Author ID 57381507000, ResearcherID AFU-7075-2022, SPIN-код РИНЦ 9339-9440, https://orcid.org/0000-0003-3776-3856

Государев Андрей Игоревич, начальник отделения разработки и масштабирования, филиал «Медгамал», ФГБУ «Национальный исследовательский центр эпидемиологии и микробиологии имени почетного академика Н.Ф. Гамалеи» Министерства здравоохранения Российской Федерации (123098, Россия, Москва, ул. Гамалеи, д. 18). E-mail: gosudarev@medgamal.ru. https://orcid.org/0000-0001-8594-2627

Ефимова Юлия Александровна, к.х.н., доцент, кафедра аналитической химии им. И.П. Алимарина, Институт тонких химических технологий им. М.В. Ломоносова, ФГБОУ ВО «МИРЭА – Российский технологический университет» (119454, Россия, Москва, пр-т Вернадского, д. 78). E-mail: efimova_yulia@bk.ru. Scopus Author ID 25228417800, https://orcid.org/0000-0002-3582-0012

Щебляков Дмитрий Викторович, д.б.н., ведущий научный сотрудник, заведущий лабораторией иммунобиотехнологии, ФГБУ «Национальный исследовательский центр эпидемиологии и микробиологии имени почетного академика Н.Ф. Гамалеи» Министерства здравоохранения Российской Федерации (123098, Россия, Москва, ул. Гамалеи, д. 18). E-mail: sdmitryv@yahoo.com. Scopus Author ID 35073056900, ResearcherID E-5899-2014, SPIN-код РИНЦ 6357-2725, https://orcid.org/0000-0002-1289-3411

Карпов Андрей Павлович, к.б.н., главный технолог, филиал «Медгамал», ФГБУ «Национальный исследовательский центр эпидемиологии и микробиологии имени почетного академика Н.Ф. Гамалеи» Министерства здравоохранения Российской Федерации (123098, Россия, Москва, ул. Гамалеи, д. 18). E-mail: ap.karpov@medgamal.ru. Scopus Author ID 22834845200.

Есмагамбетов Ильяс Булатович, к.б.н., ведущий научный сотрудник, заведующий лабораторией стромальной регуляции иммунитета, ФГБУ «Национальный исследовательский центр эпидемиологии и микробиологии имени почетного академика Н.Ф. Гамалеи» Министерства здравоохранения Российской Федерации (123098, Россия, Москва, ул. Гамалеи, д. 18). E-mail: iesmagambetov@yandex.ru. Scopus Author ID 56120429700, ResearcherID E-3327-2014, SPIN-код РИНЦ 8132-2320, https://orcid.org/0000-0002-2063-2449

Translated from Russian into English by H. Moshkov
Edited for English language and spelling by Thomas A. Beavitt

Tonkie Khimicheskie Tekhnologii = Fine Chemical Technologies.
2026;21(2):212–225
ISSN 2686-7575 (Online)

Synthesis and processing of polymers and polymeric composites
Синтез и переработка полимеров и композитов на их основе

UDC 678
https://doi.org/10.32362/2410-6593-2026-21-2-212-225
EDN CDZRGI

RESEARCH ARTICLE

Structure, properties, and photodegradation of polymer biocomposites based on polylactide filled with A-Len® thermoplastic compound

Ilya Yu. Vasilyev[1,✉], Victoria S. Petrenko[1], Viktor A. Rod[1], Dmitrii A. Golobokov[2]

[1] *Moscow Polytechnic University (Mospolitech), Moscow, 107023 Russia*

[2] *Enikolopov Institute of Synthetic Polymeric Materials, Russian Academy of Sciences, Moscow, 117393 Russia*

✉ *Corresponding author, e-mail: iljanaras@ya.ru*

Abstract

Objectives. The work set out to investigate the influence of the compounding and technological parameters of polymer biocomposite materials based on polylactide (PLA) filled with the A-Len® thermoplastic compound (Alen) on their structural, thermophysical, and mechanical properties, as well as to determine the mechanism of their destruction under the impact of ultraviolet radiation.

Methods. Films of PLA and Alen, as well as polymer composites based on them (PLA/Alen), were obtained using a flat die extruder (*MashPlast*, Russia). The structural and morphological properties of the films were determined with a JCM-6000 PLUS scanning electron microscope (*JEOL*, Akishima, Tokyo, Japan); their thermal properties were obtained using a DSC 204 F1 calorimeter (*NETZSCH*, Germany). The chemical composition and degradation mechanism were analyzed by infrared spectroscopy with an FSM-1201 spectrometer (Russia) fitted with an attenuated total internal reflection attachment. The mechanical properties were examined using a Z010 ZwickRoell tensile testing machine (*Zwick Roell Group*, Germany). The effect of ultraviolet radiation was assessed using an ultraviolet chamber.

Results. It was shown that the presence of Alen in mixtures with PLA affects the formation of a heterogeneous structure due to the presence of polyethylene in the Alen composition. This mediated a reduction in Young's modulus by 34% (to 1050 MPa) in comparison with the initial value for PLA (1600 MPa). In the polymer composites, the PLA phase recrystallizes to yield a denser-ordered supramolecular structure, while in the polyethylene phase, the segmental mobility of macromolecules decreases and crystallization process is hindered by their different polarities to form an interface between the components under study.

Conclusions. The photodegradation mechanism in PLA/Alen polymer composites is shown to be primarily due to the presence of a pro-oxidant additive in Alen, which initiates the oxidation process to degrade and subsequently fragment the low-molecular fraction of polyethylene. In addition, the PLA matrix photodegrades through the Norrish Type II mechanism, which describes the oxidation of polymer chains by a radical mechanism to produce C=C bonds. The developed polymer composites are promising for the fabrication of certain polymer products due to their optimal performance characteristics and accelerated photochemical degradation kinetics.

Keywords

polylactide, A-Len®, compound, biocomposites, UV radiation, photodegradation

Submitted: 11.08.2025
Revised: 20.11.2025
Accepted: 13.02.2026

For citation

Vasilyev I.Yu., Petrenko V.S., Rod V.A., Golobokov D.A. Structure, properties, and photodegradation of polymer biocomposites based on polylactide filled with A-Len® thermoplastic compound. *Tonk. Khim. Tekhnol. = Fine Chem. Technol*. 2026;21(2):212–225. https://doi.org/10.32362/2410-6593-2026-21-2-212-225

НАУЧНАЯ СТАТЬЯ

Структура, свойства и фотодеструкция полимерных биокомпозиционных материалов на основе полилактида, наполненного термопластичным компаундом A-Len®

И.Ю. Васильев[1]✉, В.С. Петренко[1], В.А. Род[1], Д.А. Голобоков[2]

[1] *Московский политехнический университет (Мосполитех), Москва, 107023 Россия*

[2] *Институт синтетических полимерных материалов им. Н.С. Ениколопова Российской академии наук, Москва, 117393 Россия*

✉ *Автор для переписки, e-mail: iljanaras@ya.ru*

Аннотация

Цели. Изучить влияние рецептурно-технологических параметров полимерных биокомпозиционных материалов на основе полилактида (ПЛА), наполненного термопластичным компаундом A-Len® (Alen), на структурные, теплофизические и деформационно-прочностные свойства, а также определить механизм деструкции под действием ультрафиолетового излучения.

Методы. В работе исследовали пленки на основе ПЛА и Alen, а также полимерные композиции на основе ПЛА и Alen (ПЛА/Alen), которые получали на плоскощелевом экструдере фирмы «*МашПласт*» (Россия). Для вышеуказанных объектов определяли структурно-морфологические свойства на сканирующем электронном микроскопе JCM-6000 PLUS (*JEOL*, Акисима, Токио, Япония), теплофизические свойства на калориметре DSC 204 F1 (*NETZSCH*, Германия). Химический состав, а также определение механизма деструкции осуществляли методом инфракрасной спектроскопии на приборе ФСМ-1201 (Россия) с приставкой нарушенного полного внутреннего отражения. Деформационно-прочностные свойства исследовали на разрывной машине Z010 ZwickRoell (Германия). Воздействие ультрафиолетового излучения определяли с помощью ультрафиолетовой камеры.

Результаты. Показано, что Alen в смесях с ПЛА влияет на образование гетерогенной структуры вследствие наличия в его составе полиэтилена (ПЭ). Этим опосредовано снижение модуля упругости на 34% (1050 МПа) в сравнении с исходной величиной ПЛА — 1600 МПа. При этом для фазы ПЛА в полимерных композициях осуществляется перекристаллизация с более плотным упорядочиванием надмолекулярной структуры, а для фазы ПЭ происходит снижение сегментальной подвижности макромолекул и затруднение процесса кристаллизации вследствие их разной полярности с формированием границы раздела фаз между исследуемыми компонентами.

Выводы. Механизм фотодеструкции полимерных композиций ПЛА/Alen осуществляется за счет наличия в составе термопластичного компаунда прооксидантной добавки, инициирующей процесс окисления, после чего происходит разрушение низкомолекулярной фракции ПЭ с последующей ее фрагментацией. Наряду с этим, фотодеструкция матрицы ПЛА протекает по механизму Норриша II, заключающемся в окислении полимерных цепей по радикальному типу с образованием C=C-связи. Таким образом, разработанные биокомпозиционные полимерные материалы являются перспективными для изготовления полимерных изделий из них, характеризуются оптимальными эксплуатационными свойствами и ускоренной кинетикой фотохимической деструкции.

Ключевые слова

полилактид, A-Len®, компаунд, биокомпозиты, УФ-излучение, фотодеструкция

Поступила: 11.08.2025
Доработана: 20.11.2025
Принята в печать: 13.02.2026

Для цитирования

Васильев И.Ю., Петренко В.С., Род В.А., Голобоков Д.А. Структура, свойства и фотодеструкция полимерных биокомпозиционных материалов на основе полилактида, наполненного термопластичным компаундом A-Len®. *Тонкие химические технологии*. 2026;21(2):212–225. https://doi.org/10.32362/2410-6593-2026-21-2-212-225

INTRODUCTION

The growing relevance of using biodegradable polymers is driven by the possibility of creating promising, environmentally friendly materials to reduce environmental impacts for use in the packaging, medical, and agricultural industries [1]. The leading position of synthetic thermoplastics in the packaging industry is accompanied by an uncontrolled amount of polymer waste, most of which accumulates in landfills to pollute the environment. However, in many cases, polymers synthesized from petrochemical feedstocks [2–4] can be made biodegradable by modifying them with natural fillers.

The modification of synthetic polyolefins with natural polymers accelerates the fragmentation of the polymer matrix due to the rapid biodegradation of the filler. Such modifying additives include starch [5], chitin [6], chitosan [7], and other natural polymers [8–10]. However, the formation of such composites can be complicated by insufficient adhesion of the synthetic matrix to the natural filler. An additional complicating factor is the limited filler concentration (typically up to 30 wt %), which is due to the technological complexity of producing dispersed filled systems. Increasing the natural polymer content in the synthetic polymer matrix above 30 wt % gives rise to a large number of agglomerates, which may lead to defects in the production of such composites [11–13].

A promising direction in recent years involves the creation of biodegradable materials based on polymers synthesized from renewable raw materials, in particular polylactide (PLA), which reduces the dependence on petroleum-derived polymers [14–16]. PLA is a synthetic polymer made from the lactide monomer, which can exist in two optically active isomeric forms, L- and D-lactide, as well as in the optically inactive form of meso-lactide. PLA is a strong and rigid polymer comparable in performance properties to polyethylene terephthalate and, following appropriate plasticization, to polyethylene (PE) and polyvinyl chloride [17]. PLA can be processed both by extrusion to produce flexible films and by thermoforming to produce rigid containers [18]. Although PLA is a biodegradable polymer, it is important to note that its biodegradation only occurs under certain conditions (high temperature, pH, and humidity). Therefore, PLA, like other polymers, is typically modified with additives of various origins [19–21], although the desired properties are not always achievable due to of their low technological compatibility [22].

Another method for modifying synthetic thermoplastics is the use of pro-oxidant additives, e.g., transition metal (Mn, Fe, Mg) stearates, which initiate the decomposition of the polymer matrix and promote accelerated oxidative degradation [23]. The main advantage of using transition metal stearates consists in their ability to modify a wide range of thermoplastic polymers, including PLA, as well as their processing on existing equipment designed for thermoplastics, their low toxicity, and—unlike natural fillers—the short oxidative degradation time of polymer materials produced at a low mass fraction within the synthetic polymer [24].

Therefore, it is of scientific and practical interest to analyze the properties of ternary composites based on PLA filled with the thermoplastic compound A-Len® (Alen) and determine their degradation mechanism, which is currently insufficiently understood.

EXPERIMENTAL

Materials

The polymer matrix for the production of polymer composites was made of the aliphatic polyester PLA grade 524 (China). The additive used to initiate the degradation of the polymer matrix was the thermoplastic compound A-Len® TECH BD00TY (India) with an active (organic) substance content of 10 wt %. Table 1 presents the characteristics of the initial components.

Research methods

The components were mixed, plasticized, and subsequently cast using a flat die extruder (*MashPlast*, Russia) at a varying Alen content in mixtures with PLA from 5 to 20 wt %. The resulting polymer composites were films having a thickness of 60 ± 3 μm. Table 2 presents the temperature conditions to produce the initial PLA and Alen films, as well as the polymer composites based on them. Table 3 shows the compositions of the polymer composites.

The effect of ultraviolet (UV) radiation on the samples was determined using an UV chamber containing two PRK-4 quartz (mercury) lamps producing radiation with a wavelength of λ = 254 nm. 150 × 150 mm film samples were placed 30 cm from the UV lamps, isolated from any external radiation source, and exposed for 150 h with collection of control samples every 25 h.

The thermophysical properties of the samples were determined using differential scanning calorimetry on a DSC 204 F1 calorimeter (*NETZSCH*, Germany) in a temperature range from 20 to 200°C at a scanning rate of 10°C/min and a sample weight of 10 ± 1 mg under a flow of inert argon gas. When studying the thermophysical properties, the enthalpy of melting ΔH_m (J/g), melting point T_m (°C), and glass transition temperature T_g (°C) were determined. The degrees of crystallinity α (%) of Alen and PLA, as well as polymer composites based on

Table 1. Characteristics of the initial components

Component	Melt flow index, g/10 min	Young's modulus, MPa	Elongation at break, %	Density, g/cm^3
PLA	8.7	1600	4.2	1.24
Alen	17	600	3.2	0.97

Table 2. Temperature conditions to produce polymer composites

Polymer composites	Temperature conditions of flat die extruder zones, °C				
	Zone 1	Zone 2	Zone 3	Zone 4	Zone 5
PLA	165	168	170	173	175
Alen	120	125	130	135	140
PLA/Alen	165	168	170	173	175

Table 3. Compositions of polymer composites

Polymer composites	Concentration, wt %	
	PLA	Alen
PLA	100	–
Alen	–	100
PLA/Alen5	95	5
PLA/Alen10	90	10
PLA/Alen15	85	15
PLA/Alen20	80	20

them, were found using the enthalpies of melting of fully crystalline PE (293 J/g) and for PLA (93.7 J/g) according to ISO 11357-1:2023 "Plastics. Differential scanning calorimetry (DSC). General principles"[1].

The chemical composition and photodegradation mechanism were determined by FTIR spectroscopy with an attenuated total internal reflection (ATR) attachment using an FSM-1201 spectrometer (Russia) with a resolution of 1.0 cm^{-1} (spectral wavenumber range of 4000–375 cm^{-1}) at a temperature of 23 ± 2°C according to GOST 57939-2017[2].

Performance properties were measured in accordance with ISO 527-3:2018 "Plastics. Determination of tensile properties"[3]. Tests were conducted on a ZwickRoell Z010 tensile testing machine (*ZwickRoell Group*, Germany). Specimens for testing strength and deformation properties were obtained using a type 1B punch (EN ISO 527-3:2018) with dimensions of 50 × 10 mm. The maximum permissible error of load measurements did not exceed 1%. The maximum deviation in specimen width was ±0.1 mm. The average value was determined from 10 measurements. Tests were carried out at a sample deformation rate of 50 mm/min. The strength properties were measured as Young's modulus (E) and tensile stress at break (σ), while the deformation properties were determined as elongation at break (ε).

1 ISO 11357-1:2023. Plastics — Differential scanning calorimetry (DSC). Part 1: General principles. https://www.iso.org/standard/83904.html. Accessed January 22, 2026.

2 GOST 57939-2017. National Standard of the Russian Federation. Polymer composites. Infrared spectroscopy. General principles. Moscow: Standartinform; 2019.

3 ISO 527-3:2018. Plastics — Determination of tensile properties. Part 3: Test conditions for films and sheets. https://www.iso.org/standard/70307.html. Accessed January 22, 2026.

The structural and morphological properties of gold-sputtered samples were examined using scanning electron microscopy with a JCM-6000 PLUS microscope (*JEOL*, Akishima, Tokyo, Japan) with a secondary electron detector at accelerating voltages of 10 and 15 kV.

RESULTS AND DISCUSSION

Thermophysical characteristics

The thermal analysis curve of PLA (Fig. 1a) contains two peaks: the first at 65°C corresponds to the glass transition temperature, while the second identifies the presence of a crystalline phase at a melting point of 157°C. Figure 1b depicts a characteristic endothermic melting peak at 125°C corresponding to the melting point of PE, which is part of the thermoplastic compound. The thermal analysis curve of the PLA/Alen polymer composite containing 20 wt % Alen (Fig. 1c) contains two endothermic peaks corresponding to the melting points of PE at 118°C and PLA at 153°C.

The addition of Alen to PLA at a content of 20 wt % causes an increase in the enthalpy of melting and degree of crystallinity of the PLA phase (Table 4). This occurs as a result of recrystallization, which causes a denser ordering of the PLA supramolecular structure due to the presence of the crystalline PE phase in the polymer composite. The shift of the endothermic peak of PE melting to a lower temperature of 118°C indicates the formation of more defective small crystals, which is caused by a decrease in the segmental mobility of PE macromolecules which hinders the crystallization process.

Following 150 h of exposure to UV radiation, the thermophysical properties of films based on the initial PLA and Alen components, as well as the PLA/Alen polymer composites, are observed to change (Fig. 2). For the irradiated PLA-based film, in comparison with the initial, the enthalpy of melting increases by more than 3.5 times and a cold crystallization peak appears on the thermal analysis curve at 105°C. At the same time, the melting point decreases by 5.2°C. The increase in the enthalpy of melting under UV irradiation is due to the partial degradation of the amorphous phase of PLA, which leads to a change in the supramolecular structure of the crystalline phase, namely, the formation of denser and larger crystals. Another explanation is that the presence of a metastable crystalline structure of PLA under UV irradiation is likely to promote continued crystallization by breaking stressed tie molecules, thereby increasing its degree of crystallinity [25].

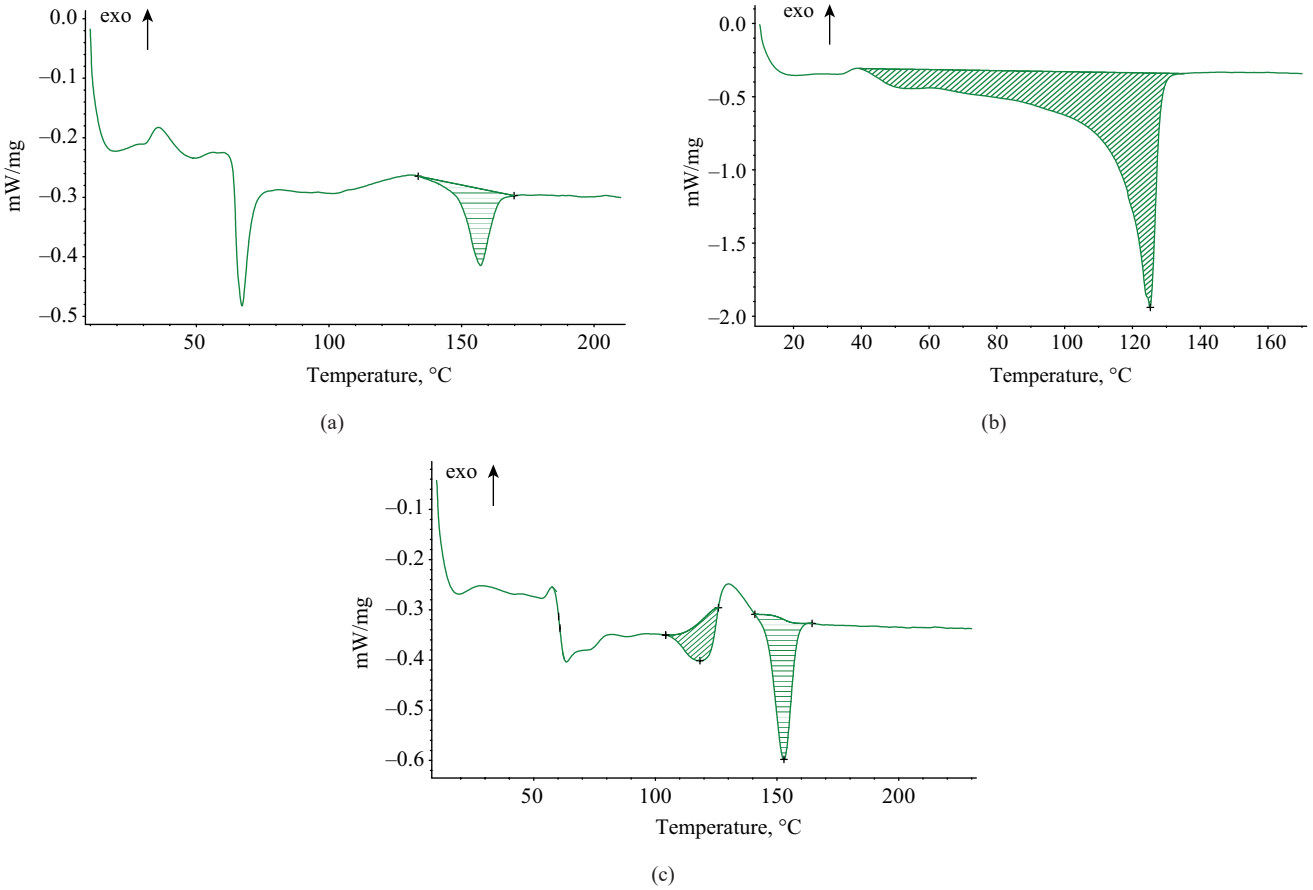

Fig. 1. Thermal analysis curves of melting of (a) PLA, (b) Alen, and (c) PLA/Alen20

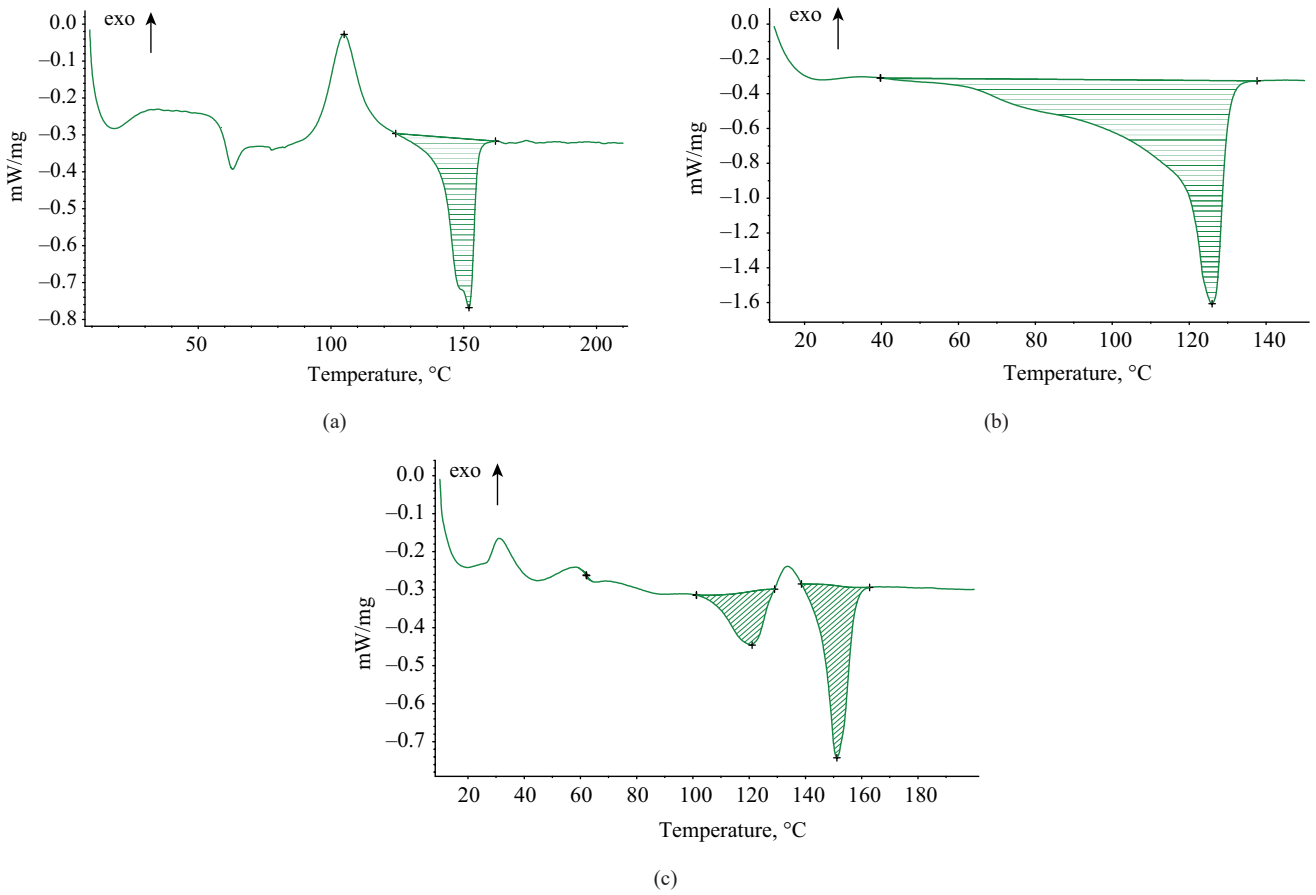

Fig. 2. Thermal analysis curves of melting of (a) PLA, (b) Alen, and (c) PLA/Alen20 following 150 h of UV irradiation

Table 4. Thermophysical properties of polymer composites

Exposure, h	Sample	T_m, °C	ΔH_m, J/g	α, %
0	PLA	157	8.7	9.3
	Alen	125	176	60.0
	PLA/Alen20	153/118	14.5/5.9	15.5/2.0
150	PLA	152	30	32
	Alen	125	155	52.9
	PLA/Alen20	151/121	23.9/12.0	25.5/4.1

For the Alen-based film (Fig. 2b), the enthalpy of melting decreases by 12%. The difference in the melting point before and after UV irradiation does not exceed 1°C. The specific energy of the endothermic process of the PLA/Alen20 polymer composite (Fig. 2c) also increases in comparison with the initial (Table 4). For example, for PE, the enthalpy of melting doubles, while for PLA it increases by 1.7 times. Furthermore, the melting point for the PE phase increases by 3°C, while for the PLA phase it decreases by 1.6°C.

IR spectrum characteristics

The presence of intense absorption bands in the IR spectrum of PLA (Fig. 3a) in the range of 1180–1077 cm^{-1} indicates the presence of rocking vibrations of the methyl CH_3 group, which identifies high-molecular-weight PLA obtained by ring-opening polymerization. Thus, PLA is an optically active poly(D,L-lactide). The IR spectrum of Alen (Fig. 3b) contains absorption bands at 2914 and 2847 cm^{-1},

indicating the presence of an asymmetric CH_2 group and a symmetric CH_2 group, as well as an absorption band at 1462 cm^{-1} characteristic of a scissoring CH_2 group. The IR spectrum also includes a pronounced absorption band near 1740 cm^{-1}; this band is not characteristic of PE, but indicates that Alen includes a second component, which contains a functional carbonyl C=O group.

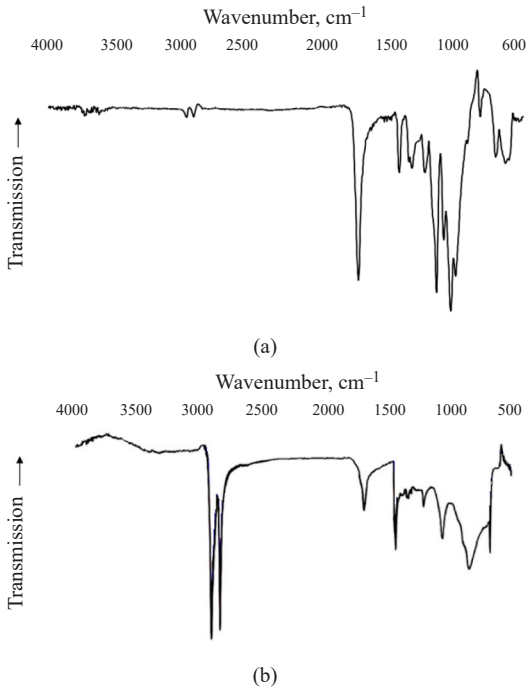

Fig. 3. IR spectra of (a) PLA and (b) Alen

The presence of PE and the carbonyl C=O group constitutes an additive—a masterbatch, which also contains active transition metal elements (Mn, Fe, Mg) initiating the decomposition of the polymer matrix through oxidative degradation [26]. Thus, Alen is a PE composite with a pro-oxidant additive in the form of transition metal stearates.

Apparently, the photodegradation mechanism of PLA/Alen polymer composites is mediated by the pro-oxidant additive in Alen, which then decomposes and fragments the low-molecular-weight PE fraction. The PLA matrix photodegrades by the Norrish Type II mechanism [27], a radical oxidation to form a C=C bond, which appears as an absorption band in the IR spectrum at 1654 cm^{-1} (Fig. 4). The IR spectrum also demonstrates a change in the intensity of the characteristic absorption bands of the PLA/Alen polymer composite, which also confirms the process of photodegradation.

Scanning electron microscopy

The surface of the extruded PLA film (Fig. 5) is characterized by a minimum number of defects, which are presumably related to the manufacturing

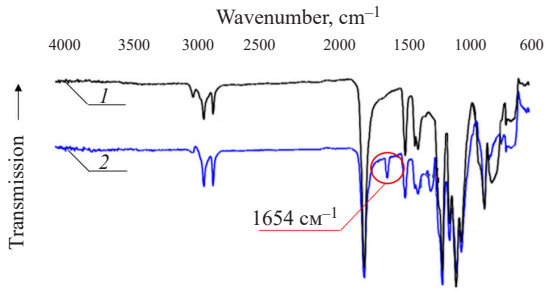

Fig. 4. IR spectra of the PLA/Alen20 polymer composite: (*1*) initial and (*2*) after 150 h of UV irradiation

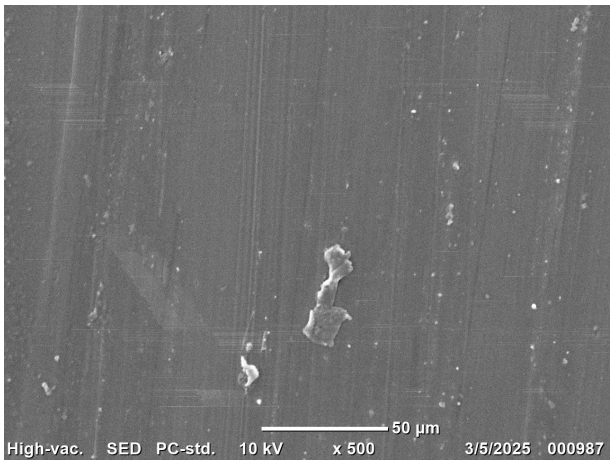

Fig. 5. Morphology of the surface of the PLA film: (a) initial, (b) after 150 h of UV irradiation

process. After 150 h of UV irradiation, the surface remained unchanged, indicating no visible signs of photodegradation throughout the entire experiment.

The surface of the Alen film (Fig. 6a) shows scratches, presumably formed during the extrusion process, and spherulites (Fig. 6b) (average size in the image is ~7 µm). As the result of photodegradation following 150 h of UV exposure, wide through cracks (Fig. 6c) formed on

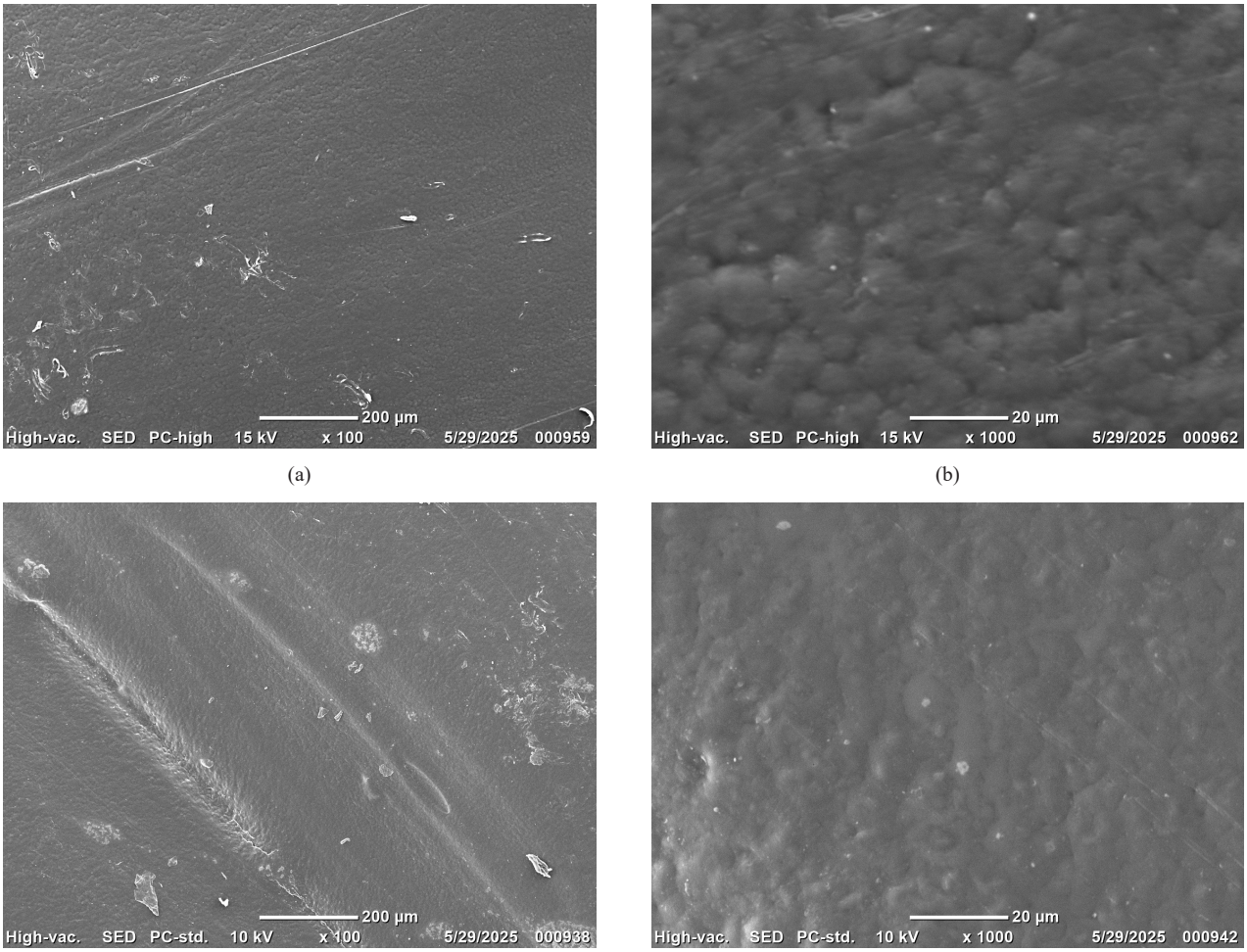

Fig. 6. Surface morphology of the Alen film: (a) and (b) initial, (c) and (d) after 150 h of UV radiation

the film surface, the number of defects increased, and the spherulitic structure became less visible (Fig. 6d).

Figure 7 presents the surface morphology of the PLA/Alen polymer composite. When this composite is produced by extrusion, a structurally heterogeneous film forms (Fig. 7a). Higher magnification reveals domains formed by phase separation of PLA and Alen (Fig. 7b). Following 150 h of exposure in a UV chamber, microcracks form on the surface (Figs. 7c and 7d), indicating photodegradation, most likely of the Alen phase.

Mechanical properties

For the initial PLA and Alen films, the tensile stress at break is 67.2 and 19.2 MPa, respectively, and the Young's modulus is 1600 and 600 MPa. Increasing the Alen content in PLA blends to 20 wt % decreases the tensile stress at break by 53% (to 31.5 MPa), elongation at break by 29% (to 3.0%), and the Young's modulus by 34% (to 1050 MPa) (Fig. 8). This is due to the formation of a heterogeneous structure because of low intermolecular interactions for the reason of the different polarities of the initial components. The elongation at break for the initial PLA film is 4.2%, while for the Alen film it is 3.2%.

Following 150 h of exposure to UV radiation, the tensile stress at break for the PLA film decreases by 67%, the elongation at break by 33%, and the elastic modulus by 50% (to 800 MPa) (Table 5). The mechanical properties of the Alen film cannot be determined because of the presence of a large number of through holes, which also act as stress concentrators. For the PLA/Alen20 polymer composite, the tensile stress at break, like the Young's modulus, decreases by 82% of the initial value, primarily failing at the PLA/PE interface. The elongation at break, which remains virtually unchanged in comparison with the initial value of the PLA/Alen20 polymer composite, amounts to 2.8%.

Thus, the developed polymer biocomposite materials are promising for the manufacture of polymer products due to their optimal performance properties and accelerated photochemical degradation kinetics.

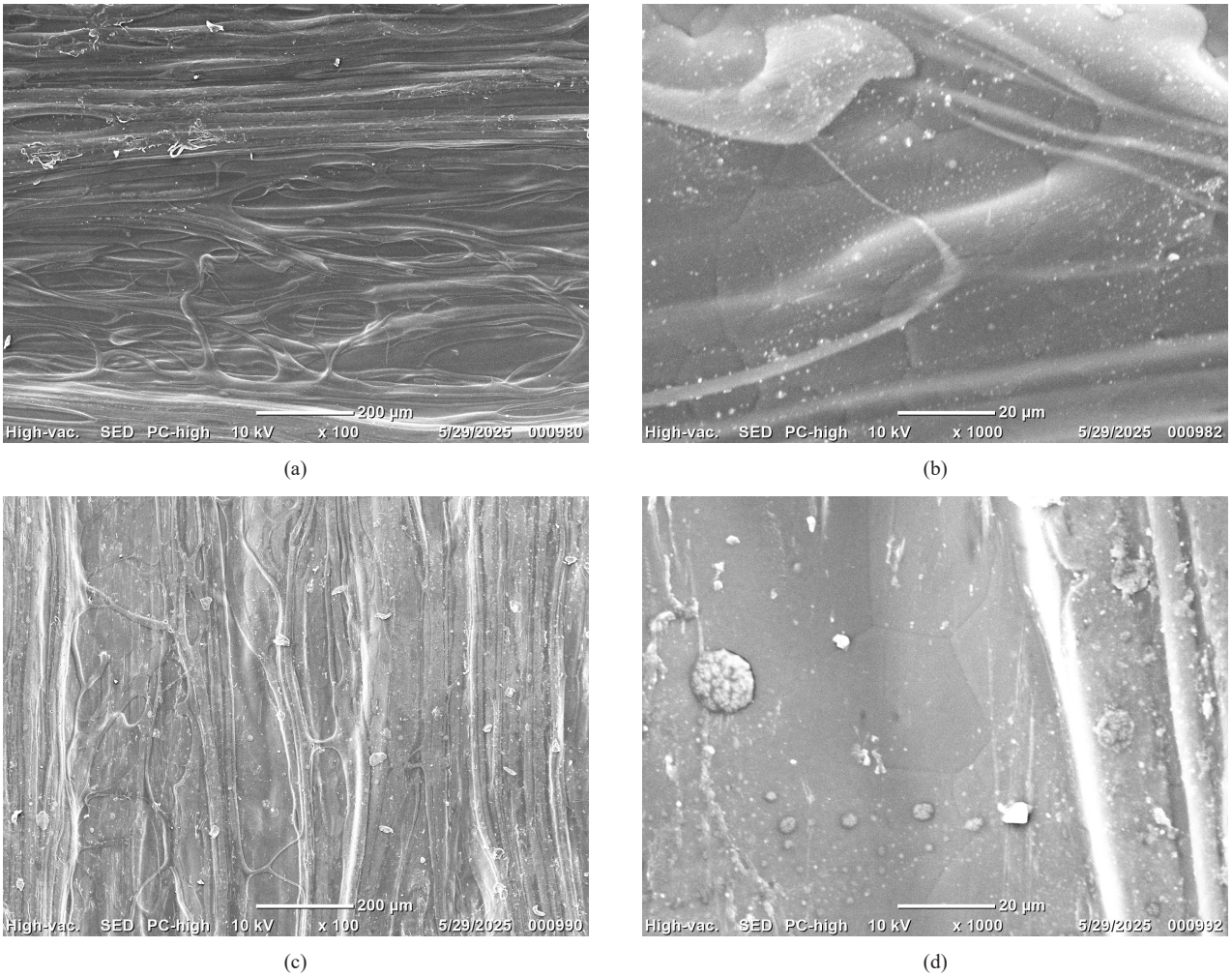

Fig. 7. Surface morphology of the PLA/Alen20 film: (a) and (b) initial, (c) and (d) after 150 h of UV radiation

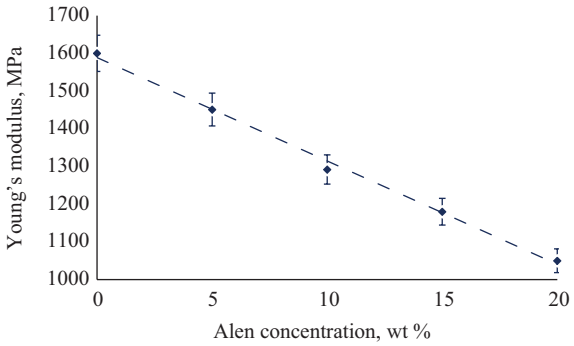

Fig. 8. Effect of the Alen concentration on the Young's modulus of the PLA/Alen polymer composite

CONCLUSIONS

The photochemical degradation of polymer composites based on PLA filled with A-Len® thermoplastic compound was studied. During extrusion of the polymer composites, the PLA phase mixed with A-Len® undergoes a change in its supramolecular structure, which manifests itself as an increase in crystallinity. This is caused by the presence of the PE phase. For this phase, the segmental mobility of macromolecules is reduced, which causes the formation of more defective and smaller crystals, resulting in decreased crystallinity. The identified structural features of the polymer composites contribute to a decrease in their performance properties due to the different polarities of the initial components.

Exposure of Alen and PLA/Alen to UV radiation leads to the formation of structural defects along with a reduction in deformation and strength properties. The most likely explanation for photodegradation is the presence of a pro-oxidant additive in Alen. In this case, the low-molecular-weight fraction of PE undergoes primary degradation, followed by fragmentation of the PE matrix. PLA undergoes photochemical degradation via the Norrish II mechanism, an oxidative degradation by a radical mechanism to form a C=C bond.

Table 5. Deformation and strength properties of polymer composites

Composites	Deformation and strength properties		
	Tensile stress at break, MPa	Elongation at break, %	Young's modulus, MPa
0 h of exposure			
PLA	67.2	4.2	1600
Alen	19.2	3.2	600
PLA/Alen5	55.1	3.8	1451
PLA/Alen10	44.0	3.4	1292
PLA/Alen15	37.8	3.2	1181
PLA/Alen20	31.5	3.0	1050
150 h of exposure			
PLA	22.4	2.8	800
Alen	–	–	–
PLA/Alen5	19.8	3.0	660
PLA/Alen10	12.6	2.9	421
PLA/Alen15	7.2	2.9	239
PLA/Alen20	5.7	2.8	189

The determined characteristics are of utility for the development of biocomposite materials having accelerated photochemical degradation kinetics.

Acknowledgments

Scanning electron microscopy of the materials used in this work was performed using equipment at the Polymer Research Center, a shared-use facility of the Enikolopov Institute of Synthetic Polymer Materials, Russian Academy of Sciences.

Authors' contributions

I.Yu. Vasilyev—experiment planning, writing and editing the text of the article.

V.S. Petrenko—conducting the study.

V.A. Rod—conducting the study.

D.A. Golobokov—conducting the study, writing and editing the text of the article.

The authors declare no conflicts of interest.

REFERENCES

1. Povernov P.A., Shibryaeva L.S., Anshin S.M. Influence of modifying additives on the structure and properties of biodegradable mixtures based on poly-3-hydroxybutyrate and nitrile butadiene rubber. *Tonk. Khim. Tekhnol. = Fine Chem. Technol.* 2024;19(6): 517–527. https://doi.org/10.32362/2410-6593-2024-19-6-517-527
2. Studenikina L.N., Protasov A.V., Melnikov A.A., Povalyayeva T.R., Leonova A.A. Composite materials based on polysaccharide-filled polyethylene: production, application, disposal. *Inzhenernye Tekhnologii = Engineering Technologies.* 2025;1(9):126–133 (in Russ.).
3. Abushakhmanova Z.R., Mastalygina E.E., Pantyukhov P.V., *et al.* Structure Formation and Interaction of Polyethylene and Polycaprolactone in Blends. *Russ. J. Phys. Chem.* 2024;98(7): 1363–1371. https://doi.org/10.1134/S0036024424700353, https://www.elibrary.ru/qyhchh
[Original Russian Text: Abushakhmanova Z.R., Mastalygina E.E., Pantyukhov P.V., Olkhov A.A., Brovina S.D., Guyvan M.Yu., Popov A.A. Structure Formation and Interaction of Polyethylene and Polycaprolactone in Blends. *Zhurnal Fizicheskoi Khimii.* 2024;98(7):3–12 (in Russ.). https://doi.org/10.31857/S0044453724070012, https://www.elibrary.ru/pwvunn]
4. Pekhtasheva E., Mastalygina E., Leonova I., Palanisamy S., Alagarsamy A., Ayrilmis N., Sillanpää M., Al-Farraj S.A. Investigation of toxicity in textile materials from natural and synthetic-based polymers utilizing bioassay performances. *BioResources.* 2024;20(1):765–789. https://doi.org/10.15376/biores.20.1.765-789
5. El-Taweel S.H., Al-Hamdi A. Starch as a successful biodegradable nucleating agent in biodegradable PHBV/PHO blends. *J. Therm. Anal. Calorim.* 2024;149(4):1351–1364. https://doi.org/10.1007/s10973-023-12791-0
6. Yazlakowa Z., Amangeldyewa M., Amanowa G., Rejepowa S. Chitin films and their applications in modern technologies. *Ceteris Paribus.* 2025;4:33–35 (in Russ.).
7. Futoryanskaya A.M., Kudyshkin V.O. Modification of low molecular weight polyethylene with maleic anhydride and chitosan. *Plasticheskie Massy.* 2024;6:40–42 (in Russ.). https://doi.org/10.35164/0554-2901-2024-06-40-42
8. Gul-E-Nayyab, Zakaria M.R.Sh.B., Abid M.B., Shamim A., Suradi S.S., Marsi N.B., Kormin F.Bt. A review on biodegradable composite films containing organic material as a natural filler. *J. Inorgan. Organomet. Polym. Materials.* 2024;35:2126–2161. https://doi.org/10.1007/s10904-024-03217-x
9. Monina A.P., Apryatina K.V., Zaitsev S.D., Smirnova O.N., Yunin P.A., Smirnova L.A. Biodegradable material based on starch-g-polyvinyl acetate copolymer with bactericidal properties. *Polym. Bull.* 2024;81:10609–10630. https://doi.org/10.1007/s00289-024-05205-0
10. Liu Sh., Tang Sh., Lu Yu., Su T., Wang Zh. Preparation of esterified starches with different amylose content and their blending with polybutylene succinate. *Int. J Mol. Sci.* 2024;25(12):6301. https://doi.org/10.3390/ijms25126301
11. Olkhov A.A., Pantyukhov P.V., Mastalygina E.E., Abushakhmanova Z.R., Ovchinnikov V.A., Kupinsky N.G., Popov A.A. Technological challenges in the production of goods from dispersed-filled polymer composite materials. *Plekhanovskii Nauchnyi Byulleten'.* 2024;1(25):132–138 (in Russ.). https://www.elibrary.ru/tyzgcb
12. Kuzmin A.M., Ayrilmis N., Özdemir F., Kanat G. Effect of content and particle size of used beverage carton pieces on the properties of HDPE composites. *BioResources.* 2023;18(2):2815–2825. https://doi.org/10.15376/biores.18.2.2815-2825

СПИСОК ЛИТЕРАТУРЫ

1. Повернов П.А., Шибряева Л.С., Аншин С.М. Влияние модифицирующих добавок на структуру и свойства биоразлагаемых смесей на основе поли-3-гидроксибутирата и бутадиен-нитрильного каучука. *Тонкие химические технологии.* 2024;19(6):517–527. https://doi.org/10.32362/2410-6593-2024-19-6-517-527
2. Студеникина Л.Н., Протасов А.В., Мельников А.А., Поваляева Т.Р., Леонова А.А. Композитные материалы на основе наполненного полисахаридами полиэтилена: получение, применение, утилизация. *Инженерные технологии.* 2025;1(9):126–133.
3. Абушахманова З.Р., Масталыгина Е.Е., Пантюхов П.В., Ольхов А.А., Бровина С.Д., Гуйван М.Ю., Попов А.А. Исследование закономерностей формирования структуры и характера взаимодействия полиэтилена и поликапролактона в смесях. *Журн. физ. химии.* 2024;98(7):3–12. https://doi.org/10.31857/S0044453724070012, https://www.elibrary.ru/pwvunn
4. Pekhtasheva E., Mastalygina E., Leonova I., Palanisamy S., Alagarsamy A., Ayrilmis N., Sillanpää M., Al-Farraj S.A. Investigation of toxicity in textile materials from natural and synthetic-based polymers utilizing bioassay performances. *BioResources.* 2024;20(1):765–789. https://doi.org/10.15376/biores.20.1.765-789
5. El-Taweel S.H., Al-Hamdi A. Starch as a successful biodegradable nucleating agent in biodegradable PHBV/PHO blends. *J. Therm. Anal. Calorim.* 2024;149(4):1351–1364. https://doi.org/10.1007/s10973-023-12791-0
6. Язлакова З., Амангелдиева М., Аманова Г., Реджепова С. Хитиновые пленки и их использование в современных технологиях. *Ceteris Paribus.* 2025;4:33–35.
7. Футорянская А.М., Кудышкин В.О. Модификация низкомолекулярного полиэтилена малеиновым ангидридом и хитозаном. *Пластические массы.* 2024;6:40–42. https://doi.org/10.35164/0554-2901-2024-06-40-42
8. Gul-E-Nayyab, Zakaria M.R.Sh.B., Abid M.B., Shamim A., Suradi S.S., Marsi N.B., Kormin F.Bt. A review on biodegradable composite films containing organic material as a natural filler. *J. Inorgan. Organomet. Polym. Materials.* 2024;35:2126–2161. https://doi.org/10.1007/s10904-024-03217-x
9. Monina A.P., Apryatina K.V., Zaitsev S.D., Smirnova O.N., Yunin P.A., Smirnova L.A. Biodegradable material based on starch-g-polyvinyl acetate copolymer with bactericidal properties. *Polym. Bull.* 2024;81:10609–10630. https://doi.org/10.1007/s00289-024-05205-0
10. Liu Sh., Tang Sh., Lu Yu., Su T., Wang Zh. Preparation of esterified starches with different amylose content and their blending with polybutylene succinate. *Int. J Mol. Sci.* 2024;25(12):6301. https://doi.org/10.3390/ijms25126301
11. Ольхов А.А., Пантюхов П.В., Масталыгина Е.Е., Абушахманова З.Р., Овчинников В.А., Купинский Н.Г., Попов А.А. Технологические вызовы при производстве изделий из дисперсно-наполненных полимерных композиционных материалов. *Плехановский научный бюллетень.* 2024;1(25):132–138. https://www.elibrary.ru/tyzgcb
12. Kuzmin A.M., Ayrilmis N., Özdemir F., Kanat G. Effect of content and particle size of used beverage carton pieces on the properties of HDPE composites. *BioResources.* 2023;18(2):2815–2825. https://doi.org/10.15376/biores.18.2.2815-2825
13. Brovina S.D., Mastalygina E.E., Trofimchuk E.S., Popov A.A. Development of materials based on poly(lactic acid) and copper(II) sulfate impregnated by the crazing method. *Colloid J.* 2024;86(1):4–13. https://doi.org/10.1134/S1061933X23601178

13. Brovina S.D., Mastalygina E.E., Trofimchuk E.S., Popov A.A. Development of materials based on poly(lactic acid) and copper(II) sulfate impregnated by the crazing method. *Colloid J.* 2024;86(1):4–13. https://doi.org/10.1134/S1061933X23601178
14. Sirazetdinov A.V., Nikiforov A.A., Volfson S.I. Polymer composites based on polylactide. *Kauchuk i Rezina.* 2021;80(6):326–336 (in Russ). https://doi.org/10.47664/0022-9466-2021-80-6-326-336
15. Shapovalov V.M., Vinidiktova N.S., Kovalenko M.A., Konakova O.V. Biodegradable plastics based on plant raw materials: varieties, properties, applications. *Polimernye Materialy i Tekhnologii = Polymer Materials and Technologies.* 2024;10(2):6–19 (in Russ.). https://doi.org/10.32864/polymmattech-2024-10-2-6-19
16. Poddenezhny E.N., Drobysheskaya N.E., Boiko A.A., Shapovalov V.M. The use of flax fiber for forming biodegradable composites with a polylactide matrix. *Vestnik Gomel'skogo gosudarstvennogo tekhnicheskogo universiteta imeni P.O. Sukhogo.* 2023;4(95):22–29 (in Russ.). https://www.elibrary.ru/eelvwg
17. Michurov D.M., Shkuro A.E., Glukhikh V.V. Study of the physical and mechanical properties of composites with a polymer phase of polylactide and hemp shives. *Vestnik Tekhnologicheskogo Universiteta = Herald of Technological University.* 2024;27(1):59–63 (in Russ.). https://doi.org/10.55421/1998-7072_2024_27_1_59
18. Tertyshnaya Y.V., Podzorova M.V., Karpova S.G., *et al.* Structural Features of Polylactide and Natural Rubber Films Produced by Solution Casting. *Russ. J. Phys. Chem. B.* 2024;18(2):592–598. https://doi.org/10.1134/S1990793124020313 [Original Russian Text: Tertyshnaya Yu.V., Podzorova M.V., Karpova S.G., Krivandin A.V. Structural Features of Polylactide and Natural Rubber Films Produced by Solution Casting. *Khimicheskaya Fizika.* 2024;43(4):110–118 (in Russ.). https://doi.org/10.31857/S0207401X24040133]
19. Poddenezhny E.N., Boiko A.A., Drobysheskaya N.E., Shapovalov V.M. Biodegradable polymer composites filled with corn starch (Review). *Polimernye materialy i tekhnologii = Polymer Materials and Technologies.* 2024;10(3):6–19 (in Russ.). https://doi.org/10.32864/polymmattech-2024-10-3-6-19
20. Bazhenov N.S., Gubanova M.I., Kirsh I.A., Bannikova O.A., Dymytsky V.A. Current state and use of biodegradable materials. *Health, Food & Biotechnology.* 2024;6(3):42–56 (in Russ.). https://doi.org/10.36107/hfb.2023.i3.s232
21. Lytkina D.N., Shalygina K.D., Gigilev A.S., Korotchenko N.M., Kurzina I.A., Kozik V.V. Physicochemical properties of biocompatible composites based on hydroxyapatite and copolymer of lactide and glycolide. *Vestnik Tomskogo gosudarstvennogo universiteta. Khimiya = Tomsk State University Journal of Chemistry.* 2023;29:116–139 (in Russ.). https://doi.org/10.17223/24135542/29/11
22. Mironov V.V., Trofimchuk E.S., Zagustina N.A. *et al.* Solid-Phase Biodegradation of Polylactides (Review). *Appl. Biochem. Microbiol.* 2022;58(6):665–676. https://doi.org/10.1134/s0003683822060102 [Original Russian Text: Mironov V.V., Trofimchuk E.S., Zagustina N.A., Ivanova O.A., Vanteeiva A.V., Bochkova E.A., Ostrikova V.V., Zhang Sh. Solid-Phase Biodegradation of Polylactides (Review). *Prikladnaya Biokhimiya i Mikrobiologiya.* 2022;58(6):537–550 (in Russ.). https://doi.org/10.31857/S0555109922060101]
14. Сиразетдинов А.В., Никифоров А.А., Вольфсон С.И. Полимерные композиционные материалы на основе полилактида. *Каучук и резина.* 2021;80(6):326–336. https://doi.org/10.47664/0022-9466-2021-80-6-326-336
15. Шаповалов В.М., Винидиктова Н.С., Коваленко М.А., Конакова О.В. Биоразлагаемые пластики на основе растительного сырья: разновидности, свойства, области применения. *Полимерные материалы и технологии.* 2024;10(2):6–19. https://doi.org/10.32864/polymmattech-2024-10-2-6-19
16. Подденежный Е.Н., Дробышевская Н.Е., Бойко А.А., Шаповалов В.М. Применение льнокостры для формирования биоразлагаемых композитов с полилактидной матрицей. *Вестник Гомельского государственного технического университета им. П.О. Сухого.* 2023;4(95):22–29. https://www.elibrary.ru/eelvwg
17. Мичуров Д.М., Шкуро А.Е., Глухих В.В. Исследование физико-механических свойств композитов с полимерной фазой полилактида и кострой конопли. *Вестник Технологического университета.* 2024;27(1):59–63. https://doi.org/10.55421/1998-7072_2024_27_1_59
18. Тертышная Ю.В., Подзорова М.В., Карпова С.Г., Кривандин А.В. Структурные особенности пленок полилактида и натурального каучука, полученных из раствора. *Химическая физика.* 2024;43(4):110–118. https://doi.org/10.31857/S0207401X24040133
19. Подденежный Е.Н., Бойко А.А., Дробышевская Н.Е., Шаповалов В.М. Биоразлагаемые полимерные композиты, наполненные кукурузным крахмалом (обзор). *Полимерные материалы и технологии.* 2024;10(3):6–19. https://doi.org/10.32864/polymmattech-2024-10-3-6-19
20. Баженов Н.С., Губанова М.И., Кирш И.А., Банникова О.А., Дымицкий В.А. Современное состояние и использование биоразлагаемых материалов. *Health, Food & Biotechnology.* 2024;6(3):42–56. https://doi.org/10.36107/hfb.2023.i3.s232
21. Лыткина Д.Н., Шалыгина К.Д., Гигилев А.С., Коротченко Н.М., Курзина И.А., Козик В.В. Физико-химические свойства биосовместимых композитов на основе гидроксиапатита и сополимера лактида и гликолида. *Вестник Томского государственного университета. Химия.* 2023;29:116–139. https://doi.org/10.17223/24135542/29/11
22. Миронов В.В., Трофимчук Е.С., Загустина Н.А., Иванова О.А., Вантеева А.В., Бочкова Е.А., Острикова В.В., Чжан Ш. Твердофазная биодеградация полилактида (обзор). *Прикладная биохимия и микробиология.* 2022;58(6):537–550. https://doi.org/10.31857/S0555109922060101
23. Купинский Н.Г., Пантюхов П.В., Абушахманова З.Р., Ольхов А.А., Масталыгина Е.Е., Попов А.А. Изучение возможности использования стеаратов переходных металлов в качестве основы прооксидантной добавки. В сб.: *Новые материалы и технологии для устойчивого развития: Материалы III Международной научной конференции.* М.; 2024. С. 110–113. https://www.elibrary.ru/xfngwe
24. Купинский Н.Г., Абушахманова З.Р., Пантюхов П.В., Масталыгина Е.Е., Овчинников В.А., Ольхов А.А., Попов А.А. Стеараты переходных металлов как оксодобавки для полиолефинов. В сб.: *Экологические аспекты в науке и образовании: Материалы межвузовской научной конференции.* М.; 2023. С. 34–35. https://www.elibrary.ru/wejqrx
25. Подзорова М.В., Тертышная Ю.В., Московский М.Н. Фотодеградация композиционных материалов полилактид – натуральный каучук. *Известия Кабардино-Балкарского государственного университета.* 2022;12(4):118–123. https://www.elibrary.ru/bkzwgo

23. Kupinskii N.G., Pantyukhov P.V., Abushakhmanova Z.R., Olkhov A.A., Mastalygina E.E., Popov A.A. Study of the potential use of transition metal stearates as a basis for a pro-oxidant additive. In: *New Materials and Technologies for Sustainable Development*: *Proceedings of the Third International Scientific Conference.* Moscow; 2024. P. 110–113 (in Russ.). https://www.elibrary.ru/xfngwe
24. Kupinskii N.G., Abushakhmanova Z.R., Pantyukhov P.V., Mastalygina E.E., Ovchinnikov V.A., Olkhov A.A., Popov A.A. Transition metal stearates as oxo-additives for polyolefins. In: *Environmental Aspects in Science and Education*: *Proceedings of the Interuniversity Scientific Conference.* Moscow; 2023. P. 34–35 (in Russ.). https://www.elibrary.ru/wejqrx
25. Podzorova M.V., Tertyshnaya Yu.V., Moskovskiy M.N. Photodegradation of composite materials polylactide – natural rubber. *Izvestiya Kabardino-Balkarskogo Gosudarstvennogo Universiteta = Proceedings of the Kabardino-Balkarian State University.* 2022;12(4):118–123 (in Russ.). https://www.elibrary.ru/bkzwgo
26. Ovchinnikov V.A., Abushakhmanova Z.R., Mastalygina E.E., Pantyukhov P.V., Mamin E.A., Kupinskiy N.G., Popov A.A. Kinetic features of oxidative degradation of polyethylene with addition of stearates of various transition metals. *Vse Materialy. Ehntsiklopedicheskii Spravochnik.* 2024;1:31–36 (in Russ.). https://www.elibrary.ru/yuokwo
27. Mikheev Yu.A., Lomakin S.M., Usachev S.V., Koverzanova E.V., Artsis M.I., Stoyanov O.V. Photodegradation of semi-crystalline polylactide under UV radiation. II. Stages of matrix transformation according to the DSC method. *Vestnik Tekhnologicheskogo Universiteta = Herald of Technological University.* 2024;27(10):16–22 (in Russ.). https://doi.org/10.55421/1998-7072_2024_27_10_16
26. Овчинников В.А., Абушахманова З.Р., Масталыгина Е.Е., Пантюхов П.В., Мамин Э.А., Купинский Н.Г., Попов А.А. Кинетические особенности окислительной деструкции полиэтилена при добавлении стеаратов различных переходных металлов. *Все материалы. Энциклопедический справочник.* 2024;1:31–36. https://www.elibrary.ru/yuokwo
27. Михеев Ю.А., Ломакин С.М., Усачев С.В., Коверзанова Е.В., Арцис М.И., Стоянов О.В. Фотодеградация полукристаллического полилактида под действием УФ-радиации. II. Стадии матричной трансформации по данным метода ДСК. *Вестник Технологического университета.* 2024;27(10):16–22. https://doi.org/10.55421/1998-7072_2024_27_10_16

About the Authors

Ilya Yu. Vasilyev, Cand. Sci. (Eng.), Associate Professor, Moscow Polytechnic University (38, Bolshaya Semyonovskaya ul., Moscow, 107023, Russia). E-mail: iljanaras@ya.ru. Scopus Author ID 57195569317, ResearcherID ABW-6525-2022, RSCI SPIN-code 2038-4156, https://orcid.org/0000-0001-8488-5907

Victoria S. Petrenko, Student, Moscow Polytechnic University (38, Bolshaya Semyonovskaya ul., Moscow, 107023, Russia). E-mail: petrenkoviktoria480@gmail.com. https://orcid.org/0009-0006-4131-8623

Viktor A. Rod, Student, Moscow Polytechnic University (38, Bolshaya Semyonovskaya ul., Moscow, 107023, Russia). E-mail: vikdor.andreevich@mail.ru. RSCI SPIN- code 5509-7202, https://orcid.org/0009-0008-8333-4749

Dmitrii A. Golobokov, Junior Researcher, Enikolopov Institute of Synthetic Polymeric Materials of the Russian Academy of Sciences (70, Profsoyuznaya ul., Moscow, 117393, Russia). E-mail: d.golobokov@ispm.ru. ResearcherID MBG-4040-2025, RSCI SPIN-code 7346-6740, https://orcid.org/0000-0002-4678-9866

Об авторах

Васильев Илья Юрьевич, к.т.н., доцент, ФГАОУ ВО Московский политехнический университет (Мосполитех) (107023, Россия, Москва, ул. Большая Семеновская, д. 38). E-mail: iljanaras@ya.ru. Scopus Author ID 57195569317, ResearcherID ABW-6525-2022, SPIN-код РИНЦ 2038-4156, https://orcid.org/0000-0001-8488-5907

Петренко Виктория Сергеевна, студент, ФГАОУ ВО Московский политехнический университет (Мосполитех) (107023, Россия, Москва, ул. Большая Семеновская, д. 38). E-mail: petrenkoviktoria480@gmail.com. https://orcid.org/0009-0006-4131-8623

Род Виктор Андреевич, студент, ФГАОУ ВО Московский политехнический университет (Мосполитех) (107023, Россия, Москва, ул. Большая Семеновская, д. 38). E-mail: vikdor.andreevich@mail.ru. SPIN-код РИНЦ 5509-7202, https://orcid.org/0009-0008-8333-4749

Голобоков Дмитрий Александрович, младший научный сотрудник, ФГБУН Институт синтетических полимерных материалов им. Н.С. Ениколопова Российской академии наук, (117393, Россия, Москва, ул. Профсоюзная, д. 70). E-mail: d.golobokov@ispm.ru. ResearcherID MBG-4040-2025, SPIN-код РИНЦ 7346-6740, https://orcid.org/0000-0002-4678-9866

Translated from Russian into English by V. Glyanchenko
Edited for English language and spelling by Thomas A. Beavitt

Tonkie Khimicheskie Tekhnologii = Fine Chemical Technologies.
2026;21(2):226–236
ISSN 2686-7575 (Online)

Synthesis and processing of polymers and polymeric composites
Синтез и переработка полимеров и композитов на их основе

UDC 691.175.2
https://doi.org/10.32362/2410-6593-2026-21-2-226-236
EDN DQUAQT

RESEARCH ARTICLE

Features of changes in the electrical resistance of mixtures of crystallizing polymers with carbon black upon heating

Anatoly V. Markov[1], Alexander E. Zverev[1,✉], Elena V. Kalugina[1,2], Vasily A. Markov[3]

[1] *MIREA – Russian Technological University (M.V. Lomonosov Institute of Fine Chemical Technologies), Moscow, 119454 Russia*

[2] *POLYPLASTIC Group, Moscow, 119530 Russia*

[3] *BELL INNOVATION INTEGRATOR, Moscow, 115088 Russia*

✉ *Corresponding author, e-mail: azmonst@gmail.com*

Abstract

Objectives. The effects of positive and negative temperature coefficients (PTC and NTC, respectively) in carbon black-filled conductive polymer composites based on high-density polyethylene grade 277-73 and polypropylene grade 01050 were investigated. Carbon black electrically conducting grade OMCARB C-140 (UM-76) was used as the filler.

Methods. To study the electrical characteristics of the compositions, plates were pressed with brass contact electrodes at the plate ends to simulate polymer heaters. The electrical resistance of the samples was evaluated using an ohmmeter DT9208A (*RESANTA*, Latvia). Tests at elevated temperatures were carried out in an SNOL 3.5 heat chamber (*NPF TherMIX*, Russia) with a heating rate of ~3°C/min. The crystallinity of the samples during heating was assessed by differential scanning calorimetry on a DSC 204F1 Phoenix device (*NETZSCH*, Germany) with a heating rate of 3°C/min.

Results. The complex PTC and NTC mechanisms in mixed polymer compositions are not solely related to thermal expansion and melting of the polymer. While changes in the electrical resistance of carbon-filled polymer composites are associated with the presence of crystalline regions with defects, the destruction of the conductive channels occurs at the earliest stages of polymer melting due to the formation of expanding amorphous “microdroplets” of the hot melt. For a carbon-filled, electrically conductive mixture of polyethylene and polypropylene, the magnitude and nature of the change in the peak temperature of the PTC depends on the melting onset temperature of the lowest-melting phase of polyethylene. At the same time, the heterogeneity of the mixtures of crystallizing polymers with technical carbon increases the thermal stability of the material by expanding the PTC zone into the melting region of the higher-melting phase of polypropylene. When comparing electrically conductive compositions of polymers with different melting points and carbon black, the low-melting polymer determines the temperature of self-regulation and the nature of PTC, while the high-melting polymer shifts the jump in electrical conductivity to the region of elevated temperatures.

Conclusions. The activation energies of carbon-filled mixtures of polyethylene and polypropylene, which are weakly dependent on the mixing method, are approximately 44 ± 3 kJ/mol. The obtained values are consistent with the activation energy values for the viscous melt flow process. The method of mixing the components in mixtures of carbon-filled compositions based on crystallizing polymers was found to have little effect on PTC. The use of carbon-filled polymer compositions with a mixed matrix of polyethylene and polypropylene allows for the regulation of the intensity of PTC and NTC.

Keywords

conductive polymer composites, positive and negative temperature coefficients, polyethylene, polypropylene, carbon black, degree of crystallinity, specific electrical resistance

Submitted: 07.11.2024
Revised: 27.11.2025
Accepted: 12.02.2026

For citation

Markov A.V., Zverev A.E., Kalugina E.V., Markov V.A. Features of changes in the electrical resistance of mixtures of crystallizing polymers with carbon black upon heating. *Tonk. Khim. Tekhnol. = Fine Chem. Technol.* 2026;21(2):226–236. https://doi.org/10.32362/2410-6593-2026-21-2-226-236

НАУЧНАЯ СТАТЬЯ

Особенности изменения электрического сопротивления смесей кристаллизующихся полимеров с техническим углеродом при нагревании

А.В. Марков[1], А.Е. Зверев[1,✉], Е.В. Калугина[1,2], В.А. Марков[3]

[1] *МИРЭА – Российский технологический университет (Институт тонких химических технологий им. М.И. Ломоносова), Москва, 119454 Россия*

[2] *ООО «Группа ПОЛИПЛАСТИК», Москва, 119530 Россия*

[3] *ООО «БЭЛЛ ИНТЕГРАТОР ИННОВАЦИИ», Москва, 115088 Россия*

✉ *Автор для переписки, e-mail: azmonst@gmail.com*

Аннотация

Цели. Исследовать эффекты положительного и отрицательного температурных коэффициентов (ПТК и ОТК соответственно) саженаполненных электропроводных полимерных композиционных материалов на основе полиэтилена высокой плотности марки 277-73 и полипропилена марки 01050, где в качестве наполнителя использовали технический углерод специальной электропроводной марки Omcarb C-140 (УМ-76).

Методы. Для исследования электрических характеристик композиций были отпрессованы пластины с запрессованными на концах контактными электродами из обезжиренной латунной сетки, моделирующие полимерные нагреватели. Электрическое сопротивление образцов оценивали с помощью омметра DT9208A (*РЕСАНТА*, Латвия). Испытания при повышенных температурах проводили в термошкафу СНОЛ 3.5 (*НПФ ТермИКС*, Россия) со скоростью нагревания ~3°С/мин. Степень кристалличности образцов при нагревании оценивали методом дифференциальной сканирующей калориметрии на приборе DSC 204F1 Phoenix (*NETZSCH*, Германия) со скоростью нагревания 3°С/мин.

Результаты. Показано, что механизмы ПТК и ОТК в смесевых полимерных композициях носят комплексный характер и не связаны только с тепловым расширением и плавлением полимера. Изменение электрического сопротивления саженаполненных полимерных композиций происходит из-за наличия дефектных кристаллических участков. На ранних стадиях начала плавления полимера токопроводящие каналы разрушаются за счет появления расширяющихся аморфных «микрокапель» его расплава. Для саженаполненной электропроводной смесевой композиции полиэтилена и полипропилена величина и характер изменения пика ПТК зависят от температуры начала плавления наиболее низкоплавкой фазы полиэтилена. При этом гетерогенность смесей кристаллизующихся полимеров с техническим углеродом повышает термическую устойчивость материала за счет расширения зоны ПТК в область плавления более высокоплавкой фазы полипропилена. Для электропроводных композиций двух полимеров с различной температурой плавления и технического углерода показано, что низкоплавкий полимер задает температуру «саморегулирования» и характер ПТК, в то время как высокоплавкий полимер смещает скачок электрической проводимости материала в область повышенных температур.

Выводы. Установлено, что энергии активации смесевых саженаполненных композиций полиэтилена с полипропиленом мало зависят от способов смешения и составляют 44 ± 3 кДж/моль. Полученные величины совпадают со значениями энергии активации процесса вязкого течения расплава. Установлено, что способ совмещения компонентов смесей саженаполненных композиций на основе кристаллизующихся полимеров мало влияет на эффект ПТК. Установлено, что использование саженаполненных полимерных композиций со смесевой матрицей полиэтилена и полипропилена позволяет регулировать интенсивность эффектов ПТК и ОТК.

Ключевые слова

электропроводные полимерные композиционные материалы, положительный и отрицательный температурные коэффициенты, полиэтилен, полипропилен, технический углерод, степень кристалличности, удельное электрическое сопротивление

Поступила: 07.11.2024
Доработана: 27.11.2025
Принята в печать: 12.02.2026

Для цитирования

Марков А.В., Зверев А.Е., Калугина Е.В., Марков В.А. Особенности изменения электрического сопротивления смесей кристаллизующихся полимеров с техническим углеродом при нагревании. *Тонкие химические технологии*. 2026;21(2):226–236. https://doi.org/10.32362/2410-6593-2026-21-2-226-236

INTRODUCTION

Although the effects of abnormally high positive and negative temperature coefficients (PTC and NTC, respectively) in polymer composites (PCs) have been known since the mid-20th century [1–3], researchers have yet to reach a consensus on the causes of these phenomena. At the same time, there are many patents for the application of carbon black-filled conductive polymer composites (CPCs) exhibiting PTC and/or NTC effects as various heating and thermostatic devices, heating elements with thermoregulation, self-regulating cables, etc. [4–16]. Such an abundance of patents and scientific publications, which indicates the promising industrial application of such materials, stimulates new research in the field of CPCs in order to understand the mechanism of PTC and NTC effects.

The selections of special grades of carbon black (CB) typically used as an electrically conductive filler in the production of CPCs is due to the peculiarity of the CB structure, in which the conductivity reaches 2.4 S/cm [17]. The electrical conductivity of CB polymer composites is achieved through the formation of conductive channels within the matrix structure, through which electrical charges flow [18–21]. The flow of electrons through interconnected carbon particles and their aggregates can occur through the mechanism of electronic conductivity [18, 22]. In polymer composites filled with CB, electron tunneling through thin dielectric layers (polymer matrix) at distances of ~5–10 nm also becomes possible [18, 22, 23].

In the case of crystallizing polymers, whose spherulites consist of dense crystallites and amorphous regions between them, local agglomeration of carbon particles is observed [24]. The observed concentration of carbon particles between crystallites during the growth of spherulites in polyethylene (PE) [24–27] permits the achievement of higher electrical conductivity values as compared to PCs based on amorphous polymers [28].

A significant increase in the electrical conductivity of polymer composites is achieved at a certain CB content, which is referred to as the percolation threshold, while the corresponding content at which the transition of CPCs from a dielectric to a semiconductor and further to a conductor occurs is called the percolation transition [29]. However, additional electrical conductivity with further increases in the CB content of the CPCs is impeded due to the formation of a stable electrically conductive cluster whose predominantly contact conductivity occurs in the volume of the polymer composite. The instability exhibited by the system of current-conducting channels at lower CB contents prior to the appearance of such clusters, which are stable and resistant to external influences, responds to thermal and deformation effects with a sharp increase in electrical resistance, giving rise to the PTC phenomenon in the studied polymer composites with CB.

The electrical characteristics of blended polymer compositions depend on the distribution of electrically conductive filler between polymer phases. In a study of high-density polyethylene (HDPE) compositions with polypropylene (PP) filled with CB with a primary particle diameter of 27 nm, CB was found to concentrate in the matrix of lower-melting PE [30]. The electrical conductivity of the CPCs can be increased by concentrating electrically conductive filler at the interface between the two polymers [30, 31]. The example of PE/PP mixtures shows that, despite the fact that carbon is concentrated in the PE phase, the percolation threshold of the composition remains virtually unchanged compared to filled PE [30, 32]. The distribution of CB along the phase boundary forms electrically conductive channels with a lower filler content [30, 31].

Analysis of scientific and technical information indicates accelerated annual growth in the number of publications and new developments in this field over the last two decades. However, the proportion of publications revealing the mechanism of the PTC phenomenon in polymer mixtures is relatively small. This work is devoted to the study of the peculiarities of the mechanism of the PTC phenomenon in mixtures of crystallizing polymers (PE and PP) prepared by various methods.

EXPERIMENTAL

The objects of the study were HDPE 277-73 Stavrolen (GOST 16338-85[1]) and PP 01050 Balen (CB 2211-074-05766563-2015[2]). CB grade OMCARB C-140 (UM-76)

[1] GOST 16338-85. Interstate Standard. Low-pressure polyethylene. Specifications. Moscow: Standartinform; 2005 (in Russ.).

[2] https://polimermsk.ru/image/catalog/product/passport/TU%202211-074-05766563-2015.pdf. Accessed January 21, 2026 (in Russ.).

(*Carbon*, Russia, CB 38-10001-94) was used as an electrically conductive filler. The preparation of the composite mixtures was carried out under the same conditions as in [33] using several methods to combine CB with PE and PP. The total content of CB in all composites was 20 wt % (11.7 vol %). The components were combined in two stages: following the preparation of two-component mixtures of PE/CB, PP/CB, or PE/PP, either a third component (PE, PP, or CB) was introduced or two mixtures were combined. Thus, various mixed composites (PE/CB)/PP, (PP/CB)/PE, (PE/PP)/CB, and (PP/CB)/(PE/CB) were obtained with PE and PP ratios equal to 1 to 1.

Test specimens having a length of $L = 120 \pm 2$ mm, width $b = 10 \pm 0.5$ mm, and thickness $\delta = 1.0 \pm 0.05$ mm were pressed with contact electrodes made of L-80 brass mesh (GOST 6613-86[3]) onto the ends at 180°C for 3 min and cooled in the press to 50°C. This helped to stabilize the crystal structure of the samples to prevent the appearance of the "calender" effect.

The electrical resistance of the samples was measured using a DT9208A ohmmeter (*RESANTA*, Latvia). Tests at elevated temperatures were carried out in a SNOL 3.5 oven (*ThermIKS*, Russia) at a heating rate of ~3°C/min. The temperature coefficient of electrical resistance α (1/°C) was calculated using Eq. (1):

$$\alpha = \frac{\Delta\rho}{\rho_0 \Delta T}, \quad (1)$$

where ρ is the measured specific volume electrical resistance (Ohm·cm); Δρ is the change in specific volume electrical resistance (Ohm·cm) with a change in temperature ΔT (°C); ρ_0 is the specific volume electrical resistance of samples (Ohm·cm) under normal conditions: PE/CB = 32.5 Ohm·cm and PP/CB = 11.5 Ohm·cm.

The change in the degree of crystallinity of polymers upon heating was studied using differential scanning calorimetry on a DSC 204F1 Phoenix device (*NETZSCH*, Germany) at a heating rate of 3°C/min. The degree of crystallinity D (%) was calculated using Eq. (2):

$$D = 100 \frac{\Delta H_m}{\Delta H_{cr}}, \quad (2)$$

where ΔH_m is enthalpy of melting of the crystalline phase of the sample, calculated taking into account the CB mass fraction (kJ/mol); ΔH_{cr} is the melting enthalpy of the crystalline phase of the polymer (kJ/mol). Values of D under normal conditions: PE/CB = 70.5%, PP/CB = 48.5%.

RESULTS AND DISCUSSION

Figure 1 shows the dependencies of the specific volume electrical resistances of the initial PE and PP compositions with CB during heating. The nature of the change in these dependencies corresponds to that described in the introduction. The presence of peaks on the curves ensures self-regulation of the heaters' power when the external temperature rises. The mechanism of this phenomenon was described in detail by in an earlier study [33]. The difference in the course of crystallization processes leads to a shift of the peak of the PTC of PP relative to the peak of PE to a higher temperature range, as well as to an expansion of the temperature range of the NTC of PP.

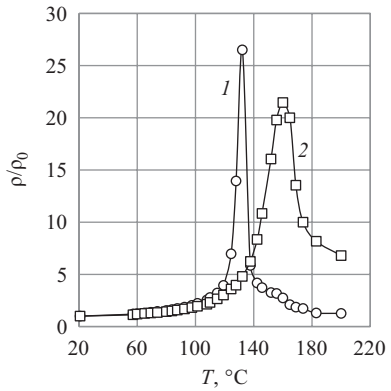

Fig. 1. Change in the specific volume electrical resistances (ρ/ρ_0) for PE/CB (*1*) and PP/CB (*2*) compositions when heated [33]

The phenomenon of NTC (decrease in electrical resistance) can result in a sharp increase in the power of the heater and its subsequent failure or even a fire. Currently, such phenomena are eliminated by radiation or chemical cross-linking of the polymer [28].

For greater clarity of these features and understanding of the mechanism of the PTC phenomenon, Fig. 2 shows graphs of the dependencies of the reduced degree of crystallinity D/D_0 (*1*) and reduced electrical conductivity σ/σ_0 (*2*) of PE (a) and PP (b) compositions with CB during heating. It should be noted that the CPCs samples were heated at a constant heating rate of ~3°C/min. For this reason, the data are considered to be kinetic, since the changes in time and temperature are proportional. The change in these dependencies for PE and PP compositions is similar, but here the electrical conductivity indicators decrease with increasing temperature. In PP CPCs, due to the higher melting point, this dependence is shifted to the higher temperature range. This indicates a connection between PTC and the

[3] GOST 6613-86. Interstate Standard. Square meshed woven wire cloths. Specifications. Moscow: Standartinform; 2005 (in Russ.).

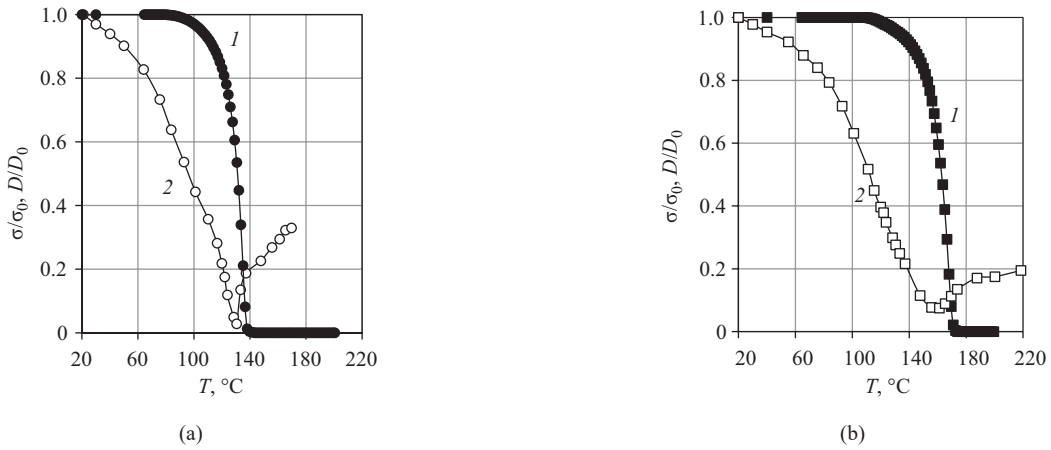

Fig. 2. Comparison of the dependence of the reduced degree of crystallinity D/D_0 (*1*) and reduced electrical conductivity σ/σ_0 (*2*) for (a) PE/CB and (b) PP/CB compositions when heated

process of decreasing crystallinity, which runs parallel to the decrease in their electrical conductivity until the onset of the NTC effect.

At the studied temperatures, the degree of crystallinity is characterized by a period of slow decline, followed by an accelerating decline until the polymer becomes completely amorphous. Unlike the degree of crystallinity, the electrical conductivity of CPCs begins to decrease significantly at much lower temperatures. This slow decrease in the electrical conductivity of CPCs can be partially attributed to thermal expansion during the heating of polymers, which is associated with the intensification of molecular thermal motion. But further in the experiment, as the temperature approaches the melting point of the crystalline formations that appeared in the final stages of polymer crystallization at low temperatures, this decline significantly outpaces the process of decreasing crystallinity. In contrast to the degree of crystallinity, which decreases to zero (Fig. 2), the PTC stage of the accelerated decrease in electrical conductivity of CPCs transitions to the NTC stage, in which electrical conductivity begins to gradually increase.

The above results of the study of the effect of heating on the properties of CPCs confirm the conclusions [28] that the mechanisms of PTC and NTC are not only related to thermal expansion and melting of CPCs. To clarify the described features of changes in electrical resistance in mixed CPCs, the activation energies of the described processes in the PTC temperature zone were determined. Figure 3 shows the dependence of the temperature coefficients of electrical resistance α on temperature in coordinates corresponding to the Arrhenius equation (the PTC temperature range of mixed compositions is highlighted with a dotted line).

The calculated activation energies of the studied mixed compositions, which are only weakly dependent on the methods of mixing the components, amount to 44 ± 3 kJ/mol. These values differ from the activation energies of their melting, but coincide with the values of the activation energy of the viscous flow of melts (E_{vf}) and the energy of destruction of conductive channels in the PTC zone (E_{el}) of the studied HDPE and PP [28]. For this reason, we may speak of their common mechanism.

Thus, the rate of increase in electrical resistance in polymer mixtures in the PTC temperature range depends on the presence of defective crystalline regions in the polymers. Due to the concentration of CB particles in the least heat-resistant interspherulite regions of crystallizing polymers and their mixtures, the destruction of conductive channels occurs at the earliest stages of polymer melting with the appearance of expanding amorphous microdroplets of its melt.

The effects of heating on changes in the electrical resistance of the CPCs under study are not limited to this phenomenon. Figure 4 shows the generalized results of electrical tests conducted on all of the above-described mixture samples. From Fig. 4 onwards, the dotted lines

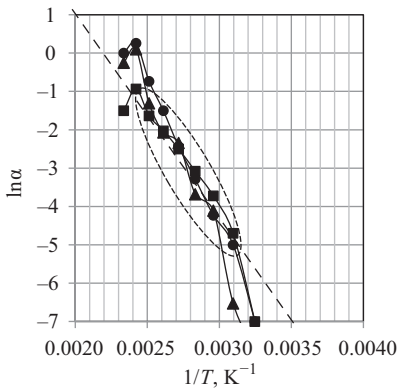

Fig. 3. Dependence of ln α on the reverse temperature ($1/T$, K^{-1}) for CPCs: (PE/CB)/PP (■), (PP/CB)/PE (▲), and (PE/PP/CB) (●)

highlight the detail previously studied [33] dependencies of two-component composites (PE/CB, PP/CB) used for comparison. Solid lines are used for three-component composites: (PE/CB)/PP, (PP/CB)/PE, (PE/PP)/CB, (PP/CB)/(PE/CB).

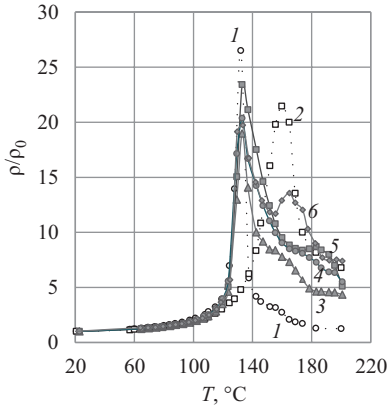

Fig. 4. Change in the specific volume electrical resistances (ρ/ρ_0) when CPCs are heated: PE/CB (*1*), PP/CB (*2*), (PE/CB)/PP (*3*), PP/CB/(PE/CB) (*4*), (PE/PP)/CB (*5*), and (PP/CB)/PE (*6*)

The first thing that catches the eye is the coincidence of all lines of mixed compositions in the PTC temperature range with the dotted line PE/CB, as well as the appearance of additional peaks of varying heights in the NTC temperature range of mixed PP/CB compositions. It should be noted that, unlike the PTC phenomenon in polymer heating devices, the NTC phenomenon is undesirable, since, at high operating temperatures of CPC heating elements, a drop in resistance can cause a sharp jump in power and destruction of the heater. As mentioned above, polymer heaters made of CPCs are currently subjected to radiation or chemical cross-linking to eliminate the NTC effect [28]. This is a technologically complex process that requires special equipment and reagents. This feature of electrical resistance change in mixed CPCs indicates the possibility of reducing the NTC effect. However, in Fig. 4 in the NTC temperature ranges, all lines diverge and intertwine, which makes it difficult to analyze the effect of the composition of mixed composites on the change in their specific volume electrical resistances (ρ/ρ_0). Therefore, the dependencies shown in the generalized Fig. 4 will be divided into three groups to take into account the intensity of the influence of the PP phase (the numbering of the lines is preserved in all figures).

The least influence on the nature of the change in specific volume electrical resistance is expected to be observed in the (PE/CB)/PP composite, in which CB is initially mixed with PE before mixing the concentrated PE/CB composition with PP. Due to the increased content of CB in the PE phase, the height of the PTC peak decreases.

Figure 5 shows the results of a study of the change in electrical resistance during heating of CPCs (PE/CB)/PP.

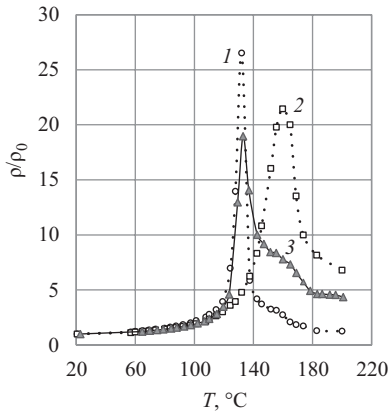

Fig. 5. Change in the specific volume electrical resistances (ρ/ρ_0) when CPCs are heated: PE/CB (*1*), PP/CB (*2*), and (PE/CB)/PP (*3*)

It should be noted that when melts with similar PE and PP contents are mixed, heterophase systems in which two continuous microfibrous phases are formed[4] [34]. The concentration of CB particles in the low-melting phase (PE) of the mixture leads to an increase in the stability of the system of conductive channels in its fibers and a consequent decrease in the peak height of the material's PTC. The NTC temperature zone of this mixture expands into the higher temperature region to partially capture the NTC zone of the PP/CB mixture. The appearance of PP traces in mixtures is commonly explained by the migration of CB particles from the PE phase into its phase [31, 32]. Although this factor cannot be ruled out, a more likely explanation may be the above-described beginning of the appearance of expanding microregions of amorphous PP melt. However, this increase (ρ increased approximately 2 times) is not sufficient for completely eliminating the undesirable NTC phenomenon in this composition.

Figure 6 shows the results of a study of changes in the electrical resistance of two CPCs with similar behavior when heated: (PE/CB)/(PP/CB) and (PE/PP)/CB.

The increased CB content in PP in these compositions results in the trace of PP in the temperature zone of its PTC becoming more noticeable and distinct to increase the resistance of the CPC data to overheating.

[4] Markov A.V. Technology of oriented multicomponent polymer films. Dr. Sci. Thesis (Eng.). Moscow: Lomonosov Moscow State Academy of Fine Chemical Technology; 2006 (in Russ.).

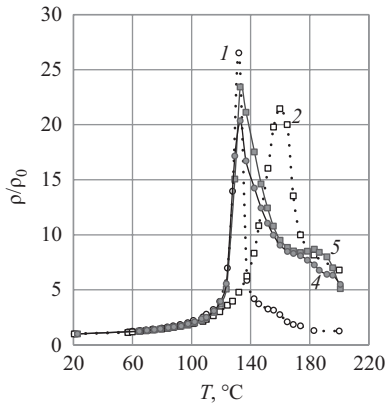

Fig. 6. Change in the specific volume electrical resistances (ρ/ρ_0) when CPCs are heated: PE/CB (*1*), PP/CB (*2*), (PE/CB)/(PP/CB) (*4*), and (PE/PP)/CB (*5*)

From the point of view of stable operation of CPCs at elevated temperatures, the best composition is (PP/CB)/PE (Fig. 7). The graph of the change in specific volume electrical resistance (ρ/ρ_0) during heating of the CPCs actually consists of two adjacent PTC peaks: the PE peak and the PP peak, which cover a wide temperature range from 120 to 160°C. This makes the latter CPCs the most resistant to overheating.

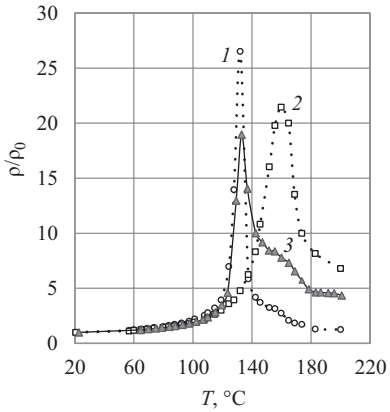

Fig. 7. Change in the specific volume electrical resistances (ρ/ρ_0) when CPCs are heated: PE/CB (*1*), PP/CB (*2*), and (PP/CB)/PE (*6*)

Thus, the method of combining components of crystallizing polymer mixtures with CB has little effect on the position of the PTC peak. The magnitude and nature of the change in the PTC peak of crystallizing polymer mixtures with CB is determined by the melting start temperature of the lowest melting phase (PE). Meanwhile, the heterogeneity of mixtures of crystallizing polymers with CB increases their thermal stability by expanding the PTC zone into the melting region of the higher-melting phase (PP).

CONCLUSIONS

The application of CPCs with a mixed polymer matrix consisting of two polymers having different melting points (e.g., PE and PP) permits adjustments to the intensity of the PTC and NTC effects. In this case, it is the low-melting polymer (PE) component of CPCs that determines the nature of PTC and the self-regulating temperature of the heater, while the higher-melting polymer with higher PTC and NTC (PP) shifts the jump in electrical conductivity of the mixed CPCs to the region of elevated temperatures, thus disrupting the operation of the heater. The results of the work made it possible to establish a number of phenomena occurring in CB-filled CPCs with PTC and NTC effects. For further research, it is necessary to consider PCs with PTC and NTC effects from the point of view of the filler, in particular, the geometric parameters of the technical specifications of special grades.

Acknowledgments

The study was carried out in accordance with research initiative topic 195-ITKhT.

Authors' contributions

A.V. Markov—conceptualization of the study, administration of the study, discussion and analysis of the results, writing the text of the article.

A.E. Zverev—setting up the experiment, studying the properties of the samples, collecting analytical data, processing, analyzing and visualizing the results, writing the text of the article.

E.V. Kalugina—consultation, discussion and analysis of the results obtained.

V.A. Markov—development of the methodology for the experimental section.

The authors declare no conflicts of interest.

REFERENCES

1. Frydman E. *Improvements in or Relating to Resistance Elements Having Positive Temperature/Resistance Characteristics:* United Kingdom Pat. GB 604695A. Current Assignee: Automatic Telephone and Electric Co. Ltd. Priority 16.11.1945; Publ. 08.07.1948.
2. Meyer J. Glass transition temperature as a guide to selection of polymers suitable for PTC materials. *Polym. Eng. Sci*. 1973;13(6):462–468. https://doi.org/10.1002/pen.760130611
3. Kohler F. *Resistance Element:* USA Pat. US 3243753. Priority 13.13.1962; Publ. 29.03.1966.
4. Markov V.A., Kandyrin L.B., Markov A.V. The effect of strain on electrical resistivity of carbon black filled polyethylene composites. *Konstruktsii iz kompozitsionnykh materialov = Composite Materials Constructions*. 2013;4:40–44 (in Russ.). https://www.elibrary.ru/rdhgqf
5. Ilyin A.P. *Plastic Hot Water Boiler:* RF Pat. RU 2680099 C1. Publ. 15.02.2019 (in Russ.).
6. Ishii T., Yasui K., Terakado S., Kohara K., Eneyama M. *Flexible Heating Element with a Positive Temperature Coefficient of Resistance and a Method for Manufacturing Such a Heating Element:* RF Pat. RU 2297112C2. Publ. 10.04.2007 (in Russ.).
7. Heinemann K., Bauer R.U., Welzel T., Schrödner M., Schubert F., Riede S. *Electroconductive Molded Article With a Positive Temperature Coefficient:* RF Pat. RU 2709631C9. Publ. 04.06.2020 (in Russ.).
8. Setnescu R., Lungulescu E.M. Novel PTC Composites for Temperature Sensors (and Related Applications). In: Sen J., Yi M., Niu F., Wu H. (Eds.). *Wireless Sensor Networks – Design, Applications and Challenges*. 2023. https://doi.org/10.5772/intechopen.110358
9. Ahn J.-H., Choi D.-S., Lee C.-Y. Resistances of carbon black and polymers in smart paints for temperature sensors. *J. Nanosci. Nanotechnol*. 2021;21(7):3716–3720. https://doi.org/10.1166/jnn.2021.19209
10. Huang Y., Ellingford C., Bowen C.R., *et al*. Tailoring the electrical and thermal conductivity of multi-component and multi-phase polymer composites. *Int. Mater. Rev.* 2020;65(3): 129–163. https://doi.org/10.1080/09506608.2019.1582180
11. Harussani M.M., Sapuan S.M., Nadeem G., *et al*. Recent applications of carbon-based composites in defence industry: A review. *Defence Technol*. 2022;18(8):1281–1300. https://doi.org/10.1016/j.dt.2022.03.006
12. Yun C.M., Tong C.T., Kuo H.C. *Conductive Composition Exhibiting PTC Behavior and Over-Current Protection Device Using the Same:* USA Pat. US 20060108566A1. Publ. 25.05.2006.
13. Wang S.C., Yang E.T. *Over-Current Protection Device:* USA Pat. US 2006089448. Publ. 27.04.2006.
14. Jeong M.W. *Composition Materials for Current Control Heating Resistor Having Elasticity and Method for Manufacturing PTC Having Elasticity:* South Korea Pat. KR 20050114005A. Publ. 05.12.2005.
15. Vasilev V.A., Khoshev A.V. *Manufacturing Method of Nano- and Micro-Sized System of Sensor of Physical Values with Specified Positive Temperature Coefficient of Resistance of Resistive Elements:* RF Pat. RU 2554083C1. Publ. 27.06.2015 (in Russ.).
16. Berlyand A.M., Ehidler E.D. *Polymer Electrically Conductive Composition:* USSR Pat. SU892479A1. Publ. 23.12.1981 (in Russ.).
17. Liu C.C., Walters A.B., Vannice M.A. Measurement of electrical properties of a carbon black. *Carbon.* 1995;33(12): 1699–1708. https://doi.org/10.1016/0008-6223(95)00125-4

СПИСОК ЛИТЕРАТУРЫ

1. Frydman E. *Improvements in or Relating to Resistance Elements Having Positive Temperature/Resistance Characteristics:* United Kingdom Pat. GB 604695A. Current Assignee: Automatic Telephone and Electric Co. Ltd. Priority 16.11.1945; Publ. 08.07.1948.
2. Meyer J. Glass transition temperature as a guide to selection of polymers suitable for PTC materials. *Polym. Eng. Sci*. 1973;13(6):462–468. https://doi.org/10.1002/pen.760130611
3. Kohler F. *Resistance Element:* USA Pat. US 3243753. Priority 13.13.1962; Publ. 29.03.1966.
4. Марков В.А., Кандырин Л.Б., Марков А.В. Влияние деформирования на электрическое сопротивление композитов на основе полиэтилена и технического углерода. *Конструкции из композиционных материалов.* 2013;4:40–44. https://www.elibrary.ru/rdhgqf
5. Ильин А.П. *Пластиковый водогрейный котел:* пат. RU 2680099 C1 РФ. Заявка № 2016117137; заявл. 29.11.2013; опубл. 15.02.2019.
6. Исии Т., Ясуи К., Теракадо С., Кохара К., Енеяма М. *Гибкий нагревательный элемент с положительным температурным коэффициентом сопротивления и способ изготовления такого нагревательного элемента:* пат. RU 2297112C2 РФ. Заявка № 2004137117/09; заявл. 16.06.2003; опубл. 10.04.2007.
7. Хайнеманн К., Бауэр Р.У., Вельцель Т., Шрёднер М., Шуберт Ф., Риде С. *Электропроводящее формованное изделие с положительным температурным коэффициентом:* пат. RU 2709631C9 РФ. Заявка № 2018141551; заявл. 22.06.2017; опубл. 04.06.2020.
8. Setnescu R., Lungulescu E.M. Novel PTC Composites for Temperature Sensors (and Related Applications). In: Sen J., Yi M., Niu F., Wu H. (Eds.). *Wireless Sensor Networks – Design, Applications and Challenges*. 2023. https://doi.org/10.5772/intechopen.110358
9. Ahn J.-H., Choi D.-S., Lee C.-Y. Resistances of carbon black and polymers in smart paints for temperature sensors. *J. Nanosci. Nanotechnol*. 2021;21(7):3716–3720. https://doi.org/10.1166/jnn.2021.19209
10. Huang Y., Ellingford C., Bowen C.R., *et al*. Tailoring the electrical and thermal conductivity of multi-component and multi-phase polymer composites. *Int. Mater. Rev.* 2020;65(3): 129–163. https://doi.org/10.1080/09506608.2019.1582180
11. Harussani M.M., Sapuan S.M., Nadeem G., *et al*. Recent applications of carbon-based composites in defence industry: A review. *Defence Technol*. 2022;18(8):1281–1300. https://doi.org/10.1016/j.dt.2022.03.006
12. Yun C.M., Tong C.T., Kuo H.C. *Conductive Composition Exhibiting PTC Behavior and Over-Current Protection Device Using the Same:* USA Pat. US 20060108566A1. Publ. 25.05.2006.
13. Wang S.C., Yang E.T. *Over-Current Protection Device:* USA Pat. US 2006089448. Publ. 27.04.2006.
14. Jeong M.W. *Composition Materials for Current Control Heating Resistor Having Elasticity and Method for Manufacturing PTC Having Elasticity:* South Korea Pat. KR 20050114005A. Publ. 05.12.2005.
15. Васильев В.А., Хошев А.В. *Способ изготовления нано- и микроразмерной системы датчика физических величин с заданным положительным температурным коэффициентом сопротивления резистивных элементов:* пат. RU 2554083C1 РФ. Заявка № 2014116189/07; заявл. 22.04.2014; опубл. 27.06.2015.

18. Gul' V.E., Shenfil' L.Z. *Ehlektroprovodyashchie polimernye kompozitsii* (*Electrically Conductive Polymer Compositions*). Moscow: Khimiya; 1984, 240 p. (In Russ.).
19. Khodabakhshi S., Fulvio P.F., Andreoli E. Carbon black reborn: Structure and chemistry for renewable energy harnessing. *Carbon*. 2020;162:604–649. https://doi.org/10.1016/j.carbon.2020.02.058
20. Aharoni S.M. Electrical resistivity of a composite of conducting particles in an insulating matrix. *J. Appl. Phys*. 1972;43(5):2463–2465. https://doi.org/10.1063/1.1661529
21. Bueche F. Electrical resistivity of conducting particles in an insulating matrix. *J. Appl. Phys*. 1972;43(11):4837–4838. https://doi.org/10.1063/1.1661034
22. Foulger S.H. Reduced percolation thresholds of immiscible conductive blends. *J. Polym. Sci. Part B: Polym. Phys.* 1999;37(15):1899–1910.
23. Sommers D.J. Carbon black for electrically conductive plastics. *Polymer-Plastics Technol. Eng*. 1984;23(1):83–89. https://doi.org/10.1080/03602558408070043
24. Beaucage G., Rane S., Schaefer D.W., *et al.* Morphology of polyethylene–carbon black composites. *J. Polym. Sci. Part B: Polym. Phys.* 1999;37(11):105–119.
25. Sircar A.K., Wells J.L. Electrothermal study of carbon loaded ethylene-vinylacetate copolymer. *Polym. Eng. Sci*. 1981;21(13):809–815. https://doi.org/10.1002/pen.760211302
26. Zhang M., Jia W., Chen X. Influences of crystallization histories on PTC/NTC effects of PVDF/CB composites. *J. Appl. Polym. Sci*. 1996;62(5):743–747. https://doi.org/10.1002/(SICI)1097-4628(19961031)62:5<743::AID-APP4>3.0.CO;2-W
27. Tang H., Chen X., Luo Y. Studies on the PTC/NTC effect of carbon black filled low density polyethylene composites. *Eur. Polym. J*. 1997;33(8):1383–1386. https://doi.org/10.1016/S0014-3057(96)00221-2
28. Markov V.A., Kandyrin L.B., Markov A.V., Sorokina E.A. Effect of silane-crosslinking on electrical properties and heat-resistance of carbon black polyethylene composites. *Plasticheskie massy*. 2013;10:21–24 (in Russ.). https://www.elibrary.ru/rrtibr
29. Marsden A.J., Papageorgiou D.G., Valles C., *et al.* Electrical percolation in graphene–polymer composites. *2D Mater.* 2018;5(3):2–19. https://doi.org/10.1088/2053-1583/aac055
30. Sumita M., Sakata K., Asai S., *et al.* Dispersion of fillers and the electrical conductivity of polymer blends filled with carbon black. *Polymer Bulletin*. 1991;25(2):265–271. https://doi.org/10.1007/bf00310802
31. Tchoudakov R., Breuer O., Narkis M. Conductive polymer blends with low carbon black loading: polypropylene/ polyamide. *Polym. Eng. Sci.* 1996;36(10):1336–1346. https://doi.org/10.1002/pen.10528
32. Markov V.A., Markov A.V., Poldushev M.A., *et al.* The influence of the method used to prepare electrically conductive composites based on polyethylene, polypropylene, and carbon black on their properties at elevated temperatures. *Int. Polym. Sci. Technol*. 2016;43(3):T13–T18. https://doi.org/10.1177/0307174x1604300303
33. Markov A.V., Zverev A.E., Markov V.A. Features of the change in the thermal coefficient of electrical resistance upon heating electrically conductive composites of crystallizable polyolefins with carbon black. *Tonk. Khim. Tekhnol. = Fine Chem. Technol*. 2024;19(5):429–440. https://doi.org/10.32362/2410-6593-2024-19-5-429-440
34. Markov A.V., Kuleznev V.N. Formation of the phase structure and its influence on the properties of oriented polypropylene-polyethylene blend films. *Polym. Sci. Ser. A.* 2008;50(4): 422–428. https://doi.org/10.1134/S0965545X0804010X

16. Берлянд А.М., Эйдлер Э.Д. *Полимерная электропроводящая композиция*: А.с. 89247 СССР. Заявка № 2911115/24-07; заявл. 14.04.1980; опубл. 23.12.1981.
17. Liu C.C., Walters A.B., Vannice M.A. Measurement of electrical properties of a carbon black. *Carbon.* 1995;33(12): 1699–1708. https://doi.org/10.1016/0008-6223(95)00125-4
18. Гуль В.Е., Шенфиль Л.З. *Электропроводящие полимерные композиции*. М.: Химия; 1984, 240 с.
19. Khodabakhshi S., Fulvio P.F., Andreoli E. Carbon black reborn: Structure and chemistry for renewable energy harnessing. *Carbon*. 2020;162:604–649. https://doi.org/10.1016/j.carbon.2020.02.058
20. Aharoni S.M. Electrical resistivity of a composite of conducting particles in an insulating matrix. *J. Appl. Phys*. 1972;43(5):2463–2465. https://doi.org/10.1063/1.1661529
21. Bueche F. Electrical resistivity of conducting particles in an insulating matrix. *J. Appl. Phys*. 1972;43(11):4837–4838. https://doi.org/10.1063/1.1661034
22. Foulger S.H. Reduced percolation thresholds of immiscible conductive blends. *J. Polym. Sci. Part B: Polym. Phys.* 1999;37(15):1899–1910.
23. Sommers D.J. Carbon black for electrically conductive plastics. *Polymer-Plastics Technol. Eng*. 1984;23(1):83–89. https://doi.org/10.1080/03602558408070043
24. Beaucage G., Rane S., Schaefer D.W., *et al.* Morphology of polyethylene–carbon black composites. *J. Polym. Sci. Part B: Polym. Phys.* 1999;37(11):105–119.
25. Sircar A.K., Wells J.L. Electrothermal study of carbon loaded ethylene-vinylacetate copolymer. *Polym. Eng. Sci*. 1981;21(13):809–815. https://doi.org/10.1002/pen.760211302
26. Zhang M., Jia W., Chen X. Influences of crystallization histories on PTC/NTC effects of PVDF/CB composites. *J. Appl. Polym. Sci*. 1996;62(5):743–747. https://doi.org/10.1002/(SICI)1097-4628(19961031)62:5<743::AID-APP4>3.0.CO;2-W
27. Tang H., Chen X., Luo Y. Studies on the PTC/NTC effect of carbon black filled low density polyethylene composites. *Eur. Polym. J.* 1997;33(8):1383–1386. https://doi.org/10.1016/S0014-3057(96)00221-2
28. Марков В.А., Кандырин Л.Б., Марков А.В., Сорокина Е.А. Влияние силанольного сшивания на электрические характеристики и теплостойкость полиэтиленовых композитов с техническим углеродом. *Пласт. массы*. 2013;10: 21–24. https://www.elibrary.ru/rrtibr
29. Marsden A.J., Papageorgiou D.G., Valles C., *et al.* Electrical percolation in graphene–polymer composites. *2D Mater.* 2018;5(3):2–19. https://doi.org/10.1088/2053-1583/aac055
30. Sumita M., Sakata K., Asai S., *et al.* Dispersion of fillers and the electrical conductivity of polymer blends filled with carbon black. *Polymer Bulletin*. 1991;25(2):265–271. https://doi.org/10.1007/bf00310802
31. Tchoudakov R., Breuer O., Narkis M. Conductive polymer blends with low carbon black loading: polypropylene/ polyamide. *Polym. Eng. Sci.* 1996;36(10):1336–1346. https://doi.org/10.1002/pen.10528
32. Markov V.A., Markov A.V., Poldushev M.A., *et al.* The influence of the method used to prepare electrically conductive composites based on polyethylene, polypropylene, and carbon black on their properties at elevated temperatures. *Int. Polym. Sci. Technol*. 2016;43(3):T13–T18. https://doi.org/10.1177/0307174x1604300303
33. Марков А.В., Зверев А.Е., Марков В.А. Особенности изменения термического коэффициента электрического сопротивления при нагревании электропроводящих композиций кристаллизующихся полиолефинов с техническим углеродом. *Тонкие химические технологии*. 2024;19(5):429–440. https://doi.org/10.32362/2410-6593-2024-19-5-429-440

[Original Russian Text: Markov A.V., Kuleznev V.N. Formation of the phase structure and its influence on the properties of oriented polypropylene-polyethylene blend films. *Vysokomolekulyarnye soedineniya. Ser. A.* 2008;50(4): 651–658 (in Russ.). https://elibrary.ru/ijkowv]

34. Марков А.В., Кулезнев В.Н. Формирование фазовой структуры и ее влияние на свойства ориентированных пленок из смесей полипропилена и полиэтилена. *Высоко-молек. соединения. Сер. А*. 2008;50(4):651–658. https://elibrary.ru/ijkowv

About the Authors

Anatoly V. Markov, Dr. Sci. (Eng.), Professor, Department of Chemistry and Technology of Plastics and Polymer Composites Processing, M.V. Lomonosov Institute of Fine Chemical Technologies, MIREA – Russian Technological University (78, Vernadskogo pr., Moscow, 119454, Russia). E-mail: markovan@bk.ru. Scopus Author ID 57222377754, RSCI SPIN-code 1127-9590, https://orcid.org/0000-0001-7952-7419

Alexander E. Zverev, Postgraduate Student, Department of Chemistry and Technology of Plastics and Polymer Composites Processing, M.V. Lomonosov Institute of Fine Chemical Technologies, MIREA – Russian Technological University (78, Vernadskogo pr., Moscow, 119454, Russia). E-mail: azmonst@gmail.com. Scopus Author ID 59394532100, ResearcherID ABJ-9575-2022, RSCI SPIN-code 3609-8535, https://orcid.org/0009-0004-4418-5825

Elena V. Kalugina, Dr. Sci. (Chem.), Deputy Director, Research Institute, POLYPLASTIC Group (18/3, Ochakovskoe sh., Moscow, 119530, Russia); Professor, Department of Chemistry and Technology of Plastics and Polymer Composites Processing, M.V. Lomonosov Institute of Fine Chemical Technologies, MIREA – Russian Technological University (78, Vernadskogo pr., Moscow, 119454, Russia). E-mail: kalugina@polyplastic.ru. Scopus Author ID 6603064139, https://orcid.org/0000-0002-1894-8604

Vasily A. Markov, Cand. Sci. (Eng.), Lead Software Engineer, Bell Integrator Innovations (1, Ramenskii bul., MSU Innovative Scientific and Technological Center “Vorob’evy Gory,” cluster “Lomonosov,” Moscow, 119192, Russia). E-mail: markov.vasily@mail.ru. Scopus Author ID 57189505018, https://orcid.org/0000-0002-5768-9107

Об авторах

Марков Анатолий Викторович, д.т.н., профессор, кафедра химии и технологии переработки пластмасс и полимерных композитов, Институт тонких химических технологий им. М.В. Ломоносова, ФГБОУ ВО «МИРЭА – Российский технологический университет» (119454, Россия, Москва, пр-т Вернадского, д. 78). E-mail: markovan@bk.ru. Scopus Author ID 57222377754, SPIN-код РИНЦ 1127-9590, https://orcid.org/0000-0001-7952-7419

Зверев Александр Евгеньевич, аспирант, кафедра химии и технологии переработки пластмасс и полимерных композитов, Институт тонких химических технологий им. М.В. Ломоносова, ФГБОУ ВО «МИРЭА – Российский технологический университет» (119454, Россия, Москва, пр-т Вернадского, д. 78). E-mail: azmonst@gmail.com. Scopus Author ID 59394532100, ResearcherID ABJ-9575-2022, SPIN-код РИНЦ 3609-8535, https://orcid.org/0009-0004-4418-5825

Калугина Елена Владимировна, д.х.н., заместитель директора НИИ ООО «Группа ПОЛИПЛАСТИК» (119530, Россия, Москва, Очаковское шоссе, д. 18, стр. 3); профессор, кафедра химии и технологии переработки пластмасс и полимерных композитов, Институт тонких химических технологий им. М.В. Ломоносова, ФГБОУ ВО «МИРЭА – Российский технологический университет» (119454, Россия, Москва, пр-т Вернадского, д. 78). E-mail: kalugina@polyplastic.ru. Scopus Author ID 6603064139, https://orcid.org/0000-0002-1894-8604

Марков Василий Анатольевич, к.т.н., ведущий инженер-программист, ООО «Белл Интегратор Инновации» (119192, Россия, Москва, Раменский бульвар, д. 1, Инновационный научно технологический центр МГУ «Воробьевы горы», кластер «Ломоносов»). E-mail: markov.vasily@mail.ru. Scopus Author ID 57189505018, https://orcid.org/0000-0002-5768-9107

Translated from Russian into English by H. Moshkov
Edited for English language and spelling by Thomas A. Beavitt

Tonkie Khimicheskie Tekhnologii = Fine Chemical Technologies.
2026;21(2):237–246 ISSN 2686-7575 (Online)

Synthesis and processing of polymers and polymeric composites
Синтез и переработка полимеров и композитов на их основе

UDC 620.194.22/ 620.169.1/620.199
https://doi.org/10.32362/2410-6593-2026-21-2-237-246
EDN GEVECB

RESEARCH ARTICLE

Study of the corrosive effect of ozone on vulcanizates

Stanislav V. Mednikov✉, Pavel D. Kravchenya, Alexander S. Ponomarev, Oleg O. Tuzhikov
Volgograd State Technical University, Volgograd, 400005 Russia
✉ *Corresponding author, e-mail: mednikov17@yahoo.com*

Abstract

Objectives. The work sets out to model the ozone corrosion of vulcanizates as a percolation phase transition, similar in the scheme of development of continual percolation on a plane, during which the growing regions of the new phase form a single "spanning" cluster. In this case, the continuity of the sample is broken, being divided into two parts. In the presented model, the ozone corrosion process is divided into two stages. At the first stage, ozone corrosion of the material occurs mainly along the perimeters of already ozonized surface areas, which leads to their growth and subsequent merging. Upon contact of adjacent surface areas consisting of ozonolysis products loaded with two-dimensional tension, corrosion cracks begin to appear on the surface. At the second stage of the corrosion process, corrosion cracks that grow deeply into the material due to its stress state lead to the penetration of ozone into the internal regions of the sample. The article presents the results of computer-simulation and real experiments carried out on ozone corrosion of technical vulcanizates in a plane stressed state.

Methods. Computer simulation of the time dependence of the total contact length of the areas of ozone corrosion products and the initial vulcanizate was carried out using a C++ program developed by the authors. Real experiments were carried out on a TOM-1000 setup. Samples for research by the TOM (technical ozone resistance of materials[1]) method comprise thin disks, which are clamped along the contour and subjected to one-sided two-dimensional tension by compressed air pressure. From the side of the opposite plane, the sample is exposed to the ozone flow. The installation makes it possible to create in the sample a relative deformation of up to 100% increase in the surface area.

Results. Computer simulation allowed, in combination with direct measurements of the time dependence of ozone absorption, the dynamics of the destruction of vulcanizates in an ozone environment to be investigated. A numerical parameter of the ozone resistance of vulcanizates—the coefficient of ozone resistance—is proposed. This coefficient is almost linearly related to the time before the onset of cracking, but it is more accurate because it does not require visual observation of the ozonolysis process.

Conclusions. The results of computer simulation are in good agreement with the results of real experiments.

Keywords

hardness, corrosion, ozonolysis, percolation phase transition, aggressiveness of vulcanizates

Submitted: 15.06.2025
Revised: 18.08.2025
Accepted: 16.02.2026

For citation

Mednikov S.V., Kravchenya P.D., Ponomarev A.S., Tuzhikov O.O. Study of the corrosive effect of ozone on vulcanizates. *Tonk. Khim. Tekhnol. = Fine Chem. Technol.* 2026;21(2):237–246. https://doi.org/10.32362/2410-6593-2026-21-2-237-246

[1] TOM (technical ozone resistance of materials) is a method patented by the authors for testing vulcanizates for ozone resistance under flat stress conditions.

НАУЧНАЯ СТАТЬЯ

Исследование коррозионного воздействия озона на вулканизаты

С.В. Медников✉, П.Д. Кравченя, А.С. Пономарев, О.О. Тужиков

Волгоградский государственный технический университет, Волгоград, 400005 Россия

✉ *Автор для переписки, e-mail: mednikov17@yahoo.com*

Аннотация

Цели. Озонная коррозия вулканизатов моделируется как перколяционный фазовый переход, аналогичный по схеме развития континуальной перколяции на плоскости, в процессе которой разрастающиеся области новой фазы образуют единый «перекидывающийся» кластер. Процесс озонной коррозии представляется разделенным на две стадии. На первой стадии процесс озонопоглощения происходит на границах корродированных участков с окружающей поверхностью вулканизата, поэтому поглощение образцом озона вначале возрастает, затем уменьшается по мере смыкания участков увеличивающейся корродированной поверхности. При соприкосновении соседних участков поверхности, состоящих из продуктов озонолиза, под воздействием двумерного напряжения на поверхности начинают появляться коррозионные трещины. На второй стадии коррозионные трещины проникают в глубь материала из-за его напряженного состояния, сопровождаясь проникновением озона во внутренние области образца. Изменение в процессе озонолиза общей длины линии контакта областей продуктов озонолиза с поверхностью, еще не подвергнутой озонной коррозии, отражает общее озонопоглощение корродирующего образца. Целью данной работы является экспериментальное исследование и компьютерное моделирование процессов зарождения трещин в образцах технических вулканизатов, находящихся в плоском напряженном состоянии, вследствие воздействия озона.

Методы. Компьютерное моделирование временной зависимости общей длины контакта областей продуктов озонной коррозии и исходного вулканизата осуществлялось с помощью разработанной авторами программы на языке C++. Реальные эксперименты по регистрации кинетики озонопоглощения озона шинными вулканизатами проводились на установке ТОМ-1000. Образцы для исследований по методу ТОМ[2] (техническая озоностойкость материалов) представляют собой тонкие диски, защемленные по контуру и подвергаемые одностороннему двумерному растяжению давлением сжатого воздуха. Со стороны противоположной плоскости образец подвергается воздействию потока озона. Установка дает возможность создания в образце относительной деформации до 100% увеличения площади поверхности.

Результаты. Компьютерное моделирование позволило, в сочетании с прямыми измерениями временной зависимости озонопоглощения, исследовать динамику процесса деструкции вулканизатов в среде озона. Предложен численный параметр озоностойкости вулканизатов — коэффициент озоностойкости, который практически линейно связан с временем до начала трещинообразования, однако более точен, т.к. не требует визуального наблюдения за процессом озонолиза.

Выводы. Результаты машинного моделирования находятся в хорошем согласии с результатами реальных экспериментов по регистрации кинетики озонопоглощения образцов шинных вулканизатов в процессе озонолиза, что свидетельствует в пользу правомерности модели двухстадийной коррозии вулканизатов в среде озона.

Ключевые слова

жесткость, коррозия, озонолиз, перколяционный фазовый переход, агрессивостойкость вулканизатов

Поступила: 15.06.2025
Доработана: 18.08.2025
Принята в печать: 16.02.2026

Для цитирования

Медников С.В., Кравченя П.Д., Пономарев А.С., Тужиков О.О. Исследование коррозионного воздействия озона на вулканизаты. *Тонкие химические технологии*. 2026;21(2):237–246. https://doi.org/10.32362/2410-6593-2026-21-2-237-246

[2] ТОМ (техническая озоностойкость материалов) — запатентованный авторами метод тестирования вулканизатов на озоностойкость в условиях плоского напряженного состояния. [TOM (technical ozone resistance of materials) is a method patented by the authors for testing vulcanizates for ozone resistance under flat stress conditions.]

INTRODUCTION

The necessity for theoretical research on various aspects of material corrosion in aggressive environments is due to the diversity both of corrosive media and materials operating in these environments. In this work, we focus primarily on describing the behavior of mechanically stressed technical vulcanizates (rubbers) in an ozone environment, to which the established term "ozone corrosion" (ozonolysis) applies.

Resistance to the aggressive impact of ozone, which leads to stress cracking of rubber components, is one of the most important operational characteristics of these materials [1–3]. The universally accepted numerical criterion for ozone resistance of vulcanizates, as prescribed by the standards of many countries, is the "time to the appearance of the first corrosion crack on the surface of a vulcanizate sample under uniaxial load in an ozone environment" [4–5]. This moment in time is generally recorded visually. With the advancement of experimental techniques, dynamic testing methods which still rely on visual observation of the crack initiation moment have appeared in the practice of ozone resistance measurements [6]. However, the main focus in improving the ozone resistance of vulcanizates is currently directed toward developing new formulations and modifying existing ones [7–9].

Recently, the processes of crack formation and evolution in materials under ultimate loads have been analyzed in terms of geometric phase transitions (percolation) [10–14]. Without delving into possible microscopic mechanisms of crack initiation in ozone-aged vulcanizates, the present work considers ozone damage to vulcanizates as a geometric phase transition. The result of this transition is the nucleation of corrosion cracks in the surface layer of a material under a plane stress state.

The process of aggressive ozone action on the surface of rubbers in a mechanically stressed state begins in those areas where the surface structure is distorted by defects, such as the presence of filler particles, areas with uneven filler distribution in the material, or irregularities in the formed vulcanization network [15]. The surface density of such distorted sites, which initiate the interaction process between ozone and the vulcanizate, varies significantly depending on the vulcanizate production technology and its components [16]. Their initial areas are usually considered to be comparable to the sizes of filler components. Since ozone action occurs primarily at the boundaries of these "defective" sites with the surrounding surface, the areas of these sites increase as the interaction process between the vulcanizate and ozone develops. Accordingly, the increased rate of ozone absorption is proportional to the total perimeter of the areas of reacted sites on the ozonated surface. However, ozone diffusion into the bulk of the vulcanizate only affects the overall ozone absorption to a minor extent.

Subsequently, the isolated reacted areas begin to merge, leading to a decrease in their total perimeter and consequent reduction in the ozone absorption rate.

When the entire sample surface has reacted, further development of ozone corrosion occurs solely due to the diffusion of ozone into the vulcanizate. This initiates the formation and growth of cracks on the surface undergoing ozonolysis. Under stressed material conditions, this leads to crack opening and propagation, along with a continuous increase in the reactive area of the vulcanizate. Consequently, ozone absorption continues to increase until a through-crack forms in the sample.

Thus, the interaction of ozone with the vulcanizate surface can be divided into two temporal stages: before and after the moment of the first corrosion cracks appearing on the surface.

The first stage—the process of growth and subsequent merging of corroded areas on the vulcanizate surface—is analogous in its development scheme to continuous percolation on a plane. This is an abstract geometric phase transition that concludes with the formation of a "spanning" cluster, which divides the surface into two parts [17, 18]. For example, when sequentially punching holes of a certain predetermined diameter into a conductive plate, whose positions are chosen randomly, the electrical conductivity of the plate decreases along a curve characteristic of second-order thermodynamic phase transitions [17]. By continuing this procedure, a chain of interconnected holes is eventually created which cut the plate into two parts in some location. At this point, current through the plate ceases due to its electrical conductivity approaching zero. The region of the plate at which it becomes divided into two parts is called the "spanning" cluster.

Unlike a thermodynamic phase transition (e.g., ferromagnetic–paramagnetic), the onset of a percolation phase transition depends on time, whereas in the former case it depends on the temperature of the substance's phase.

The difference in our model lies in the fact that it does not involve the sequential addition of new phase regions (holes), but the sequential increase in the size of existing new phase regions (ozonolysis products). These regions initially exist as an isolated system of structural defects in the vulcanizate. With a merging of the growing ozonolysis product regions, crack formation occurs on the ozonated surface because the material is in a stressed state, and the second stage begins—the propagation of corrosion cracks into the sample bulk.

EXPERIMENTAL

To confirm the percolation nature of the change in the area of the vulcanizate surface having reacted with ozone, we conducted machine modeling of the change over time of the non-corroded surface area of a sample as a function of the number of modeling steps (i.e., time).

Consider a square plate with a certain area *S*. Place a square grid of equally spaced circles with initial radii r_0 on the plate. These circles model defects in the original surface structure of the vulcanizate that initiate ozonolysis along their perimeters. At each modeling step, the perimeters of the circles increase by a certain amount. Then, calculate the new circle radii, the total area occupied by the circles, the area not yet reacted with ozone, and the total length of all circle circumferences in the grid (the total perimeter of the boundary with the unreacted surface). Within this model, the ozone absorption rate is considered proportional to the total length of this combined perimeter.

During the program's operation, the areas of the circles increase. Eventually, the circles begin to overlap, and the total length of the perimeter where the ozone-reacted surface contacts the still unreacted surface decreases. The program continues until the total area occupied by the reacted surface equals the total area of the plate *S*.

Figures 1–4 show the simulation stages for four time points, corresponding to step numbers: 100, 280, 320, and 400. In Figs. 1a–4a, the dark areas correspond to the current sizes of the reacted areas on the vulcanizate surface (hereinafter referred to as clusters). Figures 1b–4b show the time dependencies of the total length of cluster perimeters, while Figs. 1c–4c show the time dependencies of the total surface area not yet reacted at that moment. All quantities on the axes are given in arbitrary units.

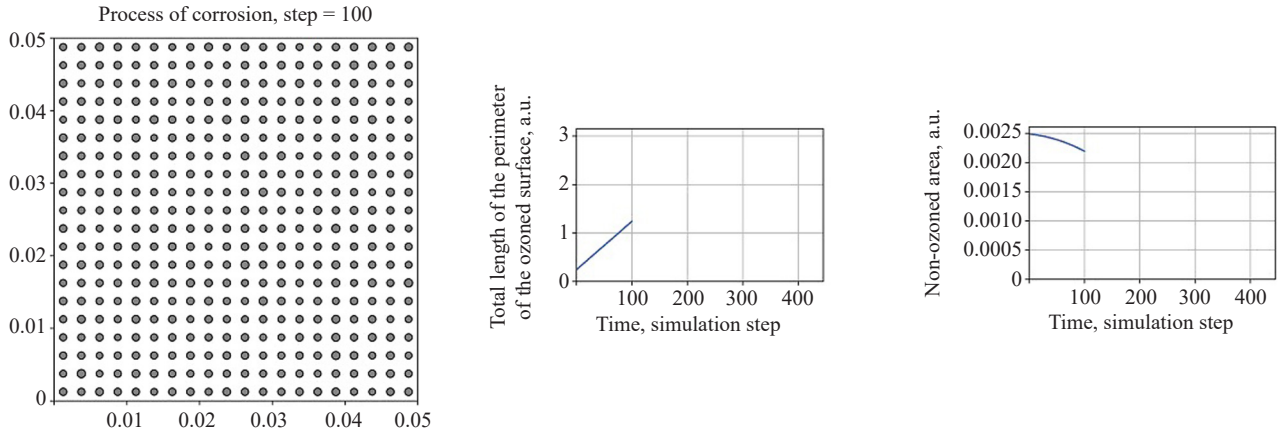

(a) (b) (c)

Fig. 1. Simulation on a time interval of isolated clusters

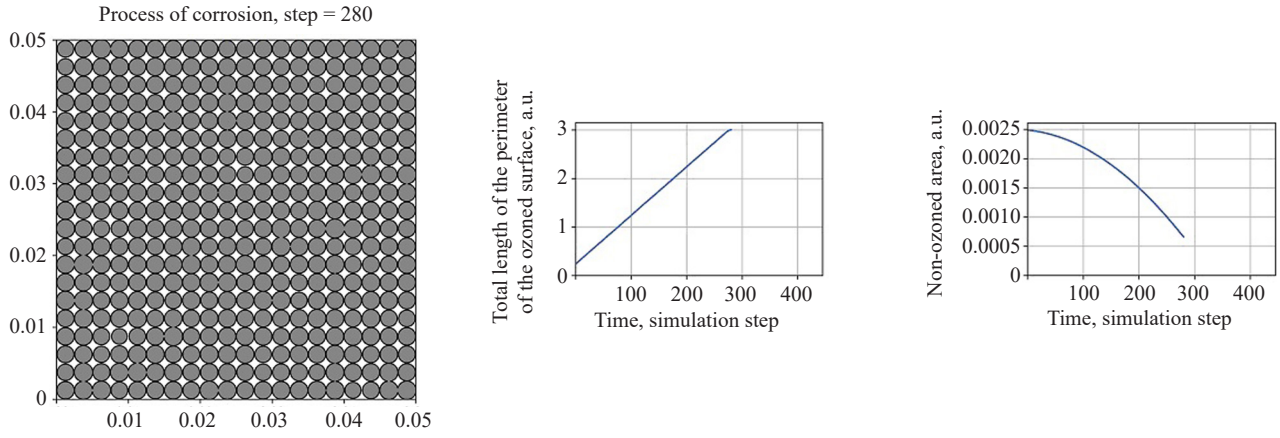

(a) (b) (c)

Fig. 2. Moment of mutual contact of corroded clusters, corresponding to the maximum rate of ozone absorption

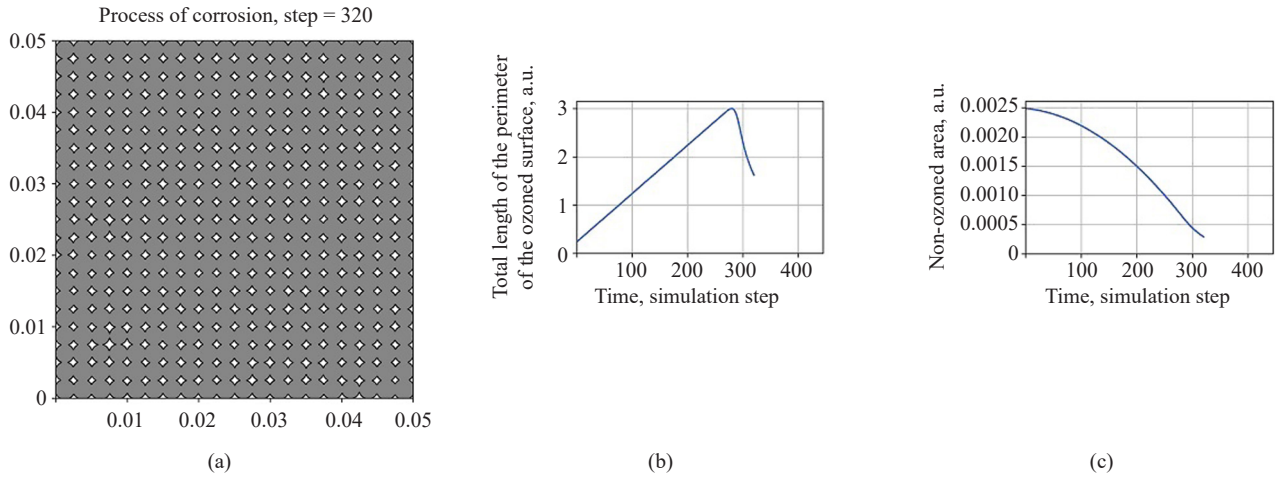

Fig. 3. Simulation on a time section of the connected clusters of the reacted surface

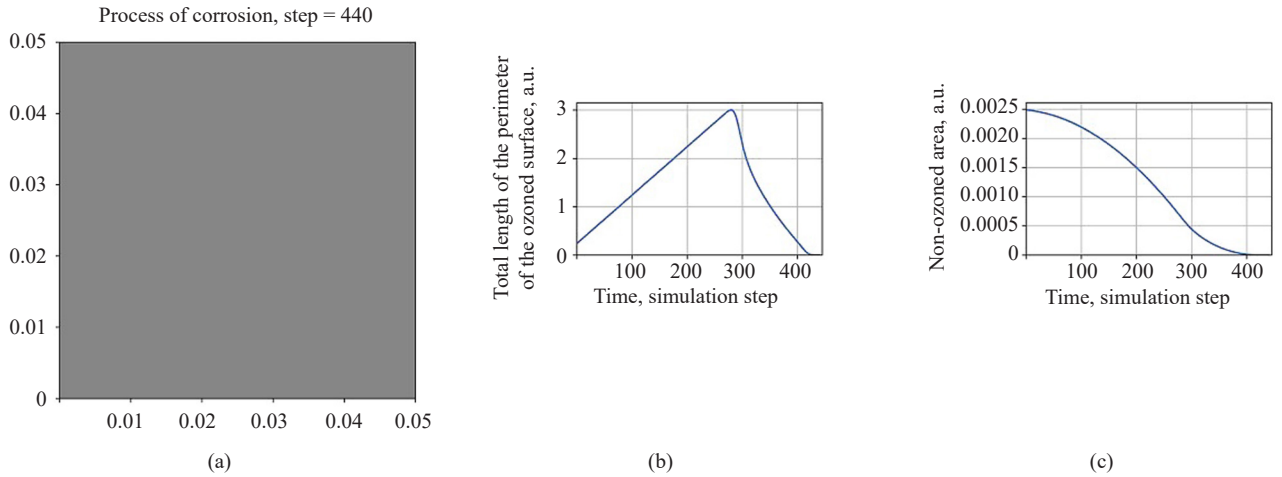

Fig. 4. Completion of the simulation. The entire surface is corroded

As the clusters grow in size, their total perimeter increases, and consequently, the ozone absorption rate increases (Fig. 1). Up to the 280th modeling step, the change in area over time resembles percolation behavior, characteristic, for example, of experiments recording current in a conductive strip as holes are punched with randomly chosen coordinates [19, 20], or in a system of parallel conductive buses as they are cut in random order [21]. Within this model, the maximum ozone absorption rate corresponds to the moment when the total perimeter of all growing clusters reaches its peak, observed when they contact each other at the 280th modeling step (Fig. 2). In continuum percolation theory, this moment corresponds to the formation of a "spanning" cluster [20]. In the conditions of our model, the total perimeter of boundaries with the unreacted surface subsequently decreases, corresponding to a reduction in the ozone absorption rate (Fig. 3). The simulation stops when the entire surface has been corroded (Fig. 4).

The rate of ozone corrosion and consequent ozone resistance of a vulcanizate can be most accurately calculated by analyzing the kinetics of ozone absorption by its surface. We investigated this process using the Technical Ozone Resistance of Materials (TOM) setup, developed at Volgograd State Technical University (Russia) [22, 23], for testing the ozone resistance of vulcanizates under conditions of a plane stress state. Ozone exposure is applied to one surface of a thin, flat disc-shaped sample, which is clamped along its perimeter and deformed on the opposite side by compressed air pressure. The TOM setup allows for the recording of the amount of ozone absorbed by the sample (i.e., reacted with the vulcanizate) during ozonolysis by measuring the ozone concentration in the ozone-air mixture to which the sample is exposed, at both the inlet and outlet of the reaction chamber. Figure 5 shows typical results of recording the time-dependent change in the ozone absorption rate (mol/s) during testing of a series of tire vulcanizate samples on the TOM setup. Comparing

the graphs in Figs. 1–4 and Fig. 5, a good agreement between the model and the results of the real ozonolysis process of a vulcanizate is observed. The formation of the first corrosion cracks, i.e., the increase in the reaction-active surface area, for this vulcanizate composition begins around the 24th second of the ozonolysis process (Fig. 5). As seen from the graph, the ozone absorption rate subsequently begins to increase again, indicating the onset of the second stage of ozonolysis that involves the propagation of corrosion cracks into the bulk of the sample.

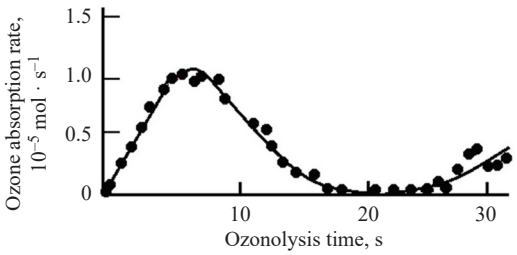

Fig. 5. Typical time dependence of the ozone absorption rate of tire vulcanizates

From a practical standpoint, it is of interest to investigate the dynamics of the deterioration (degradation) of the physicomechanical properties of a material during the first stage of ozonolysis, which concludes with the formation of corrosion cracks on its surface.

RESULTS AND DISCUSSION

The main parameter recorded during testing of vulcanizates for ozone resistance using the TOM method is the pressure of the air acting on the sample in the pressurization chamber of the setup. Ozonolysis leads to a decrease in the sample's stiffness and its subsequent deformation, which is recorded as a pressure drop. A typical view of the time dependence of pressure in the pressurization chamber during sample ozonolysis is presented in Fig. 6 [24]. The moment of crack initiation is registered by the TOM method as the beginning of the linear segment on the time dependence of pressure decrease in the setup's pressurization chamber.

A sample that has been clamped along its perimeter and subjected to compressed air pressure from the pressurization chamber side represents an elastic element, which is generally nonlinear. The deformation of this element can be characterized by the deflection w_0 at its center (the apex of the dome). For small deflection values, it can be considered a linear elastic element—a spring with stiffness k—and Hooke's law can be applied to it:

$$P \cdot B = k \cdot w_0, \quad (1)$$

where P is the current pressure of the compressed air on the sample; B is the effective area of the sample, depending on its diameter and the design features of the TOM setup; w_0 is the deflection of the apex of the sample dome loaded by the compressed air pressure from the pressurization chamber.

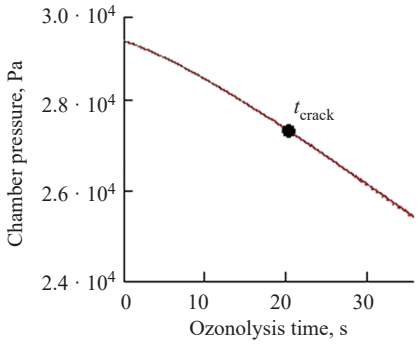

Fig. 6. Time dependence of pressure in the injection chamber. t_{crack} is the moment of the onset of crack formation in the sample

In the first stage of ozonolysis, ozone exposure affects a thin surface layer of the material. According to current understanding, the decrease in sample stiffness occurs only due to the deterioration of the physicomechanical properties of this layer. Let us model the sample as two elastic elements connected in parallel, having thicknesses h_1 and h_2 and stiffnesses k_1 and k_2. Stiffness k_1 decreases as the area of the surface not yet reacted with ozone diminishes, while stiffness k_2 decreases much more slowly during ozonolysis. At the start of ozonolysis, the material of the surface layer is identical to the rest of the sample material. Therefore, the ratio of the initial stiffnesses of the surface layer k_1^0 and the remaining material k_2^0 equals the ratio of their thicknesses, i.e.,

$$k_2^0 = \frac{h - h}{h_1} \cdot k_1^0, \quad (2)$$

where h_1 is the thickness of the surface layer; h is the thickness of the sample.

Since the total perimeter in our model is assumed to increase linearly with time (until the clusters begin to merge), the total ozonated surface area increases quadratically with time. Therefore, the time-dependent law for the decrease in stiffness of the surface layer can be written as:

$$k_1(t) = k_1^0 - k't^2,$$

where, k' characterizes the rate of decrease in the stiffness of the sample's surface layer during ozonolysis. Its reciprocal, therefore, serves as an objective criterion

for the ozone resistance of the sample material (during the first stage of ozonolysis). The total stiffness of the sample is:

$$k_{tot}(t) = k_1^0 - k't^2 + k_2(t). \quad (3)$$

Here, $k_2(t)$ accounts for the slower process of ozone diffusion through the surface layer into the depth of the sample.

For small sample deflections (less than 0.4 of the sample radius), a dependence of pressure P in the pressurization chamber on the maximum deflection w_0 (at the apex of the deformed sample's dome) was obtained in the form:

$$P(t) = \frac{P_0 V_0}{B w_0(t)}, \quad (4)$$

which represents Boyle–Mariotte's law (the ozonolysis process of vulcanizates on the TOM setup is isothermal). Here, P_0 and V_0 are the pressure and volume of compressed air in the pressurization chamber at the start of ozonolysis, while B is the effective sample area introduced earlier.

Let us write Hooke's law (1) in the form:

$$P(t)B = k_{tot}(t)w_0(t) = \left[k_1^0 - k't^2 + k_2(t)\right] \cdot w_0(t). \quad (5)$$

Expressing the deflection w_0 from (4) and substituting it into (5), we obtain the time dependence of pressure change in the pressurization chamber due to the decrease in sample stiffness on the time interval from the start of ozonation to the moment of the first corrosion crack formation:

$$P(t) = \sqrt{\frac{k_{tot}(t)P_0V_0}{B^2}} = \sqrt{\frac{\left[k_1^0 - k't^2 + k_2(t)\right]P_0V_0}{B^2}}. \quad (5a)$$

The best agreement of the obtained relationship with experimental results on the TOM setup is observed under the assumption of a linear law for the decrease in stiffness $k_2(t)$, i.e.:

$$P(t) = \sqrt{\frac{\left[k_1^0 - k't^2 + k_2^0 - k''t\right]P_0V_0}{B^2}}. \quad (6)$$

The negative root in (6) corresponds to negative gauge pressure in the pressurization chamber. In the TOM setup, this sample loading option is not used.

Neglecting the change in stiffness k'' during the first stage of ozonolysis, we can rewrite Eq. (6) as:

$$P(t) = \sqrt{\frac{\left[k_1^0 - k't^2\right]P_0V_0}{B^2}}. \quad (6a)$$

Equation (6a) allows for the calculation of the constant k' from experimental results obtained using the TOM setup, which determines the moment of crack initiation, t_{crack}, and the initial sample stiffness k_0. The initial stiffness is calculated using Eq. (1), based on the condition that at $t = 0$, $P = P_0$. The set of experimental results constitutes a two-dimensional array "time t – pressure P," which, according to Eq. (6a), expresses a quadratic dependence of pressure on the sample versus time during the first stage of ozonolysis. To obtain k' values from this data, any suitable computational environment, for example, MATHCAD, can be used.

Further, the thickness of the surface layer damaged during the first stage of ozonolysis can be calculated from the experimental results. For the series of tire vulcanizate samples used in this work, the thickness of the surface layer damaged during the first stage of ozonolysis was approximately 50 μm.

Figure 7 shows the relationship between the ozone resistance coefficient we propose and the standard ozone resistance parameter—the time to crack initiation in the ozonated vulcanizate.

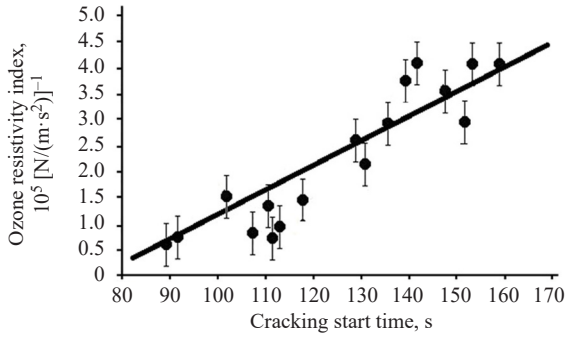

Fig. 7. Relationship between the ozone resistance coefficient and the time before crack formation in tire vulcanizate samples

The graph is based on the results of statistical processing of ozone corrosion experiments conducted on a series of 17 tire vulcanizate samples. The ozone concentration in the ozone-air mixture at the inlet of the reaction chamber was 12 mg/L ± 10% in all experiments.

As can be seen from the graph, the ozone resistance coefficient correlates well with the previously mentioned standard criterion for vulcanizate ozone resistance—the time to the first corrosion crack formation in the sample. However, it avoids the subjective aspect of the standard method, which uses visual observation to record the time of corrosion crack formation.

CONCLUSIONS

1. Crack formation arising on the surface of vulcanizates in a mechanically stressed state during corrosive exposure can be considered in terms of a percolation phase transition, similar in nature to continuous percolation.

2. A model is proposed for the decrease in mechanical stiffness during ozonation of a sample deformed by one-sided pressure. The sample is considered as a system of two elastic elements connected in parallel, whose stiffnesses decrease during the first stage of ozonolysis at significantly different rates. The model is in good agreement with experimental results obtained on the TOM setup.
3. The numerical indicator of vulcanizate resistance to aggressive ozone exposure proposed in this work—the ozone resistance coefficient—is practically linearly related to the currently accepted ozone resistance parameter, the time to crack initiation. However, the numerical indicator is more accurate as it does not require visual observation of the ozonolysis process development.

Authors' contributions

S.V. Mednikov—development of the application of percolation theory in the theoretical model of ozone corrosion of vulcanizates, participation in the development of the methodology for machine modeling, participation in the discussion of results.

P.D. Kravchenya—development of the computer program for modeling vulcanizate corrosion, execution of computer simulations, participation in the discussion of results.

A.S. Ponomarev—conducting experimental studies on the ozone resistance of tire vulcanizates using the TOM setup, participation in the discussion of results.

O.O. Tuzhikov—development of the theoretical model of ozone corrosion of vulcanizates, participation in the development of the methodology for machine modeling, participation in the discussion of results.

The authors declare no conflicts of interest.

REFERENCES

1. Razumovskii S.D., Zaikov G.E. *Ozon i ego reaktsii s organicheskimi soedineniyami* (*Ozone and its Reactions with Organic Compounds*). Moscow: Nauka; 1974, 324 p. (In Russ).
2. Zuev Yu.S., Degteva T.G. *Stoikost' ehlastomerov v ehkspluatatsionnykh usloviyakh* (*Service Life of Elastomers*). Moscow: Khimiya; 1986, 264 p. (In Russ).
3. Rakovsky S., Zaikov G. *Kinetics and Mechanism of Ozone Reactions with Organic and Polymeric Compounds in Liquid Phase*. N.Y.: Nova Science Publisher, Inc.; 1998, 345 p.
4. Dick J.S. *Tekhnologiya reziny: Retsepturostroenie i ispytaniya* (*Rubber Technology: Compounding and Testing for Performance*): transl. from Engl.; V.A. Shershnev (Ed.). St. Petersburg: Nauchnye osnovy i tekhnologii; 2010, 620 p. (In Russ.). ISBN 978-5-91703-015-9
[Dick J.S. *Rubber Technology: Compounding and Testing for Performance*; 2nd ed. Hanser Pub. Inc.; 2009, 567 p.]
5. Reznichenko S.V., Morozova Yu.L. (Eds.). *Bol'shoi spravochnik rezinshchika* (*Large Handbook of Rubber Worker*) in 2 v. V. 2. *Reziny i rezinotekhnicheskie izdeliya* (*Rubbers and Rubber Products*). Moscow: Tekhinform; 2012, 641 p. (In Russ.). ISBN 978-5-89551-025-4
6. Khorova E.A., Nagornaya M.N., Tretyakova N.A. Increasing resistance to thermal-oxidative and ozone aging of rubbers operating under dynamic loading conditions. *Kauchuk i rezina.* 2024;83(3):140–143 (in Russ.).
7. Zheng T., Zheng X., Zhan S., Zhou J., Liao S. Study on the ozone aging mechanism of Natural Rubber. *Polym. Degrad. Stab*. 2021;186(2):109514. https://doi.org/10.1016/j.polymdegradstab.2021.109514
8. Mamed Gasan-Zade D.S., Mustafayeva R.E. The preparation and study of ozone-resistant rubbers based on a blend of elastomers. *Kauchuk i rezina.* 2019;78(2):114–115 (in Russ.).
9. Bochkarev E.S., Vaniev M.A., Buravov B.A., Gubin S.G., Dang Minh Thuy, Fan Ngok Tu., Novakov I.A. The effect of rubber blend ingredients on ozone and weather aging of rubber. *Izvestiya Volgogradskogo gosudarstvennogo tekhnicheskogo universiteta* (*Izvestiya VolGGTU*) = *Izvestia VSTU*. 2022;5(264):7–19 (in Russ.). https://doi.org/10.35211/1990-5297-2022-5-264-7-19
10. Sieradzki K., Rong L. Fracture Behavior of a Solid with Random Porosity. *Phys. Rev. Lett*. 1987;56:2509–2512. https://doi.org/10.1103/PhysRevLett.58.429.

СПИСОК ЛИТЕРАТУРЫ

1. Разумовский С.Д., Заиков Г.Е. *Озон и его реакции с органическими соединениями*. М.: Наука; 1974, 324 с.
2. Зуев Ю.С., Дегтева Т.Г. *Стойкость эластомеров в эксплуатационных условиях.* М.: Химия; 1986, 264 с.
3. Rakovsky S., Zaikov G. *Kinetics and Mechanism of Ozone Reactions with Organic and Polymeric Compounds in Liquid Phase*. N.Y.: Nova Science Publisher, Inc.; 1998, 345 p.
4. Дик Дж.С. *Технология резины: Рецептуростроение и испытания:* пер. с англ.; под ред. В.А. Шершнева. СПб.: Научные основы и технологии; 2010, 620 с. ISBN 978-5-91703-015-9
5. *Большой справочник резинщика:* в 2 ч.; под ред. С.В. Резниченко, Ю.Л. Морозова. Ч. 2. *Резины и резинотехнические изделия*. М.: Техинформ; 2012, 641 с. ISBN 978-5-89551-025-4
6. Хорова Е.А., Нагорная М.Н., Третьякова Н.А. Повышение стойкости к термоокислительному и озонному старению резин, работающих в условиях динамического нагружения. *Каучук и резина*. 2024;83(3):140–143.
7. Zheng T., Zheng X., Zhan S., Zhou J., Liao S. Study on the ozone aging mechanism of Natural Rubber. *Polym. Degrad. Stab*. 2021;186(2):109514. https://doi.org/10.1016/j.polymdegradstab.2021.109514
8. Мамед Гасан-Заде Д.С., Мустафаева Р.Э. Получение и исследование озоностойких резин на основе смеси эластомеров. *Каучук и резина*. 2019;78(2):114–115.
9. Бочкарев Е.С., Ваниев М.А., Буравов Б.А., Губин С.Г., Данг М.Т., Фан Н.Ту., Новаков И.А. Влияние ингредиентов на старение резин под действием озона и атмосферных факторов. *Известия Волгоградского государственного технического университета* (*Известия ВолгГТУ*). 2022;5(264):7–19. https://doi.org/10.35211/1990-5297-2022-5-264-7-19
10. Sieradzki K., Rong L. Fracture Behavior of a Solid with Random Porosity. *Phys. Rev. Lett*. 1987;56:2509–2512. https://doi.org/10.1103/PhysRevLett.58.429
11. Морозовский А.Е., Снарский А.А. Перколяционное описание проводимости случайных сеток с широким спектром распределения сопротивлений. *Журнал экспериментальной и теоретической физики* (*ЖЭТФ*). 1993;104(6):4059–4072.
12. Чинь В.Х. Модель трещины в механизме динамического фазового перехода и физический смысл функции Качанова. *Физическая мезомеханика*. 2002;5(4):5–8.

11. Morozovskii A.E., Snarskii A.A. Percolation description of the conductivity of random networks with a broad spectrum of the distribution of resistances. *Journal of Experimental and Theoretical Physics* (*JETP*). 1993;77(6):959–965. [Original Russian Text: Morozovskii A.E., Snarskii A.A. Percolation description of the conductivity of random networks with a broad spectrum of the distribution of resistances. *Zhurnal ehksperimental'noi i teoreticheskoi fiziki* (*ZhETF*). 1993;104(6):4059–4072 (in Russ).]
12. Chin V.H. Crack model in the mechanism of dynamic phase transition and the physical meaning of the Kachanov function. *Fizicheskaya mezomekhanika = Physical Mesomechanics.* 2002;5(4):5–8 (in Russ.).
13. Khalkechev R.K. Percolated multifractal mathematical model of destruction of the gas-containing rock mass as the basis for forecasting of sudden emission of breeds and gas. *Gornyi informatsionno-analiticheskii byulleten' = Mining Informational and Analytical Bulletin.* 2015;4:359–363 (in Russ.).
14. Valishin A.A., Antonova I.V. Percolation model of micro-defects accumulation and forced elasticity area collapse before the crack fracture front in polymer and composite materials. *Inzhenernyi zhurnal: nauka i innovatsii = Engineering Journal: Science and Innovation*. 2016;11(59):1–16 (in Russ.). https://doi.org/10.18698/2308-6033-2016-11-1556
15. Dogadkin B.A., Dontsov A.A., Shershnev V.A. *Khimiya ehlastomerov* (*Chemistry of Elastomers*). Moscow: Khimiya; 1981, 376 p. (In Russ.).
16. Ikeda Y., Higashitani N., Hijikata K., Kokubo Y., Morita Y., Shibayama M., Osaka N., Suzuki T., Endo H., Kohjiya S. Vulcanization: New focus on a traditional technology by small-angle neutron scattering. *Macromolecules*. 2009;42(7): 2741–2748. https://doi.org/10.1021/ma802730z
17. Gould H., Tobochnik J. *Komp'yuternoe modelirovanie v fizike* (*Computer Modeling in Physics*): in 2 v.: transl. from Engl. V. 2. Moscow: Mir; 1990, 400 p. (In Russ.). ISBN 5-03-001594-9 [Gould H., Tobochnik J. *An Introduction to Computer Simulation Methods Applications to Physical Systems. Part 2.* Addison-Wesley; 1987, 629 p.]
18. Tarasevich Yu.Yu. *Perkolyatsiya: teoriya, prilozheniya, algoritmy* (*Percolation: Theory, Applications, Algorithms*). Moscow: URSS; 2018, 112 p. (In Russ.).
19. Watson B.P., Leath P.L. Conductivity in the two-dimensional-site percolation problem. *Phys. Rev. B.* 1975;9:4893–4896. https://doi.org/10.1103/PhysRevB.9.4893
20. Last B.J., Thouless D.J. *Percolation Theory and Electrical Conductivity. Phys. Rev. Lett*. 1971;27(25):1719–1721. https://doi.org/10.1103/PhysRevLett.27.1719
21. Mednikov S.V., Chebotarev M.A., Mednikov V.S. Percolation model of the corrosion process. *Voprosy fizicheskoi metrologii.* 2003;5:54–66 (in Russ). https://elibrary.ru/iuzzal
22. Mednikov S.V., Tuzhikov O.O., Olshanskii O.V. *Method for Determining the Durability of Structural Materials in Aggressive Environments and Device for its Implementation:* RF Pat. 2320972. Publ. 27.03.2008 (in Russ.).
23. Tuzhikov O.O., Ol'shanskii O.V., Mednikov S.V., Baierlyain R., Baierlyaen KH. "Tom – 3000" – automated test complex for determining the ozone resistance of rubber. *Kauchuk i rezina.* 2009;2:35–38 (in Russ.).
24. Mednikov S.V., Tuzhikov O.O., Ol'shanskii O.V. Chemical corrosion of elastomeric materials under conditions of plane stress state as a phase transition. *Izvestiya Volgogradskogo gosudarstvennogo tekhnicheskogo universiteta* (*Izvestiya VolGGTU*) = *Izvestia VSTU*. 2017;4(199):66–70 (in Russ.). https://elibrary.ru/ypwjdv
13. Халкечев Р.К. Перколяционная мультифрактальная математическая модель разрушения газосодержащего породного массива как основа для прогнозирования внезапного выброса пород и газа. *Горный информационно-аналитический бюллетень*. 2015;4:359–363.
14. Валишин А.А., Антонова И.В. Перколяционная модель накопления микродефектов и коллапса зоны вынужденной эластичности перед фронтом трещины разрушения в полимерных и композиционных материалах. *Инженерный журнал: наука и инновации.* 2016;11(59):1–16. https://doi.org/10.18698/2308-6033-2016-11-1556
15. Догадкин Б.А., Донцов А.А., Шершнев В.А. *Химия эластомеров*. М.: Химия; 1981, 376 с.
16. Ikeda Y., Higashitani N., Hijikata K., Kokubo Y., Morita Y., Shibayama M., Osaka N., Suzuki T., Endo H., Kohjiya S. Vulcanization: New focus on a traditional technology by small-angle neutron scattering. *Macromolecules*. 2009;42(7): 2741–2748. https://doi.org/10.1021/ma802730z
17. Гульд Х., Тобочник Я. *Компьютерное моделирование в физике:* в 2 ч.: пер. с англ. Ч. 2. М.: Мир; 1990, 400 с. ISBN 5-03-001594-9
18. Тарасевич Ю.Ю. *Перколяция: теория, приложения, алгоритмы.* М.: URSS; 2018, 112 с.
19. Watson B.P., Leath P.L. Conductivity in the two-dimensional-site percolation problem. *Phys. Rev. B.* 1975;9:4893–4896. https://doi.org/10.1103/PhysRevB.9.4893
20. Last B.J., Thouless D.J. *Percolation Theory and Electrical Conductivity. Phys. Rev. Lett*. 1971;27(25):1719–1721. https://doi.org/10.1103/PhysRevLett.27.1719
21. Медников С.В., Чеботарев М.А., Медников В.С. Перколяционная модель коррозионного процесса. *Вопросы физической метрологии.* 2003;5:54–66. https://elibrary.ru/iuzzal
22. Медников С.В., Тужиков О.О., Ольшанский О.В. *Способ определения долговечности конструкционных материалов в агрессивных средах и устройство для его осуществления:* пат. 2320972 РФ. Заявл. 11.11.2005; опубл. 27.03.2008.
23. Тужиков О.О., Ольшанский О.В., Медников С.В., Байерляйн Р., Байерляен Х. «Том – 3000» – автоматизированный испытательный комплекс для определения озоностойкости резин. *Каучук и резина*. 2009;2:35–38.
24. Медников С.В., Тужиков О.О., Ольшанский О.В. Химическая коррозия эластомерных материалов в условиях плоского напряженного состояния как фазовый переход. *Известия Волгоградского государственного технического университета* (*Известия ВолгГТУ*). 2017;4(199):66–70. https://elibrary.ru/ypwjdv

About the Authors

Stanislav V. Mednikov, Cand. Sci. (Phys.-Math), Associate Professor, Department of Physics, Volgograd State Technical University (28, pr. im. V.I. Lenina, Volgograd, 400005, Russia). E-mail: s_mednikov@vstu.ru. Scopus Author ID 57212473929, RSCI SPIN-code 1584-9501, https://orcid.org/0000-0001-6621-7550

Pavel D. Kravchenya, Cand. Sci. (Phys.-Math), Senior Lecturer, Department of Electronic Computers and Systems, Volgograd State Technical University (28, pr. im. V.I. Lenina, Volgograd, 400005, Russia). E-mail: kpd_@mail.ru. Scopus Author ID 36628612400, RSCI SPIN-code 1584-9501, https://orcid.org/0000-0002-1934-5792

Alexander A. Ponomarev, Head of the Laboratory, Department of Computer Engineering, Volgograd State Technical University (28, pr. im. V.I. Lenina, Volgograd, 400005, Russia). E-mail: alpo5404@gmail.com. https://orcid.org/0000-0002-3659-7094

Oleg O. Tuzhikov, Dr. Sci. (Eng.), Associate Professor, Head of the Department of General and Inorganic Chemistry, Volgograd State Technical University (28, pr. im. V.I. Lenina, Volgograd, 400005, Russia). E-mail: tuzhikovoleg@mail.ru. Scopus Author ID 12645529200, RSCI SPIN-code 8142-5915, https://orcid.org/0000-0001-6316-8896

Об авторах

Медников Станислав Владимирович, к.ф.-м.н., доцент, кафедра физики, ФГБОУ ВО «Волгоградский государственный технический университет» (400005, Россия, Волгоград, пр-т им. В.И. Ленина, д. 28). E-mail: s_mednikov@vstu.ru. Scopus Author ID 57212473929, SPIN-код РИНЦ 1584-9501, https://orcid.org/0000-0001-6621-7550

Кравченя Павел Дмитриевич, к.ф.-м.н., старший преподаватель, кафедра «Электронно-вычислительные машины и системы», ФГБОУ ВО «Волгоградский государственный технический университет» (400005, Россия, Волгоград, пр-т им. В.И. Ленина, д. 28). E-mail: kpd_@mail.ru. Scopus Author ID 36628612400, SPIN-код РИНЦ 1584-9501, https://orcid.org/0000-0002-1934-5792

Пономарев Алексей Сергеевич, заведующий лабораторией, кафедра «Вычислительная техника», ФГБОУ ВО «Волгоградский государственный технический университет» (400005, Россия, Волгоград, пр-т им. В.И. Ленина, д. 28). E-mail: alpo5404@gmail.com. https://orcid.org/0000-0002-3659-7094

Тужиков Олег Олегович, д.т.н., доцент, заведующий кафедрой общей и неорганической химии, ФГБОУ ВО «Волгоградский государственный технический университет» (400005, Россия, Волгоград, пр-т им. В.И. Ленина, д. 28). E-mail: cand@vstu.ru. Scopus Author ID 12645529200, SPIN-код РИНЦ 8142-5915, https://orcid.org/0000-0001-6316-8896

Translated from Russian into English by N. Isaeva
Edited for English language and spelling by Thomas A. Beavitt